



Programa de Doctorado en Química

**INNOVATIVE POLYMER NANOPARTICLES FOR  
ENERGY STORAGE AND ANTI-COUNTERFEITING  
APPLICATIONS**

Tesis Doctoral presentada por

**Amparo Fernández Benito**

**Supervisors:**

**Dr. Javier Carretero González**

**Dr. Mario Hoyos Núñez**

**Dr. Miguel Ángel López Manchado**

**Tutora: Dra. Belén Batanero Hernán**

**Alcalá de Henares, diciembre 2022**





***A los que siempre creyeron en mí, mi familia.***



## ACKNOWLEDGMENTS

Qué complicado es decir adiós a una etapa de tu vida que ha significado tanto y qué difícil resulta mostrar lo agradecida que estoy a todos los que me han acompañado durante este proceso. Hace mucho tiempo, cuando empecé la carrera de Química en la Universidad de Salamanca, mi familia me dijo que estaba empezando una carrera de resistencia, hasta ahora que me dispongo a acabar mi doctorado en Química, ¡quién me lo iba a decir!. Por eso, enfoco los agradecimientos como si todos hubierais formado parte de esa carrera de resistencia.

En primer lugar, me gustaría agradecer a la Universidad de Alcalá de Henares, a mis compañeros y a todos los profesores que me acompañaron en mi etapa como estudiante en Química. Vosotros fuisteis mis primeros entrenadores con los que fui capaz de superar estos primeros kilómetros de la carrera.

Los siguientes kilómetros fueron realizando el máster de Alta Especialización en Plásticos y Cauchos. Quiero agradecer a todos los profesores la dedicación y entusiasmo con la que me enseñaron tantísimo.

Después de estos primeros kilómetros, me disponía a afrontar la parte más dura de la carrera: empezaba mi Tesis Doctoral. Por eso quiero agradecer a Javier Carretero, Mario Hoyos y Miguel Ángel López, mis directores de Tesis, los que pensaron que era una buena candidata y los que me han acompañado en este tramo final.

Javier, mi gurú de la ciencia, nunca he conocido a nadie que tenga tanta pasión por lo que hace y que disfrute tanto enseñando como tú. Llevamos 5 años juntos, desde que fuiste mi tutor de Máster y creo que hacemos muy buen equipo, sería muy difícil imaginarme esta etapa sin ti como director. Estoy muy agradecida por permitirme aprender de ti en cada momento, por guiarme en cada paso que daba y por asegurarte que disfrutaba investigando.

Mario, nunca olvidaré la primera vez que te vi. Empezaste a hablar de productos de anti-falsificación, y fíjate, tiempo después me metí de lleno en esa aventura. Quería agradecerte que pensaras en mi como candidata para el proyecto, he tenido la oportunidad de aprender mucho de ti en todo este

tiempo, gracias por darme libertad en el proyecto, gracias a ti he aprendido a ser independiente y a ganar seguridad en mí misma.

Miguel Ángel, gracias por ser el punto de cordura que he necesitado en este tiempo, por estar ahí cuando he necesitado hablar, gracias por asesorarme y transmitirme la calma que necesitaba.

Un agradecimiento especial a mi tutora Belén Batanero, gracias por aceptar estar a mi lado cuando empezaba la etapa más dura. Gracias por las largas conversaciones, los cafés y el apoyo.

También me gustaría dar las gracias a la empresa Inentia Arô S.L., a Daniel y Ramón, por confiar en mí y por darme la oportunidad de crecer profesionalmente.

No puedo olvidarme de dar las gracias a los miembros y compañeros del *Grupo de Compuestos Poliméricos del Instituto de Ciencia y Tecnología de Polímeros (ICTP)*. Son muchos los que me habéis acompañado en esta carrera, desde los inicios: Laura, Emil, Paolo, Javi, Suman, Vanesa, Jorge, Francisco, Nedía y Jordy. También a los que aparecisteis a mitad de carrera: Ozden, Mena, Marta, Paula Navalpotro, Paula Cisneros y Leandro. Y los que aparecisteis en mi sprint final: Juan Carlos y Dani. En especial agradezco a Sergio haber estado todo este tiempo y sobre todo en el sprint final, gracias por todos los cafés a primera hora de la mañana. No quiero olvidar agradecer a la Dra. Raquel Verdejo y a la Dra. Marianella Hernández por los consejos y apoyo cuando lo he necesitado.

A Said, akhouya, empezamos casi a la vez y has sido la alegría del laboratorio todo este tiempo. Gracias por unir al grupo, gracias por tu buen humor todos los días, gracias por tantas charlas juntos. De ti, he aprendido a intentar no agobiarme y relativizar los problemas. Eres todo un ejemplo para mí de buena disposición y actitud ante la vida. Tengo suerte de que sigas en mi camino, mi "bestie".

A Alberto, apareciste cuando ya la carrera había empezado y no me puedo imaginar haberla acabado sin ti. Apareciste como uno más que participaba en su propia carrera de la ciencia, luego fuiste un compañero muy cercano en toda la etapa, pero me siento orgullosa de decir que acabamos siendo amigos. Y que suerte la mía de que lo seamos, gracias por todo lo que me has enseñado,

por haberme corregido el inglés siempre, por haberme dedicado tu tiempo y por estar en las buenas y en las malas.

A Mónica, salimos juntas en la carrera de la Tesis y hemos llegado a la meta más unidas que nunca. Tengo claro que, sin ti, nunca habría llegado a terminarla. Has sido mi apoyo incondicional en cada traspies que he dado, me has enseñado a no tirar nunca la toalla y a seguir creciendo. Te has convertido en una persona muy importante para mí dentro y fuera del ICTP. Solo espero poder seguir a tu lado viendo como creces profesionalmente porque nos queda un mundo lleno de oportunidades por delante y las lloraremos y celebraremos juntas.

En toda carrera de resistencia hay zonas de avituallamiento, por eso quiero agradecer a todos los que habéis formado parte de esta Tesis, porque de una forma u otra me habéis ayudado. Al *Servicio de Mantenimiento de Equipos, Infraestructuras e Informática* del ICTP: Carlos, Manuel y Alberto, a vosotros os debo muchísimo. Gracias por ayudarme siempre en todo lo que he necesitado, gracias por aguantarme cada vez que iba a veros, gracias por las largas charlas y sobre todo gracias por el apoyo en el último sprint de la carrera. Al *Servicio de Gerencia y Administración*, en especial a Conchi. Al *Servicio de Caracterización* del ICTP: Pilar Posadas, David Gómez, Esperanza Benito, Carolina García, Isabel Muñoz y Patricia Sampedro.

Agradecer a todos los grupos de investigación del ICTP que estuvieron siempre ahí para ayudarme y sin los que no podría haber acabado esta maratón. Gracias por ayudarme a esquivar los baches en la carrera y llegar con buenos resultados. Al *Grupo de Biomateriales*, en especial a María Rosa Aguilar por dejarme siempre los equipos cuando los he necesitado; y a Yeral por empezar juntos desde el máster y terminar juntos esta carrerita de resistencia, gracias por seguir a mi lado. Al *Grupo de Funcionalización de Polímeros*, en especial a Carlos Elvira y a Raúl. Gracias por ayudarme cuando lo he necesitado, siempre ha sido un placer escaparme a vuestro laboratorio para que me echarais una mano. Al *Grupo de Fotoquímica de Polímeros*, en especial a Teresa, por haberme dejado los equipos cuando más los necesitaba, pero sobre todo por las charlas y las buenas palabras que siempre has tenido para mí.

Esta carrera de resistencia me llevó a otro país, a otra ciudad, Copenhague. Donde estuve 3 meses siendo entrenada por Thomas. That is why I would like to thank *Thomas Just Sorensen's Group* for their warm welcome. Especialmente a Thomas, por dedicando su tiempo a mí y mostrando su pasión por la ciencia. También, a todo el grupo, especialmente Patrick, Lu, Yang, Rasmus, Jesper, Laura, Maria, Lea, Nickolaj, Christian, Morten and Villads por ser parte de esta gran experiencia. Gan bei!

A Laura, que estuviste conmigo desde el principio en el ICTP y nos volvimos a encontrar en Copenhague, gracias por hacer mis días más felices en las distintas etapas de la carrera.

En toda carrera siempre están aquellos en la barrera para animarte por cada calle que pasas, por cada cuesta arriba, por cada tramo. A vosotros, mis amigas y amigos que siempre habéis estado para acompañarme y animarme. Aunque no os nombre uno a uno, sabéis quienes sois, gracias de corazón.

A ti, Jaime, mi compañero de vida. No tengo palabras para poder agradecerte tanto. Has sido mi gran apoyo todo este camino, cuando me he caído siempre has estado para levantarme, has aguantado mis agobios, risas y llantos y sigues a mi lado. No podría haber elegido mejor compañero para esta carrera, gracias a ti y a tus ánimos estoy consiguiendo llegar a la meta. El camino es la mejor parte, por eso espero correr todas las carreras juntos ¡Te quiero!

A mi familia, por haber creído siempre en mí y por apoyarme en todo lo que he hecho. A ti, María, por estar siempre, por ser todo un ejemplo para mí. No podría tener mejor hermana, gracias a ti empecé a entender la química orgánica y fíjate donde estoy ahora.

Papá, mamá, gracias por confiar siempre en mí, por darme esos empujoncitos cuando los he necesitado, por haberos alegrado por cada uno de mis logros, por hacerme siempre ser mejor persona y por enseñarme a superarme a mí misma.

Os quiero muchísimo a los tres, soy lo que soy gracias a vosotros. Os estaré eternamente agradecida por haber confiado en mí siempre. Estoy llegando a la meta y sé que me estáis esperando allí para celebrarlo juntos.

*Amparo*







“Aprenda a amar a sus derrotas, pues son las que le construirán. Son sus derrotas las que darán sabor a sus victorias”.

Joel Dicker, *La Verdad sobre el caso Harry Quebert*

“Cuanto más difícil es hacer algo, mayor es la recompensa que te espera al final.”

Edward Bloom (*Big Fish*) Tim Burton



# Table of contents

<b>Abstract</b> .....	17
<b>Preface</b> .....	19
<b>Chapter 1. Introduction</b> .....	29
<b>Section I. Polymer nanoparticles for energy storage applications</b> .....	65
<b>Chapter 2.</b> Multifunctional metal-free rechargeable polymer composite nanoparticles boosted by CO <sub>2</sub> .....	85
<b>Chapter 3.</b> Novel ferrocene-containing amphiphilic block copolymer nanoparticles as high-capacity charge carriers in aqueous redox flow systems .....	129
<b>Conclusions of Section I</b> .....	175
<b>Section II. Polymer nanoparticles for anti-counterfeiting applications</b> .....	181
<b>Chapter 4.</b> New polymeric systems for anti-counterfeiting devices.....	199
<b>Chapter 5.</b> A physical unclonable function based on recyclable polymer nanoparticles for enabling the circular economy.....	245
<b>Conclusions of Section II</b> .....	271
<b>Chapter 6. Summary and final remarks</b> .....	275
<b>Appendix</b> .....	281



# Resumen

La nanociencia y la nanotecnología representan uno de los campos más interesantes de la ciencia moderna, con un carácter altamente multi- e interdisciplinar, ya que combina diferentes disciplinas como la química, la biología, la física y la ingeniería, aprovechando sus principios y procesos. Los nanomateriales han estado presentes en la naturaleza y en la vida desde tiempos ancestrales. Sin embargo, no es hasta la revolución industrial cuando se desarrollan nuevas herramientas tecnológicas que propiciarán en el futuro un gran interés por el estudio de los nanomateriales. Una de las grandes características de los nanomateriales es que presentan propiedades diferentes al disminuir su tamaño a nivel nanométrico ya que poseen una mayor área superficial.

Las nanopartículas poliméricas (PNPs) han recibido recientemente mucho interés y tienen un papel clave en diversas áreas como fotónica, electrónica, sensores, medicina, control de la contaminación y tecnología ambiental. La transformación del polímero disponible a granel en un material polimérico de tamaño nanométrico ha proporcionado la aparición de propiedades nuevas e interesantes sin cambiar la composición del polímero.

Con el fin de desarrollar nuevos dispositivos de alta tecnología para diversas aplicaciones, los investigadores necesitan controlar mejor la estructura y la función de las nanopartículas poliméricas comprendiendo el papel del tamaño, la forma y la composición. La interfaz de investigación en la que las nanopartículas poliméricas se encuentran con la química analítica, la biomedicina, la construcción, la electroquímica y otros campos ofrece ricas oportunidades para revelar nuevas propiedades químicas, médicas y biológicas de los nanomateriales y descubrir muchas funciones y aplicaciones nuevas de estos materiales.

Las nanopartículas poliméricas, por tanto, representan una plataforma para poder desarrollar nuevas aplicaciones, estudiando nuevas rutas sintéticas para obtener las propiedades óptimas para cada aplicación deseada.

En la tesis, se describen los avances recientes en la síntesis de nuevas nanopartículas poliméricas con propiedades avanzadas mediante diferentes estrategias. Las estrategias sintéticas incluyen la síntesis química y física para la producción controlada de nanopartículas poliméricas con morfologías bien definidas.

En concreto, se desarrollaron diferentes tipos de nanopartículas con altas prestaciones en aplicaciones en almacenamiento de energía y en el campo de la antifalsificación.

Los beneficios tecnológicos que se han desarrollado en la tesis doctoral residen en el diseño de los nuevos nanomateriales con potenciales aplicaciones que además pueden aportar valor a tecnologías y productos ya existentes, como además dar soluciones a problemas medioambientales y sociales actuales. Estas nuevas rutas sintéticas y pruebas de concepto creadas en la presente tesis doctoral generan nuevo conocimiento que da valor tanto a nivel académico como industrial.



# Abstract

Nanoscience and nanotechnology represent one of the most interesting fields in modern science, with a highly interdisciplinary character, as it is developed by mixing different disciplines such as chemistry, biology, physics and engineering, taking advantage of their principles and processes. Nanomaterials have always been present in nature. It was not until the industrial revolution, when new technological tools were developed, that allowed the future study of nanomaterials. One of the main characteristics of nanomaterials is that they have different properties as they decrease in size at the nanometric level because they have a larger surface area. The composition, particle size, shape, surface coatings and bond strength of the particles change, providing interesting new properties.

Polymeric nanoparticles (PNPs) have recently received much interest due to their unique properties because of their nanometer size. Without changing the polymer composition, new properties can be conferred by simply converting bulk polymers to nanoscale polymers.

In order to develop new high-tech devices for various applications, researchers want to have better control over the structure and function of polymer nanoparticles by understanding the role of size, shape and composition. The research of the interface where polymer nanoparticles meet analytical chemistry, biomedicine, construction, electrochemistry and other fields offers rich opportunities to reveal new chemical, medical and biological properties of nanomaterials and to discover many new functions and applications of these materials.

Polymeric nanoparticles, therefore, represent an alternative to develop new applications by simply studying new synthetic routes to obtain the optimal properties for each desired application.

In the Thesis, recent advances in the synthesis of new polymeric nanoparticles with advanced properties using different strategies are described. The synthetic strategies include chemical and physical synthesis for the controlled production of polymeric nanoparticles with well-defined morphologies.

Specifically, different types of nanoparticles with high performance in applications in energy storage and in the field of anti-counterfeiting were developed.

The technological benefits that have been developed in the Ph.D. Thesis lie in the design of new nanomaterials with potential applications that can also add value to existing technologies and products, as well as provide solutions to current environmental and social problems. These new synthetic routes and proofs of concept created in this Ph.D. Thesis generate new knowledge that provides value at both academic and industrial levels.

# Preface

This Ph.D. Thesis has been focused on Secure, Clean and Efficient Energy and Secure Societies Protecting Europe's Freedom and Security of H2020.

The **motivation** of this Thesis is to deepen the chemical composition, structure, and functioning mechanisms of polymeric nanoparticles (PNPs) with potential application in different fields, especially in energy storage, traceability, and anti-copying products.

The work in this PhD Thesis consists of the development of functional nanocomposites and nanostructured polymer nanoparticles with advanced properties. In order to develop these advanced systems, first we will try to control the structure and function of micro/nanomaterials through shape, composition, hybridization and dimensions. A characteristic of nanomaterials is that they generally present different properties by decreasing their dimensions to nanometric levels.

The preparation of new functional polymeric nanostructures will be investigated, from both commodity polymers and new synthetic polymers, formed through different strategies that allow the production of nanoparticles with well-defined morphologies.

These nanoparticles will be used as functional materials for different proof-of-concept tests in various applications, such as traceability and authenticity control systems in the packaging sector, and in new sustainable energy storage systems.

The **general objective** is, therefore, the design and synthesis of new polymeric nanoparticles dispersible in water and green solvents using new chemical strategies. The aim is to advance in the fundamental knowledge of the synthesis of new polymeric nanoparticles and then, in their sustainable and environmentally friendly processing, as well as in their practical applications in the area of energy storage and anti-counterfeiting.

The following specific objectives related to the main goal of this Ph.D. Thesis have been identified:

1 The synthesis of low-cost nanoparticles composed of three interpenetrated functional macromolecular networks (polypyrrole, methyl cellulose and lignin) offers the opportunity to address two major energy and environmental challenges: global warming and pollution of the atmosphere by greenhouse gas emissions and electricity generation together with energy storage from renewable sources. Batteries are potential candidates to enable both energy storage and CO<sub>2</sub> storage.

2 Synthesis of new polymeric nanoparticles, enhancing water solubility and maximizing the number of redox sites to improve the capacity (Energy) of these polymeric systems. A proof of concept is performed on an aqueous, hybrid flow battery with a zinc anode and the innovative redox block-copolymer nanoparticles developed in this Ph.D. Thesis as catholyte material in the cell.

3 Design of new luminescent polymeric nanoparticles without the use of chromophores or semiconducting polymers.

4 Application of polymer nanoparticles in the circular economy of plastics and in the field of anti-counterfeiting of products.

## THE INDUSTRIAL AND ACADEMIC STRUCTURE OF THE Ph.D. THESIS

The development of this Ph.D. Thesis is carried out within the framework of the industrial Ph.D. of the Community of Madrid (CAM). The main goal of this Ph.D. fellow is the reinforcement of the I+D+i and competitiveness of industrial partners through the development of research projects in close collaboration with the universities and public research Institutions. Besides, the Ph.D. candidate has improved her professional perspective through the acquisition of new scientific skills and the expansion of their scientific vision in different areas such as polymer science and nanotechnology, energy storage and anti-counterfeiting of great interest to society. All of this has enhanced the interaction between the industrial and academic spheres promoting knowledge transfer from research to its practical application.



Industrial and academic structure of the Ph.D. Thesis

The main partners involved in the development of the activities of this Ph.D. are the following:

- **Spanish National Research Council (CSIC).**

The Thesis has been carried out at the Institute of Polymer Science and Technology (ICTP) in the Polymer Composite Group. The Thesis has been co-directed by:

- Dr Javier Carretero González has extensive experience in the design of electroactive polymeric materials, and their study by applying advanced characterization tools to unveil their energy storage and failure mechanisms.
- Dr Mario Hoyos Nuñez is an expert in the synthesis, preparation, and physical and chemical obtaining of nanostructures, as well as the modification of their properties in the synthesis of new semiconducting polymers from specific catalysts for their subsequent use in electronic devices and anti-counterfeiting systems.
- Dr. Miguel Ángel López Manchado has extensive experience in the processing and characterization of polymer nanocomposites.

The existence of three directors in this Thesis is due to the multi- and interdisciplinary nature of the subject of the Thesis, and the evolution of their scientific content. Besides, the direction of all of them have favored the achievement of the main objectives.

- **Inentia Arô S.L.**

Part of the research has been carried out in the company; the supervisors of the industrial activities in this Ph.D. are Ramon Cisneros and Daniel Andrinal Lopez.

Inentia Arô S.L. is a company incorporated on 25/11/2016 in San Sebastian de Los Reyes, Madrid. Its CNAE is Wholesale trade of perfumery and cosmetics products. The SIC activity of INENTIA ARO SL is 5122 Drugstore, perfumery and pharmacy and its business purpose is Retail Trade by Correspondence or Internet.

The newly formed company was awarded a CDTI project for the development of a new personal device. The development of new anti-counterfeiting measures will allow the company to have a new complementary product to the basis of its market strategy. Doing the industrial doctorate with Inentia Arô S.L. allows the company to acquire specific and highly qualified knowledge relevant to its market interests.

The company had developed a new personal wearable device which they had patented and developed. The company's objective is to provide a smart packaging solution to protect, track the product and create safety links between brands and the consumer. The goal is to design a plastic cosmetic package with an anti-counterfeiting system inside the product.

- **Alcalá de Henares University (UAH):** The tutor at the university is Dr. Belén Batanero, whom has been following closely the development of the research and has advised to the Ph.D. candidate during the duration time of the Ph.D. Thesis.

## **SPECIFIC ACADEMIC AND INDUSTRIAL ACTIVITIES PERFORMED DURING THE Ph.D. THESIS**

The main objective related to the industrial activities carried out by the company was to develop new anti-counterfeiting systems inside the product for plastic cosmetic package. So, new advanced materials based on polymer nanoparticles for the development of dispersions or stable inks, processable by different methodologies on any kind of substrates were designed.

Despite the Ph.D. Thesis being planned into an industrial doctorate context, the content extended to the synthesis and study of new advanced nanoparticles that could be applied in other industrial applications such as energy storage. The main reason behind this decision was that the developments performed on that topic might enrich the research related to anti-counterfeiting.

Once put in context, the first steps to follow in this industrial Ph.D. are:

1. Find the suitable polymer for each application.
2. Optimize the material processing conditions.
3. Study under standard:  
ASTM-D543-95: Chemical and resistance evaluation.  
ASTM-D638-14: Mechanical properties.
4. Evaluate the most suitable polymer dispersion to be used.
5. Design the pattern to create a detection code and demonstrate its potential application as a traceability system.



## **Ph.D. THESIS STRUCTURE**

This Ph.D. Thesis has been divided into 6 chapters, and include the following elements:

**Chapter 1** introduces the main aspects related to the state of the art in the area of polymeric nanomaterials such as, design principles, synthesis, structural diversity, chemical functionalization, processing and potential applications of polymeric nanoparticles. It shows the trade-off between nanoparticle size, morphology and the properties of the nanoparticles.

In the **Chapters 2 and 3** involved in **Section I: "energy storage applications"**, introduce the synthesis of different nanoparticulate systems for its use as aqueous electrolytes in redox flow batteries (RFB). This will enable the development of RFBs in aqueous solution and avoid the use of toxic and hazardous solvents. In addition, the aim is to replace the existing expensive membranes with size-exclusion membranes.

**Chapters 4 and 5** involved in **section II: "anti-counterfeiting applications"** focus on the design of new anti-counterfeiting systems using nanotechnology. The objective of Inentia-Aro, S.L., enterprise responsible for the industrial doctorate, is the use of these anti-counterfeiting systems in the cosmetics-perfumery sector.

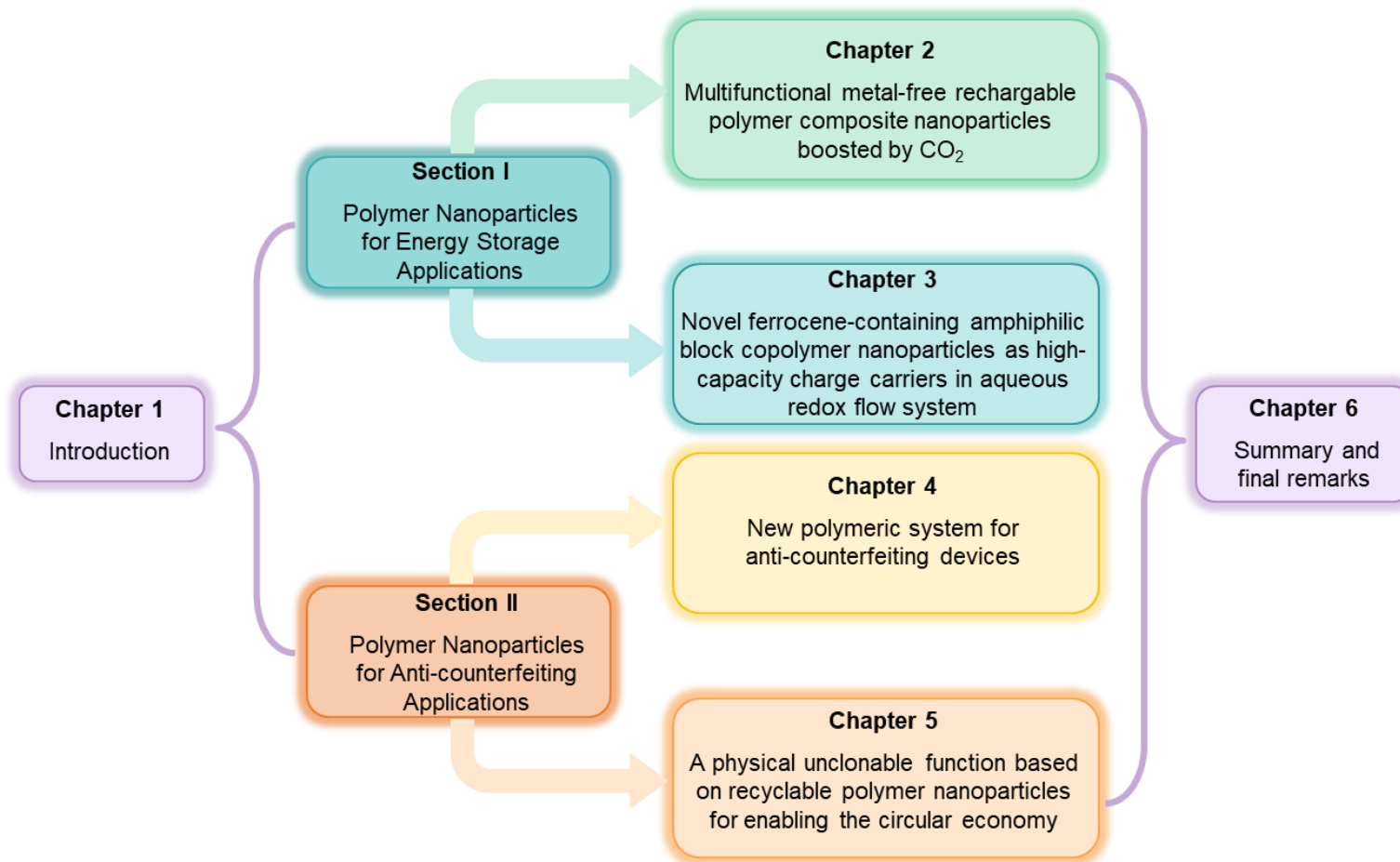
**Chapter 5** assesses the applicability of these nanoparticles as anti-counterfeiting systems on the market. Non-cloneable physical patterns are created and validated through an existing mobile application.

Finally, the conclusions of the Thesis and future outlook are given in **Chapter 6**.

The preparation of this Ph.D. Thesis has resulted in a total of three scientific articles in prestigious international journals, and two international patents under the starting hypothesis.

Most of the experimental work presented in this Ph.D. Thesis was carried out at the Institute of Polymer Science and Technology (CSIC) in Madrid (Spain). Collaborations with other institutions, however, have also taken place. In Chapter 2, part of the work has been carried out with the support of Dr. Martin Sjödin at the Department of Engineering Science, Uppsala University (Sweden). And the support of Dr. Daniel Arenas Esteban and Dr. David Avila Brande at the Department of Inorganic Chemistry, Faculty of Chemistry, Universidad Complutense de Madrid, Spain. In Chapter 3, part of the work has been carried out with the support of Francisco J. Rivera Gálvez, and Dr Carlos F. Jasso Gastinel, at Chemical Engineering Department, Universidad de Guadalajara, Guadalajara (México). On the other hand, cryoEM imaging was performed at the Centro Nacional de Biotecnología (CNB) with the assistance of Rocío Arranz. In Chapter 4, the fluorescence confocal microscopy work was carried out at the Instituto de Investigaciones Biomédicas "Alberto Solis" (CSIC-UAM) with the assistance of Mónica Martín and Lucía Guerrero. All Chapter 5 was developed at the University of Copenhagen in the TJS group, with the support of Dr. Thomas Just Sorensen.

This Ph.D. Thesis is written in English to facilitate and promote its scientific impact, although it has been developed almost entirely in Spain.



Structure of the Ph.D. Thesis by sections and chapters.



# **Chapter 1.**

## **Introduction**

---



## Introduction

Recent years have seen difficult situations such as the Covid-19 pandemic that has devastated a large part of the planet, or global warming due to increasing greenhouse gas emissions into the atmosphere that have caused extreme situations, such as the Filomena or gigantic fires in Spain. This situation must be addressed in order to avoid devastating consequences in the near future.

Therefore the 2030 Agenda of the United Nations (UN) has based its planning on the fulfillment of the Sustainable Development Goals (SDGs) (Figure 1.1) to be achieved during the period 2016-2030.



**Figure 1.1.** United Nations Sustainable Development Goals

Society is facing serious challenges, and that is why it is now when new technologies are being explored that can offer solutions in almost every aspect, from health, energy, environment, and climate either directly or indirectly [1].

Nanotechnology is part of the tools at our disposal to deal with major problems such as those we are currently observing [2-4].

## Nanotechnology

Nanotechnology has great potential for application in countless sectors that can find solutions that remedy many of the problems that need to be solved to achieve the SDGs. Nanotechnology can offer breakthroughs and innovations that can provide answers and solutions to help the environment and the society. The SDGs that will benefit from the impact of nanotechnology are 2, 3, 6, 7, 9, 11 and 12, although indirectly other SDGs will also benefit [4].

Nanotechnology can be defined as the set of knowledge and methodologies that come from different branches of science (biology, engineering, physics and chemistry among others) with which we have learned to understand and master the matter at nanometric scale, that is, at atomic and molecular scale. Nanotechnology is therefore based on the understanding and knowledge of the properties of matter at the nanometer scale of less than 1000 nm.

However, what are nanomaterials? They can be defined in several ways: they are materials that have a dimension at least  $< 100$  nm whose relative scales are shown in Figure 1.2; another definition is as materials that have special properties that depend directly on their small size. This last definition is what gives nanomaterials a high added value compared to conventional materials.

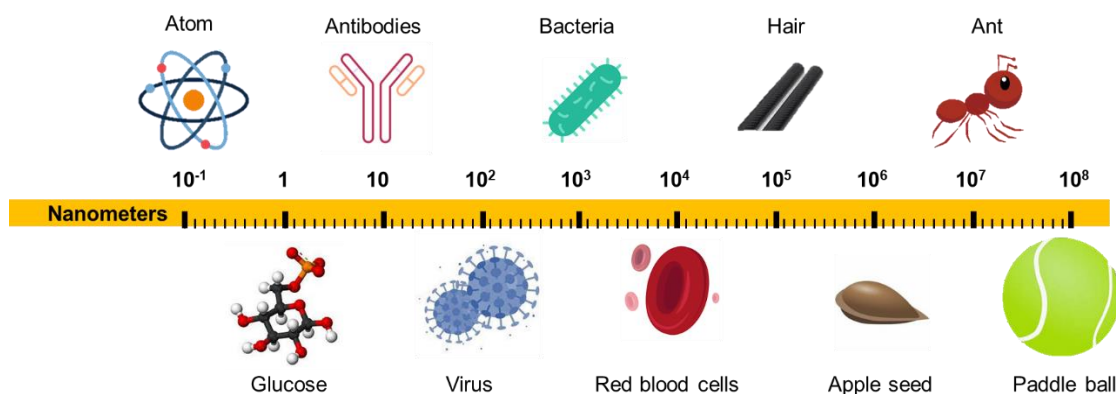


**Figure 1.2.** Dimensional scale from nanoscopic to macroscopic

Nanoscience and nanotechnology have been recognized almost modern and highly promising research topics. Nanotechnology was predicted in 1959 in Richard Feynman in his lecture's "There's Plenty of Room at the Bottom" [5], but



it was defined until 1974 by Norio Taniguchi [6]. Therefore, the field of nanotechnology has been explored for 50 years. The knowledge generated over the last 50 years and its interdisciplinary nature means that this domain of matter at the nanometer scale has great potential for cross-cutting applications in different sectors. Currently, the nanotechnology contributes to almost all fields of science such as, natural sciences and engineering, materials science, agriculture, medicine, and a myriad of fields that continue growing today [7] (Figure 1.3).

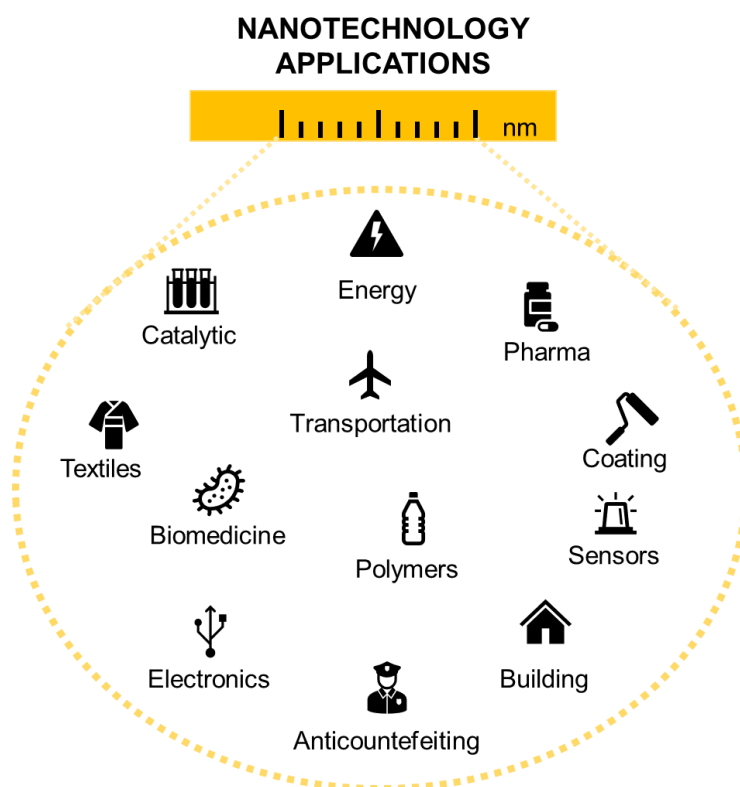


**Figure 1.3.** Diverse applications of nanotechnology

Nanomaterials present particular properties due to the effect of reduced size, surface effect and have many applications in electrochemistry, optics, electronics, analytical devices among others [8–11]. For example, nanoparticles (NPs) are atomic aggregates or solid particles with a nanometer size. The NPs can be formed by different materials with different shape and morphology [12]. The small size of the NPs gives them specific properties because they are subject to physical laws that lie between classical and quantum physics [13].

The existence of nanoparticles is not only due to man-made design and fabrication in modern research, but nanoparticles can also be found in the environment. Depending on the nature of nanoparticles these can be classified as inorganic or organic (Figure 1.4) [14,15].

For example, quantum dots, can be made either of metallic ceramic or carbonaceous materials [9,16–19].

Organic nanoparticles can be classified according to their composition and structure as micelles and liposomes, dendrimers, nanogels and polymeric nanoparticles [20]. The latter being the main subject of the Ph.D. Thesis being carried out.

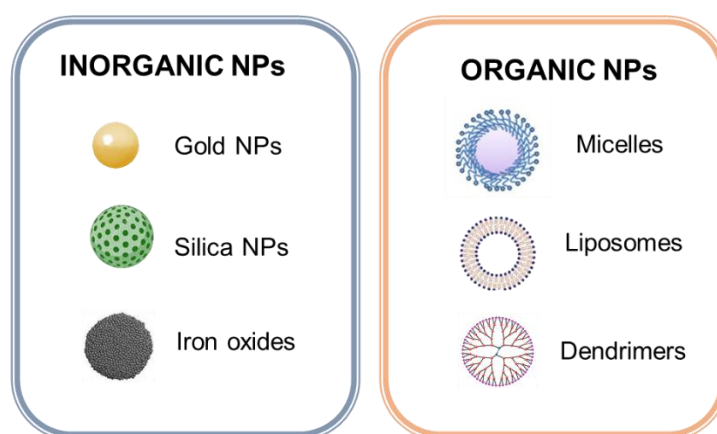


**Figure 1.4.** Schematic representation of some inorganic and organic nanoparticles

### Polymer nanoparticles

Polymer nanoparticles (PNPs) represent one family of nanoparticles, but in the last decades they are expanding rapidly and play a fundamental role in different areas. They have generated great interest as evidenced by the increasing number of associated publications [21,22]. This fact is evidenced by the increasing number of publications on polymeric nanoparticles in the last 21 years that is reflected in the following image (Figure 1.5). The data have been extracted from Scopus source.

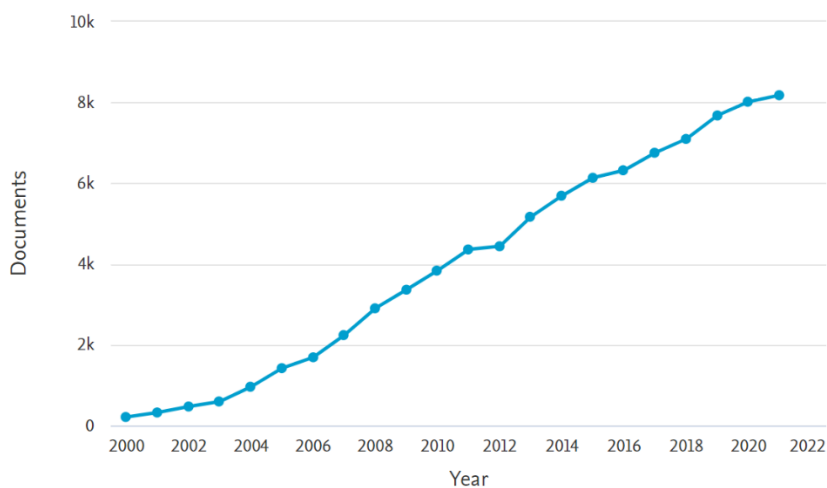


**Figure 1.5.** Articles published each year on polymeric nanoparticles

This is because polymeric nanoparticles possess unique properties that satisfy a wide range of applications (Figure 1.6).

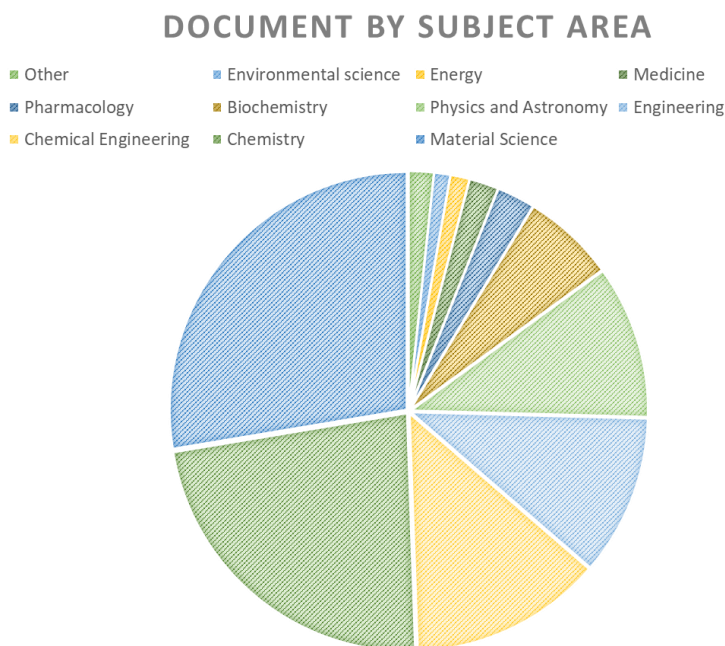


**Figure 1.6.** Document by thematic applications

Polymers confined at nanometer scale are studied to understand the size effect on their final properties. When designing nanostructures various physical

dimensions can be affected (1D, 2D and 3D) [23,24]. Nanoconfined polymeric structures can be synthesized to obtain on-demand properties [25,26].

They can be defined as colloidal systems with a diameter between 10-1000 nm, the general range being around 100-500 nm [27]. Polymer nanoparticles are defined by their polymeric composition which can be a homopolymer or copolymer [28].

These nanoparticles are often associated with novel properties mainly due to the nanometer size. By simply decreasing the size of the bulk polymer to nanometer polymer, new properties can appear without modifying the material components.

What gives value to nanotechnology and nanoscience is that the conversion to polymer nanoparticles causes their physicochemical qualities to be modified.

What really makes novel properties possible is the decrease in size, since at the nanoscale, quantum spaces prevail and the ratio between surface area and volume is multiplied, which leads to the appearance of novel and unique properties [29–33]. The following figure describes the increase in surface area in the transition from the macro to the nanoscale (Figure 1.7).

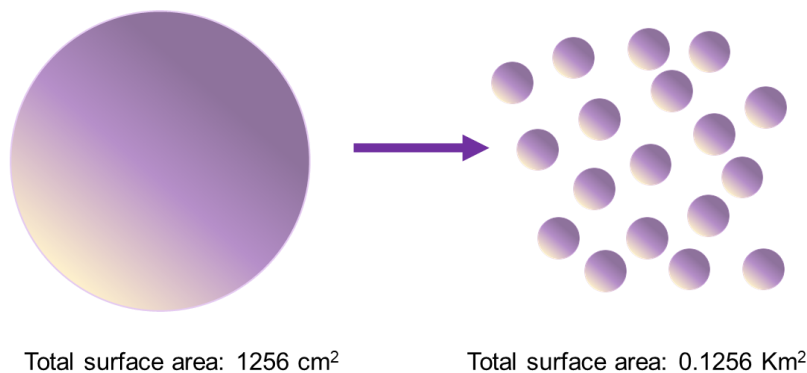


**Figure 1.7.** Large surface area with reduced particle size

The term "polymer nanoparticle" includes any type of nanometer-sized particle but focuses on polymer nanospheres and nanocapsules. Nanocapsules are vesicular systems while nanospheres are particles whose entire volume is solid

[22,27]. Spherical nanoparticles are usually obtained for the reason of lower energy [34-36].

Applications of polymer nanoparticles are affected by their physical properties and morphology. Both factors can be controlled to design nanoparticles a la carte [37-39]. The advantages of polymer nanoparticles are the potentially biodegradable properties, the ability to engineer the polymer by modifying the functional groups, and the wide variety of synthetic routes [40].

Therefore, the main objective of nanoparticle design is to create well-defined polymer nanoparticles with controllable characteristics such as particle size, morphological shape, surface charge, porosity, mechanical and chemical resistance. These properties make them suitable for applications such as drug delivery, special coatings, UV protection, among others [41–44].

### **Synthesis of polymer nanoparticles**

Advances in polymer chemistry and physicochemistry mean that the synthesis of polymer nanoparticles can provide them with countless properties [45–48]. The choice of preparation methods mentioned below depends on a number of factors, such as the type of polymer system to be used, the field of application and the size required. Therefore, a key objective is to control the structural and interfacial design of polymer nanoparticles with unique functionalities for each application.

#### **Features for nanoparticle design**

PNPs must be designed, synthesized, and optimized their properties depending on the final application. Composition, shape, size, and surface charge must be carefully considered for the design of PNPs. Well-defined structural and interfacial characteristics of PNPs are the key to an efficient outcome over different applications.

- **Size:** Due to the high surface/volume ratio, nanoscale particles hold very different properties from their bulk equivalents. The main effect observed on the size of nanoparticles is their increased interaction with active objects when the nanoparticles are smaller [32,49].

- **Morphology:** Polymers are soft, swellable, flexible, and amorphous or crystalline, so they often end up having a spherical shape since the non-spherical shape of nanoparticles of the same size have a higher surface energy than spheres at the nanoscale, and therefore, a non-spherical shape is thermodynamically unfavorable [35,50-52].
- **Surface charge:** Surface characteristics is a very important feature in desired applications. Surface ligands not only favor the stability of nanoparticles through electrostatic repulsions but also are decisive in interactions with the environment [53].
- **Chemical composition:** The individual applications of PNPs depend on the composition of the polymer, its inherent properties, and the polymerization processes [54].

PNPs can be synthesized by two different approaches that can be also used in a complementary manner [55,56]. On the one hand, the preparation of polymer nanoparticles by direct polymerization, where they are manufactured from the monomers (chemical method or bottom-up method). On the other hand, post-polymerization nanoparticle fabrication, where nanoparticles are prepared from a preformed polymer (physical or chemical method or top-down method) [57-59] (Figure 1.8).

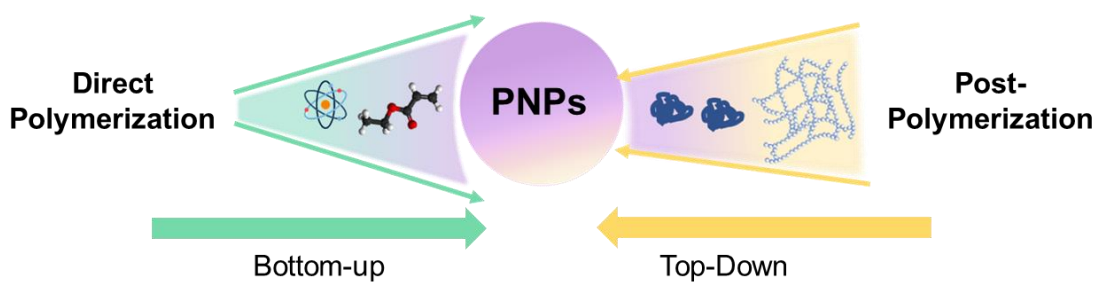


**Figure 1.8.** Schematic representation of bottom-up and top-down method for the preparation of polymer nanoparticles

## Bottom-up: Direct polymerization

The polymerization of monomers to prepare PNPs can be performed through different strategies [60].

- Conventional emulsion polymerization

This method is within the group of emulsion polymerization, being the conventional one the most used. The elements necessary are water, a monomer that is not very soluble in water (e.g., vinyl acetate, ethylene, styrene, acrylonitrile, acrylates and methacrylates, diene conjugates), an initiator (the most common are benzoyl peroxide (BPO) and 2,2'-azo-bis-isobutyronitrile (AIBN)) that is soluble in water and a surfactant. Initiation occurs when a monomer molecule that is stabilized by the surfactant contacts an initiator molecule which causes it to create free radicals and interact with the molecules of the other monomers and polymerization begins. The reaction continues until the monomer runs out. Phase separation and particle formation can occur before or at the end of the reaction. Nanoparticles with a size of around  $10^2$  nm (50-300 nm) are obtained [61–63].

- Surfactant-free emulsion polymerization

To eliminate the use of surfactants in conventional emulsion polymerization, surfactant-free polymerization has emerged. This is a simple and environmentally friendly process without the need for subsequent removal of surfactants. The ingredients used in this polymerization are water, an initiator (e.g., potassium persulfate, KPS) and monomers (usually vinyl or acrylic). Different nucleation mechanisms are proposed for the creation of polymer nanoparticles, such as homogeneous nucleation or micelle nucleation. The use of one or the other depends on the water solubility of the monomer [64–68]. Emulsion polymerizations differ from suspension polymerizations mainly in the size of the particles in which the reaction takes place (much smaller in emulsion).

- Micro-emulsion polymerization

This methodology is within the family of emulsion polymerizations. In this case, it differs from conventional emulsion polymerization due to its kinetics. In the case of conventional emulsion polymerization, there are three speed intervals while for the microemulsion only two are found. In general, smaller nanoparticles (10-30 nm) are obtained by this methodology. To carry out this method, a water-soluble initiator is needed, which is added to a stable aqueous phase containing swollen micelles. The polymerization is based on high amounts of surfactants that have an interfacial tension between the phases close to zero. In this case, the particles are coated with surfactant due to the high concentration of surfactant. In a first stage, the polymer chains are only formed in a few drops. Subsequently, due to the osmotic pressure of the chains, the microemulsions are destabilized and an increase in particle size is generated [69–72].

- Mini-emulsion polymerization

The difference with conventional emulsion polymerization lies in the use of a low molecular mass compound as a stabilizer and the use of a homogenizing device. Mini emulsions require a higher energy source in order to obtain a stable state. The necessary ingredients are an organic phase containing the initiator, an aqueous phase containing the surfactant and monomer and constant agitation. After agitation, a minimum size of nanoparticles is obtained (30-100 nm). The combinations of initiators and stabilizers are key to the nature of the nanoparticles [38,73–75].

- Interfacial polymerization

It is a widely used technique for the synthesis of polymer nanoparticles. In this case, the monomers are dispersed in two different phases (continuous phase and dispersed phase) and the reaction takes place at the interface of the two immiscible liquid phases. The most common monomers typically used in this polymerization are water-soluble diamines (such as piperazine and aromatic m-phenylenediamine) and



acid chloride monomers (such as trimesoyl chloride and isophthaloyl chloride) [76–79].

- Radical polymerization

The advantage of this methodology is the precision with which nanoparticles can be synthesized. Particle size, size distribution, particle functionalities and particle architecture can be controlled. In this case the polymerization takes place in a dispersed system, in particular in an emulsion polymerization whereby continuous addition of free radicals the polymerization takes place. There are different radical polymerization routes, such as atom transfer radical polymerization (ATRP) and reversible addition and fragmentation transfer chain polymerization (RAFT), among others [80–84]. The families of transfer agents most commonly used in RAFT polymerization are dithiobenzoates, trithiocarbonates, xanthan and dithiocaramate. Depending on the chain length of the polymers synthesized by this mechanism, different sizes of nanoparticles can be obtained, from nanometric to micrometric.

### **Top-down: post-polymerization**

The expression "top-down" means starting from a piece of a specific material and using mechanical or chemical processes to obtain the desired size and structure.

In this section we discussed the physical and chemical method for the fabrication of PNPs using preformed polymers as starting point. The methods could be subsequently applied after the chemical polymerization. Once obtain the polymer is necessary to create a dispersion to generate the nanoparticles. This section will only describe the main characteristics of each methodology how each methodology works [55,56].

- Spray Drying

This method is among the earliest technologies developed and is still considered to be one of the best methodologies for the preparation of NPs. It is a one-step production, making solid particles from the liquid phase, suitable for the manufacture of a wide range of powder with

controlled properties for application. A solution containing solvent and polymer as solute is transformed into a spray of small beads by atomization [85-88].

- Nanoprecipitation

Is based on the spontaneous precipitation of polymers in a non-solvent phase. It is also called as solvent displacement method. The basic principle of this techniques is based on the interfacial deposition of a polymer after displacement of a semipolar solvent, miscible with water, from a lipophilic solution. Polymer is mixed with intermediate polarity water-miscible organic solvent. Then, the solution is added drop by drop into the stirred aqueous phase under ambient condition. Then, the nanoparticles are collected by/on precipitation. The particle size has been regulated by the concentration of polymer, temperature, speed of stirring, rate of the injection on two phases and different kinds of solvents [89–94].

- Dialysis

Dialysis appears by the exploration of a surfactant-free nanoparticle system, which is effective for the fabrication of small and homogeneously distributed nanoparticles. For this purpose, the polymer dissolved in an organic solution is introduced into a dialysis bag with a given molecular weight cut-off. The displacement of the organic solvent by water inside the membrane leads to aggregation of the polymer due to the decrease of solubility in a different medium. In this case, the morphology and size of the nanoparticles are affected by the solvent used and the type of polymer [95–99].

- Salting out

This technique consists of two steps, in the first one the polymer is dissolved in an organic solvent that can be miscible with the aqueous solution. Subsequently the solution is emulsified in electrolytes such as magnesium chloride or calcium chloride and an aqueous solution containing a surfactant. The nanoparticles precipitate because the

organic solvent separates from the aqueous phase due to the influence of ions. The process is carried out with constant stirring which prevents the organic solvent from mixing with the aqueous solution because of salinity. Finally, the system is diluted with an excessive amount of water to increase the diffusion of the solvent in the aqueous solution, thus causing the nanoparticles to form. Its great advantage is that it does not require high temperatures, its disadvantage is the intensive washing required for the nanoparticles [100–104].

- Solvent evaporation

This method was the first used to obtain nanoparticles from a preformed dissolved polymer. In this method, the polymer is dissolved in an organic solvent with low boiling point to create an emulsion. To create the emulsion, an external energy source such as a homogenizer or ultrasound is needed, resulting in nanoparticles. Finally, to obtain the nanoparticles it is necessary to evaporate the solvent. It has been observed that the particle size is affected by the concentration of the polymer, the type of homogenizer and the stirring speed [105–109].

- Freeze-drying method

In this method the bulk polymer is dissolved in an organic solvent and completely frozen and crystals are obtained from the solution. Then the product is placed under high vacuum and the solvent is evaporated by sublimation. Finally, by evaporating the solvent under high vacuum, the polymer nanoparticles can be obtained and collected [110–113].

Depending on the requirements, it is feasible to choose the best production route and polymer type to produce nanoparticles with the preferred size range.

### **Applications of polymer nanoparticles**

The polymeric nanoparticles are used in several industrial sectors, as for example, biomedical, magnetic, catalytic, optoelectronic (Figure 1.9).

Each individual application of PNPs depends on the polymer composition of the nanoparticle. This composition depends on the inherent properties of the polymer which are influenced by the polymerization technique. In general, polymer nanoparticles possess very good structural and interfacial characteristics such as size, surface charge, shapes, porosity, swellability etc. which provides a wide range of potential applications [55,56].

The following is a brief summary of why they are used in some of the most studied applications to date.

- Biomedical application

Polymer nanoparticles have found their way into the broad field of medicine because they possess excellent chemical and physical properties compared to bulk materials. This is not the first time that nanomaterials have been used for medical applications, as inorganic and organic nanoparticles have already been used. Polymer nanoparticles, which are being further developed due to their highly valued properties such as cytotoxicity, biocompatibility and biodegradability, are used in applications such as bioimaging, controlled drug release and diagnostics among others [114–116].

- Magnetic application

Another field in which it has found a niche is in the field of magnetic nanomaterials. These nanomaterials can be used in different fields such as wastewater treatment, drug delivery, catalysis, nuclear magnetic resonance imaging, biosensors, etc. Polymer nanoparticles have great cavity in this sector because magnetic properties can be induced inside them [117–120].

- Catalytic application

With the idea always to obtain faster, less expensive, more efficient results and improve productivity, catalytic reactions appear. The search for new catalysts has been a hot topic in recent decades. Catalysts have been found that can be used in industry, which revalues their design. In order to improve the existing ones, polymer nanoparticles are part of this

challenge, in which polymer catalysts work because they can have different active sites where catalytic reactions take place. Thanks to the possibility of designing polymer nanoparticles, they have properties that make them advantageous over the rest, such as that they can be modified to give specific properties, they can be adjusted for different reactions, they are easy to recycle, and they could be easily separated by filtration [121–124].

- Optoelectronic application

Another field in which polymeric nanoparticles are used is for the manufacture of optoelectronic devices (fiber optics, laser diodes, smart TVs, cell phones, solar cells, etc.) due to their excellent electrical and optical properties. In this area, the focus is on conductive polymers, since they can be used in different parts of electronic circuits, giving them advantages such as light weight, durability, appearance and flexibility [125–129].

There is only a brief classification of possible applications of nanoparticles nevertheless there is a wide range of applications to be further developed and explored. Polymer nanoparticles can also be used as nanoparticles for self-healing materials, as construction materials, for 3D printing with magnetic properties, as polymer electrolytes, as future electrochemical devices, catalysts, luminescent markers, as anti-counterfeiting products, as flame retardant applications, and possibly as many other applications as we can imagine [130–134] (Figure 1.9).

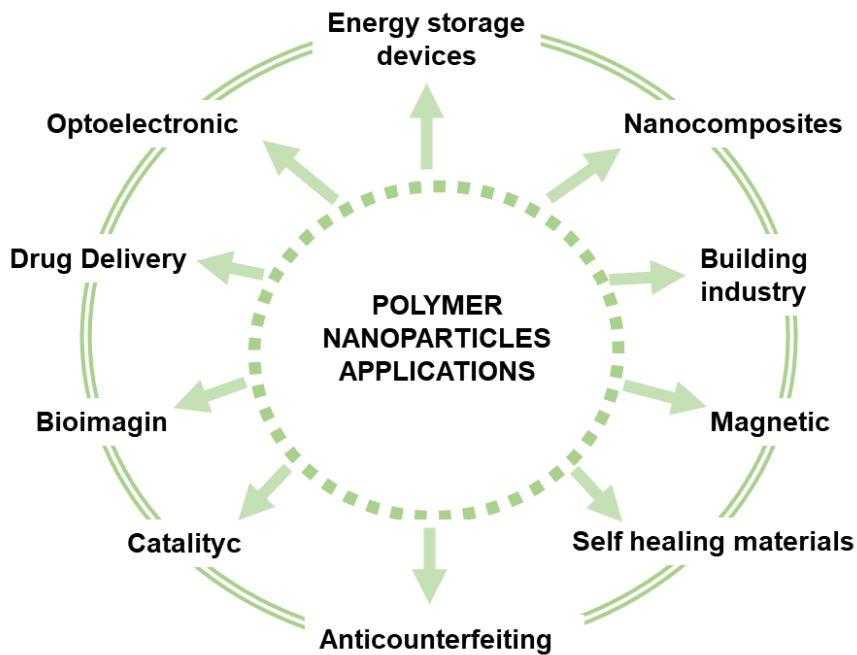


**Figure 1.9.** Applications of polymer nanoparticles

### **Closing remarks**

In the last decades, nanotechnology has already had an impact on industries such as consumer goods, weaponry, and medical treatments. This Chapter has discussed the current problems that our society has and how through nanotechnology may be able to solve some of the Sustainable Development Goals (SDGs).

As can be seen, nanotechnology has developed and is developing important advances in different sectors. Nanotechnology has the potential to improve or transform a wide range of sectors such as electronics, energy, environmental research, medicine, food production among others. Nanotechnology is poised to be a disruptive and far-reaching technology in the coming decades.

The combination of nanotechnology and polymer science can bring about a revolution in today's world if the knowledge and advantages of both are harnessed. With nanotechnology the polymer can be prepared at the nanometer scale and different optical, electrical, and magnetic properties interesting for different applications can be introduced.

In the search for information on the applications of polymer nanoparticles it is worth noting that most of them are focused on the medical sector, being applied to more sensitive diagnostic methods, therapy systems and controlled drug delivery systems. It can also be used as construction materials, raw materials for 3D printing, packaging materials, flame retardant materials, future electrochemical devices, anti-counterfeiting materials, among others.

The aim of this Thesis is to explore new synthesis routes towards polymer nanoparticles for use in potential applications, as well as to provide a deeper understanding of the basic properties of nano-objects. Disentangling the structure, stability and properties of nanoparticles is of major importance to establish a reliable structure-property relationship.

In this Thesis, three different syntheses for the preparation of polymeric nanoparticles are discussed. Detailed information on the morphology and chemical properties of the new nanoparticles is provided using a wide range of characterization techniques. In addition, proof-of-concept experiments on nanoparticles in applications such as energy storage and anti-counterfeiting are presented.

The Thesis manuscript is organized in two major sections. Section 1 presents two types of polymer nanoparticles for use as aqueous polyelectrolytes in redox flow batteries for energy storage. Section 2 presents a new polymer particle with interesting optical properties and its application in the field of anti-counterfeiting and circular economy. Finally, the conclusions of this Thesis are summarized in Chapter 6

Obtaining the desired properties of PNPs is related to their synthesis. Understanding the structure-property relationship can lead to improved capabilities across a spectrum of applications and the advancement of nanotechnology.

The polymer nanoparticles synthesized in this Ph.D. Thesis are made in order to cover other research fields in which they can be very useful and interesting.

1. Sustainable energy storage through chemical synthesis of polymer nanoparticles by different methodologies. The nanoparticles will be

stable in water and with redox properties to be used as aqueous polymer electrolytes for the production of redox flow batteries.

2. Anti-counterfeiting and traceability of goods products through the physical synthesis of polymer nanoparticles. The nanoparticles will be used to develop innovative anti-counterfeiting systems for cosmetics and perfumery sector.



---

---

## References

- [1] L. Pokrajac *et al.*, “Nanotechnology for a sustainable future: addressing global challenges with the International Network4Sustainable nanotechnology,” *ACS Nano*, vol. 15, no. 12, pp. 18608–18623, Dec. **2021**, doi: 10.1021/acsnano.1c10919.
- [2] M. C. Roco, “Environmentally responsible development of nanotechnology,” *Environ Sci Technol*, vol. 39, no. 5, pp. 106A-112A, Mar. **2005**, doi: 10.1021/es053199u.
- [3] M. S. Diallo, N. A. Fromer, and M. S. Jhon, “Nanotechnology for sustainable development: retrospective and outlook,” in *Nanotechnology for Sustainable Development*, Cham: Springer International Publishing, pp. 1–16, **2013**, doi: 10.1007/978-3-319-05041-6\_1.
- [4] P. A. Serena Domingo, “Buscando la sostenibilidad: el encaje de la nanotecnología,” *Encuentros multidisciplinares*, vol. 69, pp. 1–16, **2021**.
- [5] Feynman, Richard P. (1960) “There’s plenty of room at the bottom: An invitation to enter a new field of physics,” *Handbook of Nanoscience, Engineering, and Technology*, pp. 27–36, May **2007**, doi: 10.1201/9781420007848-8.
- [6] N. Taniguchi, “On the basic concept of nanotechnology,” in *Proceedings of the International Conference on Production Engineering*, pp. 18–23, **1974**.
- [7] J. M. A. M. Saba N, “*Nanoclay reinforced polymer composites*”. Singapore: Springer Singapore, **2016**. doi: 10.1007/978-981-10-0950-1.
- [8] S. Zeng, D. Baillargeat, H.-P. Ho, and K.-T. Yong, “Nanomaterials enhanced surface plasmon resonance for biological and chemical sensing applications,” *Chem Soc Rev*, vol. 43, no. 10, p. 3426, **2014**, doi: 10.1039/c3cs60479a.
- [9] P. Tiwari, K. Vig, V. Dennis, and S. Singh, “Functionalized gold nanoparticles and their biomedical applications,” *Nanomaterials*, vol. 1, no. 1, pp. 31–63, Jun. **2011**, doi: 10.3390/nano1010031.
- [10] J. Chomoucka, J. Drbohlavova, D. Huska, V. Adam, R. Kizek, and J. Hubalek, “Magnetic nanoparticles and targeted drug delivering,” *Pharmacol Res*, vol. 62, no. 2, pp. 144–149, Aug. **2010**, doi: 10.1016/j.phrs.2010.01.014.
- [11] E. Arici, N. S. Sariciftci, and D. Meissner, “Hybrid solar cells based on nanoparticles of CuInS<sub>2</sub> in organic matrices,” *Adv Funct Mater*, vol. 13, no. 2, pp. 165–171, Feb. **2003**, doi: 10.1002/adfm.200390024.
- [12] O. Salata, “Applications of nanoparticles in biology and medicine,” *J Nanobiotechnol*, vol. 2, no. 1, p. 3, **2004**, doi: 10.1186/1477-3155-2-3.

- [13] E. S. Papazoglou and A. Parthasarathy, "BioNanotechnology," *Synthesis Lectures on Biomedical Engineering*, vol. 2, no. 1, pp. 1–139, Jan. **2007**, doi: 10.2200/S00051ED1V01Y200610BME007.
- [14] V. G. Jesus M. de la Fuente, Nanobiotechnology: Inorganic nanoparticles vs Organic nanoparticles, *Frontiers of Nanoscience*, vol. 4. **2012**.
- [15] F. J. Heiligtag and M. Niederberger, "The fascinating world of nanoparticle research," *Materials Today*, vol. 16, no. 7–8, pp. 262–271, Jul. **2013**, doi: 10.1016/j.mattod.2013.07.004.
- [16] R. A. Sperling and W. J. Parak, "Surface modification, functionalization and bioconjugation of colloidal inorganic nanoparticles," *Phil. Trans. R. Soc. A.*, vol. 368, no. 1915, pp. 1333–1383, Mar. **2010**, doi: 10.1098/rsta.2009.0273.
- [17] K.-T. Yong *et al.*, "Preparation of quantum dot/drug nanoparticle formulations for traceable targeted delivery and therapy," *Theranostics*, vol. 2, no. 7, pp. 681–694, **2012**, doi: 10.7150/thno.3692.
- [18] V. Bagalkot *et al.*, "Quantum dot–aptamer conjugates for synchronous cancer imaging, therapy, and sensing of drug delivery based on bi-fluorescence resonance energy transfer," *Nano Lett*, vol. 7, no. 10, pp. 3065–3070, Oct. **2007**, doi: 10.1021/nl071546n.
- [19] S. M. Ng, M. Koneswaran, and R. Narayanaswamy, "A review on fluorescent inorganic nanoparticles for optical sensing applications," *RSC Adv*, vol. 6, no. 26, pp. 21624–21661, **2016**, doi: 10.1039/C5RA24987B.
- [20] I. Khan, K. Saeed, and I. Khan, "Nanoparticles: Properties, applications and toxicities," *Arab. J. Chem*, vol. 12, no. 7, pp. 908–931, Nov. **2019**, doi: 10.1016/j.arabjc.2017.05.011.
- [21] F. Alexis, E. Pridgen, L. K. Molnar, and O. C. Farokhzad, "Factors affecting the clearance and biodistribution of polymeric nanoparticles," *Mol Pharm*, vol. 5, no. 4, pp. 505–515, Aug. **2008**, doi: 10.1021/mp800051m.
- [22] N. Engelhardt, A. Ernst, A.-L. Kampmann, and R. Weberskirch, "Synthesis and characterization of surface functional polymer nanoparticles by a bottom-up approach from tailor-made amphiphilic block copolymers," *Macromol Chem Phys*, vol. 214, no. 24, pp. 2783–2791, Dec. **2013**, doi: 10.1002/macp.201300573.
- [23] Y. Dong, "Nanostructures: properties, production methods and applications", *1st ed. New York, USA: Nova Science Publishers, Inc.*, **2013**.
- [24] G. Paramasivam, V. V. Palem, T. Sundaram, V. Sundaram, S. C. Kishore, and S. Bellucci, "Nanomaterials: synthesis and applications in theranostics," *Nanomaterials*, vol. 11, no. 12, p. 3228, Nov. **2021**, doi: 10.3390/nano11123228.

- [25] T. Kitao, X. Zhang, and T. Uemura, "Nanoconfined synthesis of conjugated ladder polymers," *Polym Chem*, vol. 13, no. 35, pp. 5003–5018, **2022**, doi: 10.1039/D2PY00809B.
- [26] H. Eslami, F. Mehdipour, A. Setoodeh, and J. Rouzegar, "Nanoconfined polymers: modelling and simulation approaches," *Mol Simul*, vol. 41, no. 5–6, pp. 367–381, Apr. **2015**, doi: 10.1080/08927022.2014.954573.
- [27] X. Y. Lu, D. C. Wu, Z. J. Li, and G. Q. Chen, "Polymer nanoparticles," in *Prog Mol Biol Transl Sci.*, vol. 104, Elsevier B.V., pp. 299–323, **2011**. doi: 10.1016/B978-0-12-416020-0.00007-3.
- [28] N. Engelhardt, A. Ernst, A.-L. Kampmann, and R. Weberskirch, "Synthesis and characterization of surface functional polymer nanoparticles by a bottom-up approach from tailor-made amphiphilic block copolymers," *Macromol Chem Phys*, vol. 214, no. 24, pp. 2783–2791, Dec. **2013**, doi: 10.1002/macp.201300573.
- [29] L. S. Schadler, S. K. Kumar, B. C. Benicewicz, S. L. Lewis, and S. E. Harton, "Designed interfaces in polymer nanocomposites: a fundamental viewpoint," *MRS Bull*, vol. 32, no. 4, pp. 335–340, Apr. **2007**, doi: 10.1557/mrs2007.232.
- [30] T. Chen and P. Somasundaran, "Preparation of novel core-shell nanocomposite particles by controlled polymer bridging," *J. Am. Ceram. Soc.*, vol. 81, no. 1, pp. 140–144, Jan. **2005**, doi: 10.1111/j.1151-2916.1998.tb02305.x.
- [31] D. Gentili and G. Ori, "Reversible assembly of nanoparticles: theory, strategies and computational simulations," *Nanoscale*, vol. 14, no. 39, pp. 14385–14432, **2022**, doi: 10.1039/D2NR02640F.
- [32] S. Mourdikoudis, R. M. Pallares, and N. T. K. Thanh, "Characterization techniques for nanoparticles: comparison and complementarity upon studying nanoparticle properties," *Nanoscale*, vol. 10, no. 27, pp. 12871–12934, **2018**, doi: 10.1039/C8NR02278J.
- [33] N. Joudeh and D. Linke, "Nanoparticle classification, physicochemical properties, characterization, and applications: a comprehensive review for biologists," *J Nanobiotechnol*, vol. 20, no. 1, p. 262, Dec. **2022**, doi: 10.1186/s12951-022-01477-8.
- [34] D. Vollath, F. D. Fischer, and D. Holec, "Surface energy of nanoparticles – influence of particle size and structure," *Beilstein J. Nanotechnol.*, vol. 9, pp. 2265–2276, Aug. **2018**, doi: 10.3762/bjnano.9.211.
- [35] B. Molleman and T. Hiemstra, "Size and shape dependency of the surface energy of metallic nanoparticles: unifying the atomic and

thermodynamic approaches,” *Phys. Chem. Chem. Phys.*, vol. 20, no. 31, pp. 20575–20587, **2018**, doi: 10.1039/C8CP02346H.

[36] N. T. K. Thanh, N. Maclean, and S. Mahiddine, “Mechanisms of nucleation and growth of nanoparticles in solution,” *Chem Rev*, vol. 114, no. 15, pp. 7610–7630, Aug. **2014**, doi: 10.1021/cr400544s.

[37] M. H. N. Famili, H. Janani, and M. S. Enayati, “Foaming of a polymer-nanoparticle system: Effect of the particle properties,” *J Appl Polym Sci*, vol. 119, no. 5, pp. 2847–2856, Mar. **2011**, doi: 10.1002/app.32969.

[38] A. Gharieh, S. Khoee, and A. R. Mahdavian, “Emulsion and miniemulsion techniques in preparation of polymer nanoparticles with versatile characteristics,” *Adv Colloid Interface Sci*, vol. 269, pp. 152–186, Jul. **2019**, doi: 10.1016/j.cis.2019.04.010.

[39] R. Ridolfo, S. Tavakoli, V. Junnuthula, D. S. Williams, A. Urtti, and J. C. M. van Hest, “Exploring the impact of morphology on the properties of biodegradable nanoparticles and their diffusion in complex biological medium,” *Biomacromolecules*, vol. 22, no. 1, pp. 126–133, Jan. **2021**, doi: 10.1021/acs.biomac.0c00726.

[40] A. Gagliardi *et al.*, “Biodegradable polymeric nanoparticles for drug delivery to solid tumors,” *Front Pharmacol*, vol. 12, Feb. **2021**, doi: 10.3389/fphar.2021.601626.

[41] Z. W. Huang *et al.*, “New functional degradable and bio-compatible nanoparticles based on poly(malic acid) derivatives for site-specific anti-cancer drug delivery,” *Int J Pharm*, vol. 423, no. 1, pp. 84–92, Feb. **2012**, doi: 10.1016/j.ijpharm.2011.04.035.

[42] N. Welsch, Y. Lu, J. Dzubiella, and M. Ballauff, “Adsorption of proteins to functional polymeric nanoparticles,” *Polymer*, vol. 54, no. 12, pp. 2835–2849, May **2013**, doi: 10.1016/j.polymer.2013.03.027.

[43] H. Yang, F. Liang, Y. Chen, Q. Wang, X. Qu, and Z. Yang, “Lotus leaf inspired robust superhydrophobic coating from strawberry-like Janus particles,” *NPG Asia Mater*, vol. 7, no. 4, pp. e176–e176, Apr. **2015**, doi: 10.1038/am.2015.33.

[44] S. Li *et al.*, “Preparation and characterization of porous titania-grafted poly(styrene-divinylbenzene)/maleic anhydride nanocomposite microspheres,” *Sci China Chem*, vol. 53, no. 3, pp. 605–611, Mar. **2010**, doi: 10.1007/s11426-009-0175-z.

[45] C. Vauthier and K. Bouchemal, “Methods for the preparation and manufacture of polymeric nanoparticles,” *Pharm Res*, vol. 26, no. 5, pp. 1025–1058, May **2009**, doi: 10.1007/s11095-008-9800-3.

- [46] S. Dai, P. Ravi, and K. C. Tam, "pH-Responsive polymers: synthesis, properties and applications," *Soft Matter*, vol. 4, no. 3, p. 435, **2008**, doi: 10.1039/b714741d.
- [47] M. H. Reis, F. A. Leibfarth, and L. M. Pitet, "Polymerizations in continuous flow: recent advances in the synthesis of diverse polymeric materials," *ACS Macro Lett*, vol. 9, no. 1, pp. 123–133, Jan. **2020**, doi: 10.1021/acsmacrolett.9b00933.
- [48] C. I. C. Crucho and M. T. Barros, "Polymeric nanoparticles: A study on the preparation variables and characterization methods," *Materials Science and Engineering: C*, vol. 80, pp. 771–784, Nov. **2017**, doi: 10.1016/j.msec.2017.06.004.
- [49] D. Sharma, S. Kanchi, K. Bisetty, and V. N. Nuthalapati, "CHAPTER 1. Perspective on analytical sciences and nanotechnology," pp. 1–34, **2016**, doi: 10.1039/9781782623625-00001.
- [50] X. Chen and J. Li, "Bioinspired by cell membranes: functional polymeric materials for biomedical applications," *Mater Chem Front*, vol. 4, no. 3, pp. 750–774, **2020**, doi: 10.1039/C9QM00717B.
- [51] X. Liu, Y. Yang, and M. W. Urban, "Stimuli-responsive polymeric nanoparticles," *Macromol Rapid Commun*, vol. 38, no. 13, p. 1700030, Jul. **2017**, doi: 10.1002/marc.201700030.
- [52] S. Sacanna *et al.*, "Shaping colloids for self-assembly," *Nat Commun*, vol. 4, no. 1, p. 1688, Jun. **2013**, doi: 10.1038/ncomms2694.
- [53] J. Biener, A. Wittstock, T. Baumann, J. Weissmüller, M. Bäumer, and A. Hamza, "Surface chemistry in nanoscale materials," *Materials*, vol. 2, no. 4, pp. 2404–2428, Dec. **2009**, doi: 10.3390/ma2042404.
- [54] C. Dannert, B. T. Stokke, and R. S. Dias, "Nanoparticle-hydrogel composites: from molecular interactions to macroscopic behavior," *Polymers*, vol. 11, no. 2, p. 275, Feb. **2019**, doi: 10.3390/polym11020275.
- [55] C. Adhikari, "Polymer nanoparticles-preparations, applications and future insights: a concise review," *Polym-Plast. Tech. Mat.*, pp. 1–29, Jul. **2021**, doi: 10.1080/25740881.2021.1939715.
- [56] A. Nasir, A. Kausar, and A. Younus, "A review on preparation, properties and applications of polymeric nanoparticle-based materials," *Polym-Plast. Tech. Eng.*, vol. 54, no. 4, pp. 325–341, Mar. **2015**, doi: 10.1080/03602559.2014.958780.
- [57] J. Pecher and S. Mecking, "Nanoparticles of conjugated polymers," *Chem Rev*, vol. 110, no. 10, pp. 6260–6279, Oct. **2010**, doi: 10.1021/cr100132y.

- [58] C. Zhang, Y. Guo, and R. D. Priestley, "Confined glassy properties of polymer nanoparticles," *J Polym Sci B Polym Phys*, vol. 51, no. 7, pp. 574–586, Apr. **2013**, doi: 10.1002/polb.23268.
- [59] L. A. Renna, C. J. Boyle, T. S. Gehan, and D. Venkataraman, "Polymer nanoparticle assemblies: a versatile route to functional mesostructures," *Macromolecules*, vol. 48, no. 18, pp. 6353–6368, Sep. **2015**, doi: 10.1021/acs.macromol.5b00375.
- [60] T. Pulingam, P. Foroozandeh, J.-A. Chuah, and K. Sudesh, "Exploring various techniques for the chemical and biological synthesis of polymeric nanoparticles," *Nanomaterials*, vol. 12, no. 3, p. 576, Feb. **2022**, doi: 10.3390/nano12030576.
- [61] P. A. Lovell and F. J. Schork, "Fundamentals of emulsion polymerization," *Biomacromolecules*, vol. 21, no. 11, pp. 4396–4441, Nov. **2020**, doi: 10.1021/acs.biomac.0c00769.
- [62] S. Sahoo *et al.*, "Preparation of polymeric nanomaterials using emulsion polymerization," *Adv. Mater. Sci. Eng.*, vol. 2021, pp. 1–9, Oct. **2021**, doi: 10.1155/2021/1539230.
- [63] D. Blenner, J. Stubbs, and D. Sundberg, "Multi-lobed composite polymer nanoparticles prepared by conventional emulsion polymerization," *Polymer*, vol. 114, pp. 54–63, Apr. **2017**, doi: 10.1016/j.polymer.2017.02.080.
- [64] K. Li, L. Xie, B. Wang, J. Yan, H. Tang, and D. Zhou, "Mechanistic investigation of surfactant-free emulsion polymerization using magnetite nanoparticles modified by citric acid as stabilizers," *Langmuir*, vol. 36, no. 28, pp. 8290–8300, Jul. **2020**, doi: 10.1021/acs.langmuir.0c01493.
- [65] M. Egen and R. Zentel, "Surfactant-free emulsion polymerization of various methacrylates: towards monodisperse colloids for polymer opals," *Macromol Chem Phys*, vol. 205, no. 11, pp. 1479–1488, Jul. **2004**, doi: 10.1002/macp.200400087.
- [66] S. T. Camli, F. Buyukserin, O. Balci, and G. G. Budak, "Size controlled synthesis of sub-100nm monodisperse poly(methylmethacrylate) nanoparticles using surfactant-free emulsion polymerization," *J Colloid Interface Sci*, vol. 344, no. 2, pp. 528–532, Apr. **2010**, doi: 10.1016/j.jcis.2010.01.041.
- [67] Y. Zhao, J. Liu, Z. Chen, X. Zhu, and M. Möller, "Hybrid nanostructured particles via surfactant-free double miniemulsion polymerization," *Nat Commun*, vol. 9, no. 1, p. 1918, Dec. **2018**, doi: 10.1038/s41467-018-04320-7.
- [68] B. T. T. Pham, C. H. Such, and B. S. Hawkett, "Synthesis of polymeric janus nanoparticles and their application in surfactant-free emulsion polymerizations," *Polym Chem*, vol. 6, no. 3, pp. 426–435, **2015**, doi: 10.1039/C4PY01125B.

- [69] G. L. Rempel and H. Wang, "Microemulsion polymerization," in *Encyclopedia of Polymeric Nanomaterials*, Berlin, Heidelberg: Springer Berlin Heidelberg, pp. 1241–1250, **2015**, doi: 10.1007/978-3-642-29648-2\_262.
- [70] X.-J. Xu and L. M. Gan, "Recent advances in the synthesis of nanoparticles of polymer latexes with high polymer-to-surfactant ratios by microemulsion polymerization," *Curr Opin Colloid Interface Sci*, vol. 10, no. 5–6, pp. 239–244, Dec. **2005**, doi: 10.1016/j.cocis.2005.09.002.
- [71] R. Kanwar, J. Rathee, M. Tanaji Patil, and S. Kumar Mehta, "Microemulsions as nanotemplates: a soft and versatile approach," in *Microemulsion - a Chemical Nanoreactor*, IntechOpen, **2018**. doi: 10.5772/intechopen.80758.
- [72] L. Ren, "Electrode materials based on micro-emulsion polymerized polyaniline and their capacitive property," *Int J Electrochem Sci*, pp. 238–249, Jan. **2019**, doi: 10.20964/2019.01.10.
- [73] A. de San Luis, M. Kleinsteuber, T. Schuett, S. Schubert, and U. S. Schubert, "Miniemulsion polymerization at low temperature: A strategy for one-pot encapsulation of hydrophobic anti-inflammatory drugs into polyester-containing nanoparticles," *J Colloid Interface Sci*, vol. 612, pp. 628–638, Apr. **2022**, doi: 10.1016/j.jcis.2021.12.189.
- [74] K. Landfester, "Miniemulsion polymerization and the structure of polymer and hybrid nanoparticles," *Angew Chem Int Ed*, vol. 48, no. 25, pp. 4488–4507, Jun. **2009**, doi: 10.1002/anie.200900723.
- [75] J. M. Asua, "Miniemulsion polymerization," in *Encyclopedia of Polymeric Nanomaterials*, Berlin, Heidelberg: Springer Berlin Heidelberg, **2015**, pp. 1267–1275. doi: 10.1007/978-3-642-29648-2\_263.
- [76] G. P. Syed Ibrahim, A. M. Isloor, M. Bavarian, and S. Nejati, "Integration of zwitterionic polymer nanoparticles in interfacial polymerization for ion separation," *ACS Appl Polym Mater*, vol. 2, no. 4, pp. 1508–1517, Apr. **2020**, doi: 10.1021/acsapm.9b01192.
- [77] S. S. Guterres, M. P. Alves, and A. R. Pohlmann, "Polymeric nanoparticles, nanospheres and nanocapsules, for cutaneous applications," *Drug Target Insights*, vol. 2, p. 117739280700200, Jan. **2007**, doi: 10.1177/117739280700200002.
- [78] G. S. Lai, W. J. Lau, P. S. Goh, Y. H. Tan, B. C. Ng, and A. F. Ismail, "A novel interfacial polymerization approach towards synthesis of graphene oxide-incorporated thin film nanocomposite membrane with improved surface properties," *Arab J Chem*, vol. 12, no. 1, pp. 75–87, Jan. **2019**, doi: 10.1016/j.arabjc.2017.12.009.

- [79] H.-J. Krause, A. Schwarz, and P. Rohdewald, "Interfacial polymerization, a useful method for the preparation of polymethylcyanoacrylate nanoparticles," *Drug Dev Ind Pharm*, vol. 12, no. 4, pp. 527–552, Jan. **1986**, doi: 10.3109/03639048609048026.
- [80] M. J. Monteiro and M. F. Cunningham, "Polymer nanoparticles via living radical polymerization in aqueous dispersions: design and applications," *Macromolecules*, vol. 45, no. 12, pp. 4939–4957, Jun. **2012**, doi: 10.1021/ma300170c.
- [81] T. von Werne and T. E. Patten, "Atom transfer radical polymerization from nanoparticles: a tool for the preparation of well-defined hybrid nanostructures and for understanding the chemistry of controlled/'living' radical polymerizations from surfaces," *J Am Chem Soc*, vol. 123, no. 31, pp. 7497–7505, Aug. **2001**, doi: 10.1021/ja010235q.
- [82] W.-T. Chang *et al.*, "Synthesis of polystyrene living nanoparticles (LNPs) in water *via* nano-confined free radical polymerization," *Polym Chem*, vol. 11, no. 46, pp. 7349–7353, **2020**, doi: 10.1039/D0PY01300E.
- [83] Y. Wang and K. Matyjaszewski, "Hairy nanoparticles by atom transfer radical polymerization in miniemulsion," *React Funct Polym*, vol. 170, p. 105104, Jan. **2022**, doi: 10.1016/j.reactfunctpolym.2021.105104.
- [84] N. You *et al.*, "Facile fabrication of size-tunable core/shell ferroelectric/polymeric nanoparticles with tailorable dielectric properties via organocatalyzed atom transfer radical polymerization driven by visible light," *Sci Rep*, vol. 9, no. 1, p. 1869, Dec. **2019**, doi: 10.1038/s41598-018-38039-8.
- [85] C. Arpagaus, "PLA/PLGA nanoparticles prepared by nano spray drying," *J Pharm Investig*, vol. 49, no. 4, pp. 405–426, Jul. **2019**, doi: 10.1007/s40005-019-00441-3.
- [86] S. S. Guterres, R. C. R. Beck, and A. R. Pohlmann, "Spray-drying technique to prepare innovative nanoparticulated formulations for drug administration: a brief overview," *Brazilian J Phys*, vol. 39, no. 1a, pp. 205–209, Apr. **2009**, doi: 10.1590/S0103-97332009000200013.
- [87] R. C.R. Beck, A. F. Ourique, S. S. Guterres, and A. R. Pohlmann, "Spray-dried polymeric nanoparticles for pharmaceuticals: a review of patents," *Recent Pat Drug Deliv Formul*, vol. 6, no. 3, pp. 195–208, Aug. **2012**, doi: 10.2174/187221112802652651.
- [88] X. Li, N. Anton, C. Arpagaus, F. Belleiteix, and T. F. Vandamme, "Nanoparticles by spray drying using innovative new technology: The Büchi Nano Spray Dryer B-90," *J Control Release*, vol. 147, no. 2, pp. 304–310, Oct. **2010**, doi: 10.1016/j.jconrel.2010.07.113.



- [89] S. Hornig, T. Heinze, C. R. Becer, and U. S. Schubert, "Synthetic polymeric nanoparticles by nanoprecipitation," *J Mater Chem*, vol. 19, no. 23, p. 3838, **2009**, doi: 10.1039/b906556n.
- [90] P. R. Vuddanda, A. Mishra, S. K. Singh, and S. Singh, "Development of polymeric nanoparticles with highly entrapped herbal hydrophilic drug using nanoprecipitation technique: an approach of quality by design," *Pharm Dev Technol*, vol. 20, no. 5, pp. 579–587, Jul. **2015**, doi: 10.3109/10837450.2014.908302.
- [91] M. Beck-Broichsitter, "Solvent impact on polymer nanoparticles prepared nanoprecipitation," *Colloids Surf A Physicochem Eng Asp*, vol. 625, p. 126928, Sep. **2021**, doi: 10.1016/j.colsurfa.2021.126928.
- [92] Y. Liu *et al.*, "Stable polymer nanoparticles with exceptionally high drug loading by sequential nanoprecipitation," *Angewandte Chemie*, vol. 132, no. 12, pp. 4750–4758, Mar. **2020**, doi: 10.1002/ange.201913539.
- [93] X. Yan, J. Bernard, and F. Ganachaud, "Nanoprecipitation as a simple and straightforward process to create complex polymeric colloidal morphologies," *Adv Colloid Interface Sci*, vol. 294, p. 102474, Aug. **2021**, doi: 10.1016/j.cis.2021.102474.
- [94] S. Schubert, J. J. T. Delaney, and U. S. Schubert, "Nanoprecipitation and nanoformulation of polymers: from history to powerful possibilities beyond poly(lactic acid)," *Soft Matter*, vol. 7, no. 5, pp. 1581–1588, **2011**, doi: 10.1039/C0SM00862A.
- [95] C. Errico, C. Bartoli, F. Chiellini, and E. Chiellini, "Poly(hydroxyalkanoates)-based polymeric nanoparticles for drug delivery," *J Biomed Biotechnol*, vol. **2009**, pp. 1–10, 2009, doi: 10.1155/2009/571702.
- [96] L. Chronopoulou, I. Fratoddi, C. Palocci, I. Venditti, and M. v. Russo, "Osmosis based method drives the self-assembly of polymeric chains into micro- and nanostructures," *Langmuir*, vol. 25, no. 19, pp. 11940–11946, Oct. **2009**, doi: 10.1021/la9016382.
- [97] M. Maraldi, R. Ferrari, R. Auriemma, M. Sponchioni, and D. Moscatelli, "Concentration of polymer nanoparticles through dialysis: efficacy and comparison with lyophilization for pegylated and zwitterionic systems," *J Pharm Sci*, vol. 109, no. 8, pp. 2607–2614, Aug. **2020**, doi: 10.1016/j.xphs.2020.05.001.
- [98] J. Xie and C.-H. Wang, "Self-assembled biodegradable nanoparticles developed by direct dialysis for the delivery of paclitaxel," *Pharm Res*, vol. 22, no. 12, pp. 2079–2090, Dec. **2005**, doi: 10.1007/s11095-005-7782-y.

- [99] M. Lievonen *et al.*, “A simple process for lignin nanoparticle preparation,” *Green Chemistry*, vol. 18, no. 5, pp. 1416–1422, **2016**, doi: 10.1039/C5GC01436K.
- [100] S. R. Jitta and L. Kumar, “Salting out and ionic gelation manufacturing techniques for nanoparticles,” in *Emerging Technologies for Nanoparticle Manufacturing*, Cham: Springer International Publishing, **2021**, pp. 129–165. doi: 10.1007/978-3-030-50703-9\_7.
- [101] H. Ibrahim, C. Bindschaedler, E. Doelker, P. Buri, and R. Gurny, “Aqueous nanodispersions prepared by a salting-out process,” *Int J Pharm*, vol. 87, no. 1–3, pp. 239–246, Nov. **1992**, doi: 10.1016/0378-5173(92)90248-Z.
- [102] S. Galindo-Rodriguez, E. Allémann, H. Fessi, and E. Doelker, “Physicochemical parameters associated with nanoparticle formation in the salting-out, emulsification-diffusion, and nanoprecipitation methods,” *Pharm Res*, vol. 21, no. 8, pp. 1428–1439, Aug. **2004**, doi: 10.1023/B:PHAM.0000036917.75634.be.
- [103] E. Allémann, J. Leroux, R. Gurny, and E. Doelker, “In vitro extended-release properties of drug-loaded poly(DL-lactic acid) nanoparticles produced by a salting-out procedure,” *Pharm Res*, vol. 10, no. 12, pp. 1732–1737, **1993**, doi: 10.1023/A:1018970030327.
- [104] N. Mendoza-Munoz, D. Quintanar-Guerrero, and E. Allemann, “The impact of the salting-out technique on the preparation of colloidal particulate systems for pharmaceutical applications,” *Recent Pat Drug Deliv Formul*, vol. 6, no. 3, pp. 236–249, Aug. **2012**, doi: 10.2174/187221112802652688.
- [105] H. Yabu, T. Higuchi, K. Ijiro, and M. Shimomura, “Spontaneous formation of polymer nanoparticles by good-solvent evaporation as a nonequilibrium process,” *Chaos: An Interdisciplinary Journal of Nonlinear Science*, vol. 15, no. 4, p. 047505, Dec. **2005**, doi: 10.1063/1.2137621.
- [106] E. Pinon-Segundo, M. G. Nava-Arzaluz, and D. Lechuga-Ballesteros, “Pharmaceutical polymeric nanoparticles prepared by the double emulsion-solvent evaporation technique,” *Recent Pat Drug Deliv Formul*, vol. 6, no. 3, pp. 224–235, Aug. **2012**, doi: 10.2174/187221112802652606.
- [107] N. Mendoza-Muñoz, S. Alcalá-Alcalá, and D. Quintanar-Guerrero, “Preparation of polymer nanoparticles by the emulsification-solvent evaporation method: from vanderhoff’s pioneer approach to recent adaptations,” in *Polymer Nanoparticles for Nanomedicines*, Cham: Springer International Publishing, **2016**, pp. 87–121. doi: 10.1007/978-3-319-41421-8\_4.
- [108] L. T. M. Hoa, N. T. Chi, L. H. Nguyen, and D. M. Chien, “Preparation and characterization of nanoparticles containing ketoprofen and acrylic polymers

---

prepared by emulsion solvent evaporation method,” *J Exp Nanosci*, vol. 7, no. 2, pp. 189–197, Mar. **2012**, doi: 10.1080/17458080.2010.515247.

[109] S. Desgouilles *et al.*, “The design of nanoparticles obtained by solvent evaporation: a comprehensive study,” *Langmuir*, vol. 19, no. 22, pp. 9504–9510, Oct. **2003**, doi: 10.1021/la034999q.

[110] F. Hassouna *et al.*, “Multi-scale analysis of amorphous solid dispersions prepared by freeze drying of ibuprofen loaded acrylic polymer nanoparticles,” *J Drug Deliv Sci Technol*, vol. 53, p. 101182, Oct. **2019**, doi: 10.1016/j.jddst.2019.101182.

[111] M. E. Ali and A. Lamprecht, “Spray freeze drying as an alternative technique for lyophilization of polymeric and lipid-based nanoparticles,” *Int J Pharm*, vol. 516, no. 1–2, pp. 170–177, Jan. **2017**, doi: 10.1016/j.ijpharm.2016.11.023.

[112] G. R. Ramos Yacasi, A. C. Calpena Campmany, M. A. Egea Gras, M. Espina García, and M. L. García López, “Freeze drying optimization of polymeric nanoparticles for ocular flurbiprofen delivery: effect of protectant agents and critical process parameters on long-term stability,” *Drug Dev Ind Pharm*, vol. 43, no. 4, pp. 637–651, Apr. **2017**, doi: 10.1080/03639045.2016.1275669.

[113] P. Fonte, S. Reis, and B. Sarmiento, “Facts and evidences on the lyophilization of polymeric nanoparticles for drug delivery,” *Journal of Controlled Release*, vol. 225, pp. 75–86, Mar. **2016**, doi: 10.1016/j.jconrel.2016.01.034.

[114] A. Fabozzi, F. della Sala, M. di Gennaro, N. Solimando, M. Pagliuca, and A. Borzacchiello, “Polymer based nanoparticles for biomedical applications by microfluidic techniques: from design to biological evaluation,” *Polym Chem*, vol. 12, no. 46, pp. 6667–6687, **2021**, doi: 10.1039/D1PY01077H.

[115] B. Shkodra-Pula, A. Vollrath, U. S. Schubert, and S. Schubert, “Polymer-based nanoparticles for biomedical applications,” **2020**, pp. 233–252. doi: 10.1016/B978-0-08-102828-5.00009-7.

[116] A. Karabasz, M. Bzowska, and K. Szczepanowicz, “Biomedical applications of multifunctional polymeric nanocarriers: a review of current literature,” *Int J Nanomedicine*, vol. Volume 15, pp. 8673–8696, Nov. **2020**, doi: 10.2147/IJN.S231477.

[117] Y. Li *et al.*, “Polymer-assisted magnetic nanoparticle assemblies for biomedical applications,” *ACS Appl Bio Mater*, vol. 3, no. 1, pp. 121–142, Jan. **2020**, doi: 10.1021/acsabm.9b00896.

[118] F. Sharifianjazi *et al.*, “Polymer incorporated magnetic nanoparticles: Applications for magnetoresponsive targeted drug delivery,” *Mater Sci Eng B*, vol. 272, p. 115358, Oct. **2021**, doi: 10.1016/j.mseb.2021.115358.

- [119] Q. Lu, K. Choi, J.-D. Nam, and H. J. Choi, "Magnetic Polymer Composite Particles: Design and Magnetorheology," *Polymers*, vol. 13, no. 4, p. 512, Feb. **2021**, doi: 10.3390/polym13040512.
- [120] D. Alromi, S. Madani, and A. Seifalian, "Emerging application of magnetic nanoparticles for diagnosis and treatment of cancer," *Polymers*, vol. 13, no. 23, p. 4146, Nov. **2021**, doi: 10.3390/polym13234146.
- [121] R. Rajan *et al.*, "Polymeric nanoparticles in hybrid catalytic processing and drug delivery system," *Top Catal*, Sep. **2022**, doi: 10.1007/s11244-022-01697-0.
- [122] Y. Liu *et al.*, "Catalytically active single-chain polymeric nanoparticles: exploring their functions in complex biological media," *J Am Chem Soc*, vol. 140, no. 9, pp. 3423–3433, Mar. **2018**, doi: 10.1021/jacs.8b00122.
- [123] Y. Liu *et al.*, "Catalytic single-chain polymeric nanoparticles at work: from ensemble towards single-particle kinetics," *Mol Syst Des Eng*, vol. 3, no. 4, pp. 609–618, **2018**, doi: 10.1039/C8ME00017D.
- [124] J. Rubio-Cervilla, E. González, and J. Pomposo, "Advances in single-chain nanoparticles for catalysis applications," *Nanomaterials*, vol. 7, no. 10, p. 341, Oct. **2017**, doi: 10.3390/nano7100341.
- [125] N. K. Kwon, T. K. Lee, S. K. Kwak, and S. Y. Kim, "Aggregation-driven controllable plasmonic transition of silica-coated gold nanoparticles with temperature-dependent polymer–nanoparticle interactions for potential applications in optoelectronic devices," *ACS Appl Mater Interfaces*, vol. 9, no. 45, pp. 39688–39698, Nov. **2017**, doi: 10.1021/acsami.7b13123.
- [126] G. Moad, M. Chen, M. Häussler, A. Postma, E. Rizzardo, and S. H. Thang, "Functional polymers for optoelectronic applications by RAFT polymerization," *Polym. Chem.*, vol. 2, no. 3, pp. 492–519, **2011**, doi: 10.1039/C0PY00179A.
- [127] A. J. Kadham, D. Hassan, N. Mohammad, and A. H. Ah-yasari, "Fabrication of (polymer blend-magnesium oxide) nanoparticle and studying their optical properties for optoelectronic applications," *Bull. Electr. Eng. Inform.*, vol. 7, no. 1, pp. 28–34, Mar. **2018**, doi: 10.11591/eei.v7i1.839.
- [128] N. Maity, R. Ghosh, and A. K. Nandi, "Optoelectronic properties of self-assembled nanostructures of polymer functionalized polythiophene and graphene," *Langmuir*, vol. 34, no. 26, pp. 7585–7597, Jul. **2018**, doi: 10.1021/acs.langmuir.7b04387.
- [129] S. Li, M. Meng Lin, M. S. Toprak, D. K. Kim, and M. Muhammed, "Nanocomposites of polymer and inorganic nanoparticles for optical and magnetic applications," *Nano Rev*, vol. 1, no. 1, p. 5214, Jan. **2010**, doi: 10.3402/nano.v1i0.5214.

[130] Y. Lu, K. W. Shah, and J. Xu, "Synthesis, morphologies and building applications of nanostructured polymers," *Polymers*, vol. 9, no. 10. MDPI AG, Oct. 13, **2017**. doi: 10.3390/polym9100506.

[131] K. R. Reddy, A. El-Zein, D. W. Airey, F. Alonso-Marroquin, P. Schubel, and A. Manalo, "Self-healing polymers: Synthesis methods and applications," *Nano-Structures & Nano-Objects*, vol. 23, p. 100500, Jul. **2020**, doi: 10.1016/j.nanoso.2020.100500.

[132] C. Li *et al.*, "Ultra-stable anti-counterfeiting materials inspired by water stains," *Cell Rep Phys Sci*, vol. 2, no. 9, p. 100571, Sep. **2021**, doi: 10.1016/j.xcrp.2021.100571

[133] Y. Liu *et al.*, "Fabrication of anticounterfeiting nanocomposites with multiple security features via integration of a photoresponsive polymer and upconverting nanoparticles," *Adv Funct Mater*, vol. 31, no. 37, p. 2103908, Sep. **2021**, doi: 10.1002/adfm.202103908.

[134] L. Porcarelli *et al.*, "Single-Ion conducting polymer nanoparticles as functional fillers for solid electrolytes in lithium metal batteries," *ACS Appl Mater Interfaces*, vol. 13, no. 45, pp. 54354–54362, Nov. **2021**, doi: 10.1021/acscami.1c15771.





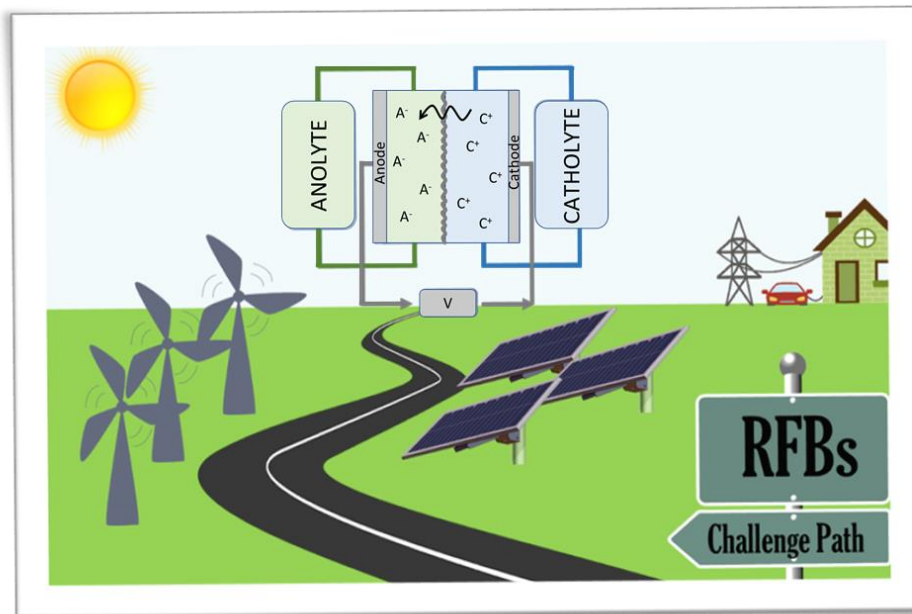




# Section I.

## Polymer Nanoparticles for Energy Storage Applications

---



*“Not all roads lead to Rome, but they do lead to renewable energies.”*

Part of the work described in this section has been published in Revista de Plásticos Modernos. **2019**, 117 (745), 21-25



## Introduction

Today, we could not conceive life without electric power; it is an invisible and omnipresent comfort that is considered a common consumer good. The great challenge of human civilization is to change the way we produced electrical energy, which comes from the combustion of fossil fuels. Since such combustion emits greenhouse gases such as CO<sub>2</sub> into the atmosphere and this is harming the planet. There has been a rapid transition to a low-carbon economy, which has driven technological development and business innovation [1].

In recent decades there has been an increase in the use of renewable sources such as solar and wind [2–4]. However, renewable energy sources present an imbalance between supply and demand. A significant portion of this energy must be stored for use at peak demand times. Therefore, energy storage is an important issue. One of the most versatile energy storage systems are the batteries. Therefore, there is a need to develop new batteries that are economical, safe and durable for large-scale stationary energy storage (Figure I.1.).

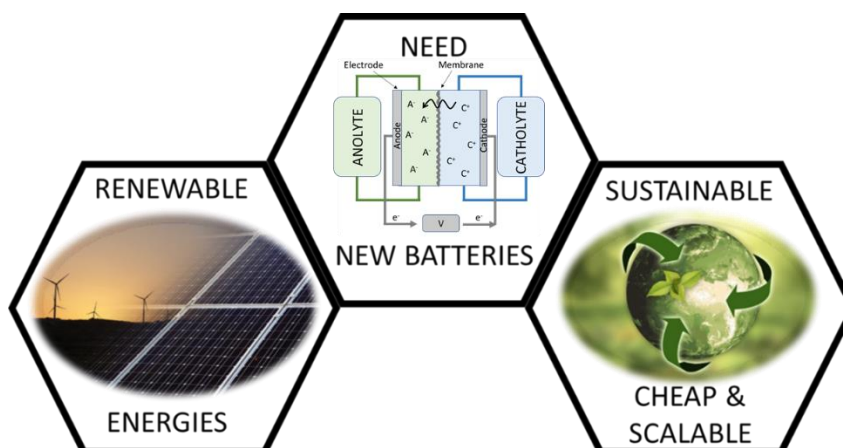


**Figure I.1.** Schematic representation of the needs of the new energy storage batteries

Electrochemical energy storage systems are considered to play a fundamental role in the energy transition to a low-carbon economy. An interesting candidate

for renewable energy storage system are redox flow batteries (RFBs) [5]. The RFBs are especially suitable due to their independent scalability of energy and power and their long cycle life. In contrast to standard batteries, the active material is not a solid electrode, but the active material is dissolved in an electrolyte. Aqueous organic redox flow batteries (AORFBs) have recently attracted much attention but it still to overcome various challenges to become a competitive technology [5–7].

In the following section it will be described how energy is stored and in how a redox flow cell works and what are its main components.

### **Electrochemical energy storage technologies**

Currently, the electricity sector model has been based on the generation of electricity through hydroelectric or thermal power plants that can vary the levels of energy production depending on the required demand. But the path of renewable energies is leading to a change in the electricity sector, towards a model where both systems will coexist, with small renewable energy facilities located close to the consumption points [8,9].

There are different technologies to convert energy according to the energy mechanism such as: electrical, chemical, thermal, mechanical and electrochemical storage [10–12]. This section focuses on electrochemical storage that store electrical energy into chemical energy. For storage to take place, at least two chemical reactions need to occur at the same time, an oxidation, and a reduction. The types of electrochemical storage vary according to the structural characteristics, design, and nature of the reactants. These energy storage systems can be classified into different categories such as primary battery, secondary battery, backup cell [13]. This section focuses on secondary batteries, i.e., electrically rechargeable batteries, more specifically on redox flow batteries.

### **What is a redox flow battery?**

Like in another type of secondary battery, redox flow batteries are capable of storing energy through an electrochemical reversible process. However, in this

type of batteries the electrolyte is in liquid phase and is stored in external tanks and pumped into the electrochemical cell and the reaction takes place on the surface of the electrodes. The electrodes are only a conductive material that allows the transfer of electrons, but they do not undergo any chemical change that causes variations in their volume or chemical structure. This process converts chemical energy into electricity and viceversa [14]. A membrane is placed between the electrodes to maintain ionic contact between the two electrodes, prevent electrical short-circuiting and prevent the electrolytes from mixing. The membrane must be impermeable to redox active materials to prevent mixing and short-circuiting contain one or more electroactive species. A simplified schematic is shown in Figure I.2.

During the charging process the cathode material get oxidizes, releasing electrons through the external electrical circuit connecting both sides of the battery, and the ions, diffuse to the opposite side of the battery through the membrane, by balancing the charge. After the charge process the catholyte material was oxidized and the anolyte reduced being stored both in their respective tanks and having converted electrical energy into chemical energy by this way. During the discharge process, the aforementioned reactions are reversed, and the electrolyte materials return to their original state, so that the reduced material is now the one that generates electrons by reversing the oxidation states to their starting point. When all the material stored in the tanks has passed through the electrochemical cell and returned to its initial oxidation state, all the chemical energy would have been converted into electrical energy, leaving the battery completely discharged.

Conventional electrolytes consist of soluble redox metal species that dissolve in the solvent and undergo rapid, reversible oxidation-reduction reactions during battery operation [15].

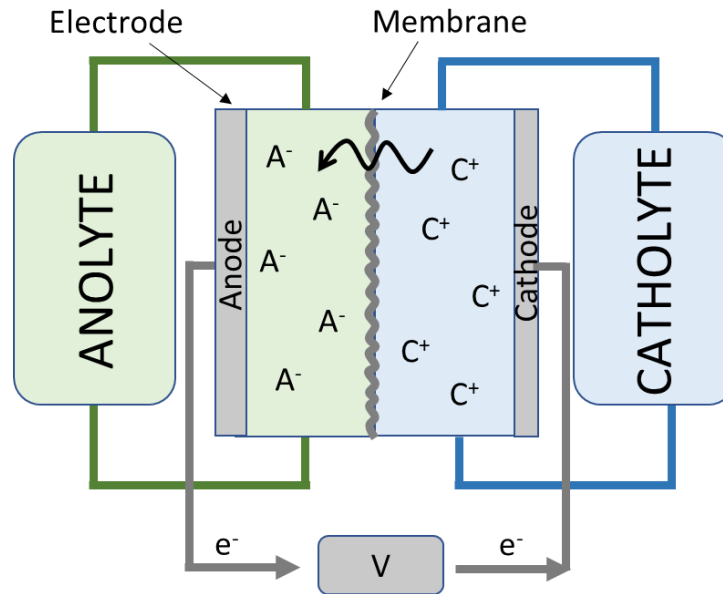


**Figure I.2.** Scheme of Redox Flow Battery

### **Advantages of redox flow batteries**

One of the main advantages of RFBs is that power and energy are decoupled, i.e., power and stored energy can be scaled independently. The energy storage capacity depends mainly on the capacity, concentration, and redox voltage of the electrolytes, while the power is defined by the surface area of the electrodes. This modular configuration will favor the scale-up and maintenance of the redox flow battery systems while the energy and power are maximum. By simply modifying the number of cells or the electrolyte concentration, more power and energy can be obtained during long periods [16].

In addition, the easy replacement of the electrolyte material in this type of batteries is another major advantage because, they can be use almost instantly by replacing the liquid electrolyte without having to replace the battery stacks as it happens with the rest of commercial batteries based on solid electrode materials.

Other advantages of this electrochemical energy storage system are long service life with a high number of life cycles, high efficiency, fast response time and low self-discharge. As the catholyte and anolyte electrolytes are stored in different external reservoirs, the phenomenon of self-discharge does not occur

---

---

and therefore the batteries can remain fully discharged for long periods of time without detrimental effects.

### **Types of redox flow batteries:**

The first generation of electrolytes for RFBs have been based on single component active materials dissolved in aqueous electrolytes such as inorganic salts and coordination compounds.

For example, the first prototype of RFBs used  $\text{Fe}^{3+/2+}$  and  $\text{Cr}^{3+/2+}$  as electroactive couples [17]. But in this prototype many problems appeared such as electrolyte mixed slowing the reaction kinetics. This prototype was the origin of the search for ion selective membranes exhibiting high conductivity for redox flow batteries and new electrolytes to make it work.

The most common of these are transition metals (e.g., Fe, Cr, V) [14], as these metals have multiple oxidation states and some of the transitions between these oxidation states occurs at a desirable standard reduction potential (SRP) that is within the kinetically favorable stability window of water. Therefore, different systems have been developed based on: Fe-Cr, Br-polysulfite, Zn-Br, Fe, V [18-21]. In addition, other molecular reagents such as  $\text{H}_2$  and halogens have also been used.

Currently, two of the most extended commercial RFBs are: Vanadium (VRB) and Zinc-Bromine (Zn-Br), but they use compounds of high cost (vanadium) and danger (bromine).

Because of the need of find low-cost, safe and highly-efficient redox electrolytes for aqueous RFBs the research on this type of systems is constantly evolving. Several research groups have started to develop new RFB chemistries, which use novel approaches such as: flow batteries with non-aqueous electrolyte [22,23], membrane-less flow batteries [24–27], batteries roasted in organic and organometallic species in aqueous electrolytes [28–30], polymer redox flow batteries [5,31–35], hybrid flow batteries [36–39], semi-solid flow batteries [40–43], or redox mediated batteries [24,44,45] among others.

This section focuses on aqueous polymer RFBs. These drawbacks could be reduced by using polymer redox electrolytes to reduce the crossover between poly(catholyte) and poly(anolyte) materials and allow the availability of low-cost porous membranes on the market [35,46].

Currently, there is a growing interest in the use of organic-based polymer redox architectures in energy storage due to the advantages of organic molecules compared to inorganic or metallic materials.

### **Why use organic materials?**

Active organic materials are interesting for electrochemical energy storage devices because they are low cost, and environmentally friendly. In addition, they possess a large molecular and structural diversity that can be tailored by relatively simple synthesis methods. One way to tailor their redox potential, solubility, chemical and electrochemical stability, and electron transfer rate is to modify the chemical structure of the organic molecule. Therefore, these materials possess the necessary characteristics to be able to lead innovative technologies.

Due to the wide range of possibilities when synthesizing new organic molecules major developments in computational chemistry are being made to provide screening tools for choosing organic electrode and electrolyte materials [47], being able to test and explore all the possibilities involves the consumption of resources and time.

Organic materials can be applied to different energy storage devices depending on their physicochemical and electrochemical properties. Therefore, the same organic compound can be used for different materials. In the case of being used as redox active electrolytes, it is necessary that they also possess high solubility.

Recent research on RFBs using redox-active organic materials has been comprehensively reviewed by the group of Prof. U. Schubert [48]. In the following Figure I.3, some representative families of organic redox species developed for RFB are summarized.



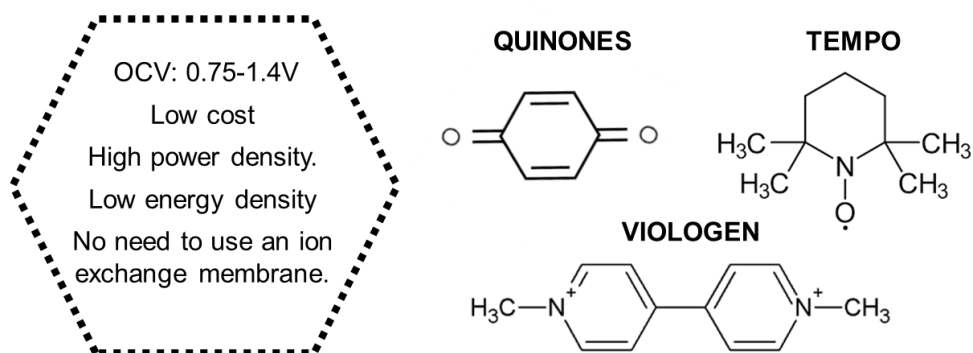


**Figure I.3.** Schematic summary of the most common redox organic molecules used in aqueous BFRs. OCV: open-circuit voltage

The first example of an aqueous organic molecules for redox flow batteries was proposed by Yang et al. in 2014 [49]. The electrolytes of the catholyte and anolyte were based on quinones, anthraquinones, and benzoquinones. The battery exhibited a 90 % retention capacity after 12 cycles, and a voltage of 0.75V. After the study of many different quinones for RFs, other organic molecules in aqueous media have been studied.

In 2016 Liu et al. [50] proposed a redox flow battery of viologen (4,4'-bipyridine) and TEMPO (2,2,6,6,-tetramethylpiperidinyloxy) as anolyte and catholyte respectively, dissolved in aqueous solution at neutral pH. The TEMPO molecule was functionalized with hydroxyl groups to improve its solubility in water. The open circuit potential (OCV) was 1.25V. Functionalization of TEMPO was also a usual strategy of Prof U. Schubert group [51] to increase the performance of a RFB based on the same TEMPO molecule. In this latter case, the cell showed an OCV of 1.4 V and a cyclability of more than 100 cycles.

The same group proposed the first polymer RFB in 2015 [35]. This battery is composed of redox polymers containing viologen and TEMPO in their macromolecular chain and dissolved in an aqueous medium at neutral pH value. This development is very important since it minimizes the dynamic viscosity in the electrolyte. The main advantage of using polymer RFBs is the possibility of replacing the high-costly perfluorinated membranes used so far, by low-cost, size-exclusion membranes. Two polymers, P1 containing the TEMPO unit and P2 containing the methylviologen (MV) units, were synthesized and investigated as redox-active materials (Figure I.4). The redox potential of P1

and P2 was determined as 0.7 V and 0.425 V vs. Ag/AgCl, respectively, suggesting a battery voltage of approximately 1.12 V.

In 2016, Winsberg et al. [52] studied a hybrid redox flow battery using methacrylate/styrene block copolymers (PTMA-b-PS) and TEMPO as electroactive material for the cathode and Zn<sup>2+</sup>/Zn pair for the anode. With this approach, they implement for the first time polymeric micelles as charge carriers in polymer RFBs. They have shown excellent cyclic stability of more than 1000 cycles with stable voltage, the battery has a capacity of 54 Ah l<sup>-1</sup> at a cell voltage of 1.4V.

The same group developed and studied a new bipolar redox active material for organic flow batteries based on boron dipyrromethanes (BODIPYs) [53] with high electrochemical reversibility. they found that the new redox polymer electrolytes have also an excellent electrochemical stability. They achieved an average voltage of 1.28 V for the discharge process, and stable capacity for 90 cycles.

As a summary, the most studied redox species in these poly(analytes) are limited to a few molecule derivatives such as quinone [54,55], viologen [56,57], TEMPO [46,52,57] and ferrocene (Fc) [56,58,59].

### **Future changes and research line.**

With the emergence field of redox active organic molecules and polymers for RFBs, a range of new opportunities opens. Moreover, the understanding the physicochemical and electrochemical aspects governing the storage mechanism of the organic-based electrolytes is also essential to overcome the failure of the battery and then extend their lifetime. In addition, it is important to be able to find the optimal process conditions of the new sustainable electrolytes, i.e., find compatible membranes, salt support and electrode materials for the system to work efficiently.

Based on the development of the last few years, the following challenges must be faced:

- Enhance the solubility of the redox active species.

- Increase chemical and electrochemical stability of the active species
- Minimize cross-over through the membrane
- In-depth study of the electrode/electrolyte interface
- Create multifunctionality in the redox species

In order to achieve all these goals, an enormous effort is being made in this area, which has become a hot topic in energy storage. The properties of all the components in redox flow batteries, i.e. electrolytes, separator membrane, and electrodes are constantly evolving. This means that major improvements in their properties are expected over the next few years.

In summary, the Section I of this Ph.D. Thesis focuses on the development of redox active polymer nanoparticles for aqueous redox flow batteries using organic active materials. The use of organic molecules leads to a significant economic decrease compared to the previously used inorganic compounds. Because domestic-sized RFBs, which can be used in combination with decentralized PV electricity production on rooftops, safe battery systems are necessary. In addition, special attention must be paid to the safety of the system, in terms of flammability and toxicity.

This Section I has focused on one of the main points discussed above to improve the existing materials for redox flow batteries. The main objective is the substitution of expensive anionic membranes by size exclusion membranes, in addition to the use of water as solvent of the redox flow batteries, to mitigate the toxicity and price of them. For this purpose, different types of polymers with electroactive capacity to store energy in an aqueous medium have been synthesized. New size-exclusion polymer nanoparticles with electroactive capacity soluble in water as high-capacity charge carriers have been designed, developed and studied. Besides, some of these nanoparticles can react with carbon dioxide boosting their charge storage properties.

The combination of nanotechnology and polymer chemistry is the core of this Section I. Furthermore, the advantages of using polymer nanoparticles as potential aqueous electrolytes for subsequent use in redox flow batteries are demonstrated, making these methodologies attractive in this field.

Chapters 2 and 3 present the different proposals to solve the challenges discussed above by designing new water-stable polymer nanoparticles with electroactive species capable of storing energy.

The selection of the appropriate polymers to prepare water stable dispersions of the nanoparticles for use as an electrolyte material in redox flow batteries is a critical step of great importance. Therefore, the polymer nanoparticles must meet several requirements:

1. Allow the charge transport intra- and inter-nanoparticles so an efficient energy storage take place. The synthesized polymer nanoparticles must be water-soluble or create stable dispersions in water in order to maximize the amount of energy stored.
2. The nanoparticles must be homogeneous in size and not pass through the size exclusion membrane.

Chemically engineered polymer nanoparticles offer the possibility of creating all these requirements, as their chemical composition, size and morphology can be controlled.

Considering these aspects, a hierarchical polymer composed of sustainable biopolymers such as cellulose and lignin and a conducting polymer such as polypyrrole, with a nanoparticulate morphology and easily dispersed in water, has been synthesized. This new polymeric material would not only be able to store energy, but also has the advantage of tackling another major problem in society such as CO<sub>2</sub> capture.

In Chapter 3 we described the preparation of a completely different, water-soluble, electroactive polymeric material, with micellar morphology. By means of a RAFT-type synthesis of an amphiphilic copolymer with dimethylaminoferrocene (electroactive compound) inserted by way of a chemical exchange. These new micellar ferrocene nanoparticles exhibited a high capacity that allow us to use it in a redox flow battery. A proof of concept is carried out in a hybrid flow battery with a zinc anode. Hybrid flow batteries should be investigated technological systems that include a Zn anode, as this metal extends the usable voltage in water and can be acquired at low cost.

---

---

## References

- [1] B. Obama, “The irreversible momentum of clean energy,” *Science* (1979), vol. 355, no. 6321, pp. 126–129, Jan. **2017**, doi: 10.1126/science.aam6284.
- [2] P. Ravestein, G. van der Schrier, R. Haarsma, R. Scheele, and M. van den Broek, “Vulnerability of European intermittent renewable energy supply to climate change and climate variability,” *Renew Sust Energy Rev*, vol. 97, pp. 497–508, Dec. **2018**, doi: 10.1016/J.RSER.2018.08.057.
- [3] D. Greenwood, S. Walker, N. Wade, S. Munoz-Vaca, A. Crossland, and C. Patsios, “Integration of high penetrations of intermittent renewable generation in future electricity networks using storage,” *Future Energy Elsevier*, pp. 649–668, Jan. **2020**, doi: 10.1016/B978-0-08-102886-5.00030-X.
- [4] H. Zsiborács *et al.*, “Intermittent renewable energy sources: the role of energy storage in the european power system of 2040,” *Electronics*, vol. 8, no. 729, Jun. **2019**, doi: 10.3390/electronics8070729.
- [5] Y. Y. Lai, X. Li, and Y. Zhu, “Polymeric active materials for redox flow battery application,” *ACS Appl Polym Mater*, vol. 2, no. 2, pp. 113–128, Feb. **2020**, doi: 10.1021/acsapm.9b00864.
- [6] V. Singh, S. Kim, J. Kang, and H. R. Byon, “Aqueous organic redox flow batteries,” *Nano Research*, vol. 12.9, pp 1988-2001, **2019**, doi: 10.1007/s12274-019-2355-2.
- [7] C. Ye *et al.*, “Development of efficient aqueous organic redox flow batteries using ion-sieving sulfonated polymer membranes”, *Nat. Commun.*, vol. 13(1), pp 1-13, **2022**, doi: 10.1038/s41467-022-30943-y.
- [8] O. Kuik, F. Branger, and P. Quirion, “Competitive advantage in the renewable energy industry: Evidence from a gravity model,” *Renew Energy*, vol. 131, pp. 472–481, Feb. **2019**, doi: 10.1016/j.renene.2018.07.046.
- [9] I. Capellán-Pérez, Á. Campos-Celador, and J. Terés-Zubiaga, “Renewable energy cooperatives as an instrument towards the energy transition in Spain,” *Energy Policy*, vol. 123, pp. 215–229, Dec. **2018**, doi: 10.1016/j.enpol.2018.08.064.
- [10] A. G. Olabi, C. Onumaegbu, T. Wilberforce, M. Ramadan, M. A. Abdelkareem, and A. H. al – Alami, “Critical review of energy storage systems,” *Energy*, vol. 214, Jan. **2021**, doi: 10.1016/j.energy.2020.118987.
- [11] M. Sterner and F. Bauer, “Definition and classification of energy storage systems,” in *Handbook of Energy Storage*, Berlin, Heidelberg, pp. 23–47, **2019**. doi: 10.1007/978-3-662-55504-0\_2.

- [12] H. Ibrahim, A. Ilinca, and J. Perron, "Energy storage systems-characteristics and comparisons," *Renew Sust Energ Rev*, vol. 12, no. 5. pp. 1221–1250, Jun. **2008**. doi: 10.1016/j.rser.2007.01.023.
- [13] M. S. Guney and Y. Tepe, "Classification and assessment of energy storage systems," *Renew Sust Energ Rev*, vol. 75. Elsevier Ltd, pp. 1187–1197, **2017**. doi: 10.1016/j.rser.2016.11.102.
- [14] A. Z. Weber, M. M. Mench, J. P. Meyers, P. N. Ross, J. T. Gostick, and Q. Liu, "Redox flow batteries: a review," *J Appl Electrochem*, vol. 4, pp. 1137–1164, **2011**, doi: 10.1007/s10800-011-0348-2.
- [15] J. Noack, N. Roznyatovskaya, T. Herr, and P. Fischer, "The chemistry of redox-flowbatteries," *Angew Chem Int Ed*, vol. 54, pp. 9776–9809, **2015**, doi: 10.1002/ange.201410823.
- [16] E. Sánchez-Díez *et al.*, "Redox flow batteries: Status and perspective towards sustainable stationary energy storage," *J Power Sources*, vol. 481, Jan. **2021**, doi: 10.1016/j.jpowsour.2020.228804.
- [17] L. H. Thaller, "Electrically rechargeable redox flow cells," *In 9th Intersociety Energy Conversion Engineering Conference*, pp. 924–928, **1974**.
- [18] Y. K. Zeng, X. L. Zhou, L. Zeng, X. H. Yan, and T. S. Zhao, "Performance enhancement of iron-chromium redox flow batteries by employing interdigitated flow fields," *J Power Sources*, vol. 327, pp. 258–264, Sep. **2016**, doi: 10.1016/j.jpowsour.2016.07.066.
- [19] A. A. Chilenskas *et al.*, "Zinc-Bromine Secondary Battery," *J Electrochem Soc*, vol. 124, no. 8, pp 1154, **1977**. doi 10.1149/1.2133517.
- [20] M. Skyllas-Kazacos, M. Rychcik, R. G. Robins, A. G. Fane, and M. A. Green, "New all-vanadium redox flow cell," *J Electrochem Soc*, vol. 133, no. 5, pp. 1057–1058, **1986**. doi: 10.1149/1.2108706.
- [21] R. Monteiro, J. Leirós, M. Boaventura, and A. Mendes, "Insights into all-vanadium redox flow battery: A case study on components and operational conditions," *Electrochim Acta*, vol. 267, pp. 80–93, Mar. **2018**, doi: 10.1016/j.electacta.2018.02.054.
- [22] K. Gong, Q. Fang, S. Gu, S. F. Y. Li, and Y. Yan, "Nonaqueous redox-flow batteries: organic solvents, supporting electrolytes, and redox pairs," *Energy Environ Sci*, vol. 8, no. 12, pp. 3515–3530, **2015**, doi: 10.1039/C5EE02341F.
- [23] S. K. Park *et al.*, "Electrochemical properties of a non-aqueous redox battery with all-organic redox couples," *Electrochem commun*, vol. 59, pp. 68–71, Jul. **2015**, doi: 10.1016/j.elecom.2015.07.013.

- [24] S. Gentil, D. Reynard, and H. H. Girault, "Aqueous organic and redox-mediated redox flow batteries: a review," *Curr Opin Electrochem*, vol. 21, pp. 7–13, Jun. **2020**, doi: 10.1016/j.coelec.2019.12.006.
- [25] W. A. Braff, M. Z. Bazant, and C. R. Buie, "Membrane-less hydrogen bromine flow battery," *Nat Commun*, vol. 4, no 1, pp. 1-6, **2013**, doi: 10.1038/ncomms3346.
- [26] P. Navalpotro *et al.*, "Critical aspects of membrane-free aqueous battery based on two immiscible neutral electrolytes," *Energy Storage Mater*, vol. 26, pp. 400–407, Apr. **2020**, doi: 10.1016/j.ensm.2019.11.011.
- [27] P. Navalpotro, J. Palma, M. A. Anderson, and R. Marcilla, "A membrane-free redox flow battery with two immiscible electrolytes," *ECS Meeting Abstracts*, vol. MA2018-02, no. 1, pp. 31–31, Jul. **2018**, doi: 10.1149/MA2018-02/1/31.
- [28] B. Huskinson *et al.*, "A metal-free organic–inorganic aqueous flow battery," *Nature*, vol. 505, no. 7482, pp. 195–198, Jan. **2014**, doi: 10.1038/nature12909.
- [29] D. G. Kwabi *et al.*, "Alkaline quinone flow battery with long lifetime at pH 12," *Joule*, vol. 2, no. 9, pp. 1894–1906, Sep. **2018**, doi: 10.1016/j.joule.2018.07.005.
- [30] Y. Ji *et al.*, "A Phosphonate-functionalized quinone redox flow battery at near-neutral pH with record capacity retention rate," *Adv Energy Mater*, vol. 9, no. 12, p. 1900039, Mar. **2019**, doi: 10.1002/aenm.201900039.
- [31] Y. Liu *et al.*, "A Long-Lifetime All-organic aqueous flow battery utilizing TMAP-TEMPO radical," *Chem*, vol. 5, no. 7, pp. 1861–1870, Jul. **2019**, doi: 10.1016/j.chempr.2019.04.021.
- [32] J. Winsberg *et al.*, "Poly(boron-dipyrromethene)—a redox-active polymer class for polymer redox-flow batteries," *Chem Mater*, vol. 28, no. 10, pp. 3401–3405, May **2016**, doi: 10.1021/acs.chemmater.6b00640.
- [33] E. C. Montoto, G. Nagarjuna, J. S. Moore, and J. Rodríguez-López, "Redox active polymers for non-aqueous redox flow batteries: validation of the size-exclusion approach," *J Electrochem Soc*, vol. 164, no. 7, pp. A1688–A1694, Jun. **2017**, doi: 10.1149/2.1511707jes.
- [34] J. Winsberg, S. Benndorf, A. Wild, M. D. Hager, and U. S. Schubert, "Synthesis and characterization of a phthalimide-containing redox-active polymer for high-voltage polymer-based redox-flow batteries," *Macromol Chem Phys*, vol. 219, no. 4, p. 1700267, Feb. **2018**, doi: 10.1002/macp.201700267.

- [35] T. Janoschka *et al.*, “An aqueous, polymer-based redox-flow battery using non-corrosive, safe, and low-cost materials,” *Nature*, vol. 527, no. 7576, pp. 78–81, Nov. **2015**, doi: 10.1038/nature15746.
- [36] A. Khor *et al.*, “Review of zinc-based hybrid flow batteries: From fundamentals to applications,” *Mater Today Energy*, vol. 8, pp. 80–108, Jun. **2018**, doi: 10.1016/j.mtener.2017.12.012.
- [37] A. Dinesh *et al.*, “Iron-based flow batteries to store renewable energies,” *Environ Chem Lett*, vol. 16, no. 3, pp. 683–694, Sep. **2018**, doi: 10.1007/s10311-018-0709-8.
- [38] L. Zhang and G. Yu, “Hybrid electrolyte engineering enables safe and wide-temperature redox flow batteries,” *Angew Chem Int Ed*, vol. 60, no. 27, pp. 15028–15035, Jun. **2021**, doi: 10.1002/anie.202102516.
- [39] N. Akhmetov *et al.*, “Composite lithium-conductive LATP+PVdF membranes: Development, optimization, and applicability for Li-TEMPO hybrid redox flow batteries,” *J Memb Sci*, vol. 643, p. 120002, Mar. **2022**, doi: 10.1016/j.memsci.2021.120002.
- [40] E. Ventosa, “Semi-solid flow battery and redox-mediated flow battery: two strategies to implement the use of solid electroactive materials in high-energy redox-flow batteries,” *Curr Opin Chem Eng*, vol. 37, p. 100834, Sep. **2022**, doi: 10.1016/j.coche.2022.100834.
- [41] M. Duduta *et al.*, “Semi-solid lithium rechargeable flow battery,” *Adv Energy Mater*, vol. 1, no. 4, pp. 511–516, Jul. **2011**, doi: 10.1002/aenm.201100152.
- [42] E. Ventosa, O. Amedu, and W. Schuhmann, “aqueous mixed-cation semi-solid hybrid-flow batteries,” *ACS Appl Energy Mater*, vol. 1, no 10, pp. 5158-5162 , Oct. **2018**, doi: 10.1021/acsaem.8b01418.
- [43] K. Huang, P. Zhou, and H. Chen, “Systematic optimization of high-energy-density Li–Se semi-solid flow battery,” *Energy Technol.*, vol. 9, no. 8, p. 2100371, Aug. **2021**, doi: 10.1002/ente.202100371.
- [44] R. Yan and Q. Wang, “Redox-targeting-based flow batteries for large-scale energy storage,” *Adv. Mater.*, vol. 30, no. 47, p. 1802406, Nov. **2018**, doi: 10.1002/adma.201802406.
- [45] M. L. Meyerson, S. G. Rosenberg, and L. J. Small, “A Mediated Li–S flow battery for grid-scale energy storage,” *ACS Appl Energy Mater*, vol. 5, no. 4, pp. 4202–4211, Apr. **2022**, doi: 10.1021/acsaem.1c03673.
- [46] T. Janoschka *et al.*, “Synthesis and characterization of TEMPO- and viologen-polymers for water-based redox-flow batteries,” *Polym Chem*, vol. 6, no. 45, pp. 7801–7811, **2015**, doi: 10.1039/C5PY01602A.



- [47] E. v. Carino, J. Staszak-Jirkovsky, R. S. Assary, L. A. Curtiss, N. M. Markovic, and F. R. Brushett, “tuning the stability of organic active materials for nonaqueous redox flow batteries via reversible, electrochemically mediated Li<sup>+</sup> coordination,” *Chem Mater*, vol. 28, no. 8, pp. 2529–2539, Apr. **2016**, doi: 10.1021/acs.chemmater.5b04053.
- [48] J. Winsberg, T. Hagemann, T. Janoschka, M. D. Hager, and U. S. Schubert, “Redox-Flow Batteries: from metals to organic redox-active materials,” *Angew Chem Int Ed*, vol. 56, no. 3, pp. 686–711, Jan. **2017**, doi: 10.1002/anie.201604925.
- [49] B. Yang, L. Hooper-Burkhardt, F. Wang, G. K. Surya Prakash, and S. R. Narayanan, “An inexpensive aqueous flow battery for large-scale electrical energy storage based on water-soluble organic redox couples,” *J Electrochem Soc*, vol. 161, no. 9, pp. A1371–A1380, Jun. **2014**, doi: 10.1149/2.1001409jes.
- [50] T. Liu, X. Wei, Z. Nie, V. Sprenkle, and W. Wang, “A total organic aqueous redox flow battery employing a low cost and sustainable methyl viologen anolyte and 4-HO-TEMPO catholyte,” *Adv Energy Mater*, vol. 6, no. 3, p. 1501449, Feb. **2016**, doi: 10.1002/aenm.201501449.
- [51] T. Janoschka, N. Martin, M. D. Hager, and U. S. Schubert, “An aqueous redox-flow battery with high capacity and power: the TEMPTMA/MV system,” *Angew Chem Int Ed*, vol. 55, no. 46, pp. 14427–14430, Nov. **2016**, doi: 10.1002/anie.201606472.
- [52] J. Winsberg *et al.*, “Polymer/zinc hybrid-flow battery using block copolymer micelles featuring a TEMPO corona as catholyte,” *Polym Chem*, vol. 7, no. 9, pp. 1711–1718, **2016**, doi: 10.1039/C5PY02036K.
- [53] J. Winsberg *et al.*, “Poly(boron-dipyrromethene)—A Redox-Active Polymer Class for Polymer Redox-Flow Batteries,” *Chem. Mater.*, vol. 28, no. 10, pp. 3401–3405, May **2016**, doi: 10.1021/acs.chemmater.6b00640.
- [54] J. Chai, X. Wang, A. Lashgari, C. K. Williams, and J. Jiang, “A pH-neutral, aqueous redox flow battery with a 3600-cycle lifetime: micellization-enabled high stability and crossover suppression,” *ChemSusChem*, vol. 13, no. 16, pp. 4069–4077, **2020**, doi: 10.1002/cssc.202001286.
- [55] W. Yan *et al.*, “All-polymer particulate slurry batteries,” *Nature*, vol. 10, no. 2513, **2019**, doi: 10.1038/s41467-019-10607-0.
- [56] E. C. Montoto *et al.*, “Redox active colloids as discrete energy storage carriers,” *J Am Chem Soc*, vol. 138, no. 40, pp. 13230–13237, **2016**, doi: 10.1021/jacs.6b06365.
- [57] J. Winsberg *et al.*, “Poly(TEMPO)/Zinc hybrid-flow battery: a novel, ‘green,’ high voltage, and safe energy storage system,” *Adv Mater*, vol. 28, no. 11, pp. 2238–2243, **2016**, doi: 10.1002/adma.201505000.

[58] P. S. Borchers *et al.*, “Regaining potential: studies concerning 2-ferrocenylethyl methacrylate, its polymers, and application in redox flow batteries,” *Macromolecules*, vol. 55, no 5, p. 1576-1589, Feb. **2022**, doi: 10.1021/acs.macromol.1c02565.

[59] P. S. Borchers *et al.*, “Aqueous redox flow battery suitable for high temperature applications based on a tailor-made ferrocene copolymer,” *Adv Energy Mater*, vol. 10, no. 41, **2020**, doi: 10.1002/aenm.202001825.

[60] R. M. Darling, K. G. Gallagher, J. A. Kowalski, S. Ha, and F. R. Brushett, “Pathways to low-cost electrochemical energy storage: a comparison of aqueous and nonaqueous flow batteries,” *Energy Environ Sci*, vol. 7, no. 11, pp. 3459–3477, Sep. **2014**, doi: 10.1039/C4EE02158D.





# Chapter 2.

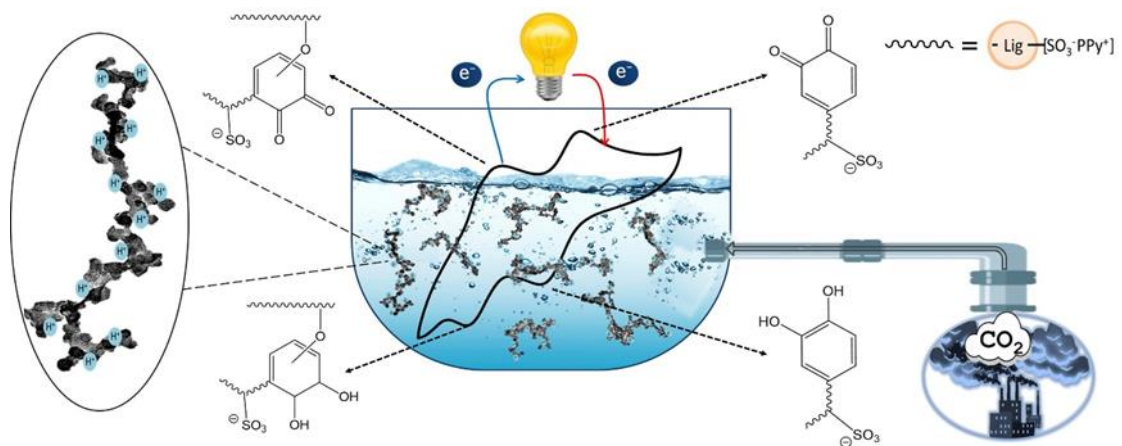
## Multifunctional metal-free rechargeable polymer composite nanoparticles boosted by CO<sub>2</sub>

Part of the work described in this Chapter has been published in *Materials Today Sustainability*, **2020**, 10, 100048.

A European patent application (EP19382731) has been filed by Consejo Superior de Investigaciones Científicas



The 45 % of the CO<sub>2</sub> emissions from burning fossil fuels and industrial chemical reactions is located in the atmosphere contributing significantly to the global warming. The transition to low-carbon energy and climate resilient future will be promoted by innovative, highly efficient and low-priced large-scale CO<sub>2</sub> and energy storage methods adapted to urban and industrial areas. Because of their diversity and versatile materials chemistry, batteries are potential candidates to enable both energy and CO<sub>2</sub> storage, shifting the current paradigm in the field mainly focusing on the electrochemical accumulation and release of electricity. The creation of advanced rechargeable materials by using sustainable precursors and preparation routes will allow the transition towards energy storage systems for the future.



## Abstract

Herein, we present a multigram scale-up route for the preparation of novel polymer composite nanoparticles as potential multifunctional rechargeable material of sustainable batteries for the future. The nanoparticles (20 nm) comprise three innocuous and functional interpenetrated macromolecular networks: polypyrrole, methylcellulose, and lignin. They are uniquely assembled in strands or chains (~200 nm) such as *necklace beads* and show long-time stability when dispersed in water. We find that under benign aqueous conditions, a suspension of this hierarchical nanomaterial is able to develop two sets of reversible redox peaks from the catechol moieties of lignin biopolymer separated by ~600 mV. Remarkably, the addition of carbon dioxide further boosted one of the electroactive processes by 500 %. Importantly, the three redox stages occur in the presence of the same nanostructured polymer so being a potentially bifunctional material to be used in advanced electrochemical systems. The new properties are attributed to an intrinsic chemical and electronic coupling at the nanoscale among the different building blocks of the metal-free polymer composite and the structural rearrangement of the interpenetrated polymer network by the incorporation of CO<sub>2</sub>. We have provided both a new electrochemically multifunctional hierarchically-structured material and a facile route that could lead to novel sustainable energy applications.



---

---

## Scientific background and state of the art

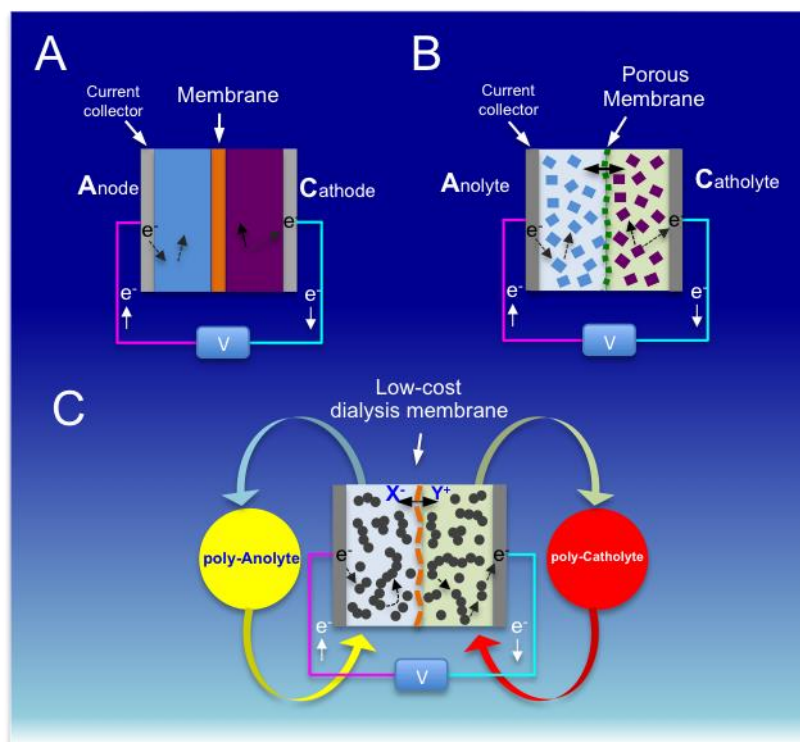
The increase of air-pollution levels in the atmosphere and their impact on global human health and climate change are pushing towards the rapid integration of energy from wind and sun into the electric grid and the electrification of transport [1,2]. To move towards a low-carbon and climate-resilient future a highly efficient, low-priced and large-scale methods to decrease the CO<sub>2</sub> concentration from urban and industrial areas are also needed [3,4]. Batteries have not yet achieved the degree of versatility and functionality to store for instance simultaneously electricity and CO<sub>2</sub> cost-efficiently. In addition, the use of more sustainable energy storage materials to minimize the original carbon dioxide footprint of fabricating and recycling the battery is highly needed [5].

In search of superior battery performance, one of the strategies adopted by researchers has been the creation of electroactive materials within the nanometer scale [6]. By diminishing the particle size [7] or the thickness [8] of the electrodes to the nanometer size, both the electrolyte's ion diffusion paths between active sites decreases while the amount of surface area being able to allocate the charges increases enabling capacity values close to the theoretical ones even at high cycling rates. Nanostructured electrodes can also accommodate large strain without pulverization, providing good electronic contact and conduction [9].

However, the fabrication of nanostructured electrodes and electroactive nanoparticles normally involves the application of complex routes of synthesis with several steps and the presence of harmful chemicals. Moreover, these methods usually provide a very low amount of functional material making the overall process highly costly and difficult to scale. The electroactive nanoparticles are usually of low density resulting in challenges to pack them into highly compact electrodes and thus diminishing the possibility to enhance the volumetric energy density of the battery. From a practical point of view, if both solid micrometer thick electrodes in a conventional secondary battery (Scheme 1A) were split off into a massive number of nanoparticles (Scheme 1B), dispersed in a liquid solvent and then charged and discharged, an increase of the capacity and the power capability of the battery system might be

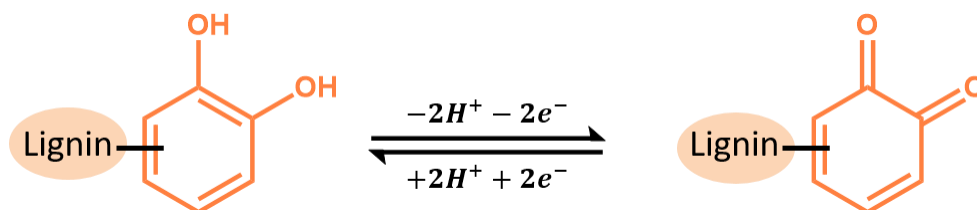
expected. The main reason for this is the decreased restrictions due to the length scales for ion insertion, which are reduced to short distances. Compared to the low mass-content of a solid thin-film electrode, where the energy and power are coupled indistinguishably, a fundamental advantage of using electroactive nanoparticles in solution is the larger amount of energy that could be stored. Moreover, if enough dense these nanoparticles will ensure a high battery's volumetric energy density too.

This description is closely related to what occurs in flowable electroactive suspensions moving back and forth of the cell [10]. The energy limitation of these systems is the partial dispersibility of the redox-active material in the liquid solvent. In most cases, researchers have implemented organic solvents [11] to maximize the concentration of the redox species and the voltage window; but the battery system would be expensive and unsafe if a massive volume of flammable organic solvent is needed. The utilization of organic solvents may also result in low ion mobility and poor rate capability [12]. Therefore, in order to achieve cost-efficient and safer electrochemical systems to store a large amount of energy from renewable sources, the use of water as the main solvent is desired. Recently, a flow battery based on aqueous-dispersed ( $1 \text{ mol}\cdot\text{l}^{-1}$ ), micro-sized all-polymer redox-active particulates have been developed showing excellent electrochemical properties such as highly reversible multi-electron redox process, rapid electrochemical kinetics and ultra-stable long-term cycling capability [13]. The application of electroactive polymer particulate slurries [11], solutions [14] or colloids electrolytes [15] also makes it possible to replace expensive ion-conducting membranes with much cheaper, commercial dialysis membranes through the mechanism of size exclusion (Scheme 2.1C). However, because many redox-active materials are not soluble in water the dispersion and stabilization without using surfactants or emulsifiers will be challenging.



**Scheme 2.1.** Configurations of different electrochemical cells: A) Conventional battery system with thick solid-state electrodes, B) semi solid-like battery and C) a redox-active particulate electrolyte flow battery

Chapter 2 details a sustainable route for the preparation of highly-water dispersible and electrochemically rechargeable polymer composite nanoparticles. These nanomaterials comprise renewable, abundant, and non-toxic active components enabling advanced redox properties under benign conditions. Methylcellulose has been selected as a dispersing agent to aid the creation of nanoparticles during colloidal polymerization and to vouch for the long-term stability of the suspensions in water. The other two functional components were lignin and polypyrrole. The former is the most abundant aromatic biopolymer on earth and can reversibly store charge through the reduction and oxidation of catechol moieties (Scheme 2.2) [16]. The latter is a low-cost biocompatible conjugated polymer that will enhance the charge transport properties in the composite nanomaterial. This new redox-active polymer composite is easy to make and does not require additional metal or expensive components.



**Scheme 2.2.** Electrochemical oxidation and reduction of catechol moieties of lignin biopolymer in protic media

Polymer composites made of polypyrrole and cellulose derivatives [17] or redox-active lignin [6] have been studied before as a solid electrode material. In this Chapter, is studied the enhanced reactivity at the nanoscale to trigger enhanced functionality in these composites made of interpenetrated networks of lignin, cellulose and polypyrrole. The main objective is the preparation of an electrochemically active polymer material with the ability to be dispersed in an aqueous medium.

## Experimental Methods

### Materials

Three different polymers have been used for the synthesis of the nanoparticulated polymer hybrid electrodes:

- **Methyl cellulose** (biopolymer) (Figure 2.1), whose function is to provide stability of the nanoparticle dispersion in the aqueous phase and to act as a nucleating agent during the polymerization reaction. An initial study in the group established that the optimal viscosity of the methyl cellulose was 4000 cP.

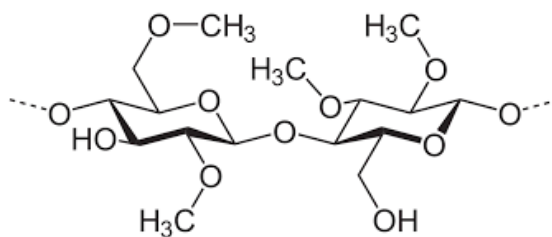


**Figure 2.1.** Molecular structure of methyl cellulose

**-Polypyrrole**, which was prepared from the pyrrole monomer by oxidative polymerization in the presence of iron trichloride which acts as a catalyst for the reaction (Figure 2.2). The function of this polymer is to provide the material with good electronic conductivity.

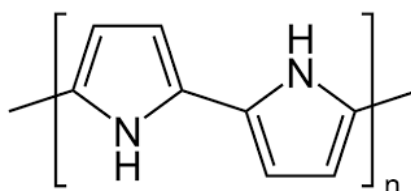


**Figure 2.2.** Molecular structure of polypyrrole

**-Lignin** (biopolymer), whose function is to provide charge and discharge storage capacity through a reversible redox process of the quinone groups present in the molecular structure. During the charging process, the ortho-quinone groups are transformed into catechol by capturing 2 electrons and 2 protons via electrochemical reaction (Scheme 2.2). Three types of lignin with different content of sulfonic groups, low, medium and high, have been used. The synthesis of different nanoparticulate hybrid polymeric materials has been carried out varying only the type of lignin.

### **Preparation of the multifunctional polymer composites**

The preparation method of the multifunctional nanomaterials containing the three macromolecules was as follows: 0.16 g of methylcellulose (Sigma-Aldrich) was dissolved in deionized water (200 ml) at 60 °C for 60 min. After cooling down to room temperature, 1 g of lignin biopolymer (Sigma-Aldrich), with a

variable content of sulfonic groups in its composition (see Table 2.2), 0.25 g of pyrrole monomer (Sigma-Aldrich) and 0.5 g of FeCl<sub>3</sub> (Sigma-Aldrich) as catalyst were added progressively. Then, the mixture was stirred for 1 h. The solution turned out black immediately, so as a sign that the polymerization started and then after a few minutes a black solid precipitate to the bottom of the reaction flask. Subsequently, the solid was separated from the solution by centrifugation. After that, the solid was washed with deionized water and centrifuged again. This process was repeated up to three times. Next, the solid was freeze-dried overnight and stored in the fridge at 2 °C until use. The terminology to designate the polymer composite samples was the following: *MPLX*, where *M*, *P*, and *L* mean methylcellulose, polypyrrole, and lignin, respectively, and *X* indicates the content of sulphonic groups in lignin estimated from elemental analysis of sulfur. So, *X* is designated as *L* when the amount of elemental sulfur in lignin is 1.6 wt.%, *M* means medium and corresponds to a content of 3.7 wt.% and *H* are used to denote the lignin with the higher sulfur content which is 4.9 wt.% (Table 2.1). The composites containing either polypyrrole-lignin or a methylcellulose-polypyrrole couple are denoted *PLX* and *MP*, respectively.

**Table 2.1.** Materials nomenclature

<b>M</b>	<b>P</b>	<b>LL</b>	<b>LM</b>	<b>LH</b>
Methylcellulose	Polypyrrole	Sulfur in lignin 1.6 wt.%	Sulfur in lignin 3.7 wt.%	Sulfur in lignin 4.9 wt.%

Table 2.2 presents the conditions of the different synthesis carried out using the different types of lignin and incorporating or not the cellulose to make the possible evaluation of the influence of both compounds in the final material. In addition, another polymer synthesis has been performed to see the effect of the presence or absence of lignin on the morphology of the polymer. The synthesis method is the same as the one detailed above, but without incorporating lignin and adding pyrrole to the aqueous solution of cellulose at room temperature.

**Table 2.2.** Synthesis conditions

	<b>H<sub>2</sub>O Des.</b> <b>(ml)</b>	<b>MC</b> <b>(g)</b>	<b>Lignin</b> <b>(g)</b>	<b>Pyrrole</b> <b>(g)</b>	<b>FeCl<sub>3</sub></b> <b>(g)</b>
<b>MP</b>	200	0.16	-	0.248	0.5
<b>MPLL</b>	200	0.16	1	0.248	0.5
<b>PLL</b>	200	-	1	0.248	0.5
<b>MPLM</b>	200	0.16	1	0.248	0.5
<b>PLM</b>	200	-	1	0.248	0.5
<b>MPLH</b>	200	0.16	1	0.248	0.5
<b>PLH</b>	200	-	1	0.248	0.5

### Experimental techniques

- **Physico-chemical properties**

#### Electron microscopy

The morphology and dimensions of the synthesized polymer composite materials were studied by using electron microscopy: scanning (SEM) and transmission (TEM). A high-resolution scanning electron microscopy (HRSEM) in a Hitachi S-8000 model with field emission filament and a voltage of 1.0 kV.

For TEM studies, the polymer composite materials were ultrasonically dispersed in water. A few drops of the resulting suspension were deposited in a carbon-coated grid. TEM and high-angle annular dark-field imaging (HAADF) in Scanning Transmission Electron Microscopy (STEM) mode experiments were performed with a JEOL JEM 3000F microscope operating at 300 kV (double tilt ( $\pm 20^\circ$ ) (point resolution 0.17 nm in TEM mode and 0.14 nm in STEM mode)), fitted with an X-ray energy dispersive spectroscopy (XEDS) microanalysis system (OXFORD INCA). The atomic ratio of the metals has been determined by XEDS. XEDS-mappings were recorded in ADF-STEM mode using the  $K_{\alpha 1}$

lines of the elements with 256×256 pixel resolution accumulated over at least 1 h to ensure good statistics.

### **Physical gas adsorption**

The textural properties of the polymer composites such as pore size, specific surface area, and pore volume were initially studied by using N<sub>2</sub> gas adsorption at 77 K. This method is ideal for porous samples with a pore size in the range of 0.7-2 nm. However, it is evidenced very low N<sub>2</sub> adsorption values, close to the instrumental detection limit, for all the polymer composite samples, most probably due to the presence of an average pore size smaller than 1 nm. Then, it was applied CO<sub>2</sub> gas adsorption at 273 K because this molecule exhibits a smaller hydrodynamic radius and lower adsorption temperature than N<sub>2</sub> facilitating the diffusion of the gas molecules at the surface. Both N<sub>2</sub> and CO<sub>2</sub> gas adsorption measurements were carried out by using Autosorb equipment (Quantachrome). The amount of sample used for each analysis was approximately 100 mg. The samples were degassed previously under vacuum for 12 h before to start the gas adsorption isotherm. The measurements were performed at 273.15 K by applying a saturation pressure of CO<sub>2</sub> of 26142 torr. The relative pressures range for the adsorption was between  $4.51 \cdot 10^{-4}$  and  $2.90 \cdot 10^{-2}$  torr. The specific micropore surface area, average pore size, and micropore volume, were determined from the adsorption data using the Dubinin–Radushkevich and Stoeckli equations [18].

### **Ultraviolet-Visible (UV-Vis) spectroscopy**

These spectroscopic measurements were carried out in a quartz cuvette (optical path length of 10 mm) containing 0.1 g·l<sup>-1</sup> of the polymer composite, Lig-HS, and MP in water solution. The electronic processes were monitored by using a Perkin Elmer model Lambda 35 spectrophotometer over the range 200-700 nm spectrum region.

### **Elemental analysis**

The content of C, H, S, and N in the polymer samples (5 mg) was determined by combustion in a LECO CHNS-932 thermal analyzer.



---

---

### **Dynamic Light Scattering (DLS) and zeta potential**

The average particle size and surface charge of the polymer composite materials were measured by DLS using a Malvern Nanosizer NanoZS Instrument equipped with a 4 mW He-Ne laser ( $\lambda = 633 \text{ nm}$ ) at a scattering angle of  $173^\circ$ . Different samples were measured in square polystyrene cuvettes (Sarstedt®) at  $25^\circ\text{C}$ . The autocorrelation function was converted in an intensity particle size distribution with ZetaSizer Software 7.10 version, based on the Stokes-Einstein equation. The zeta potential was quantified by laser Doppler electrophoresis (LDE) using polymer composite suspension with a concentration ranging between  $0.1$  and  $0.001 \text{ g}\cdot\text{l}^{-1}$ . The zeta potentials were automatically calculated from the electrophoretic mobility using the Smoluchowski's approximation. For each sample, the statistical average and standard deviation of data were calculated from 8 measurements of 20 runs each one.

The polymer composite samples were homogenized with a bath sonicator for 40 min to allow a good dispersion without damaging the polymer materials. A tip ultrasound probe (Branson Model 250) delivering pulses of  $20.000 \text{ kHz}$  at 35 % of its nominal power (350 W) was subsequently applied. The duration of each pulse was 5 and 10 min. Each pulse lasts 0.1s and is followed by a rest time of 0.1 s.

### **Acid-base properties determination by titration experiments**

Samples with a concentration of  $1 \text{ g}\cdot\text{l}^{-1}$  of MPLH, MP, Lig-H were studied with potentiometric evaluation by using a pH meter (Schott instruments, model Handylab pH 11) using different solutions; acid solutions of 0.1 M and 0.5 M HCl and on the other hand, two basic solutions of 0.1 M and 2 M NaOH. The pH meter was calibrated with buffer solutions of pH 4, 7 and 10. The potentiometric curves were obtained by measuring the change in pH after each addition of base and acid solution, respectively; the additions were made slowly with continuous stirring.

- **Electrochemical properties**

**Preparation of polymer composite films for electrochemical tests**

2.5 ml PLH or MPLH suspension was drop-casted onto freshly polished (0.3-micron alumina) gold-disc electrodes (Bio-Logic, A-002421 AUE Gold electrode (OD: 6 mm – ID: 3.0mm)) and the suspensions were allowed to dry over-night in ambient air. The PLH and MPLH layers were then characterized electrochemically in 1M NaCl<sub>aq</sub> buffered with 10 mM Na<sub>2</sub>HPO<sub>4</sub> and 10 mM H<sub>3</sub>BO<sub>3</sub> electrolyte to pH 4.3 and purged with N<sub>2</sub> for 20 min. The electrolyte was kept under a N<sub>2</sub> atmosphere throughout the measurement. A Pt wire (Bio-Logic, A-002234 Platinum counter electrode coiled, wire diameter 0.5 mm) immersed directly into the electrolyte solution was used as a counter electrode and an Ag/AgCl 3M NaCl (Bio-Logic, A-012167 RE-1B Reference Electrode) was used as the reference electrode. A CHI660 potentiostat was used for all measurements. All electrodes were then characterized by cyclic voltammetry between -0.5 and 0.6 V at various scan rates. The quinone peak potentials were evaluated both for the oxidation (E<sub>pOx</sub>) and for the reduction (E<sub>pRed</sub>) peak by subtracting a linear base-line and fitting the peak to a Gaussian function. The average of the oxidation and reduction peak potential was taken as the quinone formal potential and the evaluated formal potential as a function of scan rate together with the peak potentials. The formal potential (E'<sub>o</sub>) for the different samples was derived by averaging the evaluated formal potentials at different scan rates. The dependence of the peak current with scan rate was investigated by determining the current at (E<sub>pOx</sub>) and (E<sub>pRed</sub>), respectively.

**Quinone and polypyrrole (PPy) estimation in the thin film polymer composite electrodes**

The total capacity was evaluated by integrating the anodic and cathodic sweeps at the lowest scan rate (0.01 V.s<sup>-1</sup>). Capacity originating from PPy was evaluated by subtracting the quinone capacity from the total capacity. Then, that value was multiplied by the weight percentage of PPy in the polymer composite estimated from the elemental analysis of nitrogen.

## Electrochemical tests of the polymer composite suspensions

Electrochemistry studies of the polymer suspensions were performed by using a three-electrode configuration with Ag/AgCl as a reference and platinum wire as a counter electrode and different working electrodes according to their surface area: glassy carbon, glassy carbon ROD, microcavity, and graphite felt (Figure 2.3). The graphite felt was thermally treated at 500 °C for 12 h before use. The three-electrode configuration cells were cycled in a VMP-300 multichannel potentiostat/galvanostat (Bio-Logic). The aqueous based-suspension was purged with N<sub>2</sub> gas for 20 min before measuring. The suspensions were titrated with dilute H<sub>2</sub>SO<sub>4</sub> to the desired pH value at 25 °C. For the series of measurements performed with CO<sub>2</sub> gas, a flow of 80 ml·min<sup>-1</sup> (P<sub>CO<sub>2</sub></sub> = 1 atm and T<sup>a</sup> = 25 °C) was passed through a volume of 20 ml containing a suspension of nanoparticles dispersed in deionized water with a concentration of 1 g·l<sup>-1</sup> for 20 min. Then, the pH was adjusted following the same titration procedure as for the aqueous suspensions without CO<sub>2</sub>.

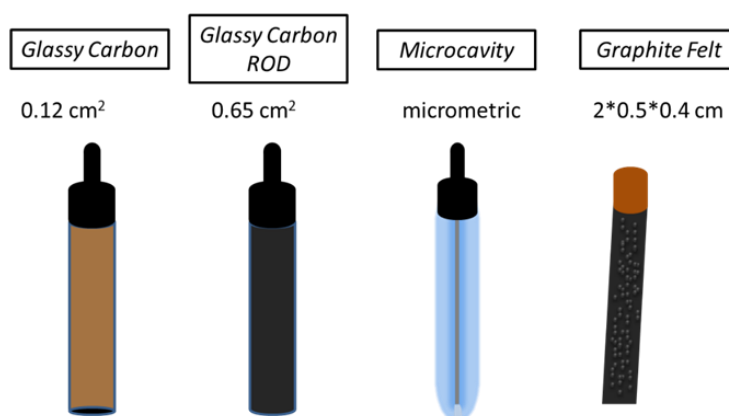


**Figure 2.3.** Working electrodes used and electrode area

## Results and discussion

For the sake of comprehensiveness, the first part of the results and discussion section shows a complete study of the preparation conditions of the new nanoparticles together with their physical and chemical characterization both in solid state and in aqueous media. The second part of the Chapter comprises

the electrochemical analysis of those nanoparticle composite materials showing the highest dispersion in water.

### Physical and chemical characterization

The chemical composition of each compound is important in the structure and morphology of the polymeric hybrids, and therefore in their electrochemical properties.

Firstly, an elemental analysis characterization of the macromolecules to be used for the synthesis of the polymers was carried out in order to evaluate the effect of the different types of lignin and the presence or absence of cellulose. In the characterization, the percentage of sulfonic groups that each type of lignin can be observed (Table 2.3).

**Table 2.3.** Elemental analysis of the components that comprise the material

	<b>LL</b>	<b>LM</b>	<b>LH</b>	<b>PPy</b>	<b>M-Celullose</b>
<b>C (%)</b>	61.6	47.2	40.3	55.6	47.7
<b>H (%)</b>	5.7	4.7	4.6	4.2	7.2
<b>N (%)</b>	0.6	0.1	0	17	0
<b>S (%)</b>	1.6	3.7	4.9	0.1	0.1

Elemental analysis of the different polymers synthesized was subsequently carried out in order to gain a better understanding of their properties (Table 2.4). The Ppy content, deduced from the elemental analysis of nitrogen, was found to be directly related to the elemental sulfur of the sulfonic groups in the lignin biopolymer. The estimated amount of Ppy within the MPLX series shown the tendency: MPLH (19.8 wt.%) > MPLM (11.1 wt.%) > MPLL (5.8 wt.%). From this trend, it was deduced that the interactions between the positive charges in the five-member ring of the pyrrole monomer and the negative charges from the sulphonic anions anchored in the lignin chains might govern a highly efficient assembling between both networks during the polymerization reaction. Besides,

it was reported that sulfonate moiety solubilizes organic substances in aqueous solutions, which might also enable the incorporation of the Ppy polymer in the composite host [19]. Regarding the role of cellulose in the chemical composition of the polymer, MPLH composite shown higher nitrogen content than in PLH (16.9 wt.% Ppy) where cellulose was absent.

**Table 2.4.** Elemental analysis of the polymer composite studied in this Chapter

	MPLL	PLL	MPLM	PLM	MPLH	PLH	MP
<b>C (%)</b>	64.6	63.6	56.7	57.5	54.5	53.9	59.1
<b>H (%)</b>	5.8	5.7	5.5	5.2	5.4	5.3	4.4
<b>N (%)</b>	1.2	1.7	3.1	2.9	4.1	3.5	15.2
<b>S (%)</b>	1.2	1.1	2.5	3.1	3.7	3.5	0.3

Figure 2.4 shows the TEM images of the polymer composites studied in this Chapter. The polymer materials are a series of composites containing either two or three macromolecules. These materials largely comprise individual particles exhibiting spherical morphology with a size ranging between 200 nm for polymers made of methyl-cellulose and polypyrrole (MP, Figure 2.4D) to 20 nm diameter for those materials containing methylcellulose, polypyrrole and highly sulfonated lignin biopolymer (MPLH, Figure 2.4C). The latter composites have a distinctive hierarchical structure with individual polymer nanoparticles assembled in strands or chains such as *necklace beads* (Figures 2.4C.1 and 2.4C.2). Interestingly, when lignin was present, the size of each polymer nanoparticle comprising the strands was one order of magnitude smaller than in MP materials containing two components. Figure 2.4A shows the MPLM sample, where it can be seen how the samples with a low sulfonation of the lignin tend to agglomerate. This agglomeration may be a result of the lower stabilization in the nanohybrid as a consequence of the few sulfonic groups present to stabilize the pyrrole.

The presence of cellulose appears to be essential in all the genesis of each nanoparticle and their assembling along the polymer strand. Cellulose might be acting as a substrate during the initial growth of the conjugated polymer nuclei, favouring the incorporation of the pyrrole and their subsequent polymerization into the nanoparticle's network [20]. The cellulose was probably also a binding agent favouring the connectivity of each nanoparticle along the chains. Besides, cellulose has an impact on the particle aggregation; its absence provokes the loss the sphericity of the nanoparticles as it was observed for those samples made of polypyrrole and highly sulphonated lignin (PLH, Figure 2.4B)

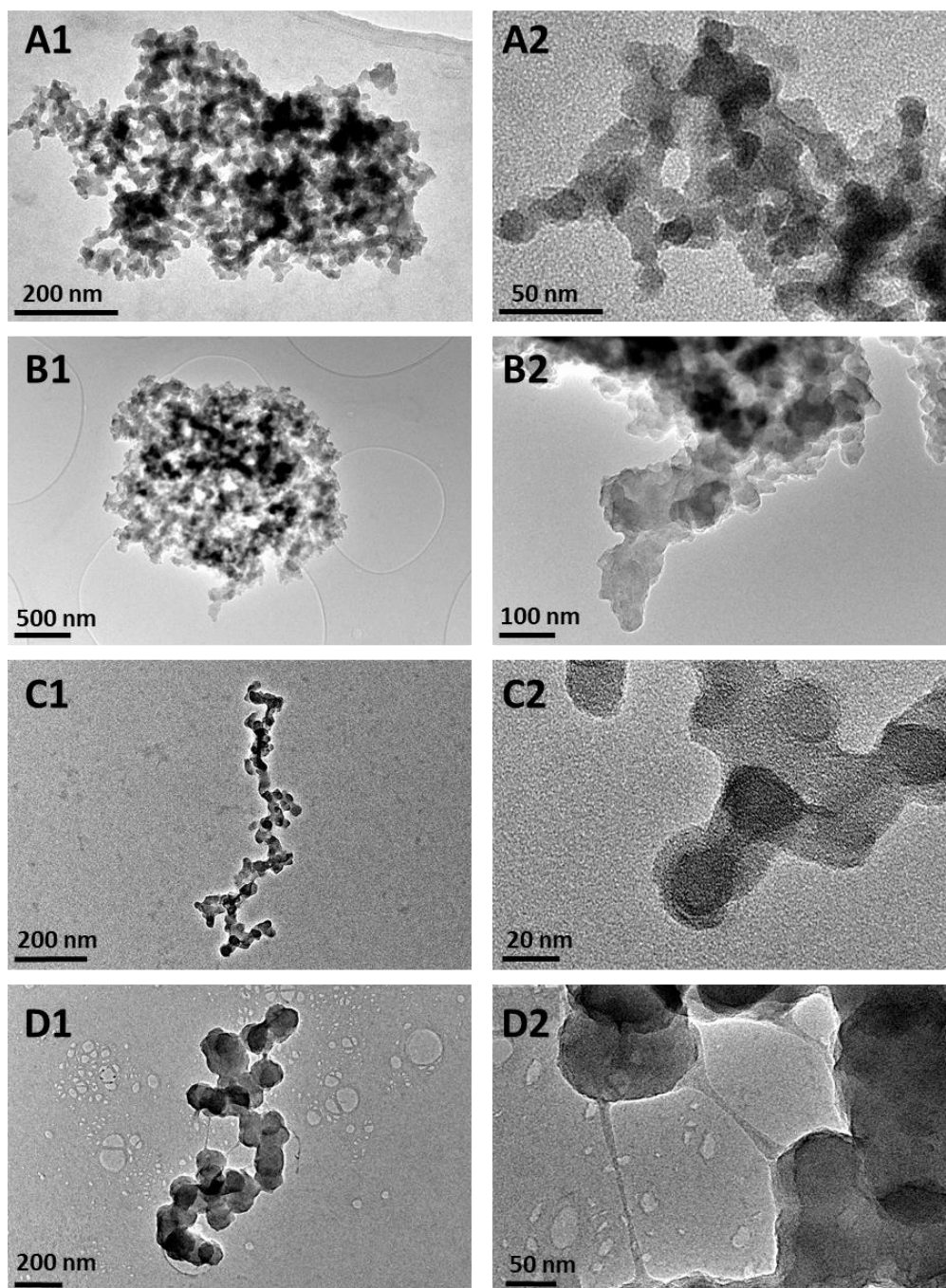


**Figure 2.4.** Transmission electron microscopy images of the different particulate polymer composite materials: A) MPLM, B) PLH, C) MPLH and D) MP. A2, B2, C2 and D2 refer to the zoomed area's from A1, B1, C1 and D1, respectively

To reveal the spatial distribution of each macromolecule in the composite material, energy dispersive X-ray spectroscopy (XEDS) of nitrogen, sulfur and carbon elements was performed during ADF-STEM mode work in the

transmission electron microscope. Figure 2.5 shows a homogeneous distribution of the three components along with the nanoparticles that form the chain confirming that the three macromolecules networks were homogeneously interpenetrated in MLPH composite. The analysis of the distribution of sulfur and nitrogen in the PLH composite also confirmed the homogeneous distribution of polypyrrole and lignin in the nanoparticles of the chains (not shown).

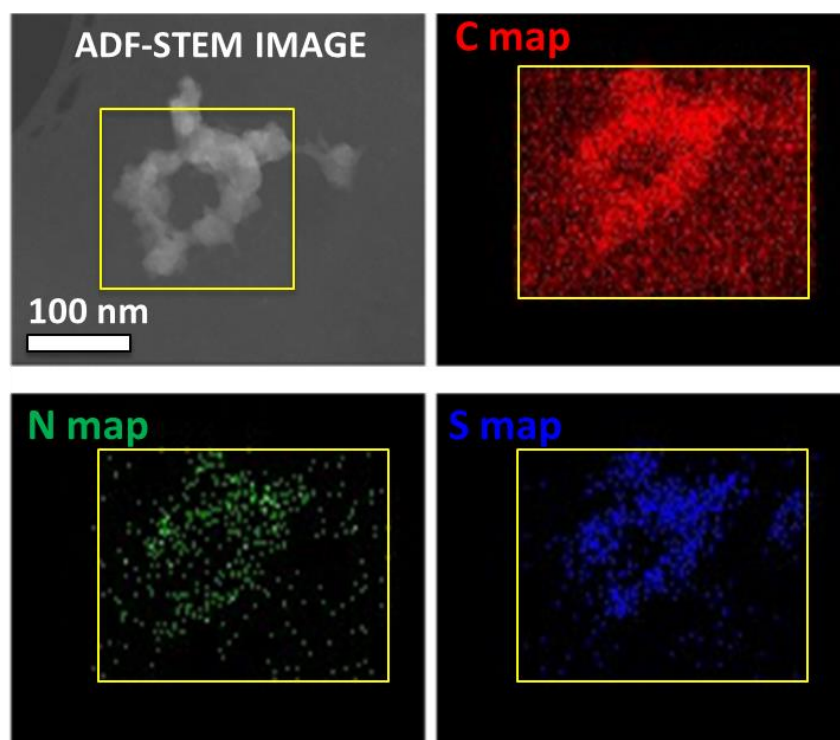


**Figure 2.5.** ADF-STEM image of MPLH and EDX maps showing the chemical distribution of the different elements (C-red, N-green, S-blue) within the structure of the nanohybrid

A shift of the absorption band corresponding to the  $\pi$ - $\pi^*$  transition from 280 nm to 286 nm was also evidenced by UV-vis spectroscopy (Figure 2.6) in the lignin biopolymer and MPLH, respectively. This fact confirms the enhancement of  $\pi$ - $\pi$  interactions between lignin chains in the composite due to the close chemical and electronic coupling at the nanoscale among the different constituents of the metal-free polymer system [21].



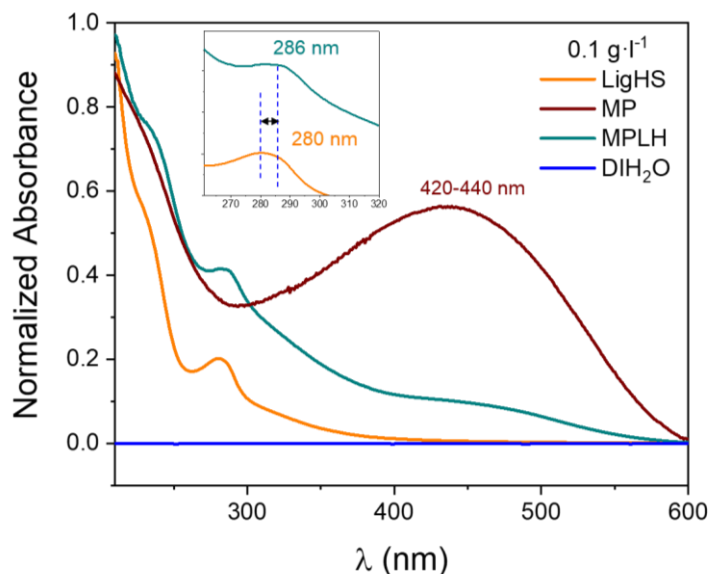


**Figure 2.6.** UV-vis characterization of the lignin biopolymer (LigHS) and the polymer composite suspensions ( $0.1 \text{ g}\cdot\text{l}^{-1}$ ) containing with (MPLH) and without lignin (MP), respectively. The UV-vis spectrum of the deionized water ( $\text{DIH}_2\text{O}$ ) is also added as comparison

The development of low-cost multifunctional electrode materials will require the precise control of their textural properties. This fact will facilitate the molecular contact of the particle surface and chemical species such as water, carbon dioxide, oxygen, hydrogen or electrolyte's ions. Thereby enabling facile catalytic and electrochemical reactions rather than relying on reactions on the limited solid surfaces and interphases. Figure 2.7 shows a comparison between the gas adsorption isotherms for a series of polymer composites. The isotherms clearly show the impact of the polymer composition on the gas up-take capacity of the composite material, and as expected, a trend is observed regarding the volume of the adsorbed gas, the pore size and the surface area (Table 2.5). For example, the hybridization of the methylcellulose with the conjugated polymer increases the pore size from 0.69 nm to 0.77 nm.

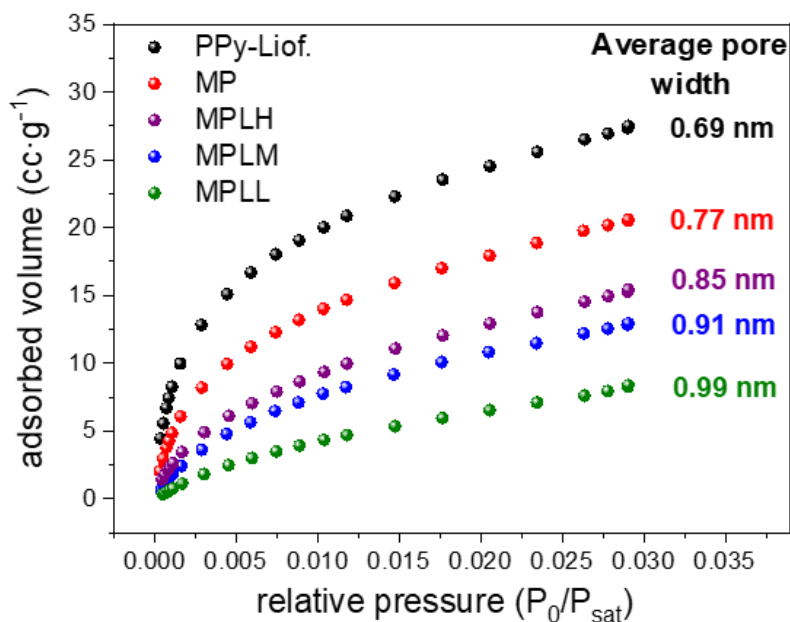


**Figure 2.7.** CO<sub>2</sub> gas adsorption isotherms for the polymer material systems studied in this work

Table 2.5 shows the values of the different textural parameters calculated from the CO<sub>2</sub> adsorption isotherms. The presence of sulphonic groups in the lignin biopolymer has a strong impact on the gas adsorption and textural properties of the MPLX composites series observing a gradual increase on the surface area as the content increases.

**Table 2.5.** Textural parameters of the series of polymer hybrids studied

	MPLL	MPLM	MPLH	PLH	MP	Ppy
<b>Average pore size (nm)</b>	0.99	0.91	0.85	0.99	0.77	0.69
<b>Micropore 106olumen (cc·g<sup>-1</sup>)</b>	0.03	0.05	0.05	0.03	0.06	0.08
<b>Surface area (m<sup>2</sup>·g<sup>-1</sup>)</b>	105	145	151	83	187	231

Moreover, there was a clear relation between the sulphonic content and the final morphology of the composites as it is shown in Figure 2.8, in comparison with the Ppy and MP materials. Noticeable differences such as nanoparticle

aggregation, porosity and particle's sphericity between the composites with three components (MPLM and MPLL) and those without cellulose (PLM and PLL) depending on the content of sulfonic groups in the lignin were also observed by electron scanning microscopy.

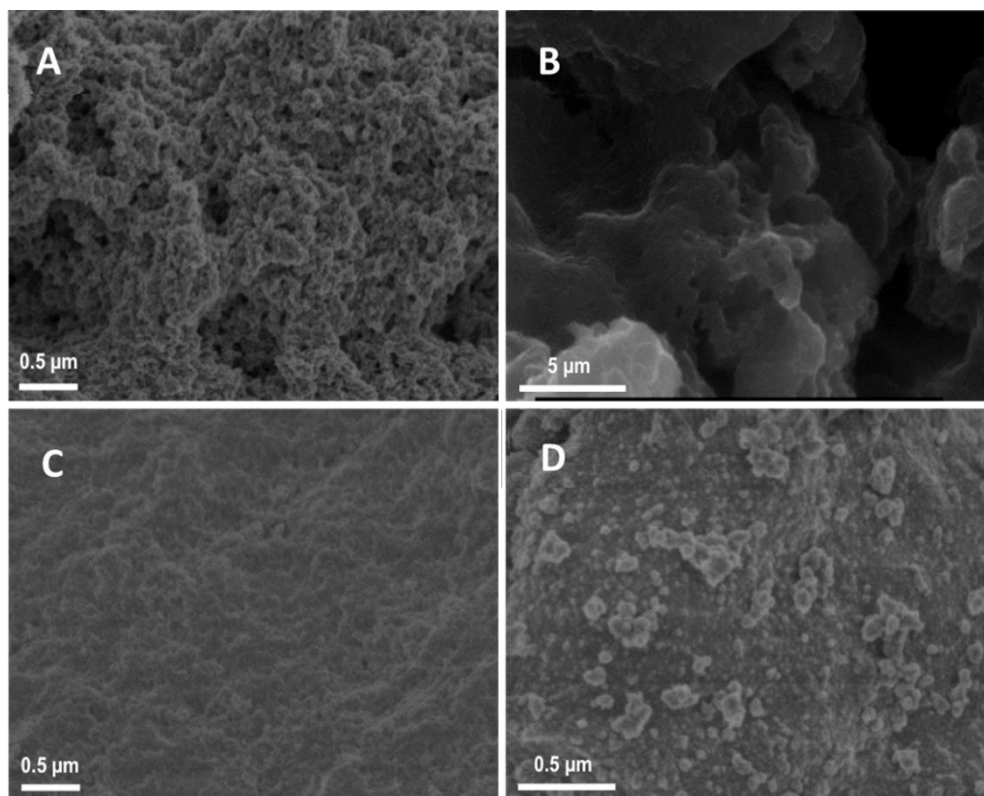


**Figure 2.8.** Scanning electron microscopy images of the polymer composite samples A) MPLM, B) MPLL, C) PLM and D) PLL

Figures 2.9 shows the impact of the chemical composition of the polymer materials on the particle size distribution determined by dynamic light scattering (DLS). As can be seen, the aggregate size distributions of each polymer composite show similar average values ( $\sim 500$  nm) in water after sonication for 15 min. The MPLH composite shows improved long-term stability in water than the PLH sample that precipitated after a few minutes, corroborating the high influence of the cellulose polymer in the stability of the composite suspensions. In addition, the polymer composites enclosing lignin with medium and low content of sulphonic groups exhibited higher aggregate size than those composites containing highly sulfonated lignin (Figure 2.9 C and D)

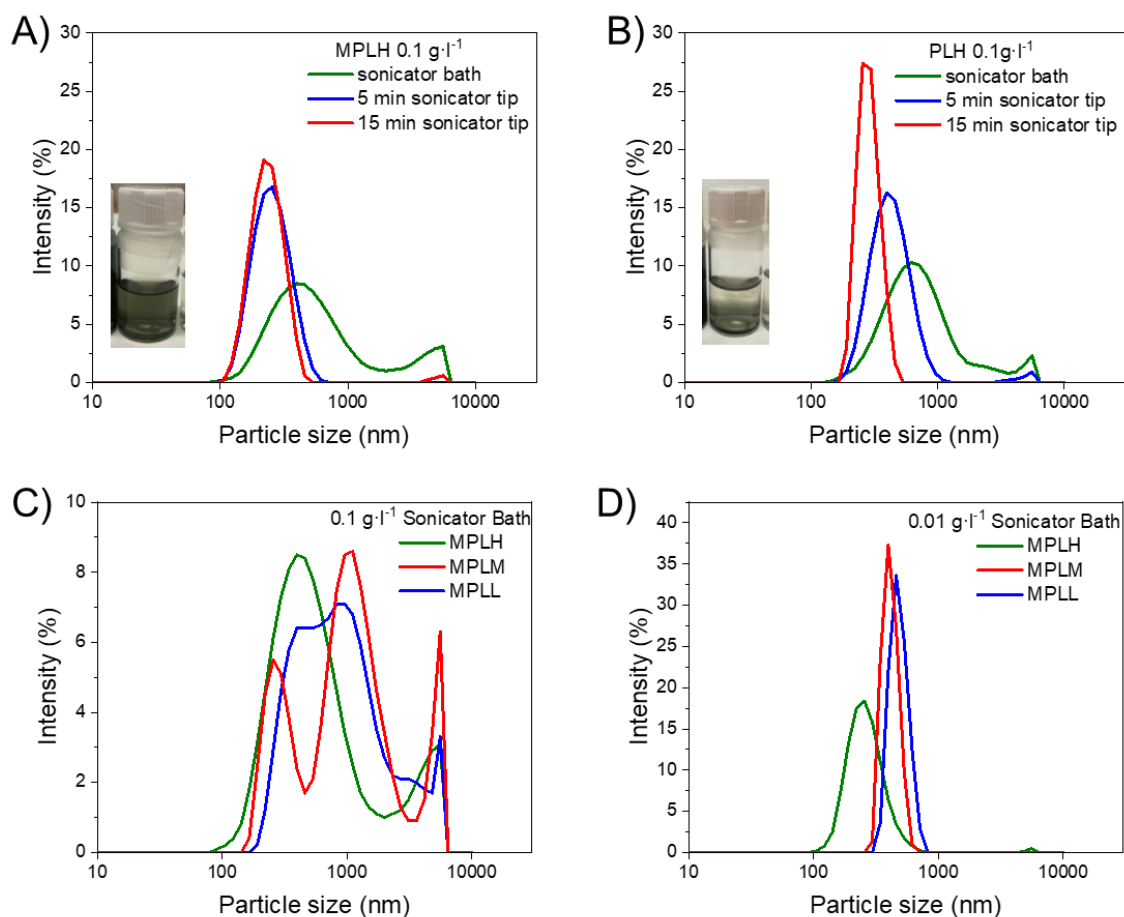


**Figure 2.9.** Characterization by dynamic light scattering (DLS) of the polymer composite suspensions containing A) MPLH and B) PLH. MPLH, MPLM, MPLL polymer suspensions with a concentration of C) 0.1g·l<sup>-1</sup> and D) 0.01 g·l<sup>-1</sup>

Figure 2.10 shows the values of zeta potential for the series of polymeric samples at different concentrations in water. The Ppy and MP suspensions exhibited positive values of zeta potential, while those samples containing lignin were in the negative zone. This fact might be due to a higher impact of the negative charges of sulfonic groups than the positive from the pyrrole monomer on the overall surface. In fact, as the content of Ppy augments, the zeta potential value also increases towards more positive values balancing the total charge. This fact makes the MPLH values higher than those of MPLM and MPLL. It is observed that as the concentration increases the values become more positive, due to increased interactions in the material resulting in less exposed surface area.

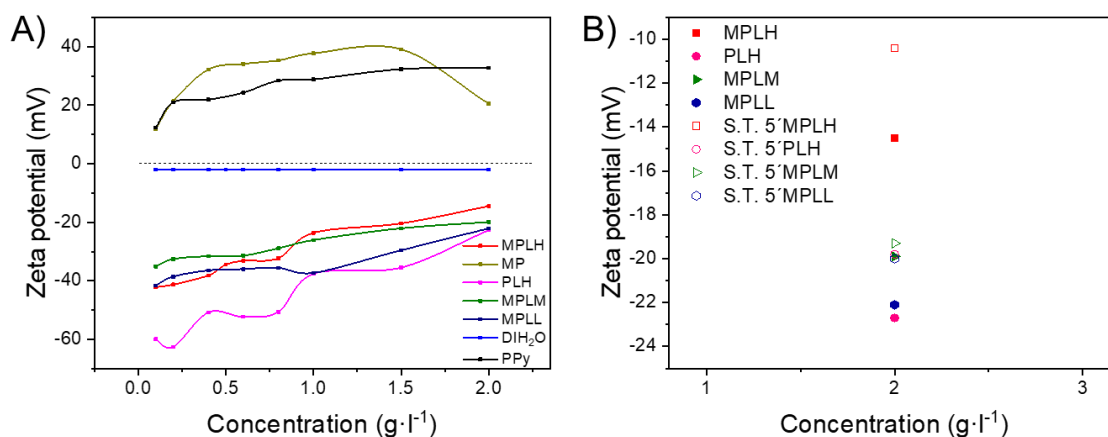


**Figure 2.10.** A) Correlation between the zeta potential values and the concentration of polymeric materials suspended in deionized water; B) zeta potential values at the same concentration (2 g·l<sup>-1</sup>) and bath sonicated for 5 min

Figure 2.11 shows the correlation between the ionization constant (pK) and the zeta potential values at different pH for an MPLH polymer suspension. A pH region with two pK's constants (pK ≈ 1.5 and 9) was found in agreement with the change of zeta potential observed at acidic and basic pH. A 1 g·l<sup>-1</sup> suspension of MPLH particles dispersed in deionized water is negatively charged, with a zeta potential value close to -30 mV and a pH value of approximately 4. In the pH range comprising the two ionization constants, this suspension preserves its stability even if a tiny amount of acid/base can easily change its pH. So, there was not a correlation between the acid-base properties, the zeta potential values and the permanence in the suspension of the MPLH composite particles. Out of this range, the polymer particles progressively lose their stability and do not remain in suspension. Therefore, the precipitation of the polymer composite particles in aqueous media might be due to the hydrolysis and oxidation of the methylcellulose polymer at low and high pH values, respectively.

In addition, cellulose has shown a negligible influence on the pH and the zeta potential values (Figure 2.11 B and C). So, the acid-base character and the charge surface values of the particles must be mainly governed by the synergistic combination of the physical and chemical properties at the

nanoscale of the Ppy and lignin macromolecules, being this interaction also mediated by the presence of the cellulose.

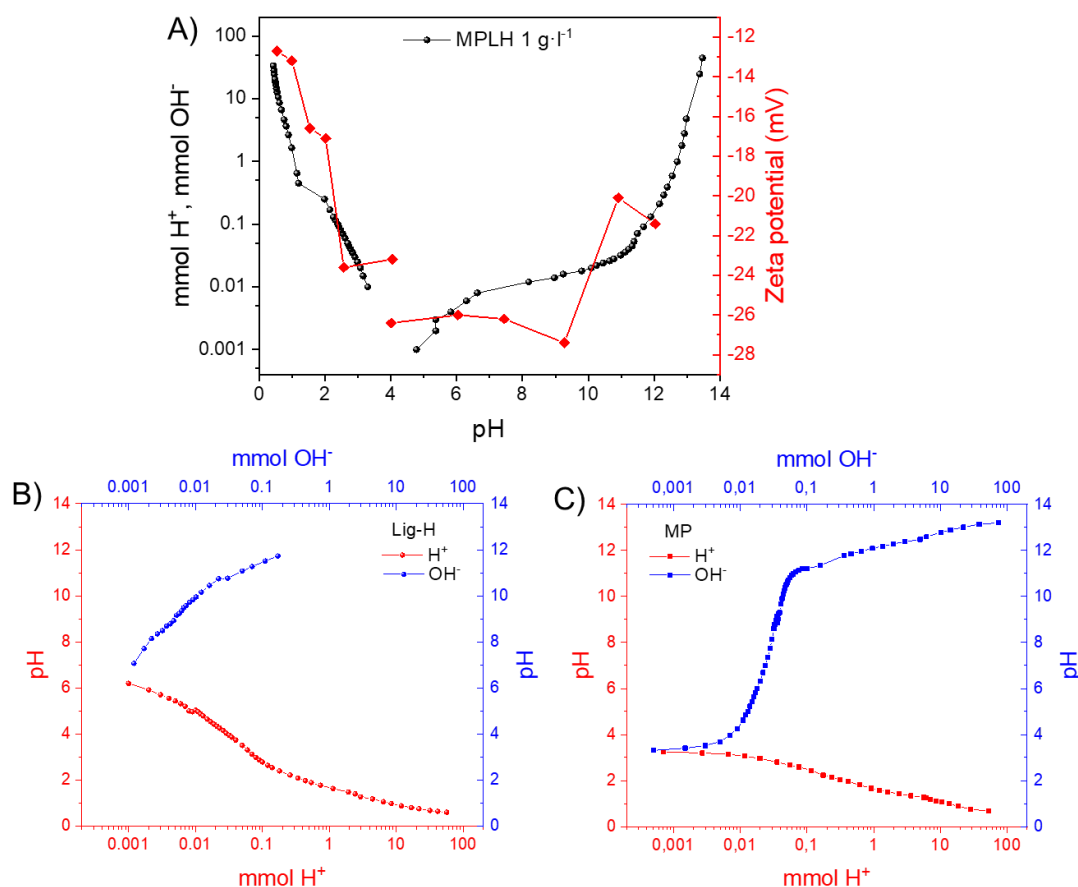


**Figure 2.11.** A) Correlation between the acid-base properties measured by titration and the zeta potential values for MPLH material. B) Acid-base titration curves of lignin biopolymer (Lig-HS) and C) methylcellulose-polypyrrole (MP) composite materials

After previous characterization studies of our batch of materials, MPLH and PLH are finally chosen as the optimal candidates for the intended application.

### Electrochemical analysis

The material has been studied by using two different electrochemical techniques, on the one hand, cyclic voltammetry, which provides qualitative information on the different redox processes and the reversibility of the redox reaction; and on the other hand, galvanostatic methods in which the material is subjected to reduction and oxidation cycles at constant current. Both techniques

have been performed at 23 °C and atmospheric pressure in a multichannel potentiostat/galvanostat.

In the electrochemical characterization, several parameters have been considered to obtain the suitable system for its characterization. On the one hand, solid measurements of the material have been carried out. It has been studied in solution varying parameters such as polymer concentration, working electrode, presence of salts, inorganic buffer medium, different acid concentrations and the effect of pH.

The electrochemistry of thin film polymer composite electrodes was studied in order to estimate the content of redox active quinone units in the polymer. Because MPLH and PLH composite materials show the highest amount of PPy in their composition they were chosen as the most suitable candidates. Figure 2.12 shows the voltammetric curves for an MPLH sample with current values normalized by the scan rates. The peak at 0.55 V vs Ag/AgCl is assigned to the lignin biopolymer as the potential agrees well with previously reported formal potentials of lignin. The capacitive response in the region -0.2 and -0.2 V vs Ag/AgCl is ascribed to the doping of the PPy component of the composite. As typical for PPy electrochemistry there is a doping on-set around -0.4 V vs Ag/AgCl [22].

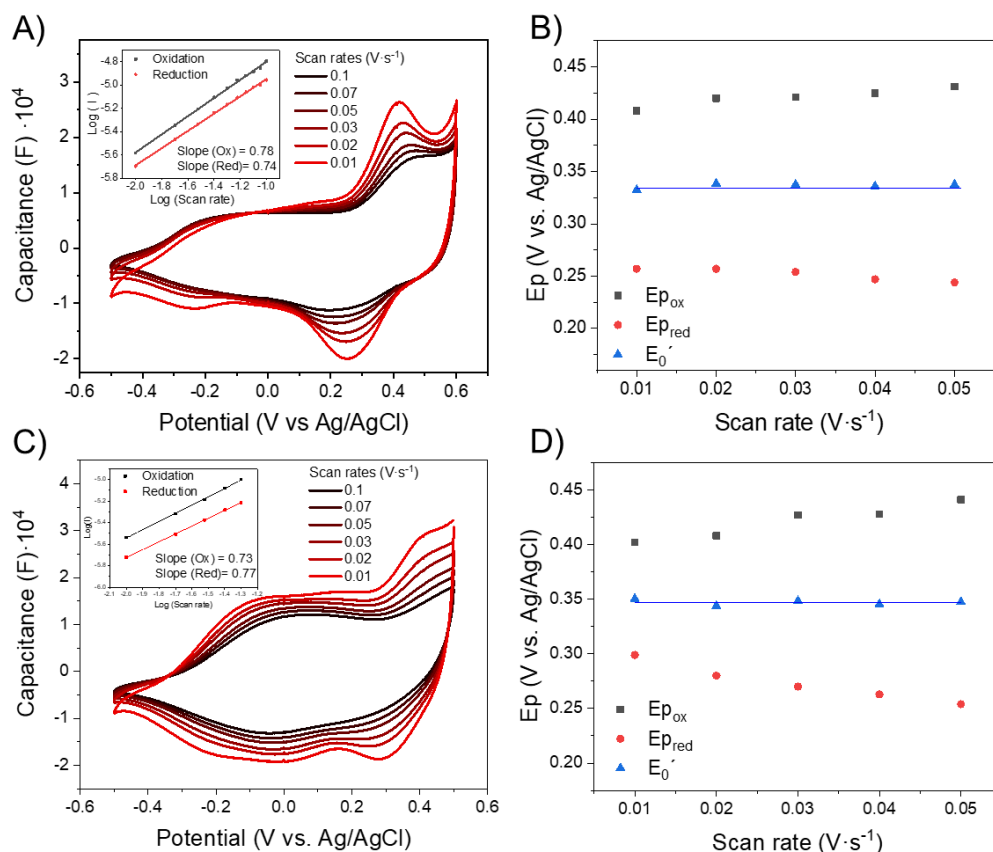


**Figure 2.12.** A) Cyclic voltammetry of a thin-layer of MPLH electrode showing the current normalized at different scan rates. Inset: log (Absolute peak currents) as a function of log (scan rate) of oxidation (black curve) and reduction (red curve) process of MPLH. MPLH layers were then characterized electrochemically in 1 M NaCl<sub>aq</sub> buffered with 10 mM Na<sub>2</sub>HPO<sub>4</sub> and 10 mM H<sub>3</sub>BO<sub>3</sub> to pH 4,3 and purged with N<sub>2</sub> for 20 min. B) Evaluated peak potentials and formal potentials at various scan rates for MPLH composite. C) Voltammetric response for the PLH sample at various scan rates (V s<sup>-1</sup>) with currents normalized to the scan rate. Inset: Log (Absolute peak currents) as function of Log (Scan rate) for PLH. D) Upper curve (black) = oxidation, lower curve (red) = reduction process. evaluated peak potentials and formal potentials at various scan rates for PLH

The dependence of both, oxidation, and reduction absolute peaks current with scan rate for MPLH and PLH electrodes are displayed in the inset plot in Figure 2.12. The corresponding slopes are between 0.7 and 0.8. Similar dependence on both oxidation and reduction peaks and slope values were found for the PLH sample. The integration of the lignin peak, after subtraction of a linear base-line,



indicates a lower capacity for PLH than for the MPLH electrode (Table 2.6). For MPLH a quinone capacity of  $1.62 \cdot 10^{-5}$  C corresponding to  $1.68 \cdot 10^{-10}$  mol charges was evidenced. This value is higher compared to the corresponding quinone capacity in PLH which was evaluated to  $5.33 \cdot 10^{-6}$  C corresponding to  $5.52 \cdot 10^{-11}$  mol charges per 2.5 ml suspension used in the preparation of the thin-film electrodes. The remaining charge was assigned to PPy and was evaluated to  $350 \text{ C} \cdot \text{g}^{-1}$  in PHL, a value more than twice the value found for the highly-water dispersible MPLH composite material of  $157 \text{ C} \cdot \text{g}^{-1}$ .

**Table 2.6.** Shows the values for the quinone and PPy concentration values inferred from electrochemical measurements. \*The meaning of C is coulombs

	<b>Quinone Capacity (C*)</b>	<b>Quinone Concentration (M)</b>	<b>PPy Capacity (C*)</b>	<b>PPy Capacity (C·g<sup>-1</sup>)</b>
<b>MPLH</b>	$1.62 \cdot 10^{-5}$	$3.36 \cdot 10^{-5}$	$7.8 \cdot 10^{-5}$	158
<b>PLH</b>	$5.33 \cdot 10^{-6}$	$1.10 \cdot 10^{-5}$	$1.4 \cdot 10^{-4}$	350

Figure 2.13A shows the cyclic voltammograms (CVs) for a suspension of the MPLH composite particles in an aqueous solution at different pH values. The voltammograms exhibit one principal redox peak over the pH range 0.8-3.7 corresponding to the reversible electrochemical transformation of the hydroquinone into quinone moieties in lignin biopolymer as it is shown in Scheme 2.2. Figure 2.13B shows the electrochemistry for the MPLH nanoparticles suspended in an aqueous acidic media saturated with CO<sub>2</sub> gas. Interestingly, the CV's show two electrochemical processes, both occurring at positive potential vs Ag/AgCl as a reference electrode. A couple of redox peaks at higher potential, Process I, corresponds to the above-mentioned redox reaction of the catechol units in lignin; the another at a lower potential, Process II, has been assigned to other catechol units with more oxygen groups coming from methoxy groups or neighboring C9-O- group directly connected to the phenyl ring [16]. Because of the strong electron-donating effect of the oxygen atoms, a significant lower redox potential value than for Process I were

observed. The consideration and subsequent discarding of other possible causes for the three redox stages support this proposition.

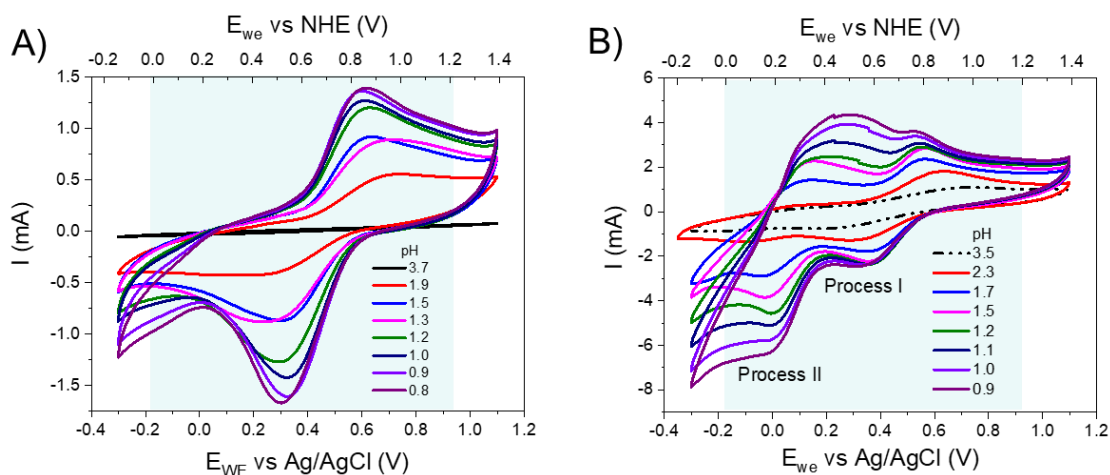


**Figure 2.13.** Electrochemical characterization of the polymer composites suspensions by using a three-electrode cell configuration. Cyclic voltammograms in an aqueous acidic media A) without and B) with  $CO_2$  of the MPLH polymer composite suspensions

For instance, the possible generation of hydrogen gas by the reduction of protons to molecular hydrogen at the surface of the working electrode has been studied. For this purpose, an electrochemical reduction at a constant current of an aqueous suspension ( $pH \sim 1$ ) of MPLH material ( $1 \text{ g}\cdot\text{l}^{-1}$ ) has been performed in an electrolyzer cell comprising three compartments separated each of them by a Nafion<sup>®</sup> 117 membranes (Figure 2.14). Because it is well known that Pt is an excellent catalyst for the  $H_2$  evolution reaction, the use of this experimental setup prevented the dissolution, migration, and deposition of Pt nanoparticles from the counter electrode to the surface of the working electrode as well as the interference of the  $H_2$  gas, sometimes visible even by the naked eye, produced also by Pt. After cycling during  $> 7 \text{ h}$  at  $0.25 \text{ mA}$ , the solid polymer nanoparticles were decanted, and the liquid supernatant phase analyzed by liquid proton NMR in an air-free tube [23].

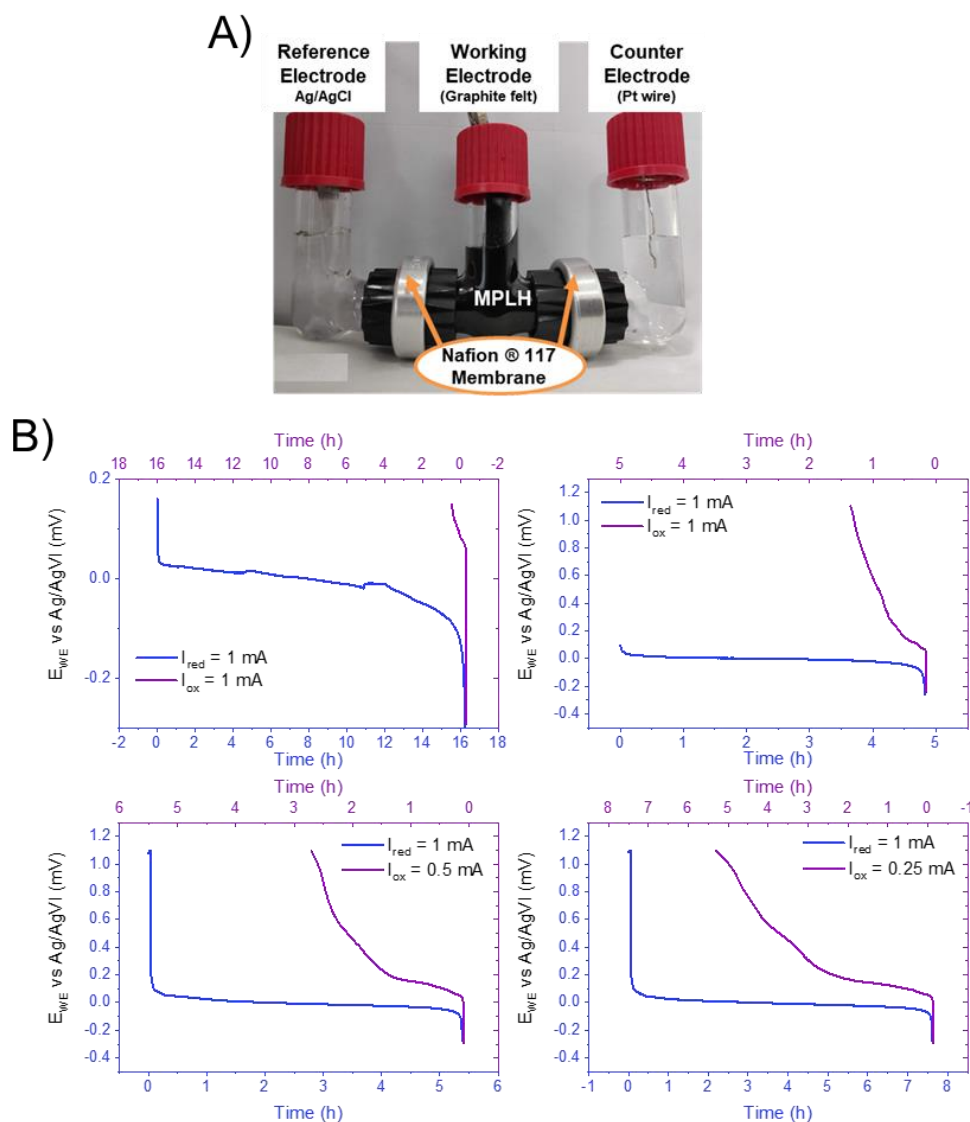


**Figure 2.14.** A) Galvanostatic study of a suspension of MPLH with a concentration of  $1 \text{ g}\cdot\text{l}^{-1}$  in an aqueous media with  $\text{CO}_2$  in an electrolyzer cell comprising three compartments separated each of them by a Nafion® 117 membrane. B) Galvanostatic reduction and oxidation cycles at different conditions

The absence in the spectra of the resonance corresponding to molecular hydrogen confirmed that Process II is not due to a reversible hydrogen reaction formation (Figure 2.15). This result was expected, as the thermodynamic potential for hydrogen evolution is much lower than the experimental one observed here under similar acidic conditions [23]. Moreover, the potential for  $\text{H}_2$  formation has also been evidenced by CV by opening the potential window

progressively while cycling an MPLH suspension (Figure 2.16). Therefore, the reorganization of the interpenetrated polymer network in the presence of CO<sub>2</sub> is considered as the most plausible reason to explain the amplification of Process II.

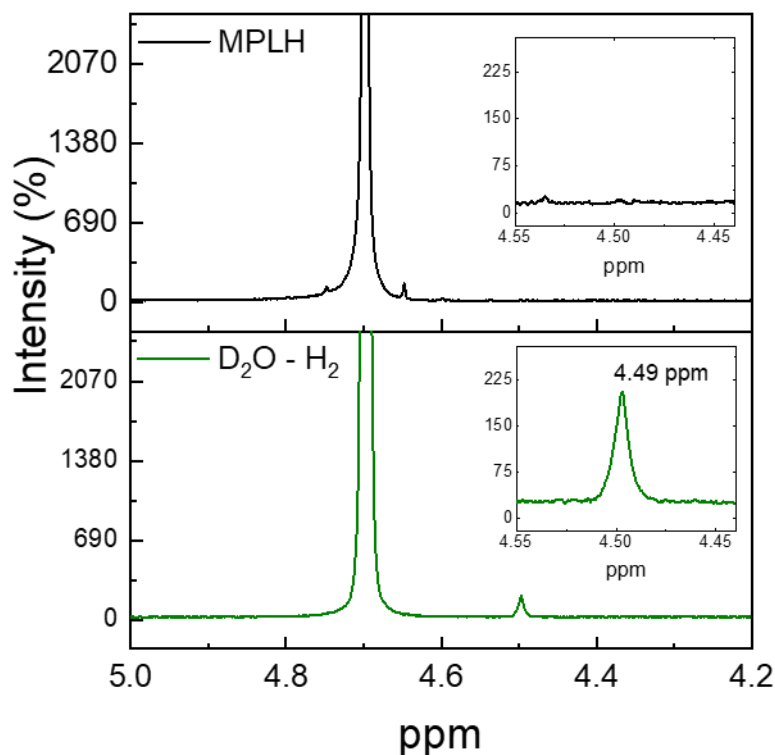


**Figure 2.15.** <sup>1</sup>H-NMR spectrum of a MPLH suspension (1 g·l<sup>-1</sup>; 5 ml) in D<sub>2</sub>O solvent reduced at 0.25 mA for > 7 h. After cycling, the solid polymer nanoparticles were decanted, and the liquid supernatant phase analyzed by liquid proton NMR in an air free tube (upper plot). The spectrum of D<sub>2</sub>O solvent containing H<sub>2</sub> gas is also shown as a comparison (bottom plot)

The presence of CO<sub>2</sub> also led enhancement of the absolute magnitudes of the anodic and cathodic current peak-heights of the Process I in the MPLH composite (Figure 2.17).

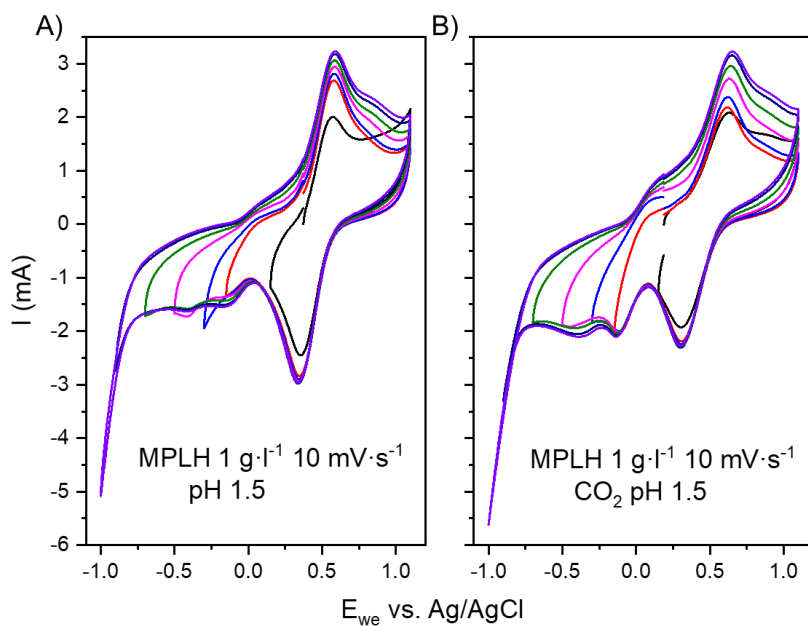


**Figure 2.16.** Potential window opening study with A) and without CO<sub>2</sub> B). In both with and without CO<sub>2</sub> when the potential window is opened, the formation of hydrogen begins to be observed

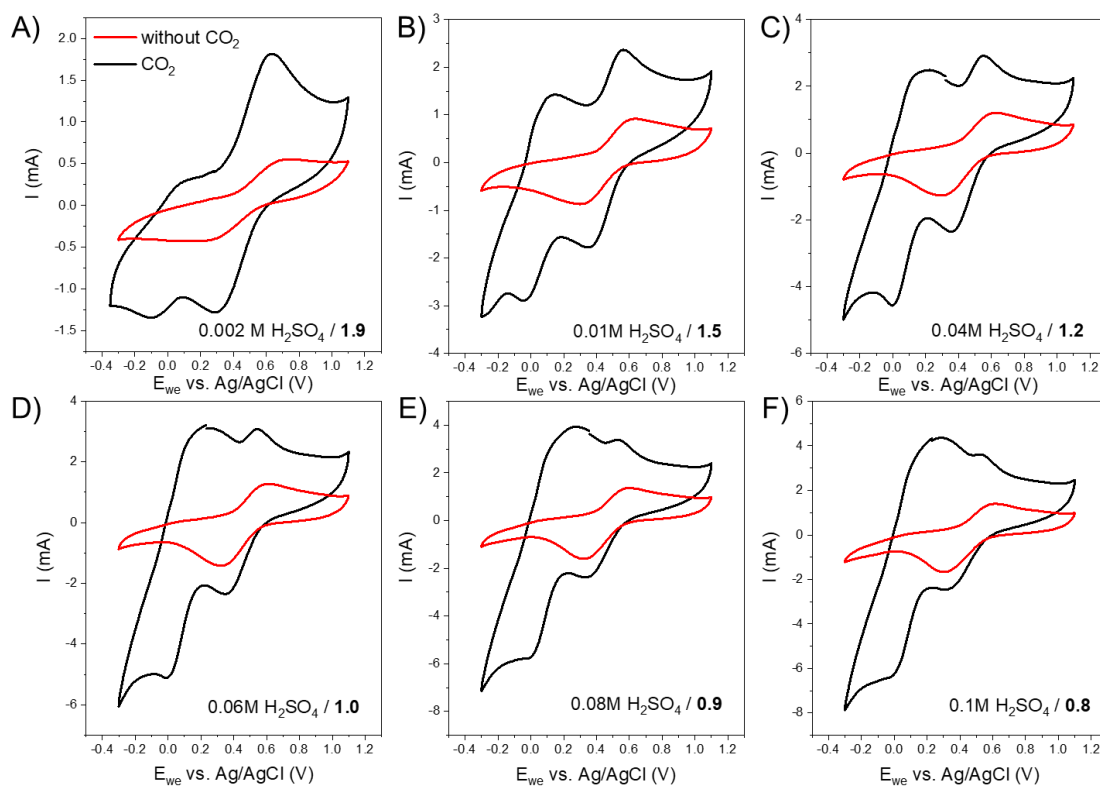


**Figure 2.17.** Effect of the presence of CO<sub>2</sub> on the electrochemistry of the polymer nanoparticle suspension at different pH. The pH value is in bold

Moreover, when lignin is nanoconfined into the MPLH's particle an anomalous pH-dependence of the equilibrium potential for the Process I was found as it is shown in Figure 2.4C. Two well-defined regions exhibiting two different slopes values were evidenced independently of whether CO<sub>2</sub> was present or not. The slope value of the equilibrium potential achieves a value of -4 mV·pH<sup>-1</sup> in the pH range between 1.2 and 3.5 in the presence of CO<sub>2</sub>. This value, closer to zero, might indicate that both oxidized and reduced chemical forms in lignin are fully deprotonated or that the local pH at the surface of the polymer composite might be buffered due to the presence of dissolved CO<sub>2</sub>. For Process II occurring in the MPLH particles, the electrochemistry with CO<sub>2</sub> shows a linear pH dependence. For the non-confined lignin biopolymer, the equilibrium potential of the Process I is pH-dependent under the presence of CO<sub>2</sub> in the whole range of pH (Figure 2.18). In fact, the average slope of the equilibrium redox potential versus pH over the pH range 0.5–4.6 is -49 mV·pH<sup>-1</sup> unit, which is close to the value of -59 mV·pH<sup>-1</sup> expected from a two-electron, two-proton process. The linear fit to the data between pH 0.9-3.5 for the Process II revealed a slope value of -98 mV·pH<sup>-1</sup>. Moreover, the anodic and cathodic intensity of the peaks corresponding to the restructured lignin moieties follows a linear dependency with the pH as it is shown in Figure 2.18B. Remarkably, the presence of carbon dioxide, a widely available greenhouse emission gas, boosted the second process reaction by 500 % at a pH value of 0.8.

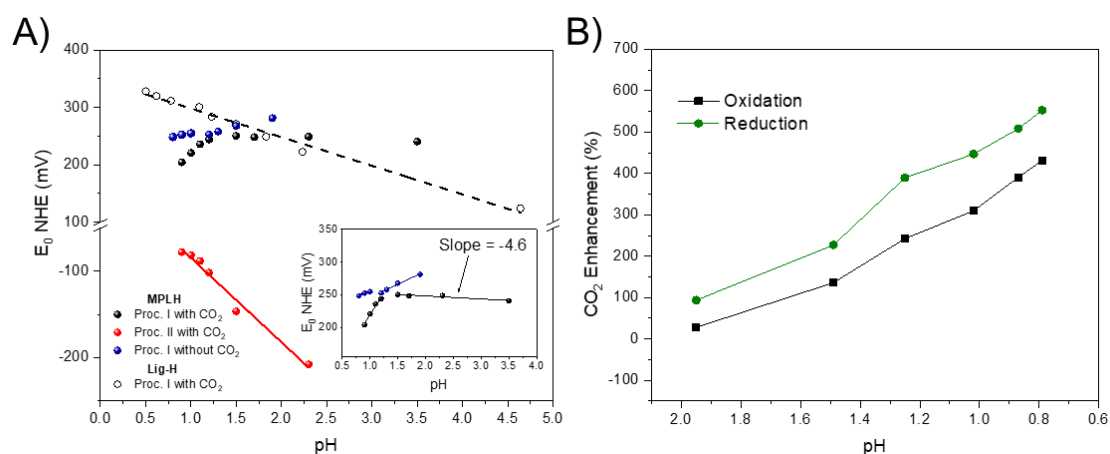


**Figure 2.18.** A) The Pourbaix diagram of MPLH water-based suspensions with and without CO<sub>2</sub>. B) Anodic and cathodic currents for the reversible

---

---

transformation of protons to hydrogen. (Pt wire was used as a counter electrode and Ag/AgCl as a reference electrode; Scan rate = 10 mV·s<sup>-1</sup>)

The same recharge experiment was performed for a solid MPLH composite electrode with and without CO<sub>2</sub> and there was no evidence of an additional redox step other than the reversible oxidation/reduction of the quinone groups on the lignin (Figure 2.19). The occurrence of three redox stages corresponding to the presence of two waves was only observed when the polymer nanoparticles were in suspension. The main reason behind this behavior might be due to the relatively larger sample volume of the particles in suspension than in the solid electrode set-up. Effectively this means that electrochemical conversion might be only related to a thin layer close to the polymer surface, which is in good agreement with the abovementioned result. In suspension, those nanoparticles that is in contact with the surface of the electrode are being constantly replaced by fresh material that was converted during cycling. Under these operation conditions, the system works at higher conversion enlightening a distinct cost-effectively approach for electrochemical charge storage.

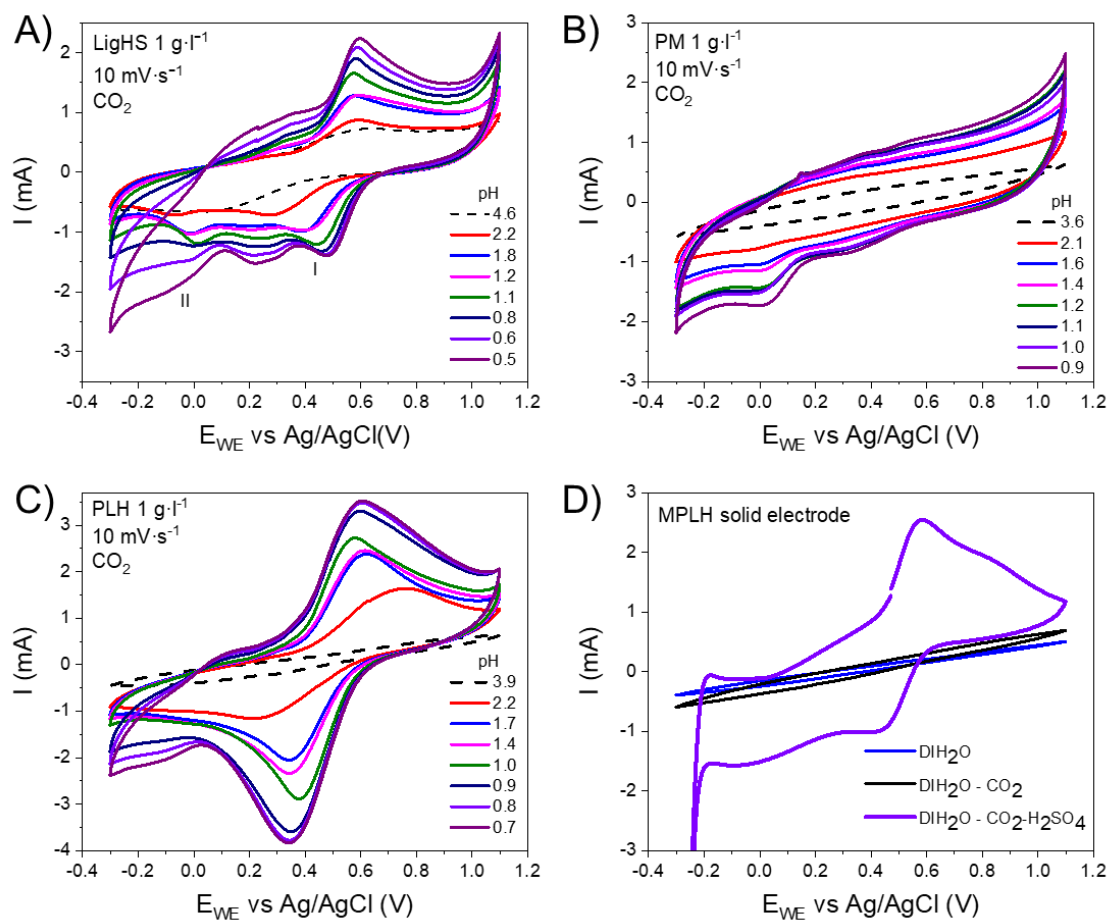


**Figure 2.19.** Electrochemical characterization of the polymer composites suspensions by using a three-electrode cell configuration (Pt wire was used as a counter electrode and Ag/AgCl as reference electrode and graphite felt as work electrode). Cyclic voltammograms in an aqueous acidic media with CO<sub>2</sub> A) of the Lig-H suspensions B) of PM suspension C) of PLH suspension. D) Electrochemical characterization of nanoparticles using three electrodes configuration, with MPLH solid electrode. In aqueous medium under different conditions, presence of CO<sub>2</sub> and acidic medium

Figure 2.20 shows the proposed mechanism's sequence to explain the electrochemical behavior observed in the polymer composite nanoparticles with and without the presence of CO<sub>2</sub> gas at different pH values. As stated above, the electrochemical processes occur most probably at the surface. Then, when the MPLH nanoparticles are placed in deionized water, the pH value is close to 4 and the surface charge value is -30 mV. These values are mainly produced by the presence of hydrated sulfonic groups on the surface of the particle. At this point, it hardly observes any redox process due to the slow kinetics of the



---

---

reaction provoked by the deficiency of protons (Figure 2.20A). When the suspension is acidified the Process I, corresponding to the reversible oxidation/reduction reaction of the catechol groups (the predominant couple) in lignin emerge. Also, the value of the zeta potential increases becoming more positive. This change in the average value of the charge at the surface provokes that part of the sulphonic groups initially doping the polypyrrole, now tend to face the nanoparticle's surface, interacting electrostatically with the protons and water molecules from the solution. Under these conditions a spatial alteration of the interpenetrated polymer network might occur (Figure 2.20B). When the CO<sub>2</sub> is added, noticeable changes are reflected in the CV such as the appearance of the Process II coexisting with the Process I. This situation might be favoring the structural rearrangement of the interacting macromolecules along the interpenetrated network [24]. For example, the polypyrrole may act as an electrophile interacting with the bicarbonate anion forming a stable adduct, then changing their physical and chemical interrelation with the biopolymers (Figure 2.20C) [25].

Therefore, here CO<sub>2</sub> is not electro reduced and is simply acting as a precursor of the species formed after hydration (carbonic acid, bicarbonate anion) [26]. It cannot be ruled out also the possible formation of a carbonate between the CO<sub>2</sub> molecule and the semiquinone that can be protonated at low pH and appear or consume protons also promoting the rearrangement of the interpenetrated polymeric network [27].

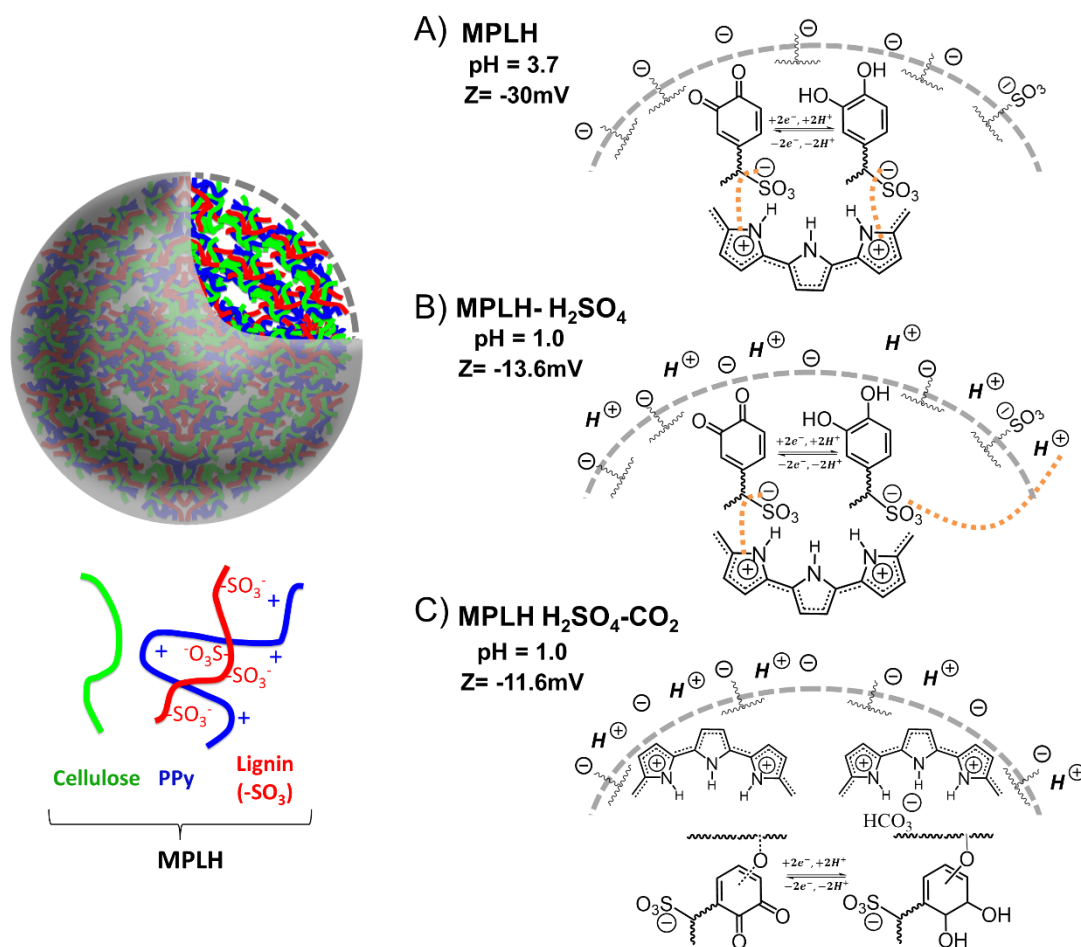


**Figure 2.20.** The proposed mechanism to explain the presence of three redox stages in the polymer composite nanomaterial in the presence of CO<sub>2</sub>

## Conclusions

In this Chapter, a new sustainable multifunctional nanomaterial has been designed that uses CO<sub>2</sub> as a useful resource to reversibly store electricity. The novel material is a hierarchically structured polymer composite that is made of inexpensive and environmentally friendly macromolecules such as methylcellulose, which assisted the creation of the nanoparticles during the colloidal polymerization and endorsed long-time stability to the polymer active suspensions in water. From cyclic voltammetry measurements, two main reversible processes were observed corresponding to the redox reaction of the lignin biopolymer. The process at the lower potential is enhanced by up to 500 % by the presence of carbon dioxide. The novel properties might be originated from an intimate chemical and electronic connection at the nanoscale among

the different components of the polymer composite and the structural rearrangement of the lignin biopolymer by the incorporation of CO<sub>2</sub>.

This creative strategy enjoys multiple advantages such as the utilization of low-cost raw matters and sustainable pathways for designing advanced multifunctional materials; the application of greenhouse gases such as CO<sub>2</sub> to promote chemical reactions by the same active multifunctional nanostructured material dispersed in water. The proposed metal-free polymer composite–CO<sub>2</sub> system could potentially serve as a new CO<sub>2</sub> utilization technology in the time of pursuing sustainable energy and environmentally friendly systems for the future. The new low-cost advanced functional nanomaterial offers the opportunity to address two main energy and environmental challenges: global warming and polluting atmosphere from greenhouse gas emissions and the generation of electricity along with energy storage from renewable sources.

## References

- [1] D. Greenwood, S. Walker, N. Wade, S. Munoz-Vaca, A. Crossland, and C. Patsios, "Integration of high penetrations of intermittent renewable generation in future electricity networks using storage," *Future Energy: Improved, Sustainable and Clean Options for Our Planet*, pp. 649–668, Jan. **2020**, doi: 10.1016/B978-0-08-102886-5.00030-X.
- [2] H. Zsiborács *et al.*, "Intermittent renewable energy sources: the role of energy storage in the european power system of 2040," *Electronics 2019, Vol. 8, Page 729*, vol. 8, no. 7, p. 729, Jun. **2019**, doi: 10.3390/ELECTRONICS8070729.
- [3] S. Chu, Y. Cui, and N. Liu, "The path towards sustainable energy," *Nat Mater*, vol. 16, no. 1, pp. 16–22, Jan. **2017**, doi: 10.1038/nmat4834.
- [4] A. I. Hassan and H. M. Saleh, "Nanomaterials for the conversion of carbon dioxide into renewable fuels," in *Advanced Technology for the Conversion of Waste Into Fuels and Chemicals*, Elsevier, **2021**, pp. 1–20. doi: 10.1016/B978-0-323-90150-5.00005-4.
- [5] D. Larcher and J.-M. Tarascon, "Towards greener and more sustainable batteries for electrical energy storage," *Nat Chem*, vol. 7, no. 1, pp. 19–29, Jan. **2015**, doi: 10.1038/nchem.2085.
- [6] A. S. Aricò, P. Bruce, B. Scrosati, J.-M. Tarascon, and W. van Schalkwijk, "Nanostructured materials for advanced energy conversion and storage devices," in *Mater Renew Sustain Energy*, Co-Published with Macmillan Publishers Ltd, UK, **2010**, pp. 148–159. doi: 10.1142/9789814317665\_0022.
- [7] B. Kang and G. Ceder, "Battery materials for ultrafast charging and discharging," *Nature*, vol. 458, no. 7235, pp. 190–193, Mar. **2009**, doi: 10.1038/nature07853.
- [8] G. Milczarek and O. Inganäs, "Renewable cathode materials from biopolymer/conjugated polymer interpenetrating networks," *Science (1979)*, vol. 335, no. 6075, pp. 1468–1471, Mar. **2012**, doi: 10.1126/science.1215159.
- [9] C. K. Chan *et al.*, "High-performance lithium battery anodes using silicon nanowires," *Nat Nanotechnol*, vol. 3, no. 1, pp. 31–35, Jan. **2008**, doi: 10.1038/nnano.2007.411.
- [10] K. B. Hatzell, M. Boota, and Y. Gogotsi, "Materials for suspension (semi-solid) electrodes for energy and water technologies," *Chem Soc Rev*, vol. 44, no. 23, pp. 8664–8687, **2015**, doi: 10.1039/C5CS00279F.
- [11] M. Duduta *et al.*, "Semi-solid lithium rechargeable flow battery," *Adv Energy Mater*, vol. 1, no. 4, pp. 511–516, Jul. **2011**, doi: 10.1002/aenm.201100152.
- [12] P. Leung *et al.*, "Recent developments in organic redox flow batteries: A critical review," *J Power Sources*, vol. 360, pp. 243–283, Aug. **2017**, doi: 10.1016/j.jpowsour.2017.05.057.
- [13] W. Yan *et al.*, "All-polymer particulate slurry batteries," *Nat Commun*, vol. 10, no. 1, p. 2513, Dec. **2019**, doi: 10.1038/s41467-019-10607-0.

- [14] T. Janoschka *et al.*, “An aqueous, polymer-based redox-flow battery using non-corrosive, safe, and low-cost materials,” *Nature*, vol. 527, no. 7576, pp. 78–81, Nov. **2015**, doi: 10.1038/nature15746.
- [15] E. C. Montoto *et al.*, “Redox Active Colloids as Discrete Energy Storage Carriers,” *J Am Chem Soc*, vol. 138, no. 40, pp. 13230–13237, Oct. **2016**, doi: 10.1021/jacs.6b06365.
- [16] G. Milczarek, “Preparation and Characterization of a Lignin Modified Electrode,” *Electroanalysis*, vol. 19, no. 13, pp. 1411–1414, Jul. **2007**, doi: 10.1002/elan.200703870.
- [17] G. Nyström, A. Razaq, M. Strømme, L. Nyholm, and A. Mihranyan, “Ultrafast all-polymer paper-based batteries,” *Nano Lett*, vol. 9, no. 10, pp. 3635–3639, Oct. **2009**, doi: 10.1021/nl901852h.
- [18] F. Stoeckli, E. Daguerre, and A. Guillot, “The development of micropore volumes and widths during physical activation of various precursors,” *Carbon N Y*, vol. 37, no. 12, pp. 2075–2077, **1999**, doi: 10.1016/S0008-6223(99)00220-1.
- [19] B. Zinger, “Electrochemistry of quinoid dopants in conducting polymers,” *Synth Met*, vol. 30, no. 2, pp. 209–225, May **1989**, doi: 10.1016/0379-6779(89)90791-1.
- [20] A. Razaq, A. Mihranyan, K. Welch, L. Nyholm, and M. Strømme, “Influence of the Type of Oxidant on Anion Exchange Properties of Fibrous Cladophora Cellulose/Polypyrrole Composites,” *J Phys Chem B*, vol. 113, no. 2, pp. 426–433, Jan. **2009**, doi: 10.1021/jp806517h.
- [21] F. Xiong *et al.*, “Preparation and Formation Mechanism of Renewable Lignin Hollow Nanospheres with a Single Hole by Self-Assembly,” *ACS Sustain Chem Eng*, vol. 5, no. 3, pp. 2273–2281, Mar. **2017**, doi: 10.1021/acssuschemeng.6b02585.
- [22] H. Olsson, D. O. Carlsson, G. Nyström, M. Sjödín, L. Nyholm, and M. Strømme, “Influence of the cellulose substrate on the electrochemical properties of paper-based polypyrrole electrode materials,” *J Mater Sci*, vol. 47, no. 13, pp. 5317–5325, Jul. **2012**, doi: 10.1007/s10853-012-6418-y.
- [23] J. Y.-C. Chen, A. A. Martí, N. J. Turro, K. Komatsu, Y. Murata, and R. G. Lawler, “Comparative NMR properties of H<sub>2</sub> and HD in Toluene-*d*<sub>8</sub> and in H<sub>2</sub>/HD@C<sub>60</sub>,” *J Phys Chem B*, vol. 114, no. 45, pp. 14689–14695, Nov. **2010**, doi: 10.1021/jp102860m.
- [24] C. Costentin, J.-M. Savéant, and C. Tard, “Catalysis of CO<sub>2</sub> electrochemical reduction by protonated pyridine and similar molecules. useful lessons from a methodological misadventure,” *ACS Energy Lett*, vol. 3, no. 3, pp. 695–703, Mar. **2018**, doi: 10.1021/acsenerylett.8b00008.
- [25] M. F. Cunningham and P. G. Jessop, “Carbon dioxide-switchable polymers: where are the future opportunities?,” *Macromolecules*, vol. 52, no. 18, pp. 6801–6816, Sep. **2019**, doi: 10.1021/acs.macromol.9b00914.
- [26] Y. Liu, H.-Z. Ye, K. M. Diederichsen, T. van Voorhis, and T. A. Hatton, “Electrochemically mediated carbon dioxide separation with quinone chemistry

in salt-concentrated aqueous media,” *Nat Commun*, vol. 11, no. 1, p. 2278, Dec. **2020**, doi: 10.1038/s41467-020-16150-7.

[27] G. Milczarek, “Lignosulfonate-modified electrodes: electrochemical properties and electrocatalysis of NADH oxidation,” *Langmuir*, vol. 25, no. 17, pp. 10345–10353, Sep. **2009**, doi: 10.1021/la9008575.







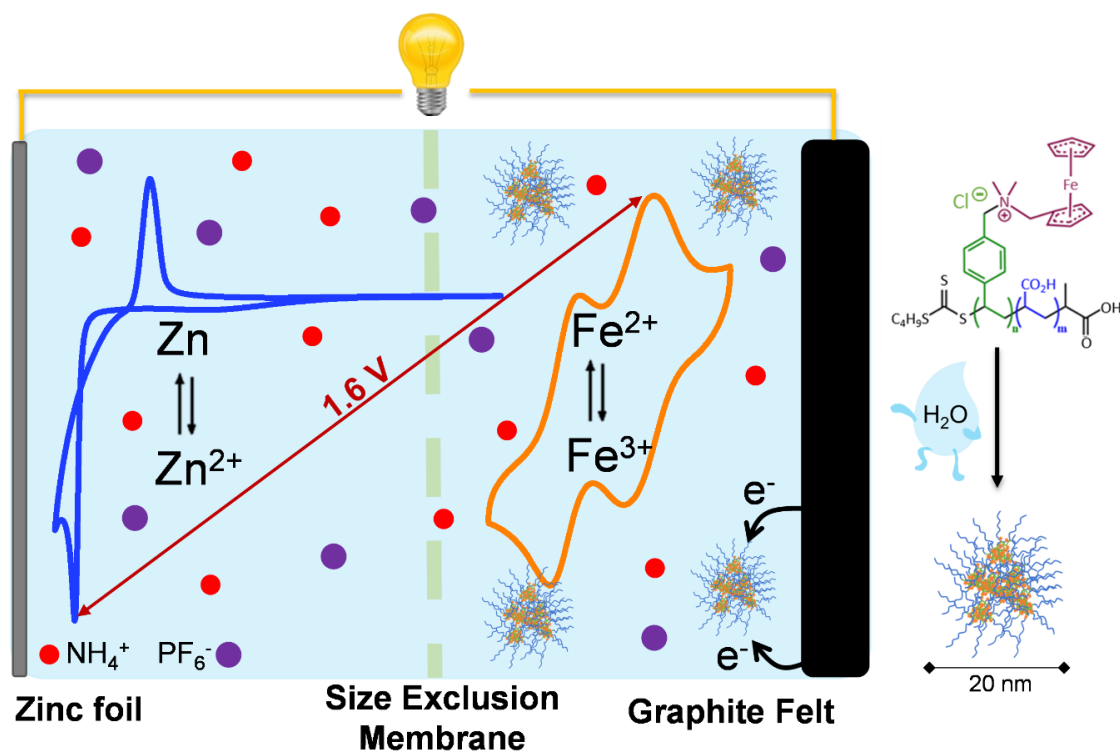
## Chapter 3.

Novel ferrocene-containing  
amphiphilic block copolymer  
nanoparticles as high-capacity  
charge carriers in aqueous redox  
flow systems

Part of the work described in this Chapter has been published in *Materials Today Chemistry*, **2023**, 27, 101271



Highly-water dispersible ferrocene-containing block copolymer nanoparticles have been developed as size-exclusion electrolytes showing a high capacity to store charges electrochemically. Besides, the scalable redox polymer electrolyte nanoparticles offer the opportunity to address two main energy and environmental challenges: global warming and polluting atmosphere from greenhouse gas emissions and the energy storage from renewable sources.



### **Abstract**

Size-exclusion polymer electrolytes are promising charge carriers to diminish the crossover and allowing commercially available low-cost porous membranes in redox-flow batteries (RFBs). Boosting the solubility in water and maximizing the number of redox sites to enhance the capacity of these polymeric systems is challenging. New highly-water dispersed amphiphilic diblock copolymers are reported here, with an average concentration value of  $1.7 \cdot 10^{-3}$  mmol of Ferrocene (Fc) linked moieties per mg of polymer, determined by Total X-ray Reflection Fluorescence. These redox amphiphilic block copolymers are stabilized in water as spherical nanoparticles (20 nm) by using a simple phase solvent inversion procedure. We evidence a maximum polymer dispersibility value of  $6 \text{ g} \cdot \text{l}^{-1}$  in water, for long-term stable polymer nanoparticle suspensions, yielding a theoretical capacity value of 4.78 mA·h at 10.5 mM Fc. Further adjustment of the ionic conductivity and pH of these stable redox block copolymer suspensions has rendered a conductivity value of  $44.5 \text{ mS} \cdot \text{cm}^{-1}$  at pH values close to a neutral one, by adding a variety of salt supports. Studies using a 3-electrode configuration cell reveal an efficient charge transport between each of the Fc motifs in the polymer nanoparticle. A capacity value of 3.1 mA·h with no transient of the polymer nanoparticles crosswise the cheap porous membrane is evidenced when cycled as polycatholyte material in a Zn hybrid aqueous redox flow battery. The particle size and electronic changes of these novel amphiphilic redox block copolymer electrolytes during consecutive redox cycles have also been monitored by Dynamic Light Scattering and UV-vis spectroscopy, respectively. The analysis of the results enables the understanding of the main mechanisms behind their non-fully reversible capacity. Among them: aggregation and sedimentation, along with retention inside the graphite felt electrode acting the latter as a filter. These insights will aid the design of future polymer electrolyte materials and redox flow battery components with better performance and cost.

---

---

## Scientific background and state of the art

Replacing non-renewable energy sources with sustainable alternatives such as solar and wind energies is crucial for the ecological transition towards a safe, zero-carbon future [1-4]. Redox flow batteries (RFBs) show promise for large-scale energy storage from these intermittent renewable sources [5]. Generally, RFBs are comprised of two electrolytes containing redox active compounds that are continuously pumped from two external tanks into an electrochemical cell where the electroactive species are oxidized or reduced swapping electrons through the external circuit. Ions migrate through an ion-selective polymer membrane to balance the charges. So far, the most studied and commercially extended RFB system has been based on vanadium chemistry [6] but it requires expensive membranes [7], and electrolytes that are also scarce and/or costly, and not particularly eco-friendly [8].

These drawbacks might be reduced by using redox polymer electrolytes to diminish the material crossover between the poly(catholyte) and poly(anolyte) and allow commercially available low-cost porous membranes [9,10]. In addition, the use of aqueous solutions at neutral or close to neutral pH values containing inexpensive salts (i.e., NaCl) as supporting electrolyte makes safer these polymeric systems in comparison with the RFBs based on corrosive acidic/basic solutions or flammable organic solvents [11].

The research has been increasingly focused on the development of novel organic-based polymeric architectures to boost properties such as polymer solubility, capacity and long-term cyclability of RFBs in both aqueous and organic media. The most studied redox moieties in these poly(analytes) are limited to a few derivatives of molecules such as quinone [12,13], viologen [14,15], TEMPO [15–17] and ferrocene [14,18,19]. Because of its reversible electrochemistry, harmless and low cost [20], Fc is particularly ideal in large-scale energy storage applications. The main challenge in utilizing Fc in aqueous RFBs is their extreme hydrophobicity in the uncharged state. To further promote their water solubility, and then expand the energy density of the aqueous flow battery, a wide range of chemical modifications and copolymerization strategies have been developed. For instance, water solutions containing hydrophilic Fc as catholyte with concentration values up to 4 M have evidenced high capacity,

long-term stability, and fast charge transfer kinetics in symmetric aqueous RFBs [21,22]. However, using single Fc-based organic molecules as electrolyte material still needs expensive membranes in the RFB system. In addition, highly-water soluble amphiphilic block copolymers containing electrochemically active Fc groups are limited to biomedical applications such as drug delivery and gene therapy [22–25]. Moreover, in most cases, reversibility has been achieved chemically with an external chemical agent [26].

To the best of our knowledge, only three scientific works [14,18,19] demonstrating the potential implementation of Fc-based polymers as charge carriers in RFBs have been published up to date. Rodriguez et al. [14] created highly reversible electrochemical and stable size-exclusion Fc-containing colloids with theoretical capacity values up to 1.34 mA·h at a polymer concentration of 10 mM in acetonitrile. The full access to the capacity of a symmetric colloidal polymer electrolyte RFB prototype, using a low-cost porous separator, was limited to 21 % of the theoretical one due to the low-loading and the observed sedimentation of the Fc-electrolyte in organic solvent. Another two articles show the creation of novel block copolymers exhibiting a concentration up to  $6.49 \cdot 10^{-4}$  mmol [19] and  $1.2 \cdot 10^{-3}$  mmol [18] of Fc moieties per mg of polymer, respectively. These Fc-based block copolymers rendered a maximum theoretical capacity of 7.83 mA·h and 35 mA·h, respectively. Although the Fc-polymers works robustly as a poly(catholyte) in aqueous organic RFBs, the demonstration of a potential application as size-exclusion electrolyte material was not evidenced because of the use of costly and non-porous anionic polymer membranes in both publications.

Here, the potential of Fc-containing amphiphilic block copolymer nanoparticles as size-exclusion charge carriers in aqueous redox flow systems is explored for the first time. For that, novel amphiphilic block copolymers by reversible addition-fragmentation chain transfer (RAFT) polymerization with a hydrophilic block, -poly (acrylic acid)- and other hydrophobic, -poly (4-vinylbenzyl chloride)- are prepared. Particularly interesting is to maximize the concentration of the redox-active units in the main chain of highly-water soluble polymers to increase the energy density of the RFB. For that, we first study the impact of the main parameters of the polymer synthesis and ion exchange conditions on the

---

---

number of available link-sites to redox units and the solubility of the block copolymers in water. Then, we performed a chemical substitution between the chlorine atoms in the lateral group of the hydrophobic unit and dimethyl aminomethyl ferrocene (DMAFc) molecules. The maximum concentration value of DMAFc groups linked to the main polymer chain was  $1.7 \cdot 10^{-3}$  mmol per mg of polymer, determined by Total X-ray Reflection Fluorescence (TXRF). These redox amphiphilic block copolymers are stabilized in water into spherical nanoparticles (20 nm) by using a simple phase solvent inversion procedure. The reactivity and charge capacity, long-term stability, ionic conductivity, and pH of block polymer nanoparticle suspensions at different concentrations of organic and inorganic salts are also studied. There is a trade-off between concentration of polymer nanoparticles and the inorganic/organic nature of the supporting salts and their amount affecting the ionic conductivity and pH values of the aqueous suspensions. The block copolymer nanoparticles exhibit a cyclic voltammogram in aqueous media characterized by two well-separated and reversible oxidation waves. This electrochemical behavior is consistent with interactions between the Fc units linked to the vinyl monomer along the main polymer chain [27]. Finally, charge storage properties and size-exclusion electrolyte's assessment of the new polymeric materials are tested in a hybrid zinc flow battery.

For the first time, block copolymer nanoparticles containing Fc with high-dispersibility as size-exclusion electrolytes showing a high capacity to store charges electrochemically have been developed. Besides, in situ dynamic light scattering (DLS) and UV-Vis measurements have been performed to understand the variations in battery capacity, mainly originated by aggregation of the polymer nanoparticles and sedimentation while undergoing electrochemical process. In this way, the main factors affecting the proper functioning of size-exclusion polymer electrolyte nanoparticles in RFBs have been identified. Further, this work contributes not only to the emerging field of redox polymer electrolyte nanoparticles in the area of energy storage, but also to the development of other possible electrochemical applications.

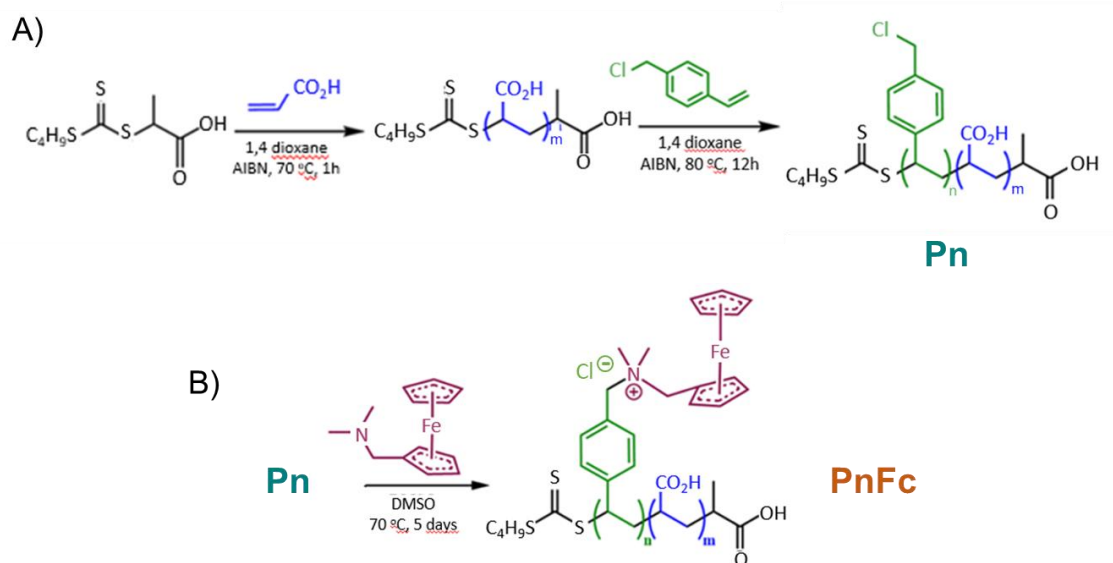
## Experimental Methods

**Materials.** All the chemicals used in this work were purchased from Sigma-Aldrich and used as received otherwise are indicated. The two monomers used to synthesize the block copolymer were acrylic acid (AA) (purity 99 %) and 4-vinylbenzyl chloride (VBC) (purity 90 %). Before they were used in the polymerization reaction, the specific inhibitor contained on each were removed by passing the VBC monomer twice through a packed column containing  $\text{Al}_2\text{O}_3$  to trap the tert-butyl catechol in the VBC monomer, or to eliminate the methyl ester hydroquinone from the AA monomer. 2,2'-Azobis(2-methylpropionitrile) (AIBN) (purity  $\geq 98$  %) was recrystallized two times in methanol before it was used as initiator in the polymerization reaction. Anhydrous 1,4-dioxane (purity  $\geq 99$  %) and nitrogen gas (Air Products, purity  $> 99$  %) were used as solvent and inert gas atmosphere respectively, in the polymerization reaction.

The redox amphiphilic diblock copolymers were prepared following the synthetic sequence shown in Scheme 1. In order to optimize the dispersibility of polymer nanoparticles, different syntheses with different ratio of hydrophilic and hydrophobic segment are performed. On the one hand, P1 is prepared by adding a longer chain of hydrophilic segment than hydrophobic segment to facilitate its dispersibility. On the other hand, P2 is prepared, adding more hydrophobic segment to allow us to subsequently anchor more electroactive units to the copolymer and study its stability in water. The synthesis procedure of the block copolymer AA:VBC 4.3:1 (P1) is used to describe the preparation route as follows (see more details in Table 3.1 and Figure 3.1): a solution containing 0.206 g ( $8.64 \cdot 10^{-4}$  mol) of RAFT agent with 0.014 g ( $8.64 \cdot 10^{-5}$  mol) of AIBN was added to a round bottom flask of 100 ml. The RAFT agent 2-[[Butylsulfanyl]carbonothioyl] sulfanyl propanoic acid was synthesized according to a reported procedure [28]. Further characterization of RAFT agent is shown in Figure 3.2. Then, 5.60 g (0.077 mol) of AA and 9.00 g ( $\text{g} \cdot \text{cm}^3$ ) of 1,4-dioxane were added to the flask. After 20 min of deoxygenation using nitrogen gas, the reaction flask was set at 70 °C for 1 h to maximize conversion. Then, it was cooled down to 50 °C and 2.80 g (0.018 mol) of VBC, and a solution containing AIBN 0.026 g ( $1.6 \cdot 10^{-4}$  mol) in 10.26 g of 1,4-dioxane was injected with a syringe to the previous system. Afterwards, the temperature was



raised to 80 °C for 12 h to maximize polymer conversion. Then, the solid product (P1) was purified first by washing it twice with acetone (purity  $\geq 97\%$ ) and secondly by dialysis in DI-H<sub>2</sub>O with a semi-permeable membrane (MWCO 3 kDa) for two days, controlling the temperature of the solution between 15-20 °C to avoid chlorine losses. Finally, supercritical CO<sub>2</sub> to eliminate the remaining unreacted monomers and traces of solvent was applied.



**Scheme 2.1.** Reaction scheme of the amphiphilic diblock copolymers with DMAFc grafted in the main chain. The synthesized polymers differ in the hydrophilic and the hydrophobic segment ratios

The chemical substitution of the chlorine atom in the amphiphilic block copolymer by the (dimethyl aminomethyl) ferrocene (DMAFc) (purity  $\geq 95\%$ ) molecule was performed according to the following procedure: first, 1.5 mol of AA-VBCI (Pn) and 1.5 mol of DMAFc were introduced in a round bottom flask. Then, 9.3 ml (8.45 g) of anhydrous DMSO were added with a syringe to allow the substitution at 70 °C for 5 days under inert (nitrogen) conditions. After, DMSO solvent was removed under reduced pressure at 90 °C. The solid obtained (PnFc) was washed three times with acetone, and then subsequently centrifuged, lyophilized and stored at 5 °C. The conversion of the linear block copolymers into water-soluble spherical polymer nanoparticles has been done by dissolving the amphiphilic block copolymer in 2.5 ml of DMSO and adding

this solution dropwise to 10 ml of deionized water under constant stirring. The final solution was dialyzed in distilled water for 48 h using a semi-permeable membrane (MWCO 3 kDa) to remove the organic solvent. The long-term water stability of block copolymer nanoparticles suspension was adjusted at different nanoparticles and supporting salt concentrations.

The synthesis of the salt support  $\text{ZnPF}_6$  used in the tests of the hybrid Zn-polymer flow battery was performed as indicated in Reference [29]. For that, ammonium hexafluorophosphate ( $\text{NH}_4\text{PF}_6$ , purity  $\geq 99\%$ ), zinc chloride ( $\text{ZnCl}_2$ , 98%), anhydrous acetonitrile ( $\text{CH}_3\text{CN}$ , 98%), silver hexafluorophosphate ( $\text{AgPF}_6$ , 98%), zinc hexafluorophosphate ( $\text{AgPF}_6$ , 98%) and zinc chloride ( $\text{ZnCl}_2$ , 98%) were used as received.

**Table 3.1.** Characteristics of the reactants and solvent used for the synthesis and chemical exchange of the block copolymers. The volume of solvent used on each step is included

Material	Synthesis of diblock copolymers				
	AA (mol · 10 <sup>2</sup> )	VBC (mol · 10 <sup>2</sup> )	RAFT agent (mol · 10 <sup>4</sup> )	AIBN (mol · 10 <sup>5</sup> )	Dioxane (ml)
<b>Hydrophilic segment</b>					
P1	7.8	-	8.6	8.6	8.7
P2	5.4	-	8.9	8.9	5.7
<b>Hydrophobic segment</b>					
P1	-	1.8	8.6	16.0	10.0
P2	-	2.9	8.9	16.0	12.5
<b>Chemical substitution of diblock copolymers</b>					
P1Fc	Diblock copolymer (Cl mol · 10 <sup>3</sup> )		Ferrocene (mol · 10 <sup>3</sup> )		
	1.5		1.5		
P2Fc	3.4		3.4		

The preparation route of the redox amphiphilic block-copolymers is displayed in Figure 3.1. Step number 1, the hydrophilic segment was synthesized in the presence of  $\text{N}_2$  for 30 min and in a bath previously heated to 70 °C for 4 h; then,

the reaction was cooled down with water. In the second step, VBCI was introduced into the reaction flask at 70 °C for 12 h, and then cooled to room temperature to incorporate the hydrophobic block into the previous reaction mixture. Finally, the third step, where the chemical substitution with the DMAFc molecule is performed, was carried out under N<sub>2</sub> gas atmosphere at 70 °C for 5 days.

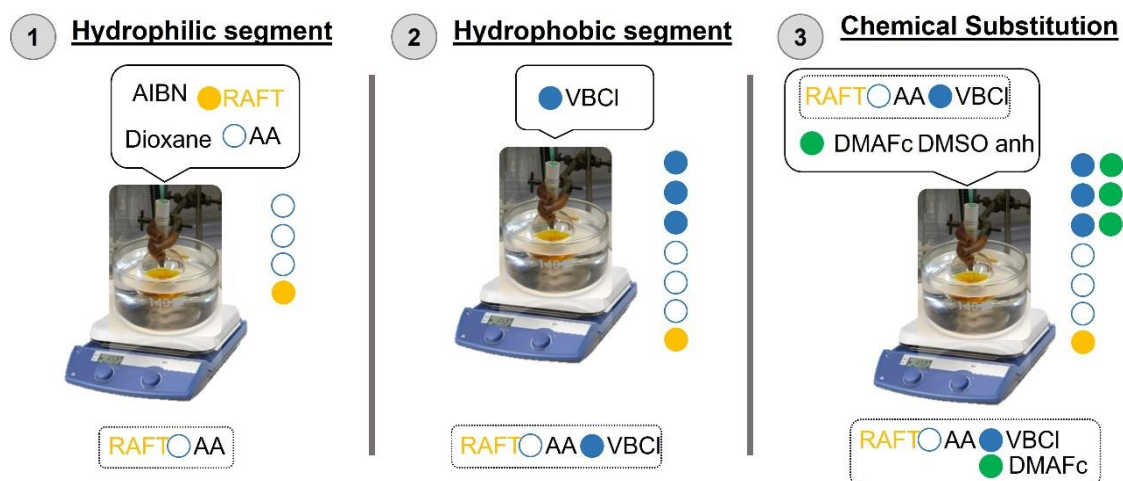


**Figure 3.1.** Synthesis and functionalization of diblock copolymers. 1) Hydrophilic segment. 2) Hydrophobic segment. 3) Chemical substitution

### Characterization.

Number-average molecular weight ( $M_n$ ), weight-average molecular weight ( $M_w$ ) and molecular-weight dispersity ( $\mathcal{D}_M = M_w/M_n$ ) were measured by size exclusion chromatography (SEC) (Waters 1515 isocratic HPLC pump, Waters 2414 refractive index detector, Waters717 autosampler) in tetrahydrofuran (THF) (5 mg of sample in 1 ml of THF).

The molecular weights and  $\mathcal{D}_M$  were derived from a calibration curve based on narrow polystyrene standards (Figure 3.2).

The polymer composition was determined by liquid <sup>1</sup>H-NMR in a magnet with a 400 MHz field (Varian Mercury) using a sample of 5 mg in 1 ml of DMSO-d<sub>6</sub>.

FT-IR spectra (Perkin Elmer Spectrum one) of Pn and PnFc were recorded in ATR mode, in a wave number range from 400 to 4000  $\text{cm}^{-1}$  at a resolution of 4  $\text{cm}^{-1}$ .

The UV-Vis spectra of the block copolymers at different concentrations in water were determined using a Nanodrop One Microvolume UV-Vis spectrophotometer (Thermo Scientific™) by fluorescence spectroscopy using 280/290 nm excitation/emission. The elemental composition of C, H, N, and S of the synthesized amphiphilic block copolymers has been determined by combustion on a LECO CHNS-932 elemental microanalyzer.

The characterization of the Fe and Cl content in the polymers was carried out by Total X-ray Reflection Fluorescence (TXRF), using a benchtop S2 PicoFox TXRF spectrometer from Bruker Nano GmbH (Germany), equipped with a molybdenum X-ray source working at 50kV and 600  $\mu\text{A}$ .

Average particle size ( $d_p$ ) as a function of reaction time was measured at 20 °C by dispersion light scattering (DLS) in a Malvern ZetasizerNano-ZS90 equipment. Pure amphiphilic block copolymer was imaged at -170 °C in a 300 kV Tecnai F30 cryoelectron microscope (CryoEM). A dilute solution of the polymers was prepared using 0.1  $\text{g}\cdot\text{l}^{-1}$ .

The block copolymer solution (3  $\mu\text{l}$ ) was added to one side of Quantifoil Cu/Rh R2/2 carbon grids, blotted, and plunged into liquid ethane in a FEI Vitrobot Mark IV. Samples were analyzed in a Talos Arctica from ThermoFisher with an X field emission gun operating at 200 kV. To acquire the images, EPU Software (Thermo Fisher Scientific®) equipped with an autoloader and a Falcon III direct electron detector was used. The analysis of the average nanoparticles was based on the counted number of particles using ImageJ analysis.

The morphology, shape, and size of the synthesized redox active amphiphilic block copolymer nanoparticle were studied by high resolution scanning electron microscopy (HRSEM) in a Hitachi SU8000 model, STEM mode, with field voltage filament and a voltage of 3.0 kV under vacuum values lower than  $1\cdot 10^{-3}$  Pa. For the observations, a dilute solution of the polymer was prepared at 0.7 mM in water. A few drops of the solution were deposited in a carbon-coated grid.

Cyclic voltammetry (CV) studies were performed with a VMP3 potentiostat (Biologic, France). A standard three-electrode configuration with a glassy carbon working electrode (3 mm diameter), an Ag/AgCl reference electrode and a platinum counter electrode were used for these measurements. To determine the diffusion coefficient, the electron transfer rate constant, and the electron transfer coefficient  $\alpha$ , rotating disc electrode (RDE) measurements were performed with the same potentiostat used for the CV studies, with a glassy-carbon working electrode (diameter 4 mm). The rotational speed was controlled externally with an RRDE-3A device (ALS, Japan). Evaluating the RDE analysis by Levich (limiting current vs. square root of the spin rate), a diffusion coefficient  $D$  was obtained with the Levich equation:

$$i_{lim}=0,62nFAD^{2/3}\omega^{1/2}\nu^{-1/6}c_0$$

where  $F$  is the Faraday constant ( $F=96485 \text{ C}\cdot\text{mol}^{-1}$ ),  $A$  is the electrode area ( $0.16 \text{ cm}^2$ ),  $\nu$  is the kinematic viscosity, and  $c_0$  is the concentration. The rate constant,  $k_0$ , has been calculated by Koutecky-Levich and later Tafel, with the equation

$$i_0=FAc_0k_0$$

where  $i_0$  is the intersection of the Tafel plot with the Y-axis. On the other hand, the electron transfer coefficient,  $\alpha$ , is obtained with the slope of the Tafel plot.

The experiments with flow were done in a flat cell type with an active membrane area of  $6.25 \text{ cm}^2$  (Jena-Batteries, Germany). For the latter study, two types of configurations have been applied. On the one hand, a 0.3 M solution of 2,7AQDS as anolyte and 2 mM P1Fc as catholyte was prepared, both with 0.5 M  $\text{NaH}_2\text{PO}_4$  as support salt. A Nafion™ 117 perfluorinated membrane was used to separate each cell side. On the other hand, for the hybrid battery, Zinc Foil was used as collector on the anolyte side and a 2 mM P1Fc solution was prepared as catholyte, both tanks with 0.1 M  $\text{NH}_4\text{PF}_6$  and  $\text{Zn}(\text{PF}_6)_2$  as support salt. A size exclusion membrane separates the two cell compartments. In both configurations, the solutions were transported through the cell at  $20 \text{ ml}\cdot\text{min}^{-1}$ .

## Results and discussion

### Chemical composition of amphiphilic block copolymers

First, a characterization of the synthesized RAFT has been carried out (Figure 3.2A-C), additionally the characterization of the block-copolymers was carried out before and after the chemical substitution with DMAFc exchange.

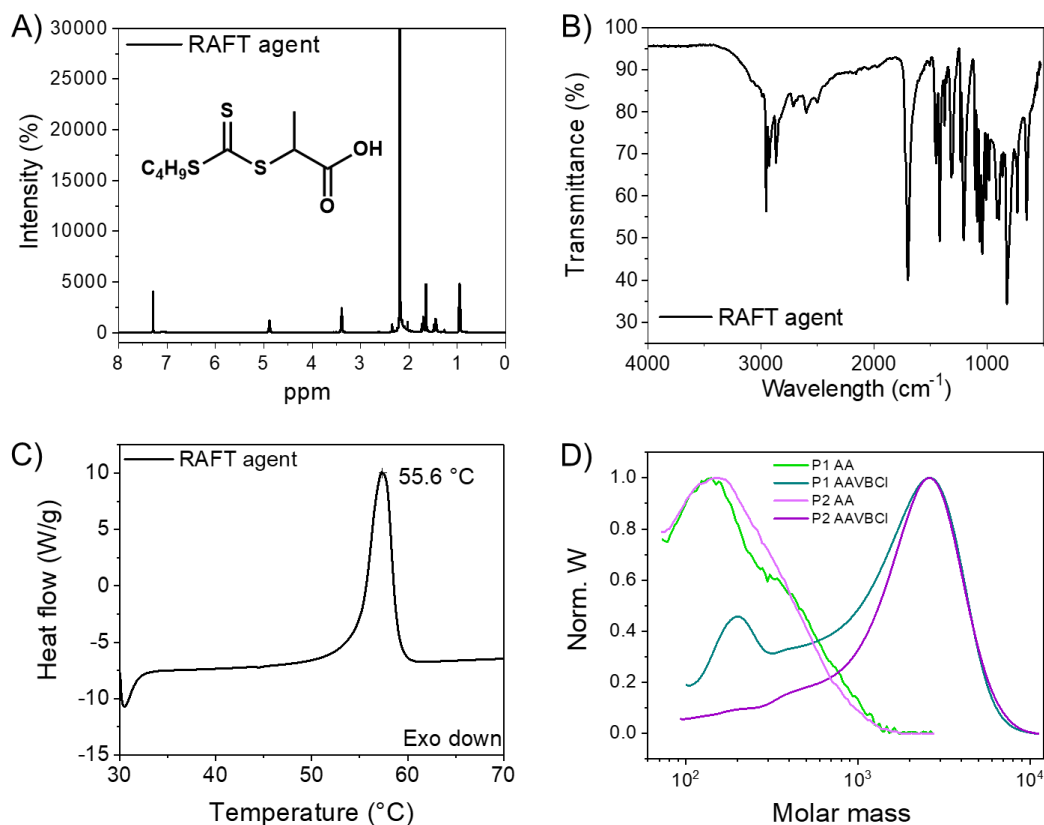


**Figure 3.2.** A)  $^1\text{H-NMR}$  in chloroform-d ( $\text{CDCl}_3$ ), B) FTIR and C) Dynamic scanning calorimetry (DSC) of RAFT agent 2-[[[(Butylsulfanyl)carbonothioyl]sulfanyl] propanoic acid. Measurement conditions: heating rate:  $10^{\circ}\text{C}\cdot\text{min}^{-1}$ ; nitrogen atmosphere. D) Molecular weight by size exclusion chromatography of block copolymers in tetrahydrofuran (THF) (5 mg of sample in 1 ml of THF)

Figures 3.3 and 3.4 show the characterizations of the block copolymers by FT-IR, UV-Vis,  $^1\text{H-NMR}$ , and elemental analysis conducted by combustion and TXRF. The spectra corresponding to both the non-substituted and the substituted block copolymers with the Fc unit are presented together in the same plot. As shown in Figure 3.3A, the FT-IR spectrum of P1 has an

absorption band  $650\text{-}700\text{ cm}^{-1}$  assigned to C-Cl stretching, bands at 2921, 2854  $\text{cm}^{-1}$  related to symmetric and asymmetric  $\text{CH}_2$  stretching, a single and intense band at  $1703\text{ cm}^{-1}$  corresponding to the C=O group from the AA block, and another band at  $1400\text{ cm}^{-1}$  due to aromatic C=C stretching. After the chemical substitution with DMAFc, the C-Cl stretching vibration disappeared and a new signal appeared at  $1503\text{ cm}^{-1}$  due to the cyclopentadienyls of Fc units, which confirms the incorporation of the electroactive group in the copolymer chain. Similar results were found for all the prepared polymers, independently of the ratio between different blocks (Figure 3.4A). UV-Vis spectroscopy in aqueous media was also performed to confirm the chemical substitution in the block copolymer as shown in Figures 3.3B and 3.4B. Before the chemically substitution, the block copolymer had presented a group of absorption bands at 212, 228 and 313 nm which are attributed to  $\pi\text{-}\pi^*$  transitions of the phenyl ring in the block containing VBC. After the incorporation of the Fc, a strong absorption band can be seen at 248 nm, which is attributed to both the absorption of Fc and the benzene ring. A change is observed in the 400-450 nm regions, due to the d-d transition in the Fc unit too. This signal is not very broad possibly due to the aggregation of the polymer nanoparticles and the enhancement of the interactions between the Fc groups inside the nanoparticles. When they are excited, a spectrum of lower intensity similar to those observed in solid-state spectroscopy is evidenced [22].

$^1\text{H-NMR}$  was used to determine the chemical composition of the block copolymers as shown in Figures 3.3C and 3.4C. The  $^1\text{H-NMR}$  spectrum featured three characteristic resonances: one at 12.3 ppm corresponds to the carboxylic (COOH) group of the acrylic acid; another one in the region 6.5-7.3 ppm corresponding to the protons of benzene ring; and a third one at 4.7 ppm from the chloromethyl group ( $-\text{CH}_2\text{Cl}-$ ) in the styrene block. After the functionalization with the DMAFc molecule, the resonance due to protons in the  $\text{CH}_2\text{Cl}$  group disappeared, and those at 4.19 ppm (1), 4.25 ppm (2), 4.3 ppm (3) and 4.4 ppm (4) due to DMAFc appeared. The new resonance at 4.5 ppm, stand for the protons presented in the new  $\text{CH}_2\text{N}$  bond. Figure 3.3D and Figure 3.4D show the elemental analysis performed by combustion and FXTR techniques. The results indicated that a decrease in the chlorine content of the

block copolymer came with the appearance of the iron and nitrogen elements as DMAFc was integrated to the polymer structure. Although traces of chlorine are still in the redox block copolymer, this chlorine is not chemically anchored to the polymer but appeared most probably counterbalancing the positive charge in the nitrogen atom just created after the chemical substitution (Scheme 2.1). From the TXFR results, the content of Fc can be estimated in the block copolymers. A maximum concentration value of Fc motifs linked to the main polymer chain up to  $0.17 \cdot 10^{-3}$  mmol per mg of polymer, was achieved.

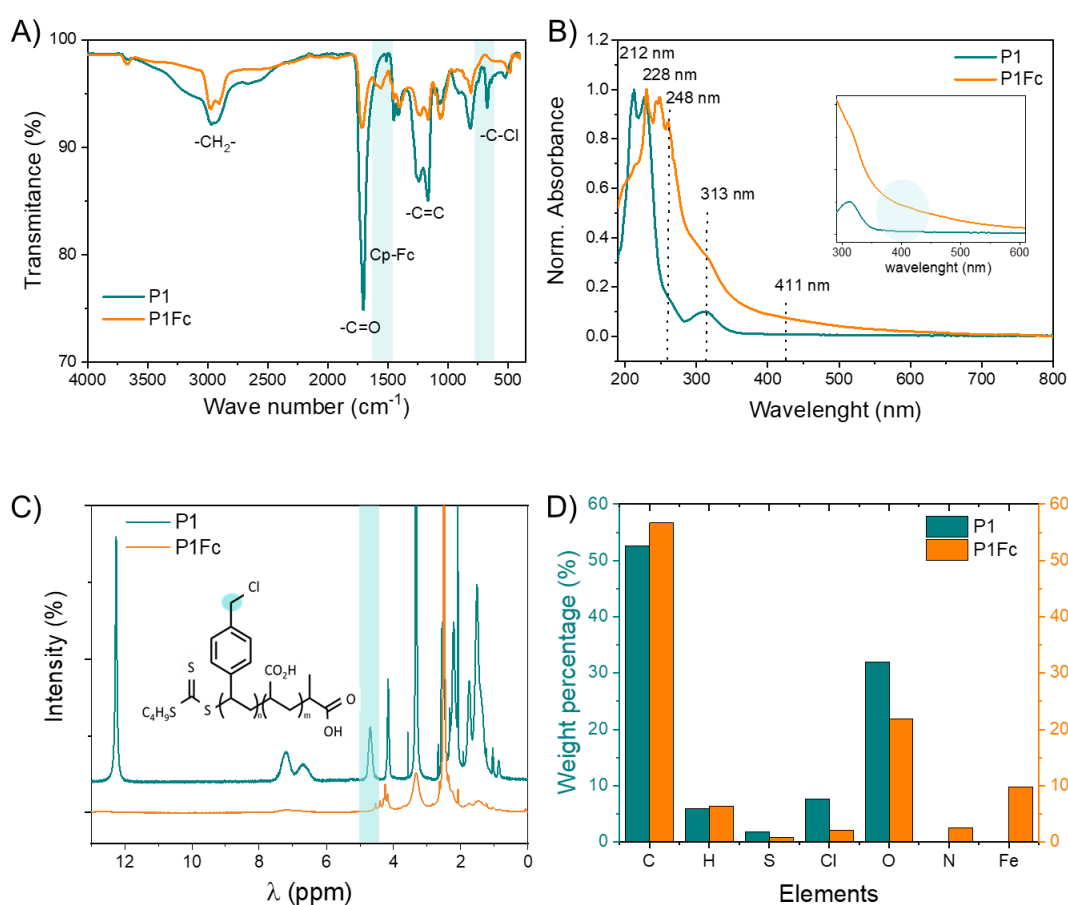


**Figure 3.3.** Characterization of the amphiphilic block copolymers before and after their functionalization with DMAFc. A) FT-IR spectra of pure solid copolymers. B) Absorption spectra of the polymers in water ( $1 \text{ g}\cdot\text{l}^{-1}$ ). C)  $^1\text{H-NMR}$  spectra of P1 and P1Fc in  $\text{DMSO-d}_6$ . D) Elemental analysis of the block copolymers performed by combustion and TXRF techniques



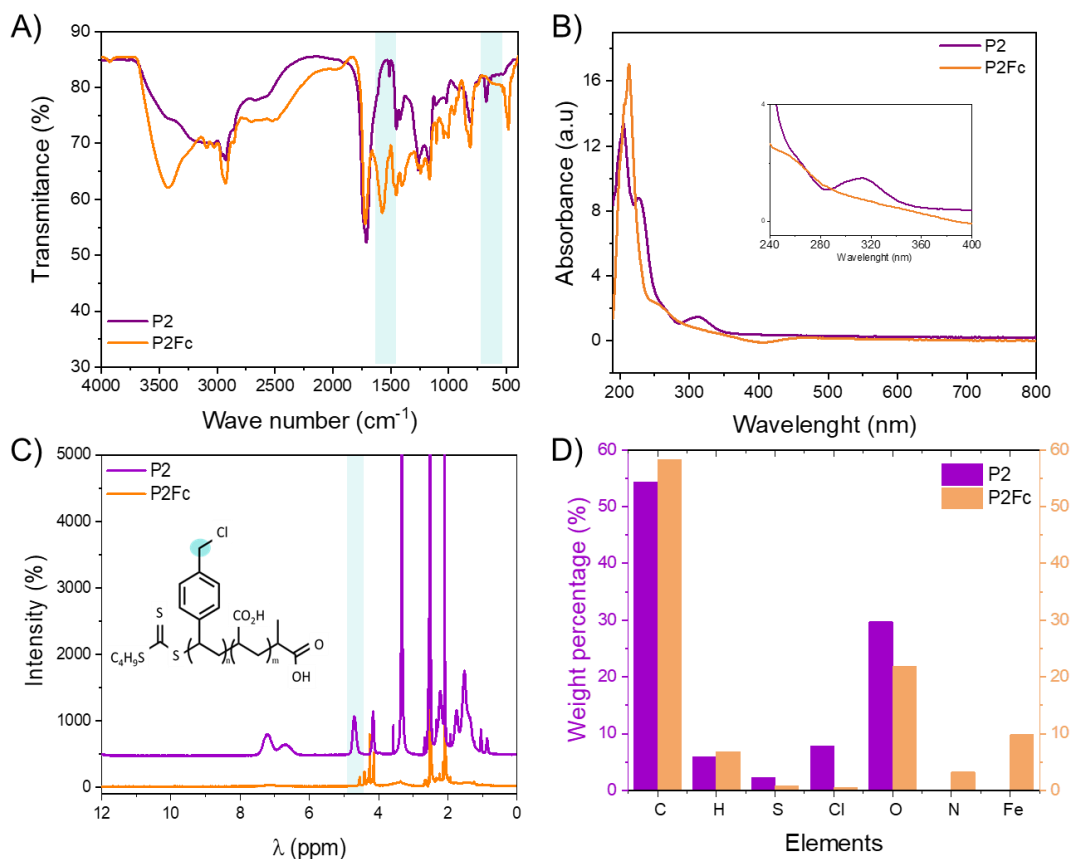


**Figure 3.4.** Characterization of one of the block-polymers synthesized in this work, P2, and their chemically substituted with DMAFc equivalent, P2Fc. A) FT-IR spectra of P2 and P2Fc. B) UV-vis absorption spectra of the polymers in water (1 g·l<sup>-1</sup>). C) <sup>1</sup>H-NMR spectra of P2 and P2Fc in DMSO-d<sub>6</sub>. D) Elemental analysis of the block-copolymers determined by combustion and TXRF analysis

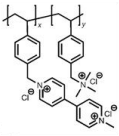
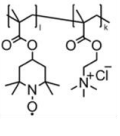
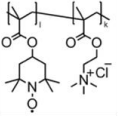
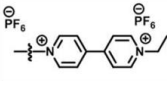
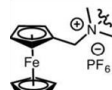
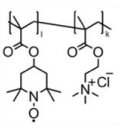
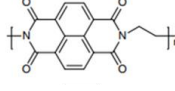
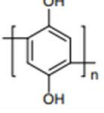
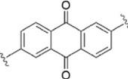
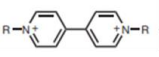
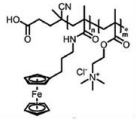
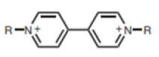
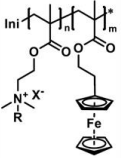
A high-value number of redox moieties in the block copolymer and a high polymer concentration in the liquid phase would be necessary to boost the energy density of an aqueous polymer RFB. Although easy to be dispersed, the long-term stability of the new amphiphilic block copolymer in water is less than 1 g·l<sup>-1</sup>, precipitating in a few h. For that reason, these amphiphilic block copolymers were transformed into long-time water-stable nanoparticles using a simple inverse-phase solvent strategy.

Generally, the determination of the amount of ferrocene moieties anchored to a polymer backbone is challenging. In this study, the amount of Fc and the weight percentage of iron in the polymer have been calculated using the total reflection X-ray fluorescence spectroscopy (TXRF). The highest iron values were 9.8

wt.% for P1Fc and P2Fc. In addition, the maximum theoretical capacity value of the Fc-containing block-copolymers has been calculated here. For that, a study for the determination of the maximum concentration of a stable dispersion of polymer nanoparticles in water without the presence of supporting salts has been pursued. Considering that the highest concentration value for a dispersion of P1Fc in water was of  $6 \text{ g}\cdot\text{l}^{-1}$ , a theoretical capacity of  $4.78 \text{ mA}\cdot\text{h}$  has been obtained.

The method allows us to reach a concentration value of up to  $6 \text{ g}\cdot\text{l}^{-1}$  of the nanoparticles in water, providing a maximum theoretical capacity value of up to  $4.78 \text{ mA}\cdot\text{h}$ , aligned with the state-of-the art on polymer-based RFBs (Table 3.2). Table 3.2 displays a comparison between the state of the art on organic-based Fc and polymeric analytes studied in redox flow batteries with the use of size-exclusion membranes and ionic membranes [11–16,18,19].

**Table 3.2.** State of the art of dome organic redox flow batteries

Negative Electrolyte	Positive Electrolyte	Environment	Membrane	Capacity	Ref
PolyViologen 	PolyTEMPO 	Aqueous NaCl	Dyalisis membrane MWCO 6000 g mol <sup>-1</sup>	10 Ah l <sup>-1</sup>	[11]
Zn	PolyTEMPO 	Aqueous NaCl-ZnCl <sub>2</sub> - NH <sub>4</sub> Cl	Dyalisis membrane MWCO 1000 g mol <sup>-1</sup>	1.1 Ah l <sup>-1</sup>	[15]
Viologen Redox Active Colloidal Particle 	Ferrocene Redox Active Colloidal Particle 	Acetonitrile LiBF <sub>4</sub>	Celgard 2325 porous separator	40 mAh g <sup>-1</sup>	[14]
Zn	Micellar PolyTEMPO 	EC/DMD/DE C Zn(ClO <sub>4</sub> ) <sub>2</sub>	Dyalisis membrane MWCO 1000 g mol <sup>-1</sup>	6.1 mAh	[16]
Poly Naphthalene 	Poly PHQ 	Aqueous H <sub>2</sub> SO <sub>4</sub>	Dyalisis membrane	8.95 Ah l <sup>-1</sup>	[13]
PEG12-AQ micellar 	Fe(CN) <sub>6</sub>	Aqueous KCl	Fumasep, cation exchanging	30.7 mAh	[12]
BTMAPV 	Ferrocene Copolymer 	Aqueous NaCl	Fumasep. Anion exchange	5.47 mAh	[19]
BTMAPV 	PnFc.METAC 	Aqueous NaCl	Fumasep. Anion exchange	29.5 mAh	[18]

### **Morphological and size characterization of amphiphilic block copolymers**

Figure 3.5 displays the characterization of the amphiphilic polymers by dynamic light scattering (DLS), cryogenic electron microscopy (CryoEM) and scanning transmission electron microscopy (STEM). Figure 3.5A shows that the block copolymers morphology consists in a hydrophobic core and a hydrophilic shell. The size corresponding to the block copolymer P1 after being dissolved and self-assembled in water was measured by DLS, observing two particle size populations centered at 68 nm and 190 nm. The particle size distribution changed after the chemical substitution with DMAFc, achieving an average nanoparticle size value of 91 nm for P1Fc. For P2Fc nanoparticles, a broader nanoparticle size distribution was observed (Figure 3.6A). Further study of the size and morphology of the block copolymers before the substitution, was performed by CryoEM. Figure 3.5B shows an average diameter of the self-assembled polymer nanoparticles of 8 nm. The CryoEM study for P2 also evidenced a larger size and a less regular spherical morphology (Figure 3.6B). Besides, the STEM images corresponding to P2Fc exhibited (Figure 3.6C) bigger particle size aggregates than the P1Fc analog. The difference in the average sizes observed by the two different characterization techniques might be because in liquid phase the amphiphilic block copolymers tend to aggregate. In any case, the results confirm that the P1 has a smaller particle size than the P2. In addition, these results also support that the P2-based polymers are not as long-term stable in an aqueous solution. Figure 3.5C displays a distribution of highly monodisperse nanoparticles of 20-40 nm of P1Fc, exhibiting few aggregates.

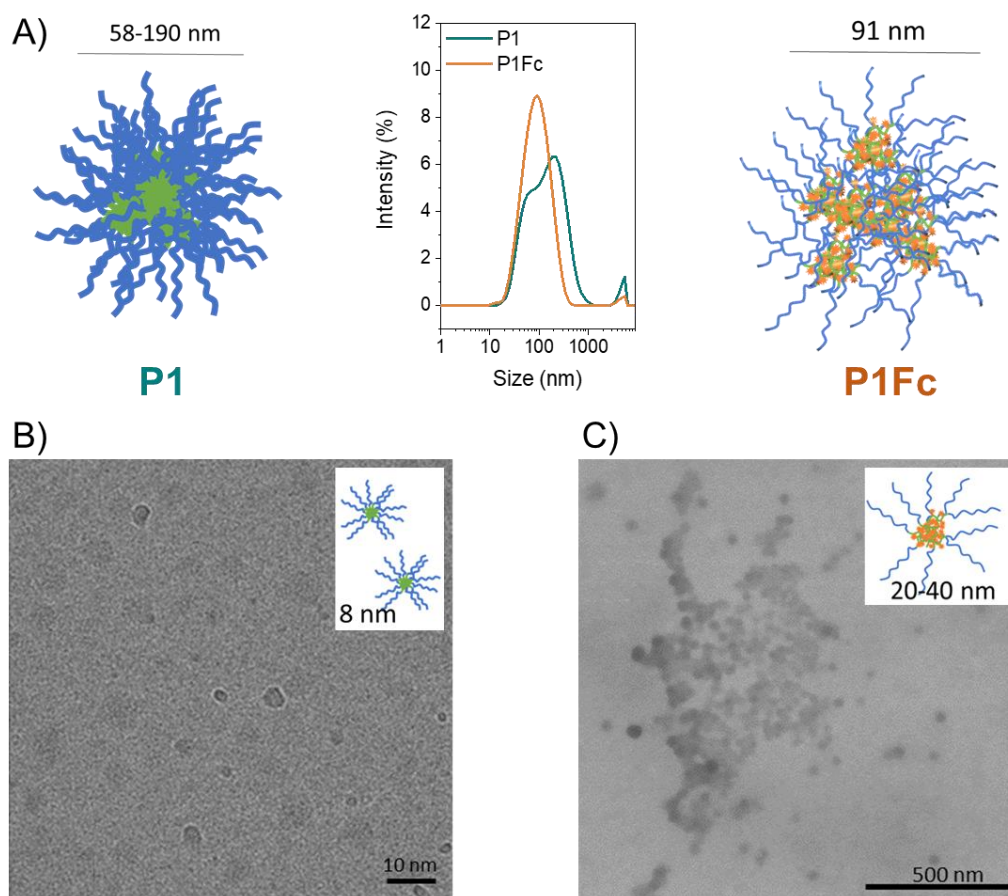


**Figure 3.5.** A) Proposed scheme for the morphology of the amphiphilic block copolymer, P1 (left) and P1Fc (right) after their self-assembly in water. DLS curves show the particle size distribution of 1 g·l<sup>-1</sup> in water (center). B) CryoEM micrograph of P1 in water C) STEM image showing nanoparticles of P1Fc

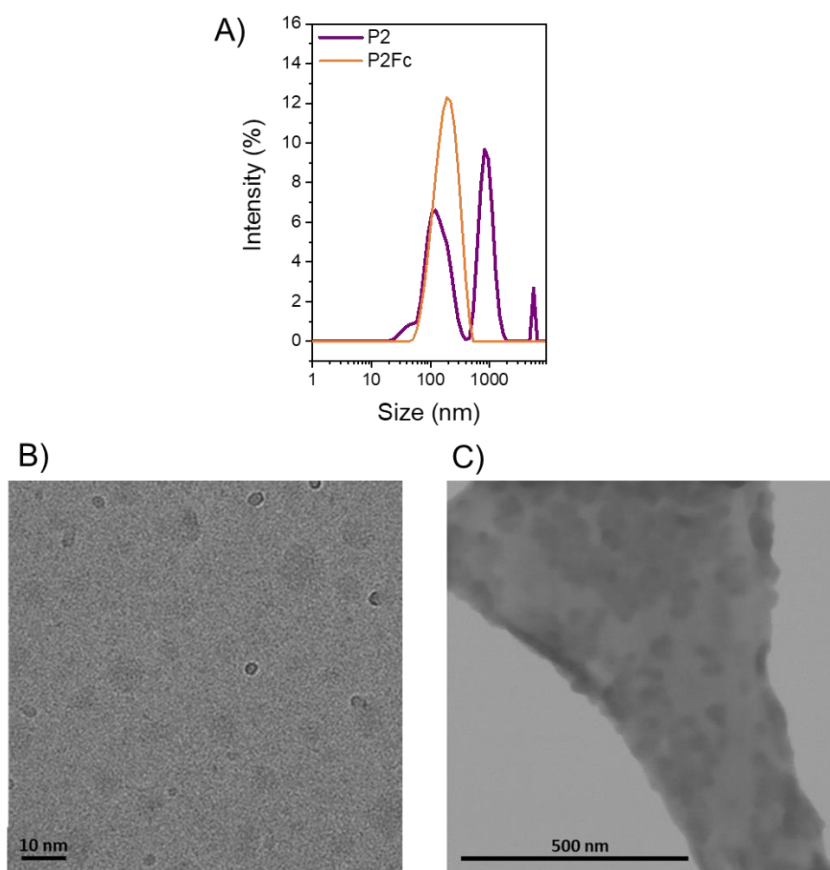


**Figure 3.6.** A) Particle size distributions of a dispersion at  $1\text{g}\cdot\text{l}^{-1}$  in water of P2 and P2Fc by DLS. B) CryoEM images of P2 in water. C) STEM images of P2Fc

### Electrochemical cell conditions and configuration

The dispersibility, time-stability, ionic conductivity, and pH relation of aqueous suspensions for the redox block copolymer nanoparticles were also studied in a broad range of concentrations and under the presence of a variety of supporting salts. A compromise can be observed between the amount of nanoparticles in the suspensions, the type and concentration of the supporting salt, the pH value and the long-term stability of the nanoparticle dispersion (Figure 3.7, Tables 3.3 and 3.4). For instance, considering the future use in a zinc hybrid battery, the polymer nanoparticles were studied in  $\text{NH}_4\text{Cl}$ , which mitigates the formation of zinc hydroxide while cycling [16]. Despite the increase in the conductivity of the redox polymer suspension, the nanoparticles ended up precipitating. Then, other salts such as  $\text{NH}_4\text{PF}_6$ ,  $\text{ZnCl}_2$ ,  $\text{Zn}_6\text{ClO}_8\cdot\text{H}_2\text{O}$ , and a combination thereof were also used. In all the cases, the conductivity improves but the polymer

precipitates with time except in the presence of  $\text{NH}_4\text{PF}_6$ . Therefore, zinc salt containing the anion  $\text{PF}_6^-$  was synthesized [29], observing the increase in conductivity and the long-term stability of the polymer nanoparticles.

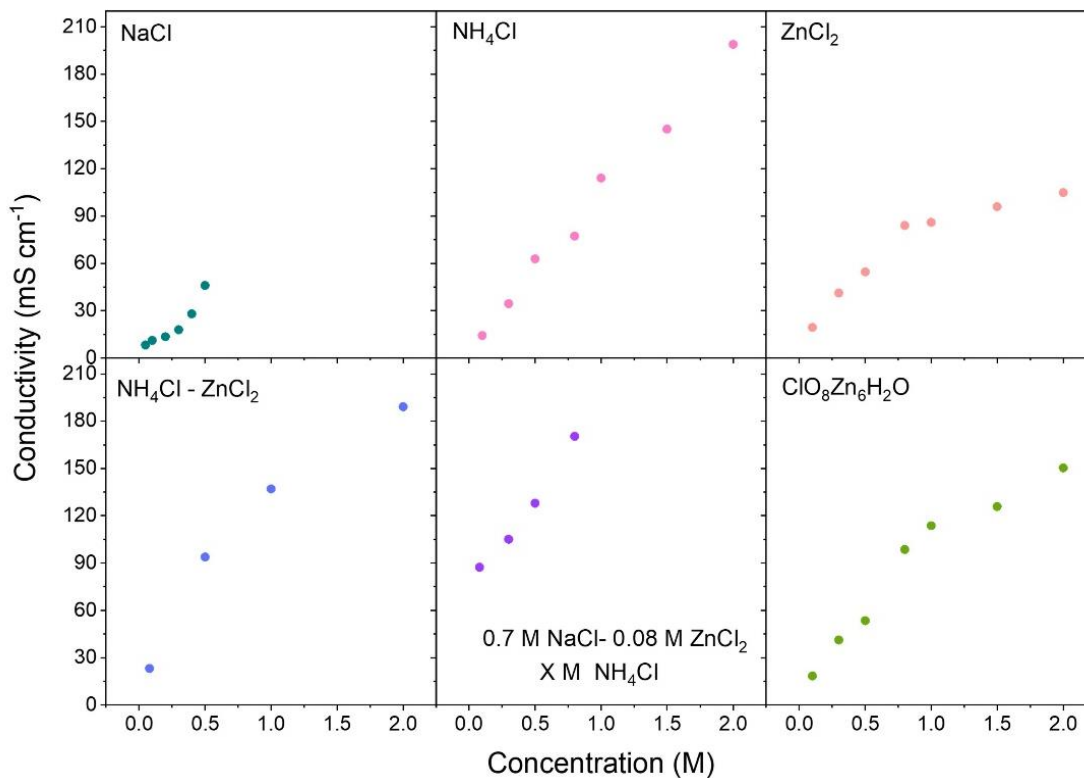


**Figure 3.7.** Ionic conductivity of the block copolymer aqueous suspensions and different electrolyte salt support at different concentrations

**Table 3.3.** Ionic conductivity and stability of a dispersion at 2 mM of P1Fc containing different supporting salts

Sample		Concentration (M)	Conductivity (mS·cm <sup>-1</sup> )	Long time stability
2 mM P1Fc +	NaCl	0.1	13.5	No
	NH <sub>4</sub> Cl	0.1	14.2	No
	NH <sub>4</sub> PF <sub>6</sub>	0.1	11.7	Yes
	NH <sub>4</sub> PF <sub>6</sub> Zn (PF <sub>6</sub> ) <sub>2</sub>	0.1 0.001	11.2	Yes
	NH <sub>4</sub> PF <sub>6</sub> Zn (PF <sub>6</sub> ) <sub>2</sub>	0.4 0.006	44.5	Yes

Therefore, by choosing the right type of anion in the ammonium salt, the time-stability of the polymer nanoparticles in the solution might increase. Conductivity values up to 44.5 mS·cm<sup>-1</sup> were achieved for an aqueous electrolyte composition at 2 mM P1Fc nanoparticles with 0.4 M NH<sub>4</sub>PF<sub>6</sub> and 6 mM Zn(PF<sub>6</sub>)<sub>2</sub> as supporting salts (Table 3.4).

**Table 3.4.** pH values of P1Fc with different concentrations and different salts

Samples	pH
4 mM P1Fc	4.73
2 mM P1Fc	4.88
2 mM P1Fc - 0.1M NaCl	4.75
2 mM P1Fc – 0.1M NH <sub>4</sub> PF <sub>6</sub>	5.00
2 mM P1Fc – 0.5M NaH <sub>2</sub> PO <sub>4</sub>	5.01
2 mM P1Fc – 0.1 M NH <sub>4</sub> PF <sub>6</sub> – 1 mM Zn(PF <sub>6</sub> ) <sub>2</sub>	3.88

However, a 2 mM concentration of an electrolyte composition containing 0.1 M NH<sub>4</sub>PF<sub>6</sub> and 1 mM Zn(PF<sub>6</sub>)<sub>2</sub> evidenced a conductivity value of 11.2 mS·cm<sup>-1</sup>, with values of pH ranging between 4 and 5 was settled for further characterization experiments due to the lower content of the supporting salts needed to maintain similar long-term stability. The efficiency and rate of charge



---

---

and discharge processes of the aqueous nanoparticle suspensions of variable supporting electrolyte salts at different concentrations were characterized under static and dynamic (i.e. steady state) conditions.

Counter-intuitively, only those electrochemical studies using porous graphite felt as received (i.e., non-thermally treated). As working electrode material, the polymer nanoparticle showed reactivity in an aqueous media (more details in Figure 3.8). The electrochemical properties of two different porous carbon electrodes as working electrode materials were studied. For this purpose, graphite felt (GF) and gas diffusion layer (GDL) materials were chosen. A heat treatment at 500 °C for 12 h on air was performed on each electrode. The electrochemical reactivity of the block-copolymer nanoparticles was studied by CV. Then, results were compared to the non-thermally treated samples. Figure 3.8 shows the electrochemical response of the different electrodes. Surprisingly, the electrochemical reactivity shown in those samples after being thermally treated was lower than the non-treated materials. The reason might be related to the fact that the heat treatment provoked the oxidation of the surface of the electrodes, making it more hydrophilic. The electrolyte nanomaterial developed here showed more reactivity when using working electrodes that are not too hydrophilic.

In order to characterize the charge and discharge properties under static conditions, a galvanostatic study of the polymer nanoparticles was carried out in a static electrochemical cell. Figure 3.9 shows the galvanic charge and discharge measurement of polymer nanoparticles that was carried out in a three-compartment cell with Ag/AgCl as reference electrode, Pt wire as counter and GF as working electrode were used inside each compartment. A dialysis membrane was used to separate the compartments. The galvanostatic study was performed at a current of 0.047 mA up to 0.7 V vs. Ag/AgCl. In the compartment containing the GF electrode there was a suspension of P1Fc nanoparticles with a 2 mM concentration and supporting salt (0.4 M  $\text{NH}_4\text{PF}_6$ ). In the other two tanks there were deionized water with supporting salt (0.1 M  $\text{NH}_4\text{PF}_6$ ). In Figure 3.9B the charge and discharge curve at constant current can be seen, where a high reversibility of the system is observed in these conditions.

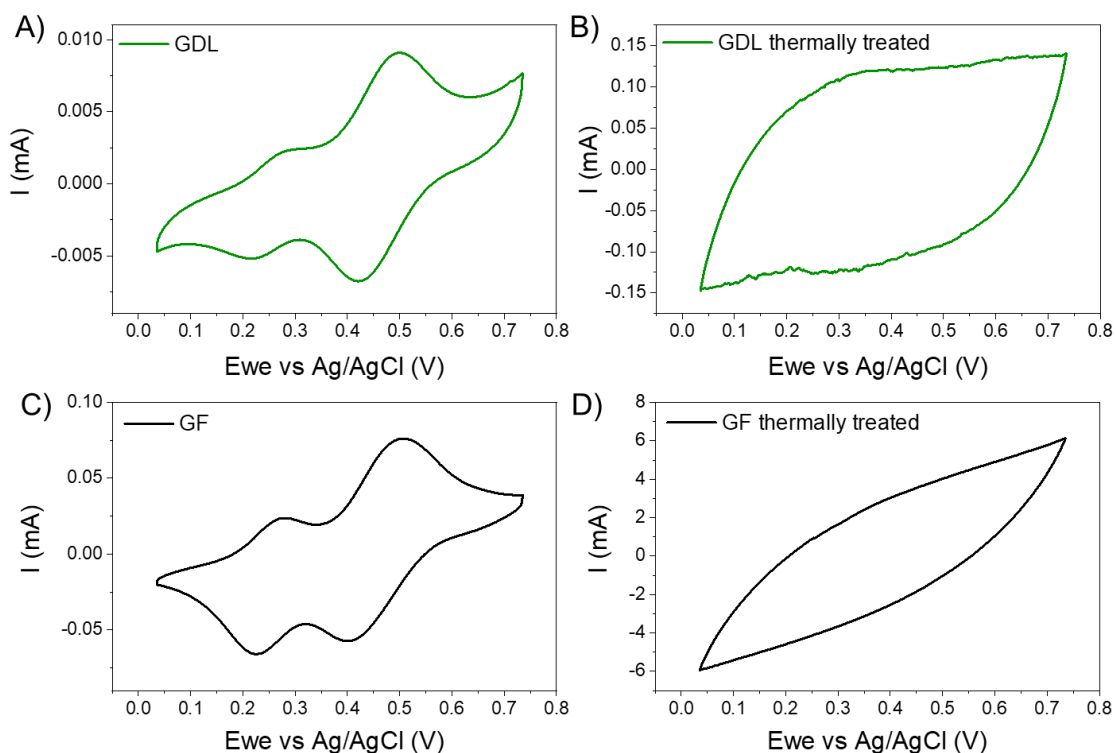


**Figure 3.8.** Analysis of the electrochemical reactivity of a suspension at 2 mM P1Fc nanoparticles with 0.1 M  $\text{NH}_4\text{PF}_6$  as salt support by using different porous carbon materials as working electrode: A) Gas diffusion layer (GDL) as received. B) GDL thermal treatment (500 °C, 12h). C) Graphite Felt (GF) as received. D) GF thermally treated (500 °C, 12h)

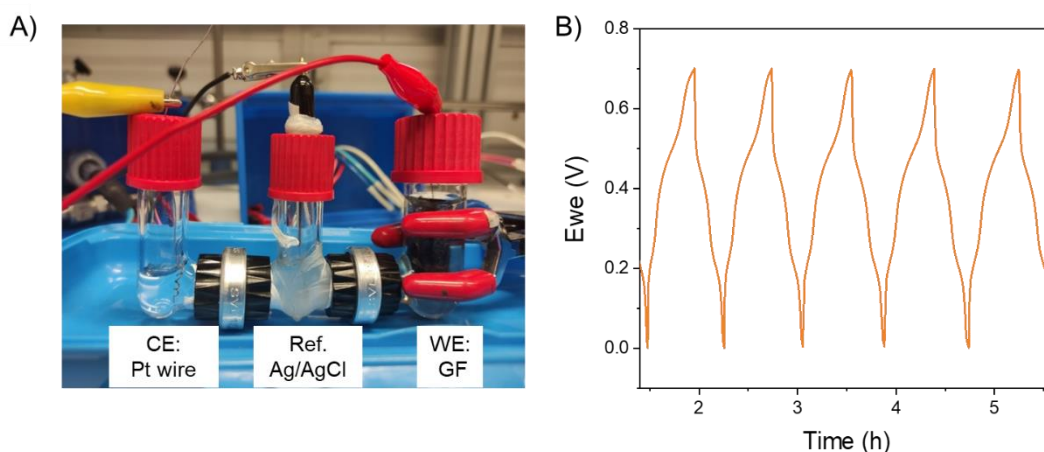


**Figure 3.9.** Long-term stability test of a suspension of P1Fc nanoparticles under static conditions in a three-compartment cell. A) Three-electrode cell used in P1Fc 2 mM with 0.1 M  $\text{NH}_4\text{PF}_6$  as salt support, B) Selected charge/discharge profiles from constant current cycling 0.047 mA shows high reversibility of the system

The amphiphilic block copolymer nanoparticles did not react when using the same porous felt as electrode material but after thermal treating on air. The block copolymer nanoparticles (2 mM P1Fc) exhibit a CV characterized by two well-separated and reversible oxidation waves at  $E_{1/2}=154$  mV and  $E_{1/2}= 369$  mV vs. Ag/AgI at  $20 \text{ mV}\cdot\text{s}^{-1}$  (Figure 3.10A). This electrochemical behaviour is consistent with interactions between the Fc units linked by the vinyl monomer along the main polymer chain. A similar cyclic voltammetric response was observed for ferrocenyl dendrons and dendrimers in solution [30]. To our knowledge, this is the first example of Fc-based polymer electrolyte nanoparticles system possessing a controlled number of interacting metal centers. A previous report on block copolymers electrolytes for RFBs with electroactive Fc moieties [14] exhibited a single reversible oxidation process, indicating that all the iron centers are essentially non-interacting. All the Fc redox-active units in those block copolymers behave independently, and exchange electrons with the electrode in a wave characteristic of a one-electron process.

## **Kinetic properties of the block copolymers**

### **Cyclic voltammetry Analysis**

Further analysis of the scan rate of the CV peak height did decisively show a strong correlation vs.  $v$  (scan rate) (Figure 3.10B and 3.10C), which suggests that the charge transport through the nanoparticle is limited by the ions and water molecules diffusion into the polymer nanoparticle. Although both anodic and the first cathodic waves have shown the form required if transport to the electrode was controlled by diffusion, the second cathodic wave did not. The correlation of the current intensity of this second cathodic peak vs.  $v$  (scan rate) was neither described by pure diffusion limited mass transfer, nor that expected for a surface-confined electroactive nanoparticle. These could be characteristic of Fc-containing nanoparticles in which oxidized form is insoluble, and the reduced form is soluble independently of having one or two waves associated with the one-electron transfer [30]. Similar behaviour has been observed before for Fc-block copolymer colloids as charge carriers for RFB in organic media. Moreover, this result could explain the sedimentation phenomena evidenced

here (see the following sections) and in the cited publication [14], when the size-exclusion electrolytes were studied in a RFB.

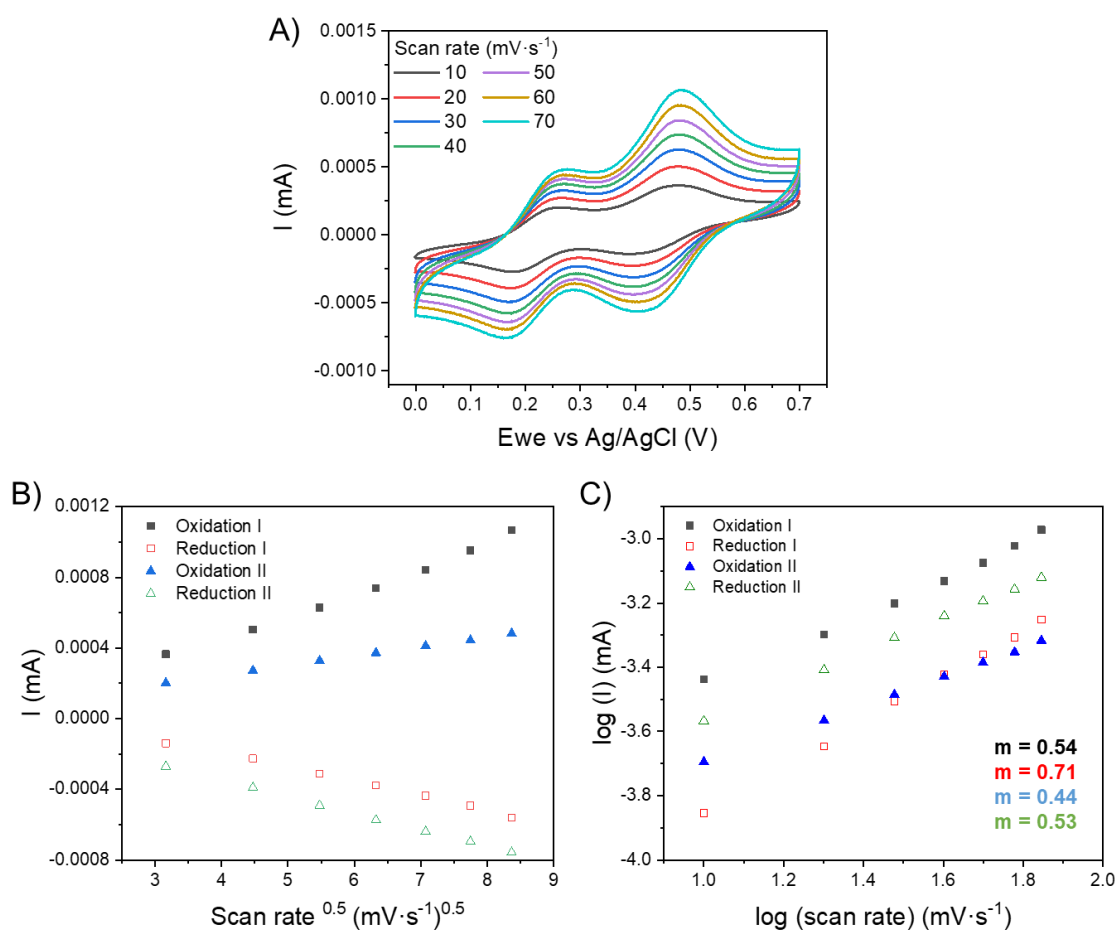


**Figure 3.10.** Electrochemical characterization of an aqueous suspension of 2 mM P1Fc nanoparticles containing 0.1 M NH<sub>4</sub>PF<sub>6</sub> as supporting salt electrolyte. A) Cyclic voltammetry at different scan rates. B) Scan-rate dependence analysis. C) Randles-Sevcik analysis

The same study has been performed for P2Fc, showing that when the scan rate increased, the current intensity increases and the potentials shifted (Figure 3.11). The Randles-Sevcik analysis suggested a diffusion-limited process, as a slope value close to 0.5 was found for a single P2Fc process. While the rest of the processes are not controlled by diffusion. This corroborates that P1Fc and P2Fc nanoparticles behave differently, possibly due to their different morphology and nanoparticle size as seen in their morphological

characterization. There must be an effect on the distribution of ferrocenes in the particle.

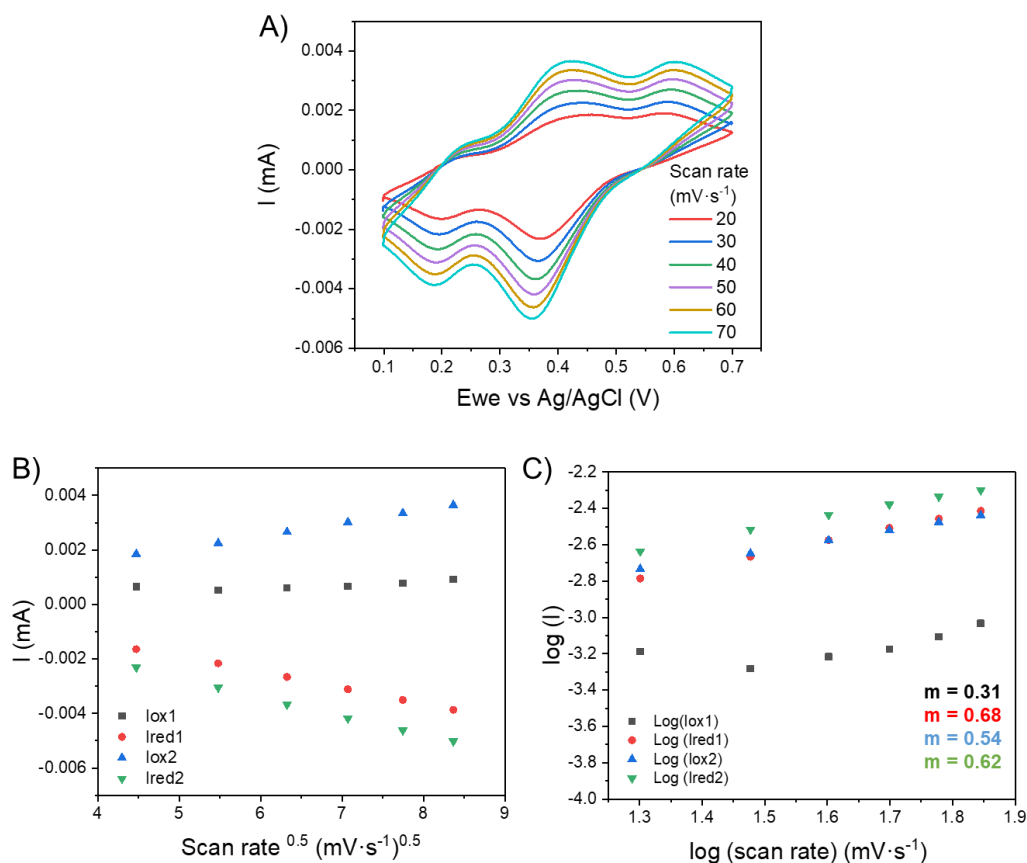


**Figure 3.11.** Electrochemical characterization of a suspension of P2Fc nanoparticles at 7 mM containing 0.1 M  $\text{NH}_4\text{PF}_6$ . A) Cyclic voltammetry at different scan rates. B) Scan-rate dependence analysis of the suspension of P2Fc nanoparticles. C) Randles-Sevcik analysis showing single anodic wave of the second process is described by diffusion-limited mass transfer

### Linear sweep voltammetry-Rotating Disk Electrode (RDE)

Taking a further step in the electrochemical study of the polymer nanoparticles, their kinetic constants were determined by linear sweep voltammetry using a glassy carbon rotating disc electrode (RDE) (Figure 3.12). Evaluating the RDE analysis by Levich (limiting current vs. square root of the spin rate), a diffusion coefficient  $D$  of  $3.3\cdot 10^{-11}$   $\text{cm}^2\cdot\text{s}^{-1}$  was obtained. This value is low compared to other electrolyte systems based on Fc-organic and polymer electrolytes studied

in RFBs, as shown in Table 3.5. However, the rate constant ( $k_0$ ) obtained, was  $6.8 \cdot 10^{-5} \text{ cm} \cdot \text{s}^{-1}$ , being in the same order of magnitude as those redox electrolytes published reports.

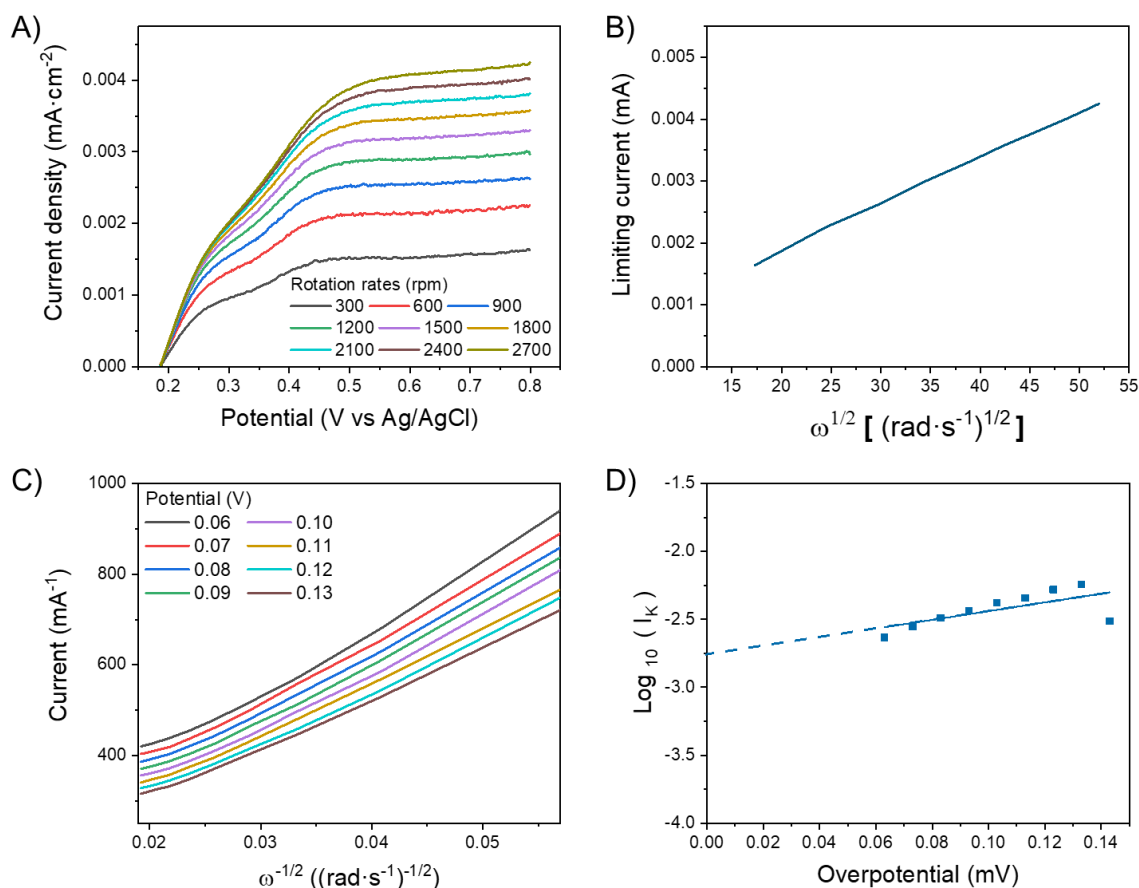


**Figure 3.12.** Electrochemical characterization of an aqueous suspension of 2 mM P1Fc nanoparticles containing 0.1 M  $\text{NH}_4\text{PF}_6$  as supporting salt electrolyte. A) RDE measurement with a scan rate of  $5 \text{ mV} \cdot \text{s}^{-1}$  from 300 to 3100 rpm. B) Levich plot at 0.8 V vs. Ag/AgCl. Using the Levich equations  $D = 3.3 \cdot 10^{-11} \text{ cm}^2 \cdot \text{s}^{-1}$  is obtained. C) Koutecky-Levich plot for different potentials. D) Tafel plot, where  $k^0 = 6.8 \cdot 10^{-5} \text{ cm} \cdot \text{s}^{-1}$  and  $\alpha = 0.19$

In view of the assessment of the block copolymer nanoparticles as the main component of an aqueous electrolyte in a hybrid zinc RFB, the electrochemistry of P1Fc in the presence of the salts that provide the best results in terms of stability and reactivity for their use in a hybrid zinc RFB combined with the P1Fc nanoparticles (Figure 3.13) have also been studied here. The value of the

kinetic parameters was in the same order as those observed for the P1Fc-Zn(PF<sub>6</sub>)<sub>2</sub> electrolyte.

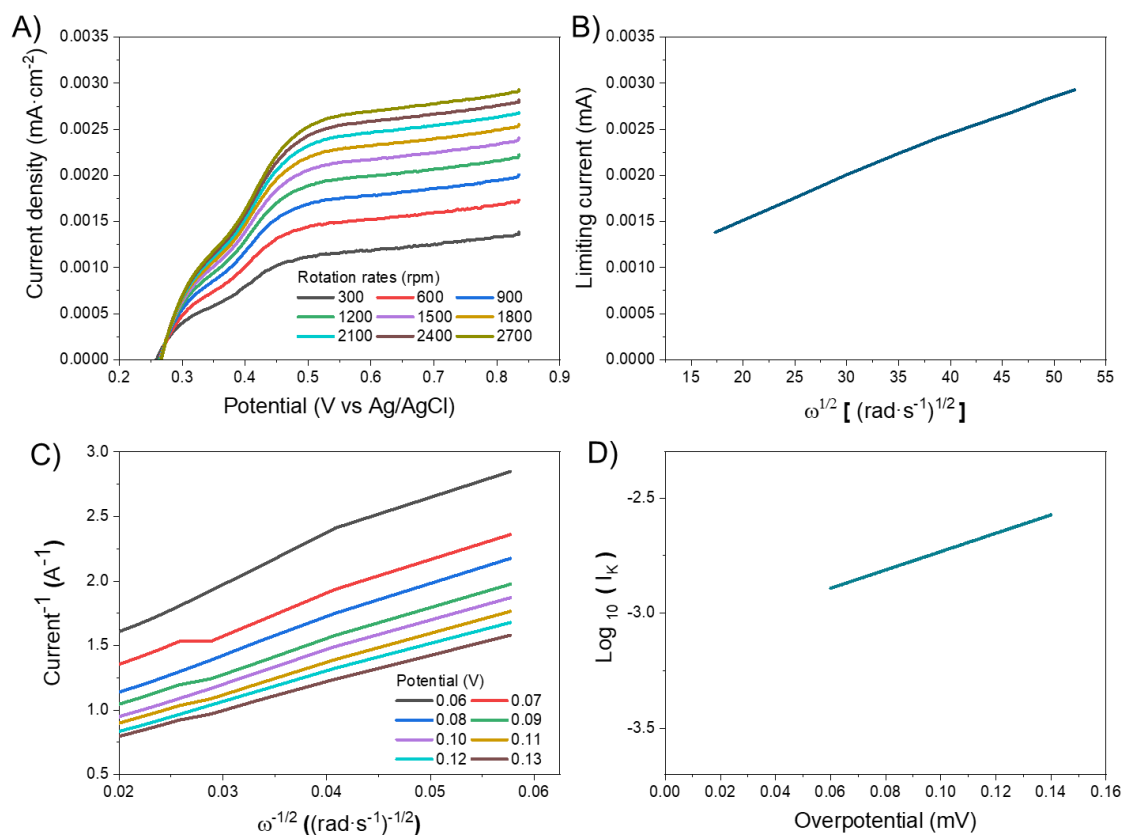


**Figure 3.13.** Electrochemical characterization of an aqueous suspension of 2 mM P1Fc nanoparticles containing 0.4 M NH<sub>4</sub>PF<sub>6</sub>, 1 mM Zn<sub>2</sub>(PF<sub>6</sub>)<sub>2</sub> as supporting salt electrolyte A) RDE measurement with a scan rate of 5 mV·s<sup>-1</sup> from 300 to 3100 rpm. B) Levich plot at 0.8 V vs. Ag/AgCl. Using the Levich equations  $D = 1.53 \cdot 10^{-11}$  cm<sup>2</sup>·s<sup>-1</sup> is obtained. C) Koutecky-Levich plot for different potentials. D) Tafel plot, where  $k^0 = 5.08 \cdot 10^{-5}$  cm·s<sup>-1</sup> and  $\alpha = 0.13$

It is observed that the values obtained from the RDE measurements are lower than other electrolyte systems based on Fc-organic electrolytes as shown in the following Table 3.5. These results prove the impact that of the nanoparticulated nature of this copolymer has on the mass transport of the charged species from the solution to the surface of the electrode, compared to other systems where the redox electrolyte behaves as a liquid solution rather than a suspended solid in water. However, these results confirm that there were no limitations for the

intra- and inter-nanoparticle (i.e., nanoparticle aggregate) electron transfer between the Fc centers.

**Table 3.5.** Comparison between electrochemical properties of the block-copolymer nanoparticles and different catholytes and anolytes

Anolyte	Catholyte	D (cm <sup>2</sup> ·s <sup>-1</sup> )	K <sub>0</sub> (cm·s <sup>-1</sup> )	α	Ref.
BTMAPV	Ferrocene methacrylamide monomer	b) 9.8·10 <sup>-7</sup> (in water)	b) 4.4·10 <sup>-4</sup>	b) 0.6	[19]
Zinc	Poly(TEMPO)	b) 1.65·10 <sup>-7</sup>	b) 9.93·10 <sup>-4</sup>	b) 0.44	[15]
PEG12-AQ	K <sub>4</sub> Fe(CN) <sub>6</sub>	a) 2.236·10 <sup>-6</sup>	a) 1.59·10 <sup>-2</sup>	a) 0.59	[12]
BTMAP-Vi	BTMAP-Fc	a) 3.3·10 <sup>-6</sup> b) 3.1·10 <sup>-6</sup>	a) 2.2·10 <sup>-2</sup> b) 1.4·10 <sup>-2</sup>	a) 0.47 b) 0.53	[21]
MV	FeNCI	3.74·10 <sup>-6</sup>	3.66·10 <sup>-5</sup>	-	[31]
Viologen-RAPs (158kDa)	Ferrocene-RAP	a) 6.7·10 <sup>-7</sup> b) 5.4·10 <sup>-6</sup>	a) 6.5·10 <sup>-3</sup> b) 2.2·10 <sup>-2</sup>	-	[32]
Viologen	TEMPO	a) 7.6·10 <sup>-7</sup> b) 7·10 <sup>-8</sup>	a) 9·10 <sup>-5</sup> b) 4.5·10 <sup>-4</sup>	- b) 0.68	[33]
Zn	P1Fc	b) 1.53·10 <sup>-11</sup>	b) 5.08·10 <sup>-5</sup>	b) 0.13	Our work

a) Anolyte data

b) Catholyte data

### Study of the charge storage properties of the amphiphilic block copolymer nanoparticles in redox flow systems

The assessment of the charge storage properties of the novel nanoparticulated polycatholyte in two-redox flow cell systems is shown in the following section.

The first redox flow system contains a 2,7-anthraquinone disulphonated (2,7 AQDS) anolyte and a non-porous, Nafion™ fluorinated membrane separating both compartments of the battery (Figure 3.14A). It was observed that the use of highly acidic or basic pH values minimized the long-term stability of the Fc-block copolymer nanoparticles in aqueous media. For that reason, the electrolyte's pH value was adjusted to 4 on both sides of the cell using 0.5 M



$\text{NaH}_2\text{PO}_4$  as supporting salt and as a buffer to keep both the electrochemical activity of the 2,7 AQDS and the long-term stability of the amphiphilic Fc-block copolymer nanoparticles in water. The redox block copolymer nanoparticles at a pH value of 4 could be paired with 2,7 AQDS anolyte in a full cell, with a theoretical cell voltage value up to 0.8 V (Figure 3.14B). The cell could be charged and discharged, but it did not retain most of its initial theoretical capacity values of 0.75 mA·h (Figure 3.14C). This drop-in capacity was probably due to the pH value of the electrolyte causing a quasi-reversible reaction of the 2,7 AQDS.

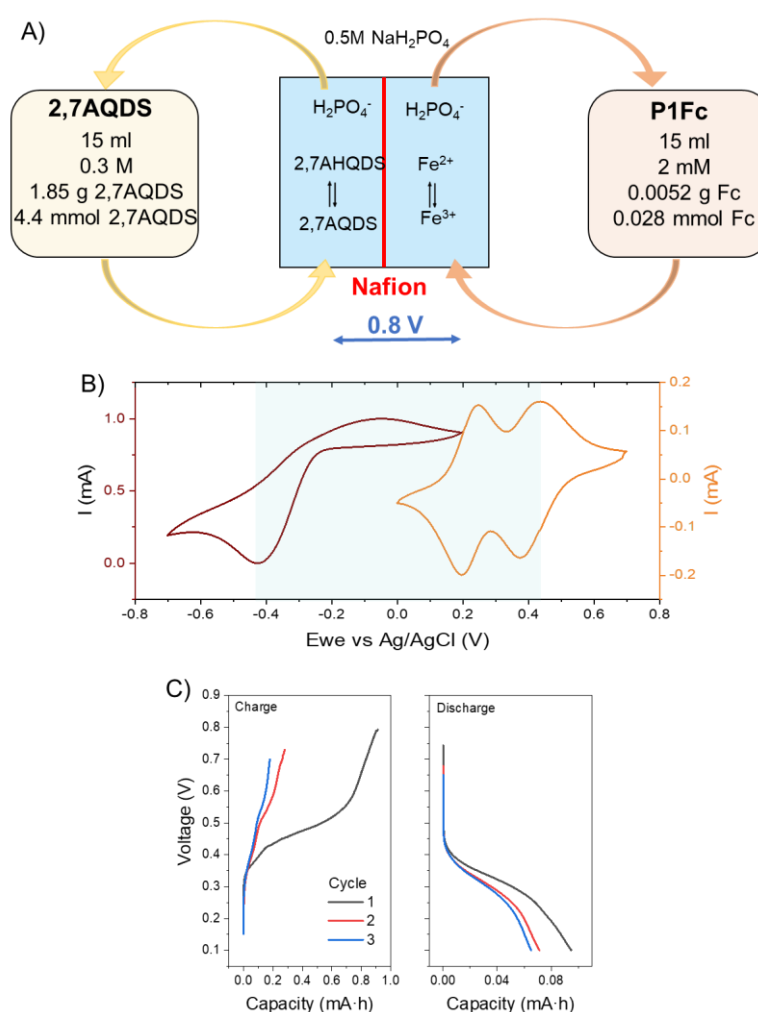


**Figure 3.14.** A) Scheme of the conditions used in each tank and the redox processes occurring inside the cell. B) Cyclic voltammogram of 0.4 M 2,7AQDS 0.5M  $\text{NaH}_2\text{PO}_4$  and 2 mM P1Fc, 0.5M  $\text{NaH}_2\text{PO}_4$ , scan rate  $10 \text{ mV}\cdot\text{s}^{-1}$ . C) Selected cycles of the redox flow battery test at 0.047mA

Besides, block copolymer sedimentation could also be one of the causes of the drop in capacity, also observed in the hybrid Zn-polymer battery used to assess the charge capacity of the active polymer nanoparticles (Figure 3.15). This hybrid flow system (Figure 3.15A) comprised a zinc foil as negative electrode of the cell separated from the polycatholyte by a porous cellulose-based dialysis membrane (2.5 x 2.5 cm) with a 2.5-3 nm pore size (Figure 3.15B). With that pore size, the dialysis membrane could effectively retain the cathode active Fc-block copolymer nanoparticles (with average particle size of 20 nm, which is ten times larger than the pore size of the dialysis membrane) but is permeable for the supporting electrolyte. The supporting electrolyte in both sides of the battery was an aqueous 0.1 M  $\text{NH}_4\text{PF}_6$  / 1 mM  $\text{Zn}(\text{PF}_6)_2$  solution with a pH value of  $\sim 4$ .

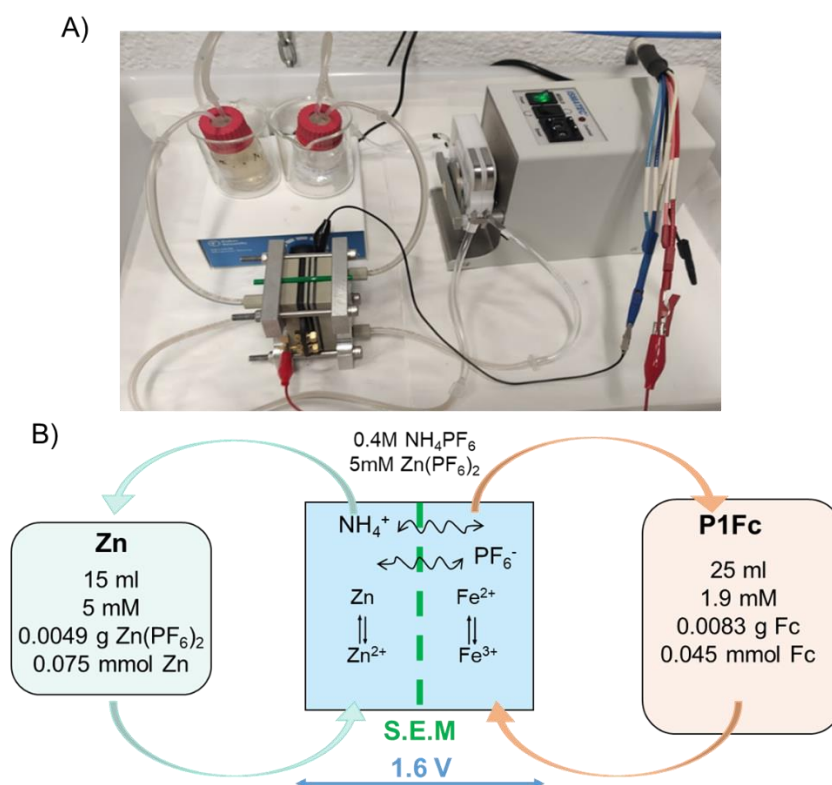


**Figure 3.15.** A) Image of the experimental setup at ambient conditions. The peristaltic pump was set to  $20 \text{ ml} \cdot \text{min}^{-1}$  to cycle the electrolyte in the cell stack, which is measured with a VMP3 potentiostat (Biologic, France). B) Scheme showing the experimental composition used in each tank and the redox processes occurring inside the cell

---

---

Three-electrode cyclic voltammetry revealed the electrodeposition of  $\text{Zn}^{2+}$  on the glassy-carbon electrode for potentials lower than  $-1.2$  V and dissolution at potentials above  $-0.98$  V vs. Ag/AgCl (Figure 3.16A). The redox reaction revealed a narrow redox wave split of  $0.21$  V. This is attributed to the unrestricted ionic conductivity of  $\text{Zn}^{2+}$  in aqueous-based electrolytes. In addition, the cyclic voltammetry of an aqueous suspension of P1Fc nanoparticles with the same salt support might lead to a potential cell voltage of  $1.6$  V when coupling both redox couples in a subsequent battery application. In fact, the cell provides an open-circuit voltage of  $1.35$  V and can be safely charged and discharged at constant current within a voltage window of  $1.60$  V (Figure 3.16B). The cell was flushed with nitrogen gas before cycling, so the evolution of oxygen or hydrogen was not observed. A maximal capacity of  $3.1$  mA·h was reached. The following charge and discharge cycles showed how the charge storage capacity decreases although the efficiency reached values of approximately  $80$  % (Figure 3.16C). This is comparable to previously reported flow battery systems based on polymer electrolytes, where maximal capacities and efficiency values in the range of  $1.1$  Ah·l<sup>-1</sup> and  $80$  % were respectively achieved [16].

The retention inside the graphite felt electrode acting the latter as a filter (Figure 3.17A) and partial clogging of the pores of the porous size-exclusion membrane by aggregation at the entrance of the redox polymer nanoparticles on the cell (Figure 3.17B) might cause the capacity decrease. The cyclic voltammograms of anolyte (blue curve) and the catholyte (orange curve) samples taken after 5 cycles corresponding to the oxidative range are shown in Figure 3.16D. The crossover of the electrolyte from the positive to the negative battery compartments was negligible as no redox activity of the Fc-block copolymer nanoparticles was observed.

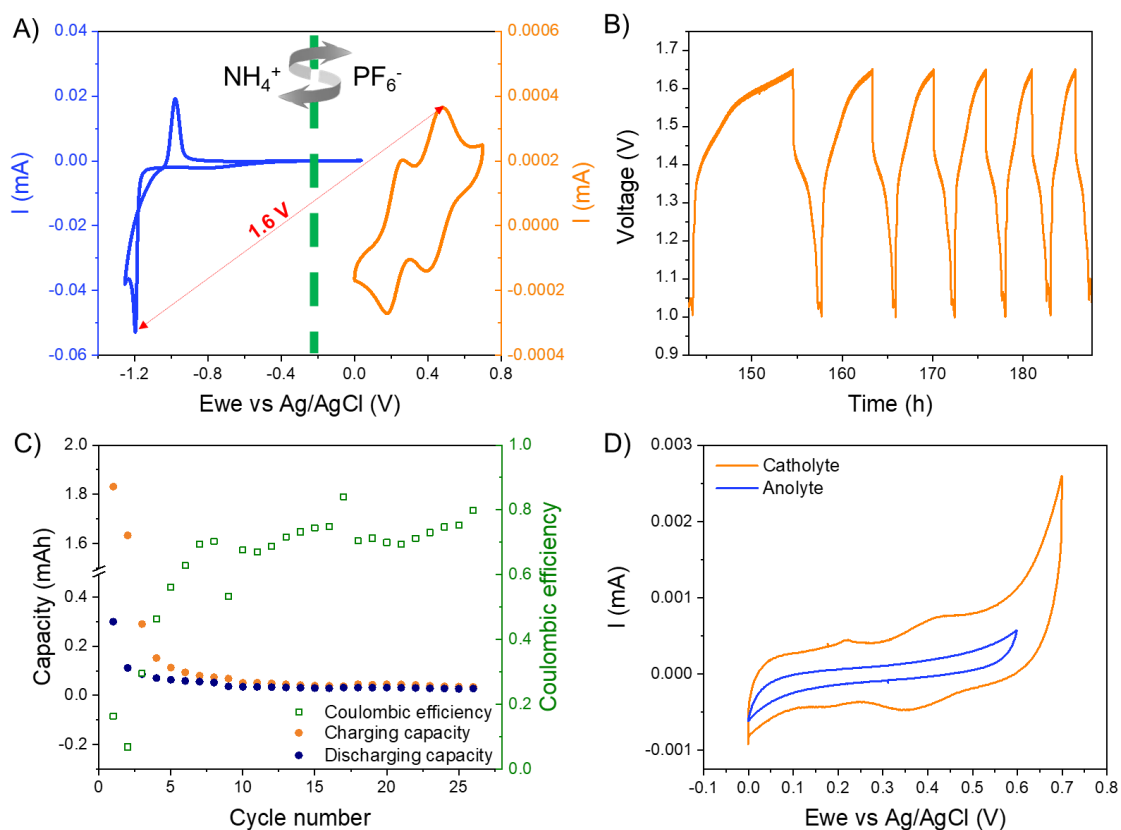


**Figure 3.16.** A) Cyclic voltammogram of an aqueous suspension of P1Fc nanoparticles at 2 mM with 0.1 M  $\text{NH}_4\text{PF}_6$  and 1 mM  $\text{Zn}(\text{PF}_6)_2$  as supporting electrolyte, scan rate  $10 \text{ mV}\cdot\text{s}^{-1}$  (blue line:  $\text{Zn}^{2+}/\text{Zn}^0$ , left y-axis; orange line:  $\text{P1Fc}^{3+}/\text{P1Fc}^{2+}$ , right y-axis). B) Exemplary charge-discharge curves at a current density of 0.027 mA. C) Capacity and coulombic efficiency of the hybrid redox flow battery over 26 cycles at a current density of 0.027 mA at room temperature. D) Analysis by CV of each of the analytes of the cell after cycling

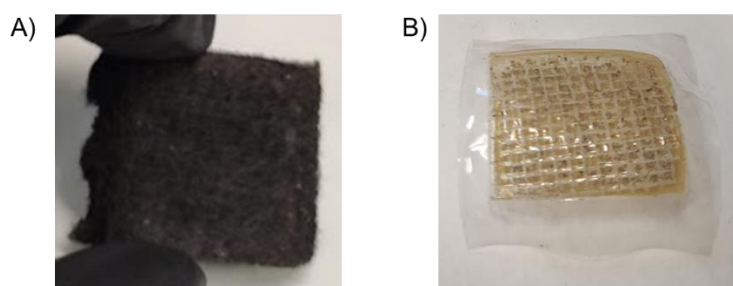


**Figure 3.17.** A) and B) show respectively the graphite felt electrode and the size-exclusion membrane after the electrochemical cycling of the redox flow battery

### Correlation between nanoparticle size, electronic and electrochemical properties

DLS and UV-Vis were coupled to galvanostatic measurements, so a deeper understanding on the function and failure mechanisms of the redox amphiphilic polymer nanoparticles can be obtained. The results are exposed together in Figure 3.18. The study monitored the average particle size distribution and the electronic properties of an aqueous suspension of the polymer nanoparticles (P1Fc) at a concentration of 2 mM with 0.1 M  $\text{NH}_4\text{PF}_6$  and 1 mM  $\text{Zn}(\text{PF}_6)_2$ , during the electrochemical oxidation and reduction processes. Typical DLS and UV-Vis cuvettes were transformed into a 3-electrode configuration cell containing an Ag/AgCl as a reference electrode; Pt wire was used as a counter electrode, and carbon fiber as a working electrode (Figure 3.18).

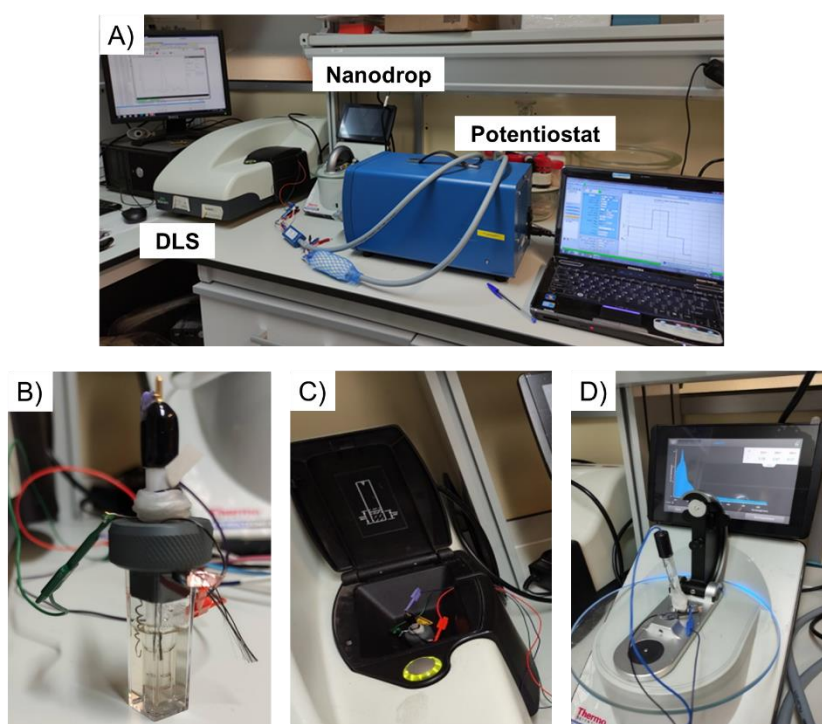


**Figure 3.18.** A) Image of techniques used to study the correlation between the nanoparticle size and the electronic properties of the polymer nanoparticles and the electrochemical oxidation and reduction processes. B) DLS and UV-Vis cuvette transformed into a 3-electrode configuration cell containing an Ag/AgCl as a reference electrode, Pt wire as a counter electrode, and carbon fiber as a working electrode. C) DLS equipment with cuvette and connections to perform the measurement. D) Image showing the Nanodrop equipment with UV-vis cuvette inside and the electrical connections to the potentiostat

The protocol consisted of cycling at a constant current (5  $\mu\text{A}$ ) up to a potential window value of 0.8 V vs. Ag/AgCl, and then holding the potential for 24 h until the current intensity was close to zero, thus ensuring that most of the Fc-block copolymer was being oxidized. A reduction up to 0 V vs. Ag/AgCl and then keeping it at that potential for 24 h. Then, both DLS and UV-Vis measurements were performed. Three oxidation and reduction cycles were applied to study the size evolution of the amphiphilic block copolymer nanoparticles. After 24 h of oxidation, the average nanoparticle size was 78 nm. After reduction for another 24 h, the size of the nanoparticles was slightly above 91 nm. In the second cycle, noticeable changes began to be observed in both oxidation and reduction processes, with the appearance of two particle size populations. In the third cycle, it was observed that the particle size distribution returned to a single size distribution after the oxidation, with an average nanoparticle size of 85 nm, while in the reduction step, a two-particle size distribution were displayed again. The average particle sizes corresponding to the two populations that appeared after the reduction process in the second and third cycles are practically the same, 68 and 396 nm. The area under the curve for the particle size distribution of the second cycle was higher than that for the third one. That must be related to the aggregation of the nanoparticles during the electrochemical reduction, leading to larger particle sizes and then precipitating to the bottom of the cuvette. The changes in the particle size between oxidation and reduction processes were probably due to the trade-off between the coulombic interactions between the  $\text{P1Fc}^{+3/+2}$  species and their hydrophilic/hydrophobic overall interactions between the blocks of the polymer and water. The increase in repulsion between the Fc centers that are in close proximity originates the separation between the nanoparticles, forming smaller nanoparticle sizes during the oxidation process. Whereas Fc was reduced, the overall charge tends to aggregate the particles. These results are consistent with the two-redox waves observed by CV analysis, caused by the interactions between the Fc units anchored in the polymer behaving dependently on each other during their exchange of electrons with the electrode. This fact might boost the intra- and internanoparticle's electrostatic interactions. These results confirmed what other groups reported before about the influence of the oxidation state of the Fc on both: (i) the copolymer structure and morphological changes [22] and; (ii) the

---

---

dispersion stability of the polymer nanoparticles in the solvent [14]. Regarding the latter, the possible block-copolymer degradation during the electrochemical cycling, which can then change the concentration of the Fc centers alongside a nanoparticle and appear to modify the polarity of the block-copolymer chains, along with their capacity, cannot be discarded. Therefore, the size distribution of the oxidized or reduced amphiphilic block-copolymer nanoparticles might be due to two opposite effects: (i) entropic effects and; (ii) electrostatic interactions. In fact, as the charge builds-up, the polymer nanoparticles might either split into smaller ones if the electrostatic interactions are higher than the polar interactions or go from smaller size aggregates to bigger ones. In that case, the increase in the particle size promotes their precipitation, and then the battery capacity drops.

Regarding the UV-vis measurements, a slight shift in the maximum absorbance value from 280 nm to 320 nm for the first oxidation-reduction cycle was observed, as it is shown in Figure 3.19. A red shift in the reduction process of the second cycle reflected the influence of the particle aggregation on the electronic structure of the polymer nanoparticles. The third cycle showed a decrease in the intensity of the maximum absorbance band, most probably due to the aggregation and sedimentation processes observed by DLS. From these results, the correlation between the electronic changes and the variation in the nanoparticle size observed by UV-vis and DLS, respectively were confirmed.

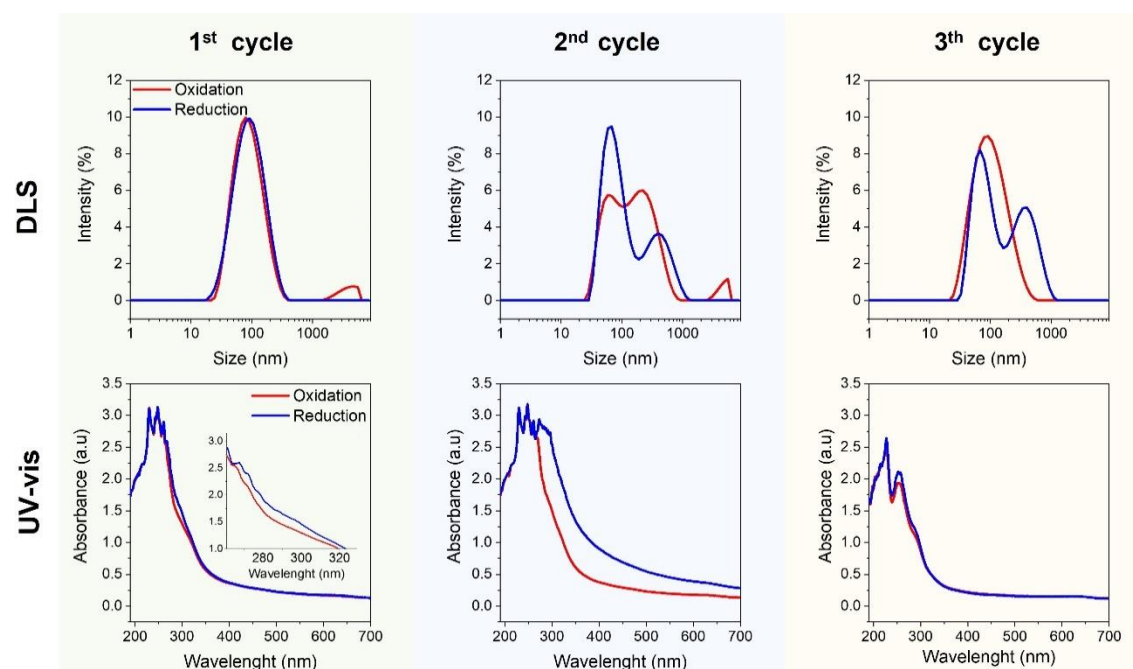


**Figure 3.19.** Particle size distribution measure by DLS (up) and optical properties study by UV-Vis spectra (down) of a concentration 2 mM of P1Fc nanoparticles containing 0.1 M  $\text{NH}_4\text{PF}_6$  supporting electrolyte when subjected to electrochemical oxidation and reduction processes

## Conclusions

Novel amphiphilic block copolymer nanoparticles containing redox active DMAFc units linked to its hydrophobic segments have been designed, prepared, and characterized in this work. The new electroactive material has showed highly-water dispersibility and an experimental capacity that is viable for practical application as a size-exclusion electrolyte in low-cost aqueous redox flow batteries. Adjusting the concentration of Ferrocenyl moieties grafted up to  $1.7 \cdot 10^{-3}$  mmol by chemical substitution, and selecting the right combination of supporting salt, an improvement in long-term stability was achieved. Besides, ionic conductivities of  $44.5 \text{ mS} \cdot \text{cm}^{-1}$  at pH close to neutral value, turns the polymer nanoparticle electrolyte quite promising compared to current redox electrolytes based on Vanadium compounds operating in highly acidic media and other organic-based polymer electrolyte systems under study, using expensive fluorinated membranes too. Electrochemical studies of the polymer nanoparticles using a 3-electrode configuration cell reveal an efficient charge



transport between each of the Fc motifs in the polymer nanoparticle while keeping the redox peaks reversibility. The implementation of the innovative nanomaterials as polycatholyte in a Zn hybrid aqueous redox flow battery display a capacity value of 3.1 mA·h and a full battery voltage of  $\approx 1.6$  V. No transient of the polymer nanoparticles crosswise the inexpensive porous membrane used in the redox flow battery is evidenced. It is the first time, that highly-water dispersible Fc-containing block copolymer nanoparticles have been developed as size-exclusion electrolytes showing a high capacity to store charges electrochemically. It is clear that the chemistry of these block-copolymer electrolyte materials can be controlled further, including for example another hydrophilic segments, or redox active groups to avoid aggregation and sedimentation of the nanoparticles, so a capacity retention and long-term cycling stability can be achieved. The proper design of current collectors and porous electrode materials with more open 3D structures will be also necessary to bring polymer nanoparticles redox flow batteries closer to practical applications. This novel and environmentally friendly aqueous analytes could also be applied to other electrochemical uses like electrocatalysts, carbon capture, and thermoelectrochemical displays.

## References

- [1] P. Ravestain, G. van der Schrier, R. Haarsma, R. Scheele, and M. van den Broek, "Vulnerability of European intermittent renewable energy supply to climate change and climate variability," *Renew Sust Energy Rev*, vol. 97, pp. 497–508, Dec. **2018**, doi: 10.1016/J.RSER.2018.08.057.
- [2] D. Greenwood, S. Walker, N. Wade, S. Munoz-Vaca, A. Crossland, and C. Patsios, "Integration of high penetrations of intermittent renewable generation in future electricity networks using storage," *Future Energy: Improved, Sustainable and Clean Options for Our Planet*, pp. 649–668, Jan. **2020**, doi: 10.1016/B978-0-08-102886-5.00030-X.
- [3] H. Zsiborács et al., "Intermittent renewable energy sources: the role of energy storage in the european power system of 2040," *Electronics*, Vol. 8, Page 729, vol. 8, no. 7, p. 729, Jun. **2019**, doi: 10.3390/ELECTRONICS8070729.
- [4] J. P. Barton and D. G. Infield, "Energy storage and its use with intermittent renewable energy," *Trans. Energy Convers.*, vol. 19, no. 2, p. 441, **2004**, doi: 10.1109/TEC.2003.822305.
- [5] Y. Y. Lai, X. Li, and Y. Zhu, "Polymeric active materials for redox flow battery application," *ACS Appl Polym Mater*, vol. 2, no. 2, pp. 113–128, **2020**, doi: 10.1021/acsapm.9b00864.
- [6] J. Noack, N. Roznyatovskaya, T. Herr, and P. Fischer, "The chemistry of redox-flow batteries," *Angew Chem Int Ed*, vol. 54, no. 34, pp. 9776–9809, Aug. **2015**, doi: 10.1002/ANIE.201410823.
- [7] L. Conte, G. P. Gambaretto, G. Caporiccio, F. Alessandrini, and S. Passerini, "Perfluoroalkanesulfonylimides and their lithium salts: synthesis and characterisation of intermediates and target compounds," *J Fluor Chem*, vol. 125, no. 2, pp. 243–252, Feb. **2004**, doi: 10.1016/J.JFLUCHEM.2003.07.003.
- [8] P. Navalpotro, E. Castillo-Martínez, and J. Carretero-González, "Sustainable materials for off-grid battery applications: advances, challenges and prospects," *Sustain Energy Fuels*, vol. 5, no. 2, pp. 310–331, Jan. **2021**, doi: 10.1039/D0SE01338B.
- [9] T. Sukegawa, I. Masuko, K. Oyaizu, and H. Nishide, "Expanding the dimensionality of polymers populated with organic robust radicals toward flow cell application: synthesis of TEMPO-crowded bottlebrush polymers using anionic polymerization and ROMP," *Macromolecules*, vol. 47, pp. 8611–8617, **2014**, doi: 10.1021/ma501632t.

- [10] Y. Zhao, S. Si, and C. Liao, "A single flow zinc//polyaniline suspension rechargeable battery," *J Power Sources*, vol. 241, pp. 449–453, **2013**, doi: 10.1016/J.JPOWSOUR.2013.04.095.
- [11] T. Janoschka et al., "An aqueous, polymer-based redox-flow battery using non-corrosive, safe, and low-cost materials," *Nature*, vol. 527, no. 7576, pp. 78–81, **2015**, doi: 10.1038/nature15746.
- [12] J. Chai, X. Wang, A. Lashgari, C. K. Williams, and J. Jiang, "A pH-neutral, aqueous redox flow battery with a 3600-cycle lifetime: micellization-enabled high stability and crossover suppression," *ChemSusChem*, vol. 13, no. 16, pp. 4069–4077, **2020**, doi: 10.1002/cssc.202001286.
- [13] W. Yan et al., "All-polymer particulate slurry batteries," *Nature*, vol. 10, no. 2513, **2019**, doi: 10.1038/s41467-019-10607-0.
- [14] E. C. Montoto et al., "Redox active colloids as discrete energy storage carriers," *J Am Chem Soc*, vol. 138, no. 40, pp. 13230–13237, **2016**, doi: 10.1021/jacs.6b06365.
- [15] J. Winsberg et al., "Poly(TEMPO)/zinc hybrid-flow battery: a novel, 'green,' high voltage, and safe energy storage system," *Adv Mater*, vol. 28, no. 11, pp. 2238–2243, **2016**, doi: 10.1002/adma.201505000.
- [16] J. Winsberg et al., "Polymer/zinc hybrid-flow battery using block copolymer micelles featuring a TEMPO corona as catholyte," *Polym Chem*, vol. 7, no. 9, pp. 1711–1718, **2016**, doi: 10.1039/c5py02036k.
- [17] T. Janoschka et al., "Synthesis and characterization of TEMPO- and viologen-polymers for water-based redox-flow batteries," *Polym Chem*, vol. 6, no. 45, pp. 7801–7811, **2015**, doi: 10.1039/c5py01602a.
- [18] P. S. Borchers et al., "Regaining potential: studies concerning 2-ferrocenylethyl methacrylate, its polymers, and application in redox flow batteries," *Macromolecules*, Feb. **2022**, doi: 10.1021/acs.macromol.1c02565.
- [19] P. S. Borchers et al., "aqueous redox flow battery suitable for high temperature applications based on a tailor-made ferrocene copolymer," *Adv Energy Mater*, vol. 10, no. 41, **2020**, doi: 10.1002/aenm.202001825.
- [20] S. Kim, D. Kim, G. Hwang, and J. Jeon, "A bromide-ligand ferrocene derivative redox species with high reversibility and electrochemical stability for aqueous redox flow batteries," *Journal of Electroanalytical Chemistry*, vol. 869, pp. 1–7, **2020**, doi: 10.1016/j.jelechem.2020.114131.
- [21] E. S. Beh, D. de Porcellinis, R. L. Gracia, K. T. Xia, R. G. Gordon, and M. J. Aziz, "A neutral pH aqueous organic- organometallic redox flow battery with extremely high capacity retention," *ACS Energy Lett*, vol. 2, no. 3, pp. 639–644, **2017**, doi: 10.1021/acsenergylett.7b00019.

- [22] L. Liu, L. Rui, Y. Gao, and W. Zhang, "Self-assembly and disassembly of a redox-responsive ferrocene-containing amphiphilic block copolymer for controlled release," *Polym Chem*, vol. 6, p. 1817, **2015**, doi: 10.1039/c4py01289e.
- [23] M. Saleem, L. Wang, H. Yu, Zain-ul-Abdin, M. Akram, and R. S. Ullah, "Synthesis of amphiphilic block copolymers containing ferrocene–boronic acid and their micellization, redox-responsive properties and glucose sensing," *Colloid Polym Sci*, vol. 295, no. 6, pp. 995–1006, Jun. **2017**, doi: 10.1007/s00396-017-4049-1.
- [24] C. Gao, C. Liu, H. Zhou, S. Wang, and W. Zhang, "In situ synthesis of nano-assemblies of the high molecular weight ferrocene-containing block copolymer via dispersion RAFT polymerization," *J Polym Sci A Polym Chem*, vol. 54, no. 7, pp. 900–909, **2016**, doi: 10.1002/pola.27947.
- [25] J. Morsbach, J. Elbert, C. Rüttiger, S. Winzen, H. Frey, and M. Gallei, "Polyvinylferrocene-Based Amphiphilic Block Copolymers Featuring Functional Junction Points for Cross-Linked Micelles," *Macromolecules*, vol. 49, no. 9, pp. 3406–3414, **2016**, doi: 10.1021/acs.macromol.6b00514.
- [26] J.-C. Eloi, D. A. Rider, G. Cambridge, G. R. Whittell, M. A. Winnik, and I. Manners, "Stimulus-Responsive Self-Assembly: Reversible, Redox-Controlled Micellization of Polyferrocenylsilane Diblock Copolymers," *J Am Chem Soc*, vol. 133, no. 23, pp. 8903–8913, May **2011**, doi: 10.1021/ja1105656.
- [27] S. Bruña et al., "Ferrocene and Silicon-Containing Oxathiacrown Macrocycles and Linear Oligo-Oxathioethers Obtained via Thiol-Ene Chemistry of a Redox-Active Bifunctional Vinylidisiloxane," *Macromolecules*, vol. 48, no. 19, pp. 6955–6969, **2015**, doi: 10.1021/acs.macromol.5b01683.
- [28] C. J. Ferguson et al., "Ab Initio Emulsion Polymerization by RAFT-Controlled Self-Assembly," *Macromolecules*, vol. 38, no. 6, pp. 2191–2204, Feb. **2005**, doi: 10.1021/ma048787r.
- [29] S. D. Han et al., "Origin of electrochemical, structural, and transport properties in nonaqueous zinc electrolytes," *ACS Appl Mater Interfaces*, vol. 8, no. 5, pp. 3021–3031, Feb. **2016**, doi: 10.1021/acsami.5b10024.
- [30] C. M. Casado et al., "Redox-active ferrocenyl dendrimers and polymers in solution and immobilised on electrode surfaces," *Coordination chemistry reviews*, 185, pp. 53-80, **1999**, doi:10.1016/S0010-8545(98)00252-5
- [31] B. Hu, C. Debruler, Z. Rhodes, and T. L. Liu, "Long-cycling aqueous organic redox flow battery (AORFB) toward sustainable and safe energy storage," *J Am Chem Soc*, vol. 139, no. 3, pp. 1207–1214, **2017**, doi: 10.1021/jacs.6b10984.

[32] M. Burgess et al., “Scanning electrochemical microscopy and hydrodynamic voltammetry investigation of charge transfer mechanisms on redox active polymers,” *J Electrochem Soc*, vol. 163, no. 4, pp. H3006–H3013, Nov. **2016**, doi: 10.1149/2.0021604jes.

[33] T. Janoschka et al., “An aqueous, polymer-based redox-flow battery using non-corrosive, safe, and low-cost materials,” *Nature*, vol. 527, no. 7576, pp. 78–81, Nov. **2015**, doi: 10.1038/nature15746.



## **Conclusions of Section I**





1. After the studies shown in this Section, it can be concluded that most of the main objectives initially planned have been achieved by fulfilling requirements such as: The synthesis and study of different redox-active polymeric nanoparticles with the capability of storing electricity and CO<sub>2</sub> in aqueous media.
2. The polymer nanoparticle suspensions were stable in water using two different chemical strategies: on the one hand, the synthesis of new amphiphilic block copolymers, and on the other hand, the synthesis of hierarchical hybrid nanoparticles. It has been possible to obtain size-exclusion nanoparticles with homogeneous size as charge carriers in aqueous media, preventing them from passing through the porous membranes acting as a separator in the electrochemical cell.







## Section II

# Polymer Nanoparticles for Anti-counterfeiting Applications

---



*"Be careful with love at first sight, it can be fake."*



## Introduction

The world is constantly growing, globalization has brought with it a multitude of new businesses and industries, but there is a dark side to the pursuit of opportunities and business, in many areas huge opportunities for counterfeiting are created. Product counterfeiting is a global business, where counterfeit products are produced and distributed, which has become an increasingly serious problem. This is because criminals are attracted by large supply chains, trade standards and high product profit margins.

According to the European Union Intellectual Property Office (EUIPO), in Spain only, the infringement of industrial property rights (IPR) in the main sectors affected means not only the loss of €5,753 million per year, but also the elimination of 44,697 jobs per year [1].

The consumption and marketing of counterfeit products not only have an economic impact, but also generate problems for public health, environmental protection and the development and growth of companies. This is why counterfeit products are now considered a public problem due to the collective negative consequences they produce.

The most common counterfeit products that expose consumers to high risks are cosmetics, perfumes, toys, car parts, clothing and pharmaceuticals [2].

The fight against counterfeiting is therefore a challenge that needs to be addressed. The first step is to raise awareness of the consumption of counterfeit and pirated products. According to the EUIPO, Europeans are aware of the negative economic, health and safety effects of counterfeit products [3].

On the other hand, technology offers numerous solutions to protect property rights and defend supply chains. This is why most industries invest heavily in anti-counterfeiting measures. Traditional anti-counterfeiting methods usually offer one-step security and due to technological advances, counterfeiters make it possible for any measure to be imitated and cracked within 18 months.

## Existing technologies

The main anti-counterfeiting technologies currently available on the market are discussed below. It offers a brief definition of each of them, describing their main characteristics. Anti-counterfeiting technologies provide tools to help identify a product or whether it is a counterfeit product. These tools can have different functions such as:

- Anti-manipulation or anti tampering of products
- Product traceability and tracking
- Product authentication

These technologies must be difficult to copy but easy to implement. In general, these technologies can be divided into direct technologies (clearly visible to the consumer) or indirect technologies (covert technologies that are not visible to the naked eye) [4].

Currently, according to the EUIPO's 2021 Anti-Counterfeiting Technology Roadmap, it consists of 6 categories [5]

- Electronic technologies: in which an electronic identification, authentication and tracking device is associated with the product, such as RFID, NFC, electronic seals and contact chips, among others [6].
- Marking technologies: in which a visible or invisible marker is incorporated to the product, such as holograms, encrypted images, watermarks, detection patterns and inks, among others [7–9].
- Chemical and physical technologies: in this case, chemical or physical processes are used to mark and verify the product, such as laser surface analysis, surface fingerprinting, use of chemical compounds to see color changes [10–13].
- Mechanical technologies: Material elements or processes are applied, such as, for example, ultra-resistant labels, laser engraving, etc. [14–16].
- Digital media technologies: information is embedded or extracted from electronic devices [17–19].

This section focuses on security labels for use as product authentication, in the category of marking technology. The field of tags has been growing



---

---

exponentially towards the shift from simple tags to tags produced by stochastic processes making them more difficult to copy [20–22].

### **Nanotechnology-based solutions**

It is hoped that nanotechnology can help in the prevention of illegal copying of products by providing innovative methods, offering new alternatives to prevent counterfeiting. Today, there are a wide range of nanomaterials that can be explored to develop new generations of anti-counterfeiting technologies.

There are currently several lines of research working on the use of nanotechnology with different technologies such as:

- **RFID:** Currently used extensively in product tracking. Nanotechnology can help this technology because of the nanoscale and printed electronics lowers the cost of tagging chips. In addition, the nanoscale can aid in the creation of unique labels [23–26].
- **Fingerprinting:** Product surfaces can be modified at the nanoscale, thus creating each product's own fingerprints. The disadvantage is that it is a very expensive technique and would only be focused on high-value products [27–29].
- **Holograms:** Holograms and logotypes have been used for a long time, but the use of nanoscale allows general nanostructures making holograms difficult to copy [30,31].
- **Barcodes:** This is one of the most widely used techniques to identify products, but it is very easy to copy. Thanks to nanotechnology, patterns can be designed at nanometer scale making the barcode more difficult to copy [32,33].
- **Nano-labels:** This technology includes the aforementioned and also metal nanoparticles or quantum dots and nanocomposite materials that can randomly generate different optical or magnetic fingerprints [34,35].

### **Use of nanoparticles against counterfeiting**

Recent research suggests using non-clonable physical functions (PUFs) to create security labels. Many methods, including PUFs, use nanoparticles because of their highly customizable characteristics. Techniques that rely on

nanoparticles are more difficult to counterfeit than molecular solutions, as their properties depend on synthesis, structure and surface charge as discussed in the main introduction of this Thesis.

The following are the most representative nanoparticles for use in anti-counterfeiting.

- **Photonic crystal:** These are optical nanostructures in which the refractive index changes periodically, which can reflect a specific wavelength band at a given angle. It has been shown that reflection colors can be controlled by solvent evaporation [36–39].
- **Semiconducting nanoparticles:** There are many types of semiconducting nanoparticles including silicon nanoparticles, group III-V quantum dots, and carbon dots among others. Semiconducting nanoparticles possess Stoke and anti-Stoke emissions due to the valence band and the conducting band, suggesting their potential for use in security inks [40–43].
  - **Silicon nanoparticle:** Due to their good stability properties, they are a good choice for use in anti-counterfeiting. By modifying silicon nanoparticles, it is possible to control their fluorescence by displaying different colors at different excitation lengths. The problem is that it requires energy expenditure to synthesize the nanoparticles [44,45].
  - **Group III-V or II-VI semiconductors:** these nanomaterials are used especially in microelectronics. Currently, there is a lot of research in this field using core/multilayer quantum dots that depend on excitation, being able to adjust the desired color for use in anti-counterfeiting. The main disadvantage is the use of toxic ions, thus limiting the market in which these nanoparticles can be used [46–48].
  - **Carbon dots:** Carbon dots are referred to as a group of carbon nanoparticles with a size of 10 nm. One of its main properties is both Stokes and anti-Stokes emissions and long persistence phosphorescence. These properties make it a good candidate for

---

---

use in anti-counterfeiting due to its high quantum yield and low toxicity [49–51].

- **Metallic nanoparticles**: These types of particles have unique optical effects such as the dependence of the absorption spectrum on the morphology and surface plasmon resonance. As a function of size, only a certain wavelength is excited and is able to map the absorption intensity [52,53].
- **Lanthanide doped nanoparticles**: In the last decades they are the most investigated nanoparticles. They have been developed as a new class of luminescent nanoparticles. Their main feature is that they exhibit unique luminescent properties such as tunable luminescence emission, excellent optical stability and long lifetimes (up to microseconds). Despite their good properties, rare earths are difficult to obtain and difficult to recycle [30], [54–57].
- **Polymer dots**: they have very good properties such as high photostability, high structural stability and are environmentally friendly. Their main feature is that they can have different colors visible under ultraviolet excitation, which allows the fabrication of multicolor structures for use as an anti-counterfeiting product. Polymer dots encompass either conjugated polymer dots or semiconducting polymer nanoparticles, which are nanoparticles prepared from organic polymers [58,59].

This Section focuses on a new category of nanoparticles that can be used for this purpose, the use of polymer nanoparticles that are neither conductive, nor carry organic dyes or rare earths anchored to them. This involves the design of polyester nanoparticles for its use as an anti-counterfeiting product, creating random patterns in the nanoscale deposited on different supports such as cardboard, glass or the same material from which the particles are made, also offering the ease of recycling.

### **Printing technologies**

There are currently several techniques for nanoparticle, pattern and anti-counterfeiting security printing, which are discussed below:

- **Inkjet printing:** This is the most widely used printing technique today. Its main advantages are the variety of substrates on which it can be used and the large dimensions in which it can be applied. In addition, it allows to recreate any image with identical reproducibility and allows mass production, which is very interesting at industrial level. It allows the creation of unique random patterns [52,60,61].
- **Screen printing techniques:** this is a technique in which ink is transferred to a substrate using a mesh with a template. It is a well-established method for transferring nanoparticles for anti-counterfeiting. By choosing the right dispersion medium for the nanoparticles, they could then be deposited on various substrates such as polymers or paper [62–64].
- **Spray coating techniques:** This is a technique in which a fine aerosol is formed by forcing a solution or printing ink through a nozzle. In this technique there are many parameters to consider such as the airbrush flow rate, the distance between the sample and the airbrush, the concentration of the solution, the type of solvent and the number of times it is sprayed. It is a very versatile technique used to create very homogeneous surfaces, forming films or nanoparticles [65–67].

In addition to these three mentioned, there are many more techniques such as stamping, photolithography technique, electrical nanoimprint lithography, drop casting among others.

In this Section, we study the aerosol spray coating and manual drop deposition to create random patterns of polymer nanoparticles onto different substrates.

### **Future changes and research line**

There are many challenges that need to be overcome for all the technologies mentioned above, one of the most important is the economic factor. Although the use of nanoparticles may allow products to be unique and irreproducible, if the cost of implementation is greater than the possible loss due to counterfeiting, there is no hope.

Nanotechnology research provides different ways to prevent product counterfeiting by creating unique non-clonable labels with characteristics at the nanoscale that are too complex to be duplicated.

Many hidden technologies exist to create anti-counterfeiting systems, including hidden printed messages, watermarks, holograms, barcodes, security inks and others. Only few technologies and devices are capable of reading all the information, but currently the systems to read the labels are expensive and difficult to obtain. That is why this Section presents the design of non-clonable physical labels on a QR code that can be read in user mode with a cell phone and a specific application.

The goal is to introduce this innovative nanoparticle system into industry and to be landed these systems have to be easily synthesized and deposited as well as use cheap recognition devices. Therefore, if an industry starts adopting these technologies, reducing costs and pollution, directly encourages other industries to adopt new technologies.

## References

- [1] “Cuantificación de la vulneración de la propiedad industrial” <https://euipo.europa.eu/ohimportal/es/web/observatory/ip-in-europe> .
- [2] “Plan nacional e integral de lucha contra la venta de productos falsificados” [https://euipo.europa.eu/tunnelweb/secure/webdav/guest/document\\_library/observatory](https://euipo.europa.eu/tunnelweb/secure/webdav/guest/document_library/observatory).
- [3] “Los ciudadanos europeos y la propiedad industrial e intelectual: percepción, concienciación y conducta – 2020. EUIPO,” [https://euipo.europa.eu/tunnelweb/secure/webdav/guest/document\\_library/observatory/documents/Perception\\_study\\_2020/Perception\\_study\\_full\\_en.pdf](https://euipo.europa.eu/tunnelweb/secure/webdav/guest/document_library/observatory/documents/Perception_study_2020/Perception_study_full_en.pdf).
- [4] L. Meraviglia, “Technology and counterfeiting in the fashion industry: Friends or foes?,” *Bus Horiz*, vol. 61, no. 3, pp. 467–475, May 2018, doi: 10.1016/j.bushor.2018.01.013.
- [5] “Anti-counterfeiting technology guide,” [https://euipo.europa.eu/tunnelweb/secure/webdav/guest/document\\_library/observatory/documents/reports/2021\\_Anti\\_Counterfeiting\\_Technology\\_Guide/2021\\_Anti\\_Counterfeiting\\_Technology\\_Guide\\_en.pdf](https://euipo.europa.eu/tunnelweb/secure/webdav/guest/document_library/observatory/documents/reports/2021_Anti_Counterfeiting_Technology_Guide/2021_Anti_Counterfeiting_Technology_Guide_en.pdf).
- [6] M. Lehtonen, T. Staake, F. Michahelles, and E. Fleisch, “The potential of RFID and NFC in anti-counterfeiting,” in *Networked RFID Systems and Lightweight Cryptography*, Berlin, Heidelberg: Springer Berlin Heidelberg, 2008, pp. 211–222. doi: 10.1007/978-3-540-71641-9\_11.
- [7] K. Ludasi *et al.*, “Anti-counterfeiting protection, personalized medicines – Development of 2D identification methods using laser technology,” *Int J Pharm*, vol. 605, p. 120793, Aug. 2021, doi: 10.1016/j.ijpharm.2021.120793.
- [8] P. di Lazzaro *et al.*, “Invisible marking system by extreme ultraviolet radiation: the new frontier for anti-counterfeiting tags,” *Journal of Instrumentation*, vol. 11, no. 07, pp. C07002–C07002, Jul. 2016, doi: 10.1088/1748-0221/11/07/C07002.
- [9] R. Azimi, A. Abdollahi, H. Roghani-Mamaqani, and M. Salami-Kalajahi, “Dual-mode security anticounterfeiting and encoding by electrospinning of highly photoluminescent spiropyran nanofibers,” *J Mater Chem C Mater*, vol. 9, no. 30, pp. 9571–9583, 2021, doi: 10.1039/D1TC01931G.
- [10] L. A. de Azevedo *et al.*, “Multi-stimuli-responsive luminescent MCM48 hybrid for advanced anti-counterfeiting applications,” *J Mater Chem C Mater*, vol. 9, no. 29, pp. 9261–9270, 2021, doi: 10.1039/D1TC01357B.
- [11] M. Moglianetti *et al.*, “Nanocatalyst-enabled physically unclonable functions as smart anticounterfeiting tags with ai-aided smartphone

---

---

authentication,” *ACS Appl Mater Interfaces*, vol. 14, no. 22, pp. 25898–25906, Jun. **2022**, doi: 10.1021/acsami.2c02995.

[12] Z. C. Kennedy *et al.*, “Enhanced anti-counterfeiting measures for additive manufacturing: coupling lanthanide nanomaterial chemical signatures with blockchain technology,” *J Mater Chem C Mater*, vol. 5, no. 37, pp. 9570–9578, **2017**, doi: 10.1039/C7TC03348F.

[13] H. Zhou, J. Han, J. Cuan, and Y. Zhou, “Responsive luminescent MOF materials for advanced anticounterfeiting,” *Chem. Eng. J*, vol. 431, p. 134170, Mar. **2022**, doi: 10.1016/j.cej.2021.134170.

[14] H. M. Abumelha *et al.*, “Development of mechanically reliable and transparent photochromic film using solution blowing spinning technology for anti-counterfeiting applications,” *ACS Omega*, vol. 6, no. 41, pp. 27315–27324, Oct. **2021**, doi: 10.1021/acsomega.1c04127.

[15] H. Wang *et al.*, “Efficient color manipulation of zinc sulfide-based mechanoluminescent elastomers for visualized sensing and anti-counterfeiting,” *J Lumin*, vol. 228, p. 117590, Dec. **2020**, doi: 10.1016/j.jlumin.2020.117590.

[16] T. Pan, S. Liu, L. Zhang, W. Xie, and C. Yu, “A flexible, multifunctional, optoelectronic anticounterfeiting device from high-performance organic light-emitting paper,” *Light Sci Appl*, vol. 11, no. 1, p. 59, Mar. **2022**, doi: 10.1038/s41377-022-00760-5.

[17] J. Deng *et al.*, “Multiplexed anticounterfeiting meta-image displays with single-sized nanostructures,” *Nano Lett*, vol. 20, no. 3, pp. 1830–1838, Mar. **2020**, doi: 10.1021/acs.nanolett.9b05053.

[18] S. Graham, “Beyond the ‘dazzling light’: from dreams of transcendence to the ‘remediation’ of urban life,” *New Media Soc*, vol. 6, no. 1, pp. 16–25, Feb. **2004**, doi: 10.1177/1461444804039905.

[19] M. Sun, J. Si, and S. Zhang, “Research on embedding and extracting methods for digital watermarks applied to QR code images,” *New Zealand J. Agric. Res.*, vol. 50, no. 5, pp. 861–867, Dec. **2007**, doi: 10.1080/00288230709510361.

[20] C. Suresh *et al.*, “Imaging sweat pore structures in latent fingerprints and unclonable anti-counterfeiting patterns by sensitizers blended LaOF:Pr<sup>3+</sup> nanophosphors,” *Opt Mater (Amst)*, vol. 100, p. 109625, Feb. **2020**, doi: 10.1016/j.optmat.2019.109625.

[21] S. Wang, E. Toreini, and F. Hao, “Anti-counterfeiting for polymer banknotes based on polymer substrate fingerprinting,” *Trans. Inf. Forensics Secur.*, vol. 16, pp. 2823–2835, **2021**, doi: 10.1109/TIFS.2021.3067440.

- [22] V. Kumar, S. Dottermusch, A. Chauhan, B. S. Richards, and I. A. Howard, "Expanding the angle of incidence tolerance of unclonable anticounterfeiting labels based on microlens arrays and luminescent microparticles," *Adv Photonics Res*, vol. 3, no. 6, p. 2100202, Jun. **2022**, doi: 10.1002/adpr.202100202.
- [23] M. Tentzeris and L. Yang, "Inkjet-printed paper-based RFID and nanotechnology-based ultrasensitive sensors: the 'green' ultimate solution for an ever improving life quality and safety?," in *International Conference on e-Democracy*. Springer, Berlin, Heidelberg, **2009**, pp. 55–63. doi: 10.1007/978-3-642-11631-5\_5.
- [24] M. M. Tentzeris, A. Rida, A. Traille, H. Lee, V. Lakafosis, and R. Vyas, "Inkjet-printed paper/polymer-based RFID and Wireless Sensor Nodes: The final step to bridge cognitive intelligence, nanotechnology and RF?," in *2011 XXXth URSI General Assembly and Scientific Symposium*, Aug. **2011**, pp. 1–4. doi: 10.1109/URSIGASS.2011.6050690.
- [25] R. Singh, E. Singh, and H. S. Nalwa, "Inkjet printed nanomaterial based flexible radio frequency identification (RFID) tag sensors for the internet of nano things," *RSC Adv.*, vol. 7, no. 77, pp. 48597–48630, **2017**, doi: 10.1039/C7RA07191D.
- [26] J. van den Hoven, "Nanotechnology and privacy: the instructive case of RFID," in *Ethics and Emerging Technologies*, London: Palgrave Macmillan UK, **2014**, pp. 285–299. doi: 10.1057/9781137349088\_19.
- [27] J. Kim, J. M. Yun, J. Jung, H. Song, J.-B. Kim, and H. Ihee, "Anti-counterfeit nanoscale fingerprints based on randomly distributed nanowires," *Nanotechnology*, vol. 25, no. 15, p. 155303, Apr. **2014**, doi: 10.1088/0957-4484/25/15/155303.
- [28] Y. Cui, R. S. Hegde, I. Y. Phang, H. K. Lee, and X. Y. Ling, "Encoding molecular information in plasmonic nanostructures for anti-counterfeiting applications," *Nanoscale*, vol. 6, no. 1, pp. 282–288, **2014**, doi: 10.1039/C3NR04375D.
- [29] K. Cheng *et al.*, "Tunable excitation-dependent-fluorescence of carbon dots: Fingerprint curves for super anti-counterfeiting," *Dyes and Pigments*, vol. 174, p. 108106, Mar. **2020**, doi: 10.1016/j.dyepig.2019.108106.
- [30] P. Kumar, S. Singh, and B. K. Gupta, "Future prospects of luminescent nanomaterial based security inks: from synthesis to anti-counterfeiting applications," *Nanoscale*, vol. 8, no. 30, pp. 14297–14340, **2016**, doi: 10.1039/C5NR06965C.



- 
- 
- [31] C. Zhang *et al.*, “Multichannel metasurfaces for anticounterfeiting,” *Phys Rev Appl*, vol. 12, no. 3, p. 034028, Sep. **2019**, doi: 10.1103/PhysRevApplied.12.034028.
- [32] S. Shikha, T. Salafi, J. Cheng, and Y. Zhang, “Versatile design and synthesis of nano-barcodes,” *Chem Soc Rev*, vol. 46, no. 22, pp. 7054–7093, **2017**, doi: 10.1039/C7CS00271H.
- [33] Y. Hou, Z. Gao, Y. S. Zhao, and Y. Yan, “Organic micro/nanoscale materials for photonic barcodes,” *Organic Chemistry Frontiers*, vol. 7, no. 18, pp. 2776–2788, **2020**, doi: 10.1039/D0QO00613K.
- [34] A. Verhagen and A. Kelarakis, “Carbon dots for forensic applications: a critical review,” *Nanomaterials*, vol. 10, no. 8, p. 1535, Aug. **2020**, doi: 10.3390/nano10081535.
- [35] F. Chen *et al.*, “Unclonable fluorescence behaviors of perovskite quantum dots/chaotic metasurfaces hybrid nanostructures for versatile security primitive,” *Chem. Eng. J.*, vol. 411, p. 128350, May **2021**, doi: 10.1016/j.cej.2020.128350.
- [36] H. Kim *et al.*, “Structural colour printing using a magnetically tunable and lithographically fixable photonic crystal,” *Nat Photonics*, vol. 3, no. 9, pp. 534–540, Sep. **2009**, doi: 10.1038/nphoton.2009.141.
- [37] W. Ma, Y. Kou, P. Zhao, and S. Zhang, “Bioinspired structural color patterns derived from 1d photonic crystals with high saturation and brightness for double anti-counterfeiting decoration,” *ACS Appl Polym Mater*, vol. 2, no. 4, pp. 1605–1613, Apr. **2020**, doi: 10.1021/acspapm.0c00047.
- [38] K. Zhu, C. Fang, M. Pu, J. Song, D. Wang, and X. Zhou, “Recent advances in photonic crystal with unique structural colors: A review,” *J Mater Sci Technol*, Oct. **2022**, doi: 10.1016/j.jmst.2022.08.044.
- [39] Pan *et al.*, “Recent advances in colloidal photonic crystal-based anti-counterfeiting materials,” *Crystals (Basel)*, vol. 9, no. 8, p. 417, Aug. **2019**, doi: 10.3390/cryst9080417.
- [40] W.-K. Tsai, Y.-S. Lai, P.-J. Tseng, C.-H. Liao, and Y.-H. Chan, “Dual colorimetric and fluorescent authentication based on semiconducting polymer dots for anticounterfeiting applications,” *ACS Appl Mater Interfaces*, vol. 9, no. 36, pp. 30918–30924, Sep. **2017**, doi: 10.1021/acscami.7b08993.
- [41] M. Ibrar and S. E. Skrabalak, “Designer plasmonic nanostructures for unclonable anticounterfeit tags,” *Small Struct*, vol. 2, no. 9, p. 2100043, Sep. **2021**, doi: 10.1002/ssstr.202100043.
- [42] L. Xu *et al.*, “Double-protected all-inorganic perovskite nanocrystals by crystalline matrix and silica for triple-modal anti-counterfeiting codes,” *ACS Appl*

*Mater Interfaces*, vol. 9, no. 31, pp. 26556–26564, Aug. **2017**, doi: 10.1021/acsami.7b06436.

[43] K. Jiang, L. Zhang, J. Lu, C. Xu, C. Cai, and H. Lin, “Triple-mode emission of carbon dots: applications for advanced anti-counterfeiting,” *Angewandte Chemie*, vol. 128, no. 25, pp. 7347–7351, Jun. **2016**, doi: 10.1002/ange.201602445.

[44] X.-B. Shen, B. Song, B. Fang, A.-R. Jiang, S.-J. Ji, and Y. He, “Excitation-wavelength-dependent photoluminescence of silicon nanoparticles enabled by adjustment of surface ligands,” *Chemical Communications*, vol. 54, no. 39, pp. 4947–4950, **2018**, doi: 10.1039/C8CC00047F.

[45] F. Li, X. Wang, Z. Xia, C. Pan, and Q. Liu, “Photoluminescence tuning in stretchable pdms film grafted doped core/multishell quantum dots for anticounterfeiting,” *Adv Funct Mater*, vol. 27, no. 17, p. 1700051, May **2017**, doi: 10.1002/adfm.201700051.

[46] J. Jie, W. Zhang, I. Bello, C.-S. Lee, and S.-T. Lee, “One-dimensional II–VI nanostructures: Synthesis, properties and optoelectronic applications,” *Nano Today*, vol. 5, no. 4, pp. 313–336, Aug. **2010**, doi: 10.1016/j.nantod.2010.06.009.

[47] C.-Z. Ning, L. Dou, and P. Yang, “Bandgap engineering in semiconductor alloy nanomaterials with widely tunable compositions,” *Nat Rev Mater*, vol. 2, no. 12, p. 17070, Dec. **2017**, doi: 10.1038/natrevmats.2017.70.

[48] N. Mir, “Rare earth–doped semiconductor nanomaterials,” in *Advanced Rare Earth-Based Ceramic Nanomaterials*, Elsevier, **2022**, pp. 291–338. doi: 10.1016/B978-0-323-89957-4.00013-X.

[49] K. Jiang, L. Zhang, J. Lu, C. Xu, C. Cai, and H. Lin, “Triple-mode emission of carbon dots: applications for advanced anti-counterfeiting,” *Angewandte Chemie*, vol. 128, no. 25, pp. 7347–7351, Jun. **2016**, doi: 10.1002/ange.201602445.

[50] J. Guo *et al.*, “Green synthesis of carbon dots toward anti-counterfeiting,” *ACS Sustain Chem Eng*, vol. 8, no. 3, pp. 1566–1572, Jan. **2020**, doi: 10.1021/acssuschemeng.9b06267.

[51] S. Kalytchuk, Y. Wang, K. Poláková, and R. Zbořil, “Carbon dot fluorescence-lifetime-encoded anti-counterfeiting,” *ACS Appl Mater Interfaces*, vol. 10, no. 35, pp. 29902–29908, Sep. **2018**, doi: 10.1021/acsami.8b11663.

[52] H. Kang, J. W. Lee, and Y. Nam, “Inkjet-printed multiwavelength thermoplasmonic images for anticounterfeiting applications,” *ACS Appl Mater Interfaces*, vol. 10, no. 7, pp. 6764–6771, Feb. **2018**, doi: 10.1021/acsami.7b19342.

- 
- 
- [53] C. Jung *et al.*, “Disordered-nanoparticle–based etalon for ultrafast humidity-responsive colorimetric sensors and anti-counterfeiting displays,” *Sci Adv*, vol. 8, no. 10, Mar. **2022**, doi: 10.1126/sciadv.abm8598.
- [54] C. Zhang *et al.*, “Dual-wavelength stimuli and green emission response in lanthanide doped nanoparticles for anti-counterfeiting,” *J Alloys Compd*, vol. 836, p. 155487, Sep. **2020**, doi: 10.1016/j.jallcom.2020.155487.
- [55] M. Ding *et al.*, “Energy manipulation in lanthanide-doped core–shell nanoparticles for tunable dual-mode luminescence toward advanced anti-counterfeiting,” *Adv. Mater.*, vol. 32, no. 45, p. 2002121, Nov. **2020**, doi: 10.1002/adma.202002121.
- [56] W. Ren, G. Lin, C. Clarke, J. Zhou, and D. Jin, “Optical nanomaterials and enabling technologies for high-security-level anticounterfeiting,” *Adv. Mater.*, vol. 32, no. 18, p. 1901430, May **2020**, doi: 10.1002/adma.201901430.
- [57] A. Abdollahi, H. Roghani-Mamaqani, B. Razavi, and M. Salami-Kalajahi, “Photoluminescent and chromic nanomaterials for anticounterfeiting technologies: recent advances and future challenges,” *ACS Nano*, vol. 14, no. 11, pp. 14417–14492, Nov. **2020**, doi: 10.1021/acsnano.0c07289.
- [58] W.-K. Tsai, Y.-S. Lai, P.-J. Tseng, C.-H. Liao, and Y.-H. Chan, “Dual colorimetric and fluorescent authentication based on semiconducting polymer dots for anticounterfeiting applications,” *ACS Appl Mater Interfaces*, vol. 9, no. 36, pp. 30918–30924, Sep. **2017**, doi: 10.1021/acsami.7b08993.
- [59] Y. Liu, C. Zheng, and B. Yang, “Phosphorus and nitrogen codoped carbonized polymer dots with multicolor room temperature phosphorescence for anticounterfeiting painting,” *Langmuir*, vol. 38, no. 27, pp. 8304–8311, Jul. **2022**, doi: 10.1021/acs.langmuir.2c00738.
- [60] Y. Liu *et al.*, “Inkjet-printed unclonable quantum dot fluorescent anti-counterfeiting labels with artificial intelligence authentication,” *Nat Commun*, vol. 10, no. 1, p. 2409, Dec. **2019**, doi: 10.1038/s41467-019-10406-7.
- [61] L. L. da Luz *et al.*, “Inkjet printing of lanthanide-organic frameworks for anti-counterfeiting applications,” *ACS Appl Mater Interfaces*, vol. 7, no. 49, pp. 27115–27123, **2015**, doi: 10.1021/acsami.5b06301.
- [62] C. Campos-Cuerva *et al.*, “Screen-printed nanoparticles as anti-counterfeiting tags,” *Nanotechnology*, vol. 27, no. 9, Jan. **2016**, doi: 10.1088/0957-4484/27/9/095702.
- [63] M. Li *et al.*, “Facile synthesis and screen printing of dual-mode luminescent NaYF<sub>4</sub>:Er,Yb (Tm)/carbon dots for anti-counterfeiting applications,” *J Mater Chem C Mater*, vol. 5, no. 26, pp. 6512–6520, **2017**, doi: 10.1039/C7TC01585B.
- 
-

[64] M. M. Abdelhameed, Y. A. Attia, M. S. Abdelrahman, and T. A. Khattab, "Photochromic and fluorescent ink using photoluminescent strontium aluminate pigment and screen printing towards anticounterfeiting documents," *Luminescence*, vol. 36, no. 4, pp. 865–874, Jun. **2021**, doi: 10.1002/bio.3987.

[65] T. A. Berfield, J. K. Patel, R. G. Shimmin, P. v. Braun, J. Lambros, and N. R. Sottos, "Micro- and nanoscale deformation measurement of surface and internal planes via digital image correlation," *Exp Mech*, vol. 47, no. 1, pp. 51–62, Feb. **2007**, doi: 10.1007/s11340-006-0531-2.

[66] F. Aziz and A. F. Ismail, "Spray coating methods for polymer solar cells fabrication: A review," *Mater Sci Semicond Process*, vol. 39, pp. 416–425, Nov. **2015**, doi: 10.1016/j.mssp.2015.05.019.

[67] M. Meikandan, P. Ganesh Kumar, D. Sakthivadivel, V. Vigneswaran, and K. Malar Mohan, "Multi-wall carbon nanotubes coating on a copper substrate using airbrush spray coating," *Proceedings of the Institution of Mechanical Engineers, Part E: J Proc Mech Eng*, vol. 235, no. 2, pp. 285–291, Apr. **2021**, doi: 10.1177/0954408920959157.





# Chapter 4.

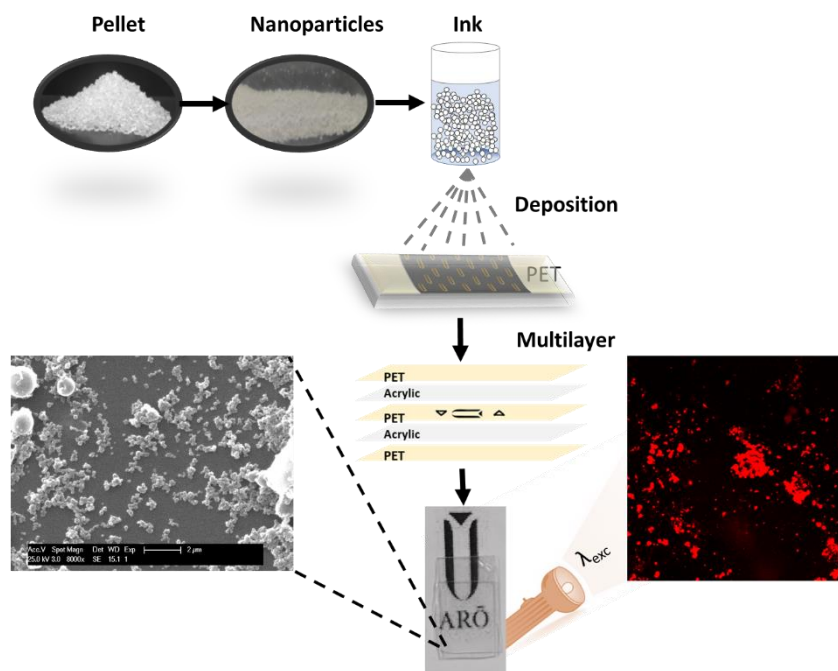
## New polymeric systems for anti-counterfeiting devices

An international patent application (PCT/ES2022/070023) has been filed by Consejo Superior de Investigaciones Científicas and Inentia Arô S. L.





Polymeric nanoparticles have been developed from the commercial polymer pellet, providing new properties to the material. In particular, a change in the photophysical properties of the material has been demonstrated, offering the opportunity to address current issues in commercial product safety.



**This first part of Chapter 4 summarizes the experimental part carried out within the company. This part shows the development of the research line and how each decision has been taken to first understand and then take actions to overcome the limitations in order to achieve the objectives of the company.**

**Why do we want to use a polymer as the support of anti-counterfeiting systems?**

The perfume market is limited in terms of container materials. The most widely used packaging so far is glass due to the excellent properties it provides, such as preserving the aroma of the product contained, it is a hygienic material that is easy to clean, odorless, can be colored and is recyclable. However, it has disadvantages, it is fragile and heavy material, its distribution is expensive, it consumes more fuel, which makes it pollute more. Therefore, it is important to find an alternative to glass for cosmetics containers.

In today's industry, some polymers have been used to replace parts of perfume/cosmetics containers. The intention is to use polymers due to their good properties in the industry such as low cost, easy manufacturing, chemical, solar and water resistance among other properties.

The plastic containers used today as packaging in general, not focused on the perfume/cosmetics sector, are thermoplastic resins that can be melted when exposed to heat and hardened with cold. This reversible characteristic allows them to be thermoformed repeatedly.

The advantages of these packages are that they are easily moldable, can tolerate high temperatures, can be reusable, are less expensive and are more resistant.

But the world of plastics as packaging is not a perfect world, they have major disadvantages such as some materials are difficult to recycle, they remain in nature for years generating more pollution. If mixed with other families of plastics, low quality products are obtained after recycling.

**Which polymer is optimal for the desired application?**

Considering that the company's product, a new device for personal use, contains perfumes/cosmetics, it was necessary to evaluate which type of polymers were optimal for their design. The company's main requirements were that the material should be chemically resistant to perfumes and cosmetics,

easily moldable and rigid. Focusing on these requirements, we find two potential materials for its use.

### Materials

- Methylene polyoxide or polyformaldehyde (POM): Delrin® DuPont. Is a high rigid semicrystalline thermoplastic, used in precision parts requiring high rigidity, low friction and excellent dimensional stability.

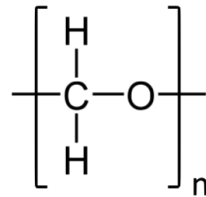


**Figure 4.1.** Methylene polyoxide molecular structure

- Poly cyclohexanedimethanol terephthalic acid (PCTA): Eastar™ copolyester AN014, Natural. Vitreous polymer, same sharpness and high brightness as crystal. High chemical and impact resistance.

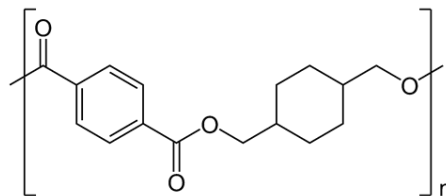


**Figure 4.2.** Poly cyclohexanedimethanol terephthalic acid molecular structure

Once the most suitable polymers for the designed container have been selected, a physical characterization of the materials was carried out to provide the company with information on processing temperatures and fundamental properties

### Characterization

#### Thermal stability

In order to study the thermal properties of the polymers we used two different techniques: TGA and DSC. Figure 4.3 shows the TGA curve obtained, showing that the degradation process occurs at 393.8 °C for PCTA and 283 °C for POM.

In both polymers, a single step is observed in the curve, indicating that all polymer decomposes at the same time under a simple mechanism [1,2].

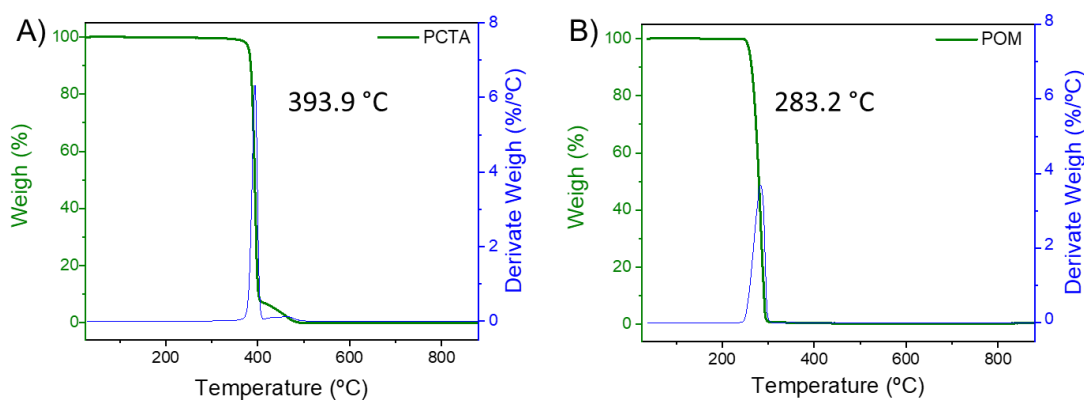


**Figure 4.3.** TGA curves of A) PCTA and B) POM

The thermal properties of both polymers were determined by DSC. The corresponding thermograms are shown in Figure 4.4. DSC measurements are recorded in the second heating cycle, the first cycle is performed to remove the thermal history of the polymer by applying a heating-cooling treatment.

For PCTA, a  $T_g$  at 79 °C and a first exothermic process with a cold crystallization temperature of 174 °C are observed. In addition, a melting endotherm is found starting at 200 °C and ending around 240 °C. In the case of POM we observe that the  $T_g$  is much lower appearing at -67.8 °C and an endothermic melting process starting around 120 °C and ending at 200 °C .

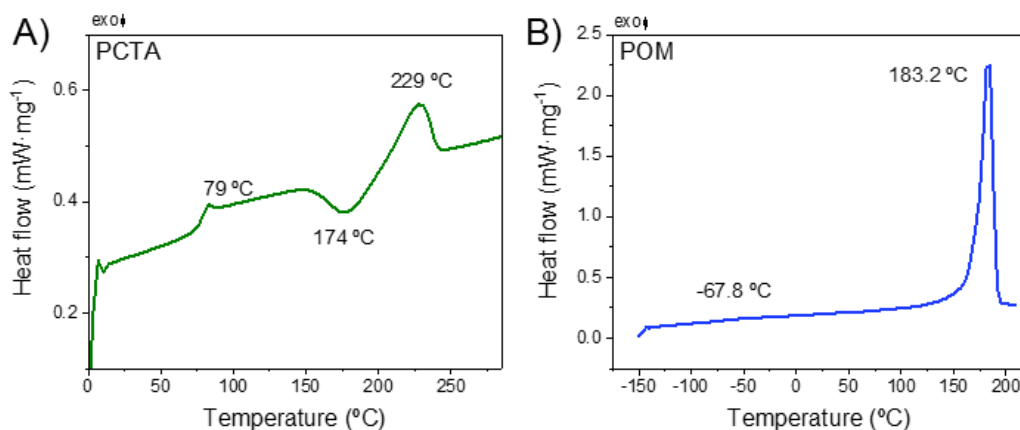


**Figure 4.4.** DSC thermograms of A) PCTA and B) POM

**Table 4.1.** Processing conditions for each material

	Tg (°C)	Melting temperature (°C)	Degradation temperature (°C)
<b>PCTA</b>	77.6	200-240	393.8
<b>POM</b>	-67.8	120-200	283.2

Moreover, processability tests were also carried out at the laboratory to provide the company with information on the processing properties of the materials. First of all, we processed the materials assisted with a mini-extruder. Further, we also tested a higher mixing capacity processing technique such as the internal mixer. Finally, best results were observed by processing aided with a laboratory platen press under selected conditions of temperature, time, and pressure (Figure 4.5). Extrusion and internal mixing were discarded on one side due to difficulty in collecting the material; and on the other hand, because of the degradation processes occurred during the shearing.



**Figure 4.5.** Equipment used for materials processing. A) Mini-extruder, B) Internal mixer, C) Automatic platen-press

The company's objective was to obtain samples of 1 mm thickness, without heterogeneities and air bubbles occluded. In order to prepare the films, we used different molds in the platen-press, which were filled with the corresponding amount of the polymer pellets to be melted at high temperatures under pressure and then cooled to room temperature.

Different temperatures were chosen to obtain films of each material, 200 °C for POM and 240 °C for PCTA. The first tests were carried out with a pressure of 100 bar in both cases. It was observed that a homogeneous material was not

obtained due to the formation of bubbles inside the film or fluidity marks (Figure 4.6). During POM processing, we observed an evolution of gases when opening the platen-press probably due to the formaldehyde formed during a possible degradation process [3]. Based on observations, an optimization on the processing of the materials was carried out with different pressure ramps, times and temperatures. Table 4.2 shows the optimum processing conditions for each polymer.

**Table. 4.2.** Processing conditions for each material

Polymer	Temperature (°C)	Pressure (bar / min)	Cooling time
POM	200	20, 40, 60, 70 bar for 1 min 30 s	6 min
PCTA	240	110 bar for 6 min	

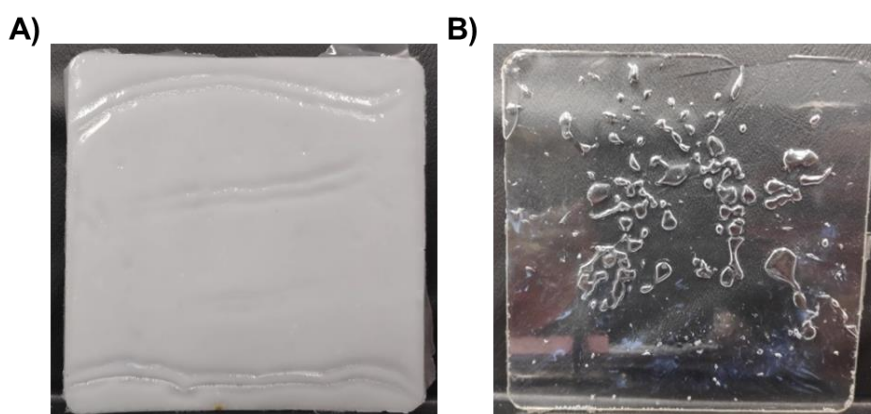


**Figure 4.6.** Photography of the processing problems found for both materials. A) POM B) PCTA

All the results described above were studied within the company. Finally, due to the degradation temperatures and its transparency, PCTA was chosen as the optimal material for packaging. Once the packaging material was selected, the next step addresses the study of its mechanical and chemical degradation properties according to the following standards.

- ASTM-D543-95: Chemical and resistance evaluation.
- ASTM-D638-14: Mechanical properties.

For both tests, it was necessary to order custom-made molds that complied with the measurements of the standard tests (Figure 4.7).

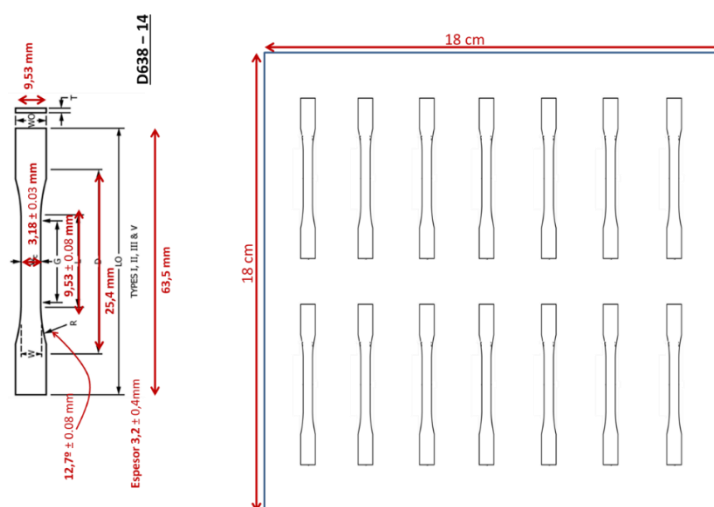


**Figure 4.7.** Mold designed for testing under chemical resistance and mechanical properties standards

### Chemical resistance or degradation

To evaluate the resistance of plastics to chemical reagents, at least three samples were used and tested for each reagent. In this case, as the company's interest is to know the resistance of cosmetic products and perfume, two types of perfumes, one with floral fragrance and the other with citrus fragrance were used as reagents.

The chemical resistance measurements are performed on halter type test tubes with the above specifications, where the polymer is immersed in the perfume for different time intervals, 24 h, 1 week and 16 weeks. Before immersion, five dry PCTA reference samples are marked with a small cut (for late identification) and all its dimensions, weight and length of the sample, length, width and thickness of the neck are measured, and their appearance, color, gloss, transparency is noted.

After each immersion, specimens are quickly dried with dust-free tissues and evaluated for variations in mass, dimensions, and appearance.



Only the weight of the samples changed, although it did not vary with immersion time. Thus, an increase of 0.15 and 0.3 wt.% for the floral and citrus perfumes, was measured, respectively. No variations were observed in the dimensions of the samples nor in their appearance, brightness, color, transparency, appearance of cracks, sticky aspect.

### Mechanical properties

The effect of immersion in the perfumes on the tensile behavior of the samples is evaluated (Table 4.3). Tensile tests are performed with a universal testing machine (Instron 3366) equipped with a 1 kN load cell. Samples were stretched until failure at a constant strain rate of 10 mm/min at a room temperature. At least five samples are analyzed for each material. The typical stress-strain curves of PCTA are shown in Figure 4.8.

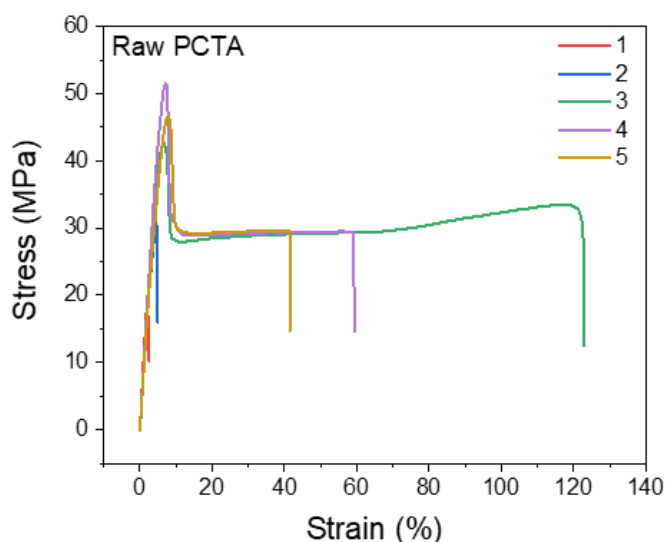


**Figure 4.8.** Raw PCTA tensile stress-strain curves

In all cases the same trend is observed, with some specimens from each study batch breaking directly and others taking longer. This effect may be due because the grippers used for the study do not always grip the specimens well, even though rough grippers are used to ensure the grip of each specimen. The polyester has a clear elastic limit before failure, which indicates that they are resistant materials [1].

In order to study the effect of perfume on the mechanical properties, Figure 4.9 shows the stress-strain curves of the raw material and of the different perfumes with different immersion time periods of the specimens. The results show a difference in the percentage of elongation at break as a function of the perfume used in the immersion due to their essences. The elongation at break of the samples immersed in the floral perfume is lower than those of the citrus perfume. This difference may be related to that the citrus essence behaves as a lubricant and the volatiles in the floral scent generated cavities which cause the material to break [4]

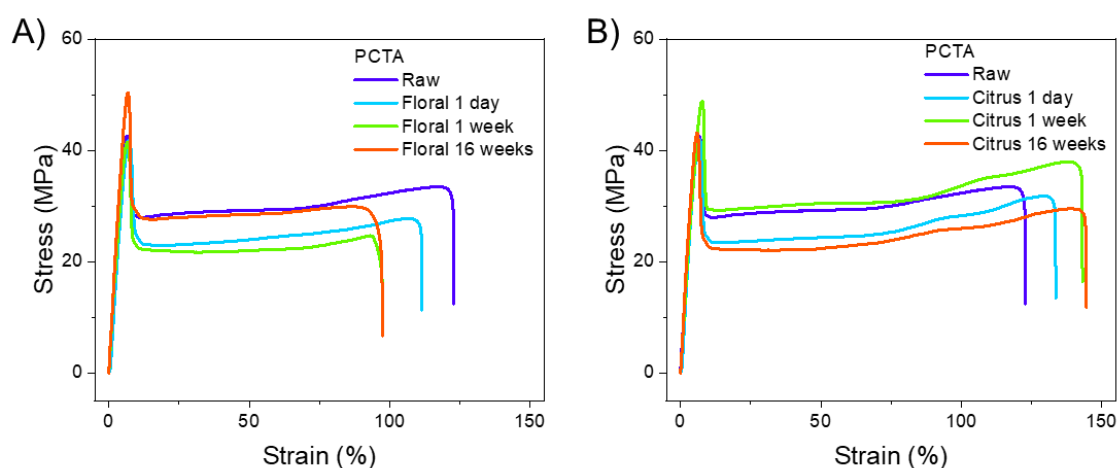


**Figure 4.9.** PCTA tensile stress-strain curves under different conditions. A) Samples immersed in floral perfume for different periods. B) Samples immersed in citrus perfume for different periods

The mechanical properties of a container are very important, but there is little information on the possible chemical-physical modifications of the containers on the interactions between the formulations and the containers [5]. It is usually very difficult to know patented chemical formulation contained in a perfume. This added to the fact that it is a previous characterization of the possible material to be used as perfume packaging. The final packaging is not only made of this material, but also usually contains antioxidants and additives. Therefore, these same experiments should be carried out with the final packaging of the production process. This study has collected the results of the mechanical properties as predictive parameters for the company.

**Table 4.3.** Effect of immersion in perfumes on the tensile behavior of samples

Polymer		Elongation break (%)	Tensile strength (MPa)	Young's modulus (MPa)
PCTA		$74 \pm 42$	$30 \pm 2$	$894 \pm 47$
Floral perfume	1 day	$80 \pm 30$	$31 \pm 4$	$844 \pm 25$
	1 week	$72 \pm 23$	$20 \pm 3$	$882 \pm 24$
	16 weeks	$87 \pm 18$	$27 \pm 3$	$936 \pm 14$
Citrus perfume	1 day	$110 \pm 26$	$32 \pm 2$	$836 \pm 52$
	1 week	$100 \pm 40$	$25 \pm 10$	$838 \pm 20$
	16 weeks	$130 \pm 20$	$28 \pm 6$	$908 \pm 71$

**Next, the second part of Chapter 4 is presented, where the anti-counterfeiting system is developed to the company.**

**Abstract**

Functional polymeric materials have evolved rapidly due to the development of modern technologies that require an unusual combination of properties that cannot be provided by polymers. Thermoplastic polymers are flexible providing good mechanical properties but are devoid of other properties that would make them more attractive, such as intrinsic luminescence. By incorporating PCTA particles with luminescent properties due to aggregation induced emission (AIE) phenomenon, multifunctional composites with the typical properties of thermoplastic polymers and optical response to UV-visible light are obtained. When the particles are dispersed in a solvent such as methanol, an increase in luminescence is observed. Confocal fluorescence microscopy demonstrates the fluorescent behavior of the particles contained in the film. These results may be used to develop a new polymeric system for traceability and anti-counterfeiting applications.

### Scientific background and state of the art

The fight against counterfeiting is an old issue [6,7], but it has been during the last decade when research works have been increasingly published exploring the complexity and singularity of nanostructures may provide the possibility of addressing effective solution for anti-counterfeiting applications [8–10].

As detailed in the introduction of **Section 2** (page 34), up-to-date there are different types of nanostructures or nanoparticles as the most representative for use in anti-counterfeiting (metallic, lanthanides, carbon, silicon, etc.). Nowadays, few research works have investigated the use of non-conductive polymers or non-fluorescence polymers as entities in the design of nanoparticles in areas as for instance bioimaging, organic light-emitting diodes (OLEDs), light-emitting electrochemical cells (LECs) or anti-counterfeiting [11–14].

Different chemical mechanisms have been reported in the literature that detail the photophysical properties of nanomaterials to overcome the aggregation-caused quenching problem (ACQ) [15–18]. The concept of aggregation induced emission (AIE) was introduced by Tang *et al.* in 2015 [19], providing fundamental insights into the photophysical processes and the ACQ of conventional aromatic luminogens [20]. Currently the development of new AIE luminogens for various applications is a hot topic [21,22].

Recently, some unconventional luminogens such as non-conjugated polymers based on saturated C=C, C=O or C=N chains or those possessing electron-rich groups such as N, S, O, P with free lone pairs, can form aggregates and emit in the visible have attracted attention for their clustering-triggered emission mechanism (CTE) [23]. Therefore, the clustering of unconventional luminogens generates a bright PL due to the effective short contacts between the electron-rich parts and increases the overlapping of electron clouds, leading to rigid conformations and the formation of an extended electron conjugation. Because of of intra- and intermolecular interactions, the emission of luminogens depends on sufficient through space conjugation (TSC) of diversified groups of subgroups [24].

---

---

Moreover, Tang *et al.* [25] studied the crystallization-induced dual emission (CIDE) of certain aromatic acids and esters such as terephthalic acid (TPA) and dimethyl terephthalate (DMTPA) under environmental conditions. It has been shown that crystallization of a non-conjugated polymer can also induce emission. Furthermore, Yuan *et al.* [26] demonstrated in 2018 crystallization-enhanced emission from polyethylene terephthalate (PET) that also showed concentration- and AIE-enhanced properties. The results showed that conformational rigidification enhances the luminous efficiency of PET films. Such emission can be explained by the CTE mechanism, as the electronic conjugation through the space of the terephthalate groups leads to extended delocalization.

Based on the results obtained with PET, a sort of commercially available PCTA with good crystallization ability is thus also expected to behave similarly. The polymer synthesized by using 1,4-cyclohexanedimethanol (CHDM) and dimethyl terephthalate (DMT) as monomers via polycondensation PCTA is obtained, which was discovered and developed at Tennessee Eastman in 1959 by Kibler *et al.* [27] and was commercialized as Kodel<sup>®</sup> fiber. Furthermore, the modification of crystallinity in PCTA with isophthalic acid is the basis of the PCTA, family of commercial resins with the trade name of Durastar<sup>®</sup> [28]. On the other hand, transparent thin-film luminescent materials are promising for many technological applications such as photovoltaic cells, photoluminescent displays, optical writing and multilayer optical storage [29–33]. In all cases, high quality transparent optical materials are required to reduce the loss of incident light [34].

The aim of this industrial research project is the preparation of multifunctional materials and control the processing for the formation of a new morphology with specific photophysical properties for its application in the packaging industry as anti-counterfeiting and traceability systems. The preparation of a novel system based on aggregated polymeric PCTA nanostructures supported on a thermoplastic material has been developed. These materials can be processed at high temperatures using injection molding technologies to directly incorporate the nanoparticles into packaging in the cosmetics and perfumery sectors (safety system).

## Experimental Methods

The shape and dimension of the synthesized nanoparticles polymer were studied by *scanning electron microscopy (SEM)* using a XL30ESEM Philips at an accelerating voltage of 25 kV. For SEM studies, the polymer was dissolved in different solvents and were dispersed by ultrasound. The nanoparticles were deposited by spray coating  $1 \text{ g}\cdot\text{l}^{-1}$  on a PET film.

The average particle size of the nanoparticle polymer was measured by *Dynamic Light Scattering (DLS)* using a Malvern Nanosizer NanoZS Instrument equipped with a 4 mW He-Ne laser ( $\lambda = 633 \text{ nm}$ ) at a scattering angle of  $173^\circ$ . Different samples were measured in square polystyrene cuvettes (Sarstedt®) at  $25^\circ\text{C}$ . The autocorrelation function was converted in an intensity particle size distribution with ZetaSizer Software 7.10 version, based on the Stokes-Einstein equation.

The polymer compositions were measured with *proton nuclear magnetic resonance ( $^1\text{H-NMR}$ )* using a Varian Mercury of 500 MHz ( $t=1''$ ;  $dl=7''$ ,  $45^\circ\text{C}$ ) taking a sample of 5 mg and added of 1 ml of deuterated trifluoroacetic acid (TFA) (Sigma-Aldrich).

*Infrared spectra* were recorded by ATR (Attenuated Total Reflection) using a Fourier transform infrared spectrometer, Perkin Elmer Spectrum One, scanning from  $400 \text{ cm}^{-1}$  to  $4000 \text{ cm}^{-1}$  with a resolution of  $1 \text{ cm}^{-1}$ .

*Differential Scanning Calorimetry (DSC)* of the PCTA particles were studied using a Netzsch DSC 214 calorimeter with standardized aluminum sample holders and caps. Samples (5-10 mg) were analyzed in  $\text{N}_2$  atmosphere from  $0^\circ\text{C}$  to  $290^\circ\text{C}$ , at a rate of  $10^\circ\text{C}\cdot\text{min}^{-1}$ , and  $T_g$  determined from second heating scan.

*Thermogravimetric analysis (TGA)* were carried out on a TA Instrument Q-500, using a heating ramp at  $20^\circ\text{C}\cdot\text{min}^{-1}$  from  $25^\circ\text{C}$  to  $700^\circ\text{C}$ , in nitrogen and air atmosphere.

*UV spectra* were monitored by using a Perkin Elmer model Lambda 35 spectrophotometer over the range 200-700 nm spectrum region. *Fluorescence*



---

---

*spectra* were recorded using a Perkin Elmer LS 55 and corrected using the response curve of the photo-multiplier.

Fluorescence confocal microscopy were measurement with SM710 spectral confocal microscope (Zeiss). It consists of an inverted transmitted light and epifluorescence microscope Observer.Z1 coupled to a spectral confocal system with 6 laser lines (405, 488, 458, 514, 561 and 633 nm). The available objectives are Plan-APOCHROMAT (10x/0.45 DIC, 25x/0.8 mm Korr DIC, 40x/1.3 Oil DIC, 63x/1.40 Oil DIC). The image acquisition and analysis software is Zen 2.3 SP1. Micrographs were analyzed with the ImageJ software.

## **Results and discussion**

### **Synthesis of PCTA nanoparticles**

As discussed in the introduction of this Ph.D. Thesis, there are two different ways to obtain nanomaterials. In this case, we have focused on the synthesis of nanoparticles by top-down methodology. This involves reducing the size of macrostructures, in this case the pellet of the material until nanoparticles are obtained. For this purpose, two different methodologies have been tested. The objective is to obtain polymeric nanoparticles with a homogeneous distribution that have the same thermal properties as the pellet in order to facilitate their subsequent recycling.

On the one hand, a synthesis methodology for PET nanoparticles has been used while maintaining the original chemistry of the material [35]. The PCTA used for the synthesis of the nanoparticles is from the pellet provided by Eastman Company. 1 g of PCTA pellet is introduced in 10 ml of *trifluoroacetic acid* (TFA, Sigma-Aldrich) (90 %) at 50 °C and stirred for 2 h until is completely dissolved and kept in agitation overnight at room temperature. In order to precipitate the nanoparticles, 10 ml of a dilute TFA solution (20 % v/v) is added under vigorous stirring, kept for 2 h and then stored overnight. Subsequently, the solution is centrifuged at 3500 rpm for 1 h and the supernatant is removed. Then, the solid is resuspended in 10 ml of water and sonicated by 5 min. Subsequently a 0.5 % solution of sodium dodecylsulfate (SDS, Sigma-Aldrich) is added and it is taken to a 250 ml test tube where it is volumetrically calibrated

to this volume. The nanoparticles are then allowed to settle in the flask overnight. The following day different fractions are observed and separated every 50 ml, centrifuged and the supernatant is removed. The resulting solid is washed with anhydrous ethanol in the centrifuge and allowed to dry completely to obtain the final particles. Aliquots of each fraction are taken to be studied by DLS to evaluate the particle size effect (Figure 4.10). The procedure for the nanoparticles preparation takes 4 days.



**Figure 4.10.** Different fractions are observed and separated every 50 ml

On the other hand, the other synthesis proposed is by nanoprecipitation. 1 g of PCTA was dissolved in 50 ml of DMSO (Sigma-Aldrich) at high temperature for 1 h. The solution was then slowly added in 500 ml of methanol (Sigma-Aldrich) under vigorous stirring. The white precipitates were collected by filtration with a sand cone funnel and a polytetrafluoroethylene (PTFE) membrane. They were then washed with methanol three times and dried under vacuum.

In order to have a better control of the nanoparticles synthesized by this method, the following parameters have been considered: temperature of the precipitation medium, precipitation solvent and dispersion solvent of the nanoparticles.

For the first parameter, three different temperatures have been selected:

- Room temperatura 25 °C (RT)
- Ice temperature 0 °C (I)
- Dry Ice -78 °C (DI)

For the case of precipitation two solvents have been studied:

- Methanol (polar)
- n-Pentane (non-polar)

Finally, for the dispersion medium, different polar protic and aprotic solvents and apolar solvents have been studied: methanol (M), ethanol (E), ether petroleum (EP), diethyl ether (EP) and N-pentane (P)

All conditions are given in the following Table 4.4.

**Table 4.4.** Conditions used for the synthesis of polymeric nanoparticle dispersions

	Temperature			Solvents
	Dry Ice	Ice	Room Temp.	
<b>Precipitates in methanol</b>	M-DI-M	M-I-M	M-RT-M	M
	M-DI-E	M-I-E	M-RT-E	E
	M-DI-EP	M-I-EP	M-RT-EP	EP
	M-DI-DE	M-I-DE	M-RT-DE	DE
	M-DI-P	M-I-P	M-RT-P	P
<b>Precipitates in n-pentane</b>	P-DI-M	P-I-M	P-RT-M	M
	P-DI-E	P-I-E	P-RT-E	E
	P-DI-EP	P-I-EP	P-RT-EP	EP
	P-DI-DE	P-I-DE	P-RT-DE	DE
	P-DI-P	P-I-P	P-RT-P	P

## Nanoparticles Characterization

### Thermal Stability

The thermal properties of the micro/nanoparticles have been studied to consider the possibility of processing them together with the plastic used for industrial packaging. A thermogravimetric analysis has been performed to know their thermal properties (Figure 4.11). It is observed that for the synthesis with TFA the nanoparticles begin to degrade at 348 °C, while by nanoprecipitation they begin to degrade at 365 °C, a difference of almost 20 °C. Considering the degradation temperature that marks the derivative, only a difference of 3 °C is observed.

These results are different in relation to PCTA pellet as previously shown in Figure 4.3 [26]. On the one hand, the degradation temperature for the nanoparticles is 20 °C lower. On the other hand, it is observed that from 400 °C another process of mass loss appears, appreciating that its thermal stability increases. The decrease in the decomposition rate that occurs in the approximate range of 17 % could be attributed to the degradation of the terephthalate groups that are stacked when forming the nanoparticles and have large electronic clouds that need higher temperature to decompose. It is proved that nanoparticles can behave differently in the thermal stability of polymers [36].

A differential scanning calorimetry (DSC) test was also performed, using the same program used for raw polymers. It can be observed that in the second heating scan, different results are obtained depending on the syntheses carried out. In the case of the synthesis of TFA, it is observed that its T<sub>g</sub> is 75 °C, and a melting temperature endotherm starting at 140 °C, obtaining its maximum at 225 °C and ending at 243 °C, being a very wide temperature range (Figure 4.12A). On the other hand, the nanoparticles synthesized by nanoprecipitation have a T<sub>g</sub> at 81.9 °C, and in this case a cold crystallization process is observed. In addition, the melting temperature in this case begins at 190 °C and ends at 243 °C obtaining a maximum at 225.9 °C (Figure 4.12B).

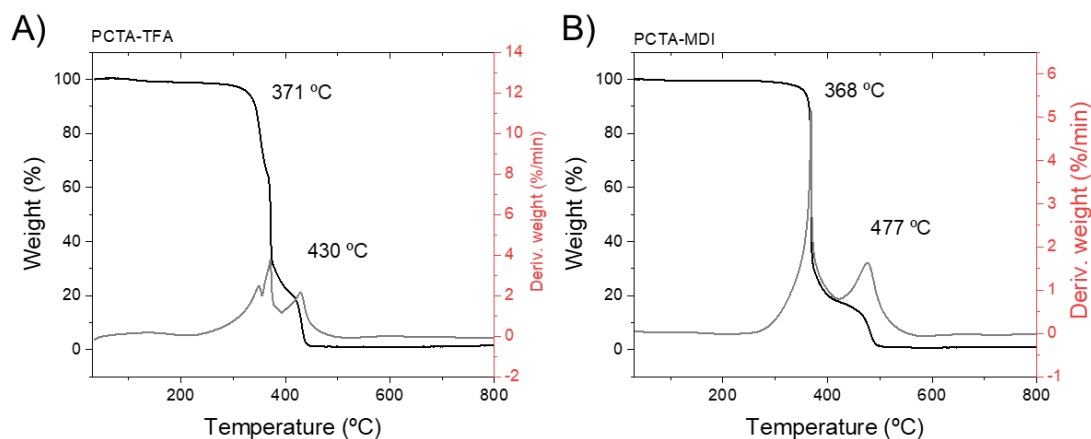


**Figure 4.11.** Thermogravimetric analysis in air atmosphere of PCTA nanoparticles synthesized by. A) TFA synthesis method. B) Nanoprecipitation method

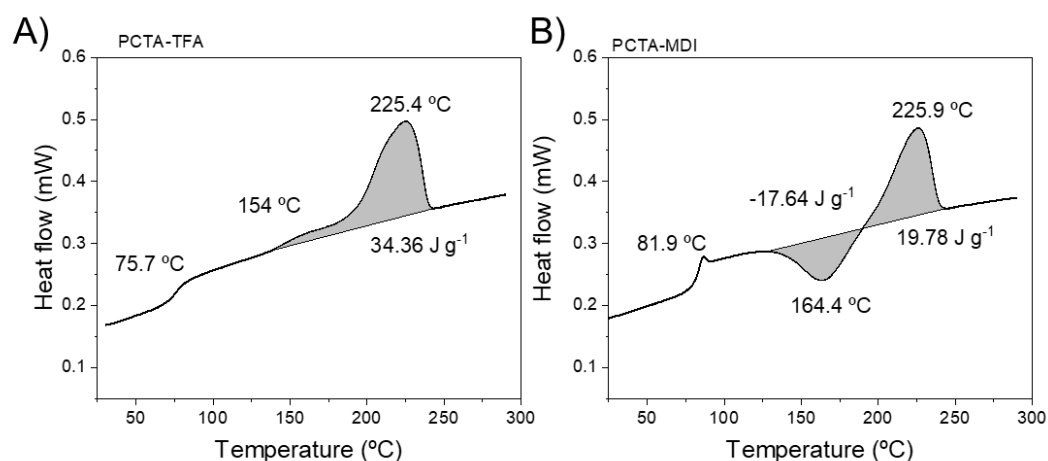


**Figure 4.12.** Differential scanning calorimetry (DSC) curves of PCTA nanoparticles synthesized by A) TFA, B) Nanoprecipitation method

Differences are observed by both methods; TGA and DSC results. Expected results would show nanoparticles with high melting and degradation temperatures, therefore the nanoprecipitation synthesis is selected for the rest of the studies.

In addition, when comparing the nanoparticles synthesized by nanoprecipitation with the commercial pellet by DSC, a similar structure is predicted with  $T_g$  values close to 80 °C and with a light decrease in the  $T_m$  of approximately 4 °C

(Figure 4.13). This difference does not represent any inconvenience when treating the nanoparticles with the virgin polymer at industrial level.

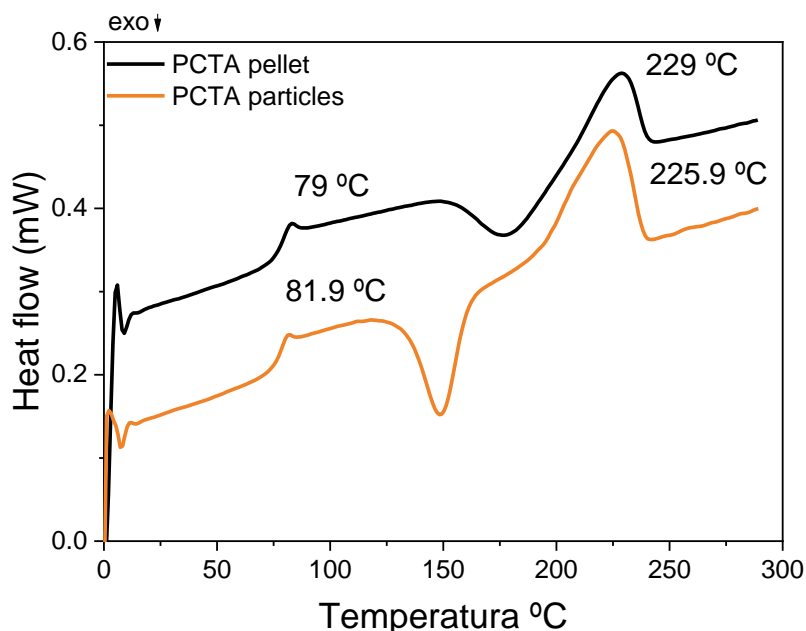


**Figure 4.13.** Differential scanning calorimetry (DSC) curves of PCTA pellet and PCTA nanoparticles

### Compositional and morphological characterization

Once the synthesis method and its optimal conditions were selected, a compositional and morphological characterization was carried out by using different techniques.

$^1\text{H-NMR}$  was used to determine the chemical composition of the synthesized nanoparticles as shown in Figure 4.14A. The  $^1\text{H-NMR}$  spectrum featured the peak at 8.76 ppm is the characteristic peak of protons in the benzene ring and stands for the total molar content of the acidic moieties. Chemically displaced partitions at 4.9 and 5.0 are attributed to the resonance peaks of methylene protons in CHDM moieties with cis and trans conformation. The signals of the methylene group at 1.93-2.03 ppm, and 1.16-1.81 ppm the signals of the methylene protons. These signals are further apart in the spectrum due to the presence in the polyester chain of cis- and trans- configurations of the

cyclohexylene group. Based on the  $^1\text{H-NMR}$  spectra, the copolymer compositions can be determined from the respective peak areas where it is confirmed that there is a percentage of 63 % trans and 36 % cis.

The structure of PCTA nanoparticles is also confirmed by a FTIR spectrometer. Figure 4.15B shows the spectrum of PCTA, showing the characteristic signals of this polymer. C=O stretching peak and ester group skeleton peak are observed at  $1715$  and  $1268\text{ cm}^{-1}$ , respectively. The C–O–C skeleton asymmetric vibration of soft segment, CH<sub>2</sub> bending vibration, C–H stretching vibration of cyclohexylene ring and C–H vibration of benzene ring appear at  $1104$ ,  $1454$ ,  $958$  and  $727\text{ cm}^{-1}$ , respectively.

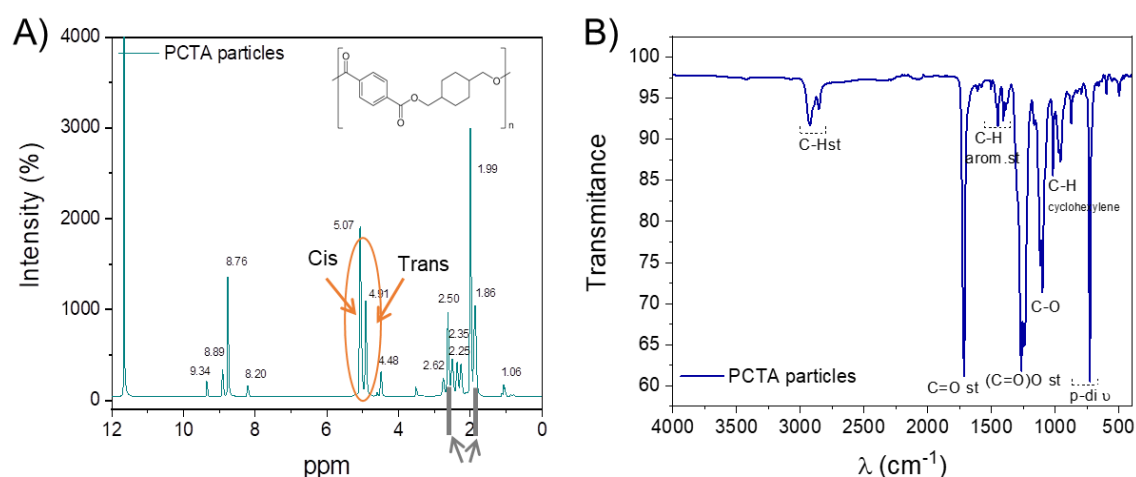


**Figure 4.14.** A)  $^1\text{H-NMR}$  spectra and characteristic peak assignment of PCTA (63.6 % trans; 36.3 % cis). B) FTIR spectra of PCTA solid particles

### Dispersion Stability

Nanoparticles precipitated in n-pentane do not disperse homogeneously in any of the solvents listed. However, nanoparticles precipitated in methanol disperse in methanol and ethanol (Figure 4.15).

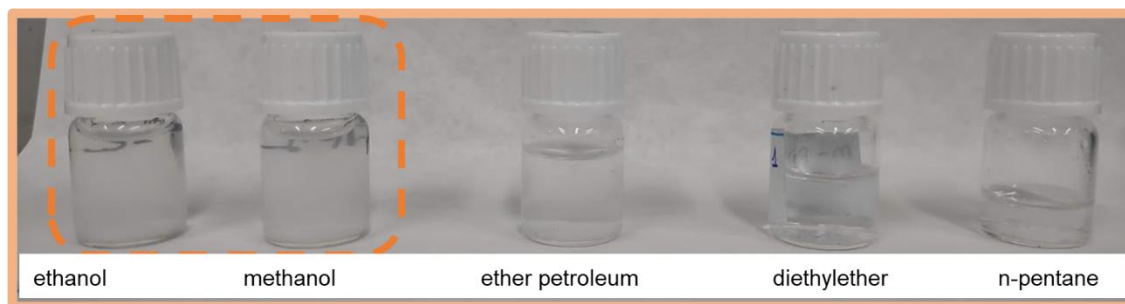


**Figure. 4.15.** Dispersion stability of nanoparticles synthesized by nanoprecipitation in methanol in the different solvents studied

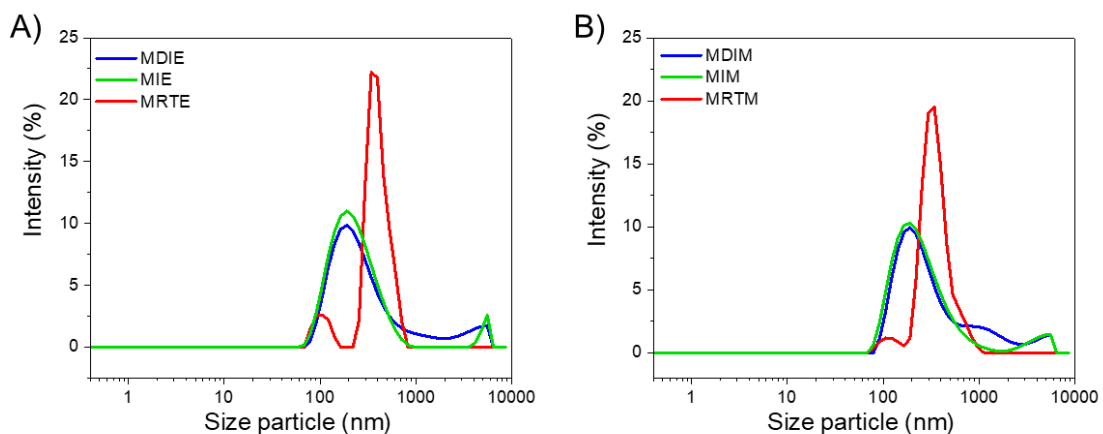
Therefore, the study focuses on nanoprecipitation in methanol. Nanoparticles are more stable dispersed in polar solvents such as methanol and ethanol, while for the rest of solvents such as EP, DE and P a stable dispersion is not obtained. Therefore, the optimal conditions to obtain stable polymeric dispersions have been found by using methanol and/or ethanol.

### Morphological and size characterization

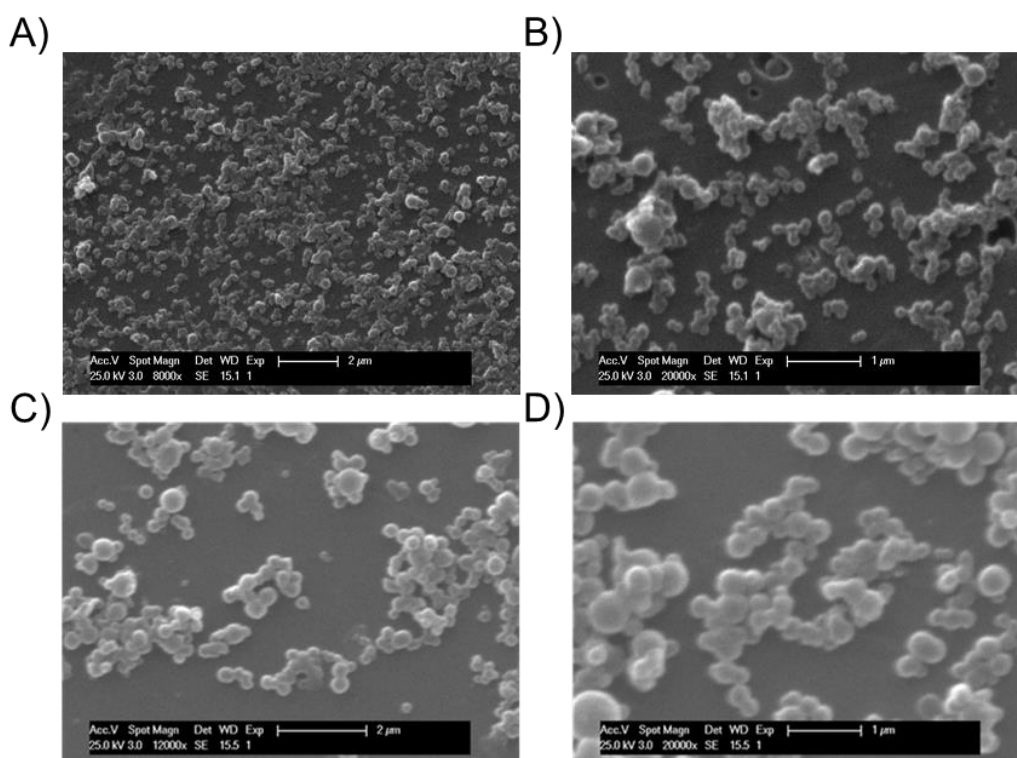
The particle size and distribution for PCTA nanoparticles were studied by DLS and SEM analysis. Figure 4.16 shows the results obtained by DLS at a concentration of  $1 \text{ g}\cdot\text{l}^{-1}$  of the nanoparticles precipitated in methanol and dispersed in ethanol or methanol as the two solvents with highest stability. In addition, the different precipitation temperatures are shown to understand the effect on the particle size. As can be seen, in both cases larger nanoparticle sizes are obtained when precipitated at room temperature regardless the solvent used to disperse. For temperatures at  $0 \text{ }^\circ\text{C}$  and  $-78 \text{ }^\circ\text{C}$  the same particle sizes are obtained. Both solvents can be used for the study, and it was decided to use the  $-78 \text{ }^\circ\text{C}$  temperature in order to have more control in the synthesis.

Figure 4.17 shows the environmental scanning electron microscopy (ESEM) images of the polymer nanoparticles studied in this Chapter. A dispersion of  $1 \text{ g}\cdot\text{l}^{-1}$  concentration of PCTA nanoparticles was prepared in ethanol and methanol, then the dispersion is sprayed on one side of a PET film and the solvent is allowed to evaporate for less than 5 min. The nanoparticles show a spherical morphology in the nanometer range (160-200 nm), although some micrometer aggregates (analyzed with ImageJ) are also found.





**Figure 4.16.** Hydrodynamic diameter distribution determined by dynamic light scattering of the prepared dispersions in A) ethanol, and B) methanol at different temperatures



**Figure 4.17.** SEM images of the synthesized PCTA nanoparticles on a PET film. A-B) nanoparticles dispersed in ethanol 1 g·l<sup>-1</sup> at different magnifications. C-D) nanoparticles dispersed in methanol 1 g·l<sup>-1</sup> at different magnifications

## Photophysical characterization

A photophysical characterization is carried out in order to understand the luminescent properties of the newly designed nanoparticles. The emission and excitation fluorescence spectra of the nanoparticles in MeOH at different concentrations have been measured.

The absorption spectrum of ultraviolet light increased with increasing concentration (Figure 4.18A). When dissolved in methanol, dilute PCTA solutions emit weak UV light at around 220 and 290 nm, which is attributed to the  $\pi \rightarrow \pi^*$  electronic transitions of the aromatic rings of the polymers. As the concentration increases, larger aggregates of the particles are formed and therefore the absorbance increases. A tail appears around 380 nm implying the presence of aggregates due to the terephthalate groups [19,26]. The phenomenon could be due to the electronic delocalization system by clustering. The absorption peaks showed a red shift with increasing concentration. This broad absorption band can be related to phenyl groups which is consistent and assignable to the emission of individual terephthalate units [26].

By comparing Figure 4.18A and B, it can be seen that the absorption and emission spectra are different. Normally the absorption and emission spectra have the same curve shape only shifted in the spectrum. In this case, the opposite is validated, the peaks of longer wavelength of their excitation are not detectable in the absorption spectrum.

As seen in the Figure 4.17B when excited at 215 nm, the intensity of the peak at 370 nm reaches a maximum at the  $2 \text{ g}\cdot\text{l}^{-1}$  concentration and then decreases, showing the typical concentration quenching effect. This quenching must come from the strong aggregation of the aromatic rings in concentrated solutions for which these wavelengths are no longer optimal. In addition, multiple emission maxima are observed at 422, 481, 526, 627 nm. The same effect occurs when excited at 280 nm.

From  $5 \text{ g}\cdot\text{l}^{-1}$  a decay in the intensity is observed, initially it is thought that it could be because of ACQ. It is presumed that in solution, when the concentration is increased, the luminescence increases due to aggregation (AIE). In this case, from a certain concentration, the opposite happens. It could be thought that

from a certain concentration the particles stack up having more  $\pi$ - $\pi$  stacking of the aromatic ones in a planar form explaining this decay. To understand what happens, this study is supported by a particle size characterization by DLS.

When the concentration is increased from 2 g·l<sup>-1</sup> to 5 g·l<sup>-1</sup> there is a decrease in particle size. It is proposed that this is due to the aggregation of the nanoparticles as the concentration increases and they precipitate at the bottom of the cuvette, so their actual size is not measured. It is assumed that the same behavior happens when the luminescence measurements are performed in the fluorimeter. As the concentration increases, the nanoparticles precipitate and that is why the increase in intensity with increasing concentration is not observed. All this is corroborated by studying the stability of the nanoparticles over time at different concentrations, observing how from a concentration of 5 g·l<sup>-1</sup> they begin to precipitate.

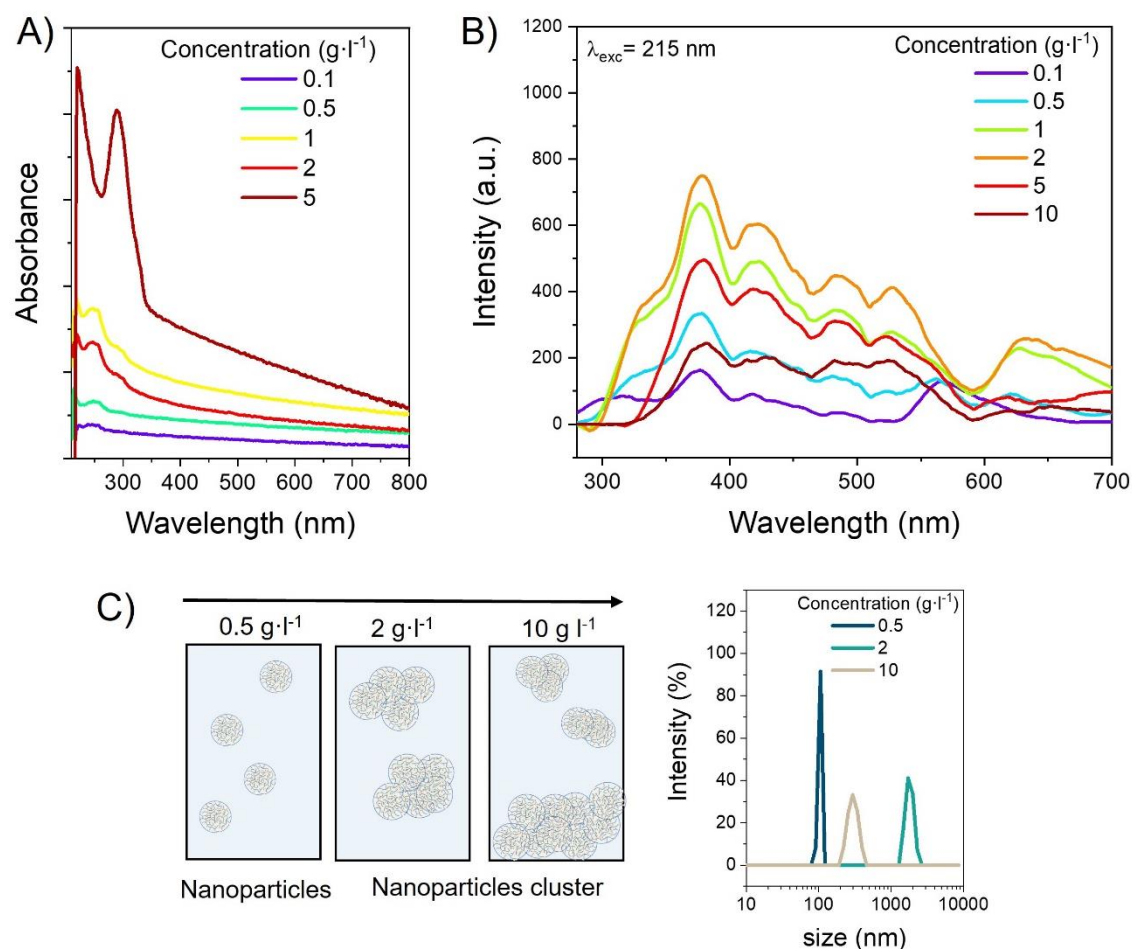


**Figure 4.18.** A) Absorption spectra PCTA nanoparticles in MeOH at different concentrations. B) Emission spectra at different concentrations of PCTA in MeOH C) Schematic illustration of nanoparticles clusterization when increases the concentration and hydrodynamic diameter distribution determined by dynamic light scattering of the prepared NanoPCTA sample in MeOH

As shown in Fig 4.19 it possesses little luminescence when the nanoparticles are dissolved in good solvents and its PL spectrum in dilute THF solution is weakly intense. However, an increase in PL intensity is seen under the same conditions when a MeOH is added to the THF solution. When the methanol fraction is 90 %, the fluorescence of the nanoparticles increases, the emission gradually intensified with increasing amount of MeOH, showing typical AIE behavior.

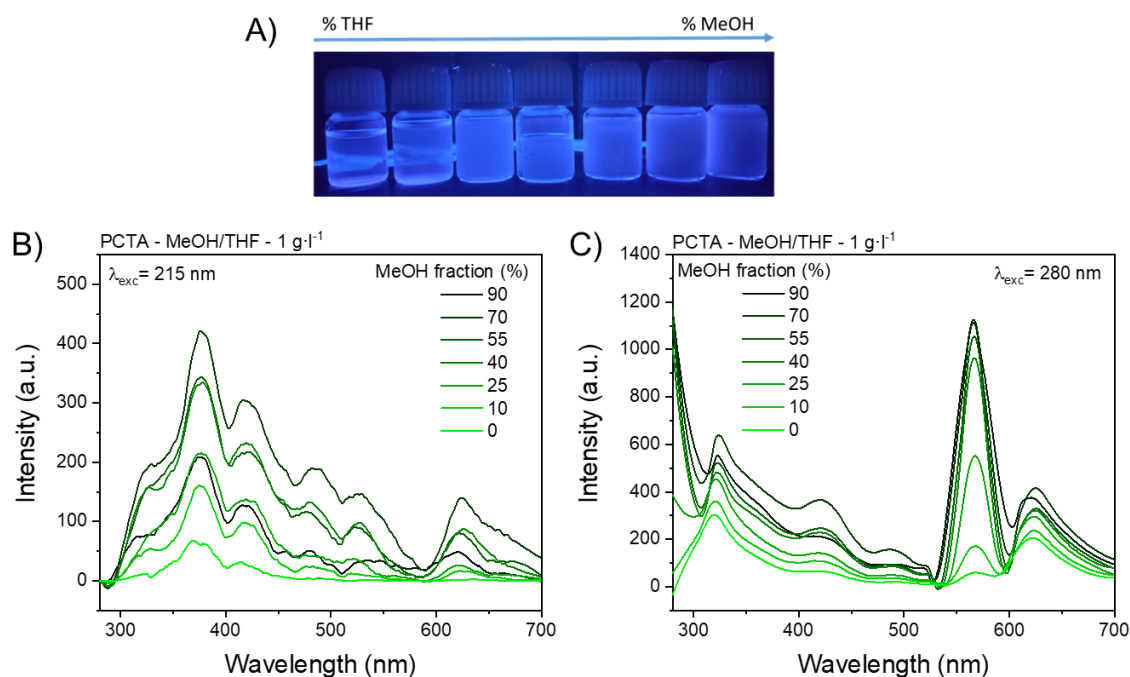


**Figure 4.19.** A) Photographs of PCTA in THF/MeOH mixtures with different MeOH fractions taken under a hand-held UV lamp with 365 nm illumination. Fluorescence emission spectra of PCTA (1g·l<sup>-1</sup>) in mixture of THF and MeOH B)  $\lambda_{exc} = 215$  nm C)  $\lambda_{exc} = 280$  nm

When we excite at different wavelengths, different emission spectrum is observed for each excitation length. For a 1 g·l<sup>-1</sup> solution different peaks are observed at 372, 422, 481, 526, and 627 nm with different excitation lengths (Figure 4.20). A dependence of the emission on the excitation is observed suggesting the presence of heterogeneous excited states. Terephthalate segments in the amorphous zone may be forced to interact with each other to generate new clusters with effective electronic communications across space such as short  $\pi$ - $\pi$ , CO--- $\pi$ , O---O, and O---CO contacts, which give rise to heterogeneous populations with different effective conjugations and, therefore, different emissions.

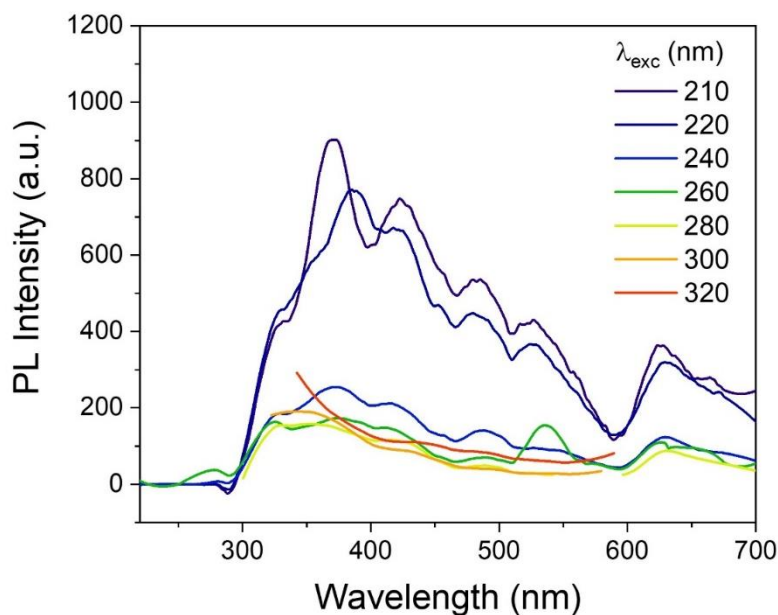


**Figure 4.20.** PL emission spectra of PCTA nanoparticles in MeOH 1 g·l<sup>-1</sup> at different wavelengths excitation

A fluorescence microscopy characterization of PCTA nanoparticles has been carried out. They have been studied in two different ways, on the one hand, in solid form, and on the other hand, in methanol dispersion. The multilayer technique has been used for this study, depositing the particles inside a sandwich formed by PET-adhesive-PET. The multilayer technique uses different sheets of thermoplastic aromatic polyester or a thermoplastic polyolefin to form a package, with an adhesive sandwiched between them to create a sandwich structure. These sheets can then be shaped into any desired design. We deposit the nanoparticles between the layers so that the aggregates are embedded in the packaging. For the deposition of the particles in dispersion, it has been done by drop-casting, subsequently allowing the drop to evaporate and closing the sandwich. In the case of the solid particles, they were deposited directly on the adhesive, ensuring a good fixation and then the multilayer structure was created. Fluorescence microscopy images show that both for solid state and when a dispersion of the nanoparticles is created to obtain smaller aggregates, they emit in the green, orange and red under different excitation wavelengths. In this case, 545 nm excitation has been used and collected with a 580 nm emission filter in front, where the red is collected. Also,

---

---

an excitation of 450-500 nm has been used and with emission filters of 510 nm forward and 540-575 nm where yellow and green are collected respectively (Figure 4.21).

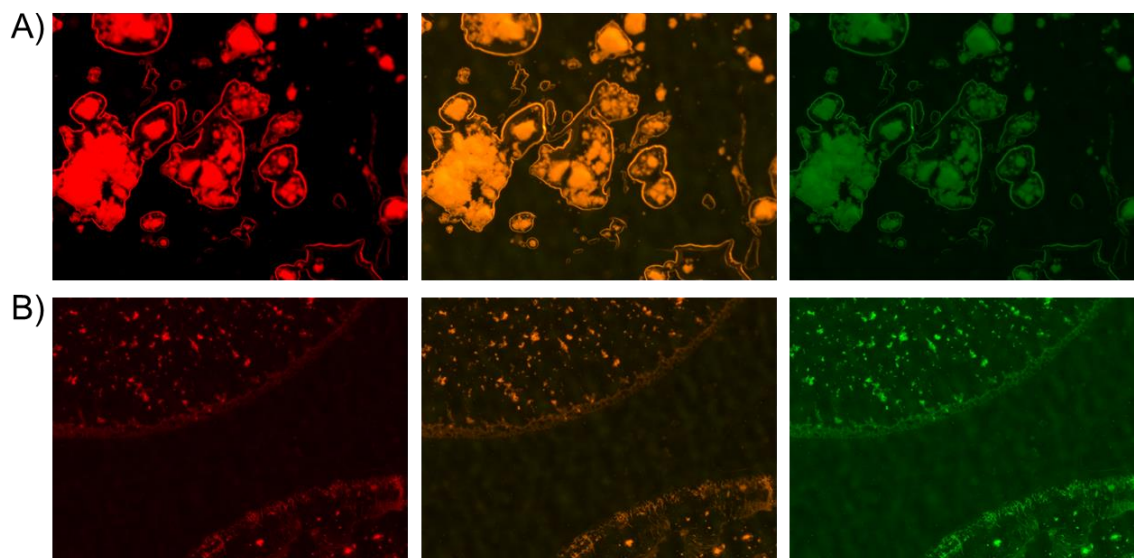


**Figure 4.21.** Fluorescence microscopy of PCTA nanoparticles in 3 layers. Fluorescence microscopy images at different excitation and emission lengths. The fluorescence images of first, second, and third column were collected in red channel (from 580 nm and up,  $\lambda_{\text{ex}} = 545$  nm), orange channel (from 510 and up nm,  $\lambda_{\text{ex}} = 450-500$  nm), and green channel (540-575 nm,  $\lambda_{\text{ex}} = 450-500$  nm). A) Powder; B) Drop casting

In addition, in previous studies performed in confocal fluorescence microscopy equipment, it was observed that it also emits blue when excited at 405 nm and collected between 420-500 nm (Figure 4.22). In the first study performed in the confocal fluorescence microscope, different excitation wavelengths were used than those used later in the fluorescence microscopy equipment, this was because the studies were performed in different research centers that had different excitation sources. Having the opportunity to use both devices has allowed us to obtain a deeper characterization of the nanoparticles under study.

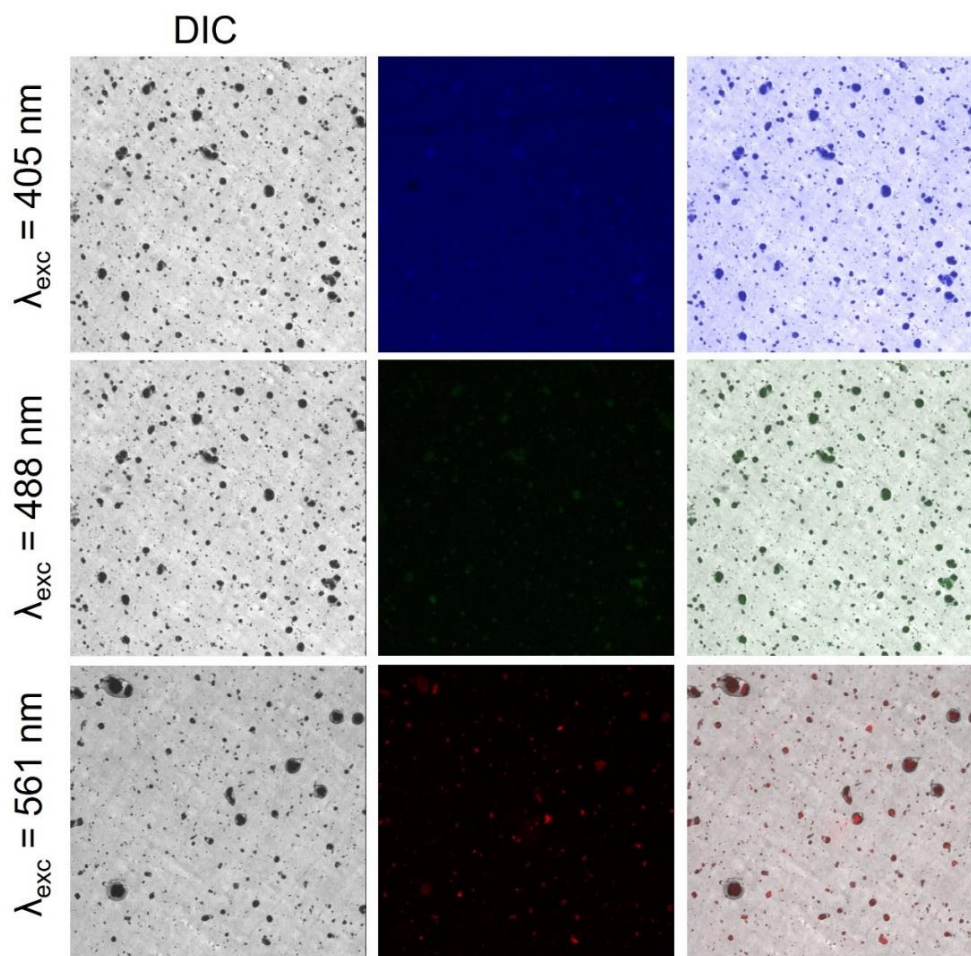


**Fig 4.22.** Fluorescence confocal microscopy of PCTA nanoparticles in 3 layers. The fluorescence images of first, second, and third line were collected in blue channel (420–500 nm,  $\lambda_{\text{ex}} = 405$  nm), green channel (500–570 nm,  $\lambda_{\text{ex}} = 488$  nm), and red channel (570–640 nm,  $\lambda_{\text{ex}} = 561$  nm). The last column is a composite images of blue, green, red channels

Between the two characterizations, the following observations were taken for determining:

- The absence of fluorescence coming from the PET film and PCTA film measured in the areas where there are no nanoparticles added.
- Depending on the wavelength used for excitation, the particles emit in different areas of the visible spectrum.
- For the case of confocal fluorescence microscopy, excitations of 405, 488 and 561 nm have been used, and emission in blue, green and red has been collected.



- 
- 
- In the case of fluorescence microscopy, excitations of 450-500 and 545 nm were used, and emission was collected using different emission filters in green, orange and red.
  - Luminescence was observed both in the particles deposited as powder and those deposited by drop-casting.

### **Discussion of the mechanism**

Being a type of non-conjugated polymer, PCTA nanoparticles do not have conventional conjugated chromophores, so it is important to understand the origin of the luminescence.

As suggested by Tang *et al.* [37,38] the fact that the CTE process occurs may be due to different processes such as, for example, that the chemical structures are apparently non-conjugated and that the functional groups without  $\pi$ -electron bonds are separated by a saturated backbone with sigma bonds. They also suggest that when the polymer is dissolved at low concentrations, luminescence does not occur. The absorption and excitation spectra are different, the longer wavelength peaks of their excitation spectra are not usually detectable as a significant feature in the absorption spectra. The wavelength of their emission depends on the excitation, where excitation at longer wavelengths results in red emission.

Several points have been justified that are due to CTE processes:

- Non-conjugated group with non-bonding or  $\pi$ -electron are separated by saturated backbone as CHDM.
- Absorption and excitation spectra are different
- Excitation dependent
- Multicolor emission resulting from different wavelength

The mechanism for understanding the CTE process can be explained by the TSC model. The TSC process proposed by Tang *et al.* [37,39] can be easily understood. It justifies that the better the degree of delocalization of the system and the closer the components are, the greater the interaction between them. Especially for systems with electron-rich atoms.

The polymer has several electron-rich subgroups such as O with lone electron pairs and unsaturated C=O. These groups exist as a common non-emitting organic group. However, when connected in macromolecules or clusters, they can give emission when aggregated. The CTE mechanism can explain the photophysical processes of these unconventional systems, the clustering of diverse groups with subsequent electron cloud and molecular rigidification [38].

Through-space conjugation (TSC) together with through-bond conjugation can explain these unusual aggregation-induced emission (AIE) systems [26,37,38,40]. Aromatic benzene rings from different molecules can be stacked in parallel creating a delocalized electron cloud allowing the TSC effect to occur. As this occurs, the gap is reduced giving a red shift to emission. Therefore, the fluorescence may be the result of the tightly packed structure of the polymer and rigidly hold the aromatic chromophores.

As observed in fluorescence microscopy there is emission in different regions of the spectrum when different wavelengths are excited, which is justified by Tang *et al.* [23] that emissions are excitation dependent, when high wavelengths are used to excite the polymer, a red shift is observed. It is possible that this is due to conjugation through the space between the aromatic rings of the PCTA.

In summary, the fluorescence of PCTA particles can be explained by the CTE mechanism. The polymer's terephthalate groups, as well as the carbonyl groups, are clustered in close proximity to each other allowing electronic communications through space (TSC), including the overlapping of pi electrons forming an extended electronic conjugation.

It is aimed to explain the effect of the nanoscale on the luminescent properties. The difference between having the polymer isolated and obtaining the nanoparticle is that the energy gap from the excited state to the ground state decreases.

It is assumed that the delocalized  $\pi$  electrons and lone pair electrons isolated in the polymer could form a variety of intrachain clusters. These  $\pi$  electrons and lone pair electrons could further delocalize through n-  $\pi$  and  $\pi$  -  $\pi$  interactions in the clusters [14]. This aggregation with shared and overlapping electron

clouds could exhibit extended conjugations and smaller energy gaps (Figure 4.23).

Also, after aggregation, the non-radiative deactivation pathways of excitons are impeded due to rigid conformations resulting from effective inter- and intramolecular interactions. Consequently, the exciton wavelength-dependent emissions of the aggregates should be attributed to the heterogeneity of the synthesized nanoparticles.

The formation of cluster luminescence occurs between the carbonyl groups and the phenyl groups. The aggregation causes a vibrational restriction to occur, thus reducing non-radiative processes. The red shifts may be due to  $n-\pi^*$  between the carbonyl groups. It appears that the presence of carbonyl groups and phenyl groups is a prerequisite for emission [41].

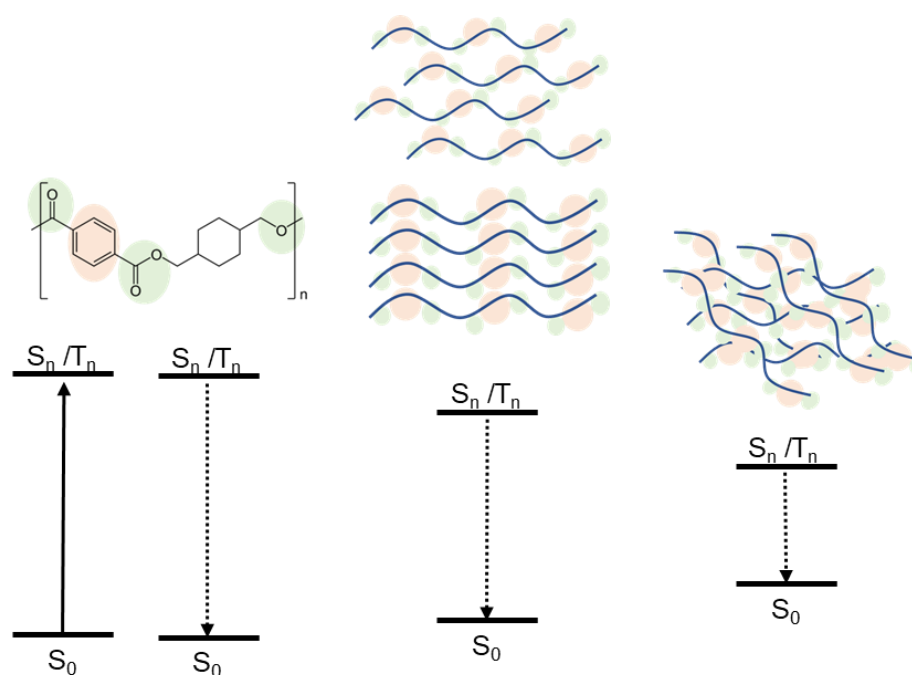


**Figure 4.23.** Schematic illustration of CTE mechanism via TSC

An XPS study is performed to evidence TSC due to the ester groups in the cluster when the nanoparticles are prepared, and to understand the difference in polymer properties when they are in film/specimen test format and when they are as nanoparticles. It helps to understand how the properties of a material change at the nanometer scale (Figure 4.24).

TSC through the terephthalate groups is vital to generate emission at higher wavelengths. One of the ways to study this is by XPS. If we compare the results obtained from the particles together with the specimen test. The XPS analysis of C1s of the particles indicates the presence of different components with binding energies of 284.47, 285.6, 286.33 and 288.9 nm corresponding to C=C, C-C, C=O, O=C-O respectively [26]. While for the specimen the contribution due to the O=C-O group is vanished. As for the study carried out for the binding energies of the O1s peak of the O=C, O-C and H-O-H units, different shifts of the signal corresponding to the C-O bond from 533.01 eV of the particle to 532.34 eV of the specimen, with a shift of 0.7 eV, are observed. These shifts indicate the increase of the electron cloud density of the terephthalate group in the particles, which is further evidence of electronic communications between the ester groups in the clusters due to a CTE mechanism via TSC.

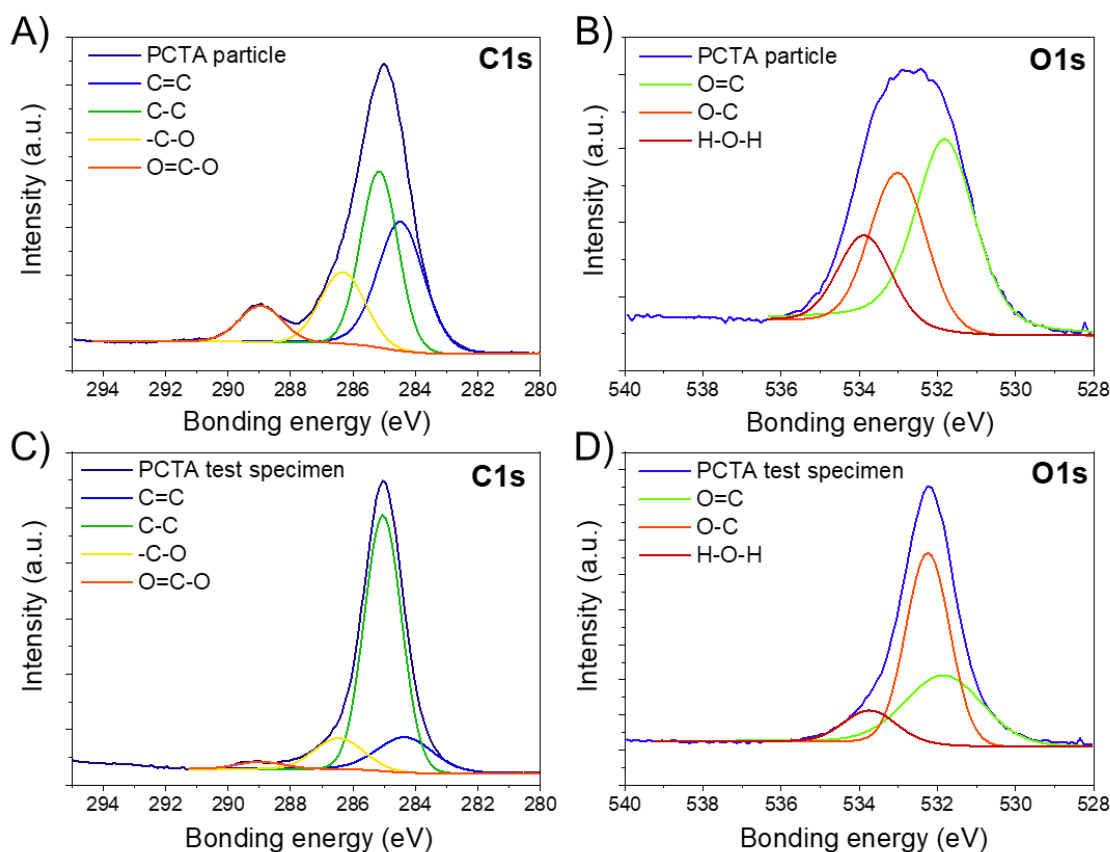


**Figure 4.24.** XPS spectra of A) and B) particle C<sub>1s</sub> and O<sub>1s</sub>; C) and D) spectra of test specimen C<sub>1s</sub> and O<sub>1s</sub>

## Conclusions

Functional polymeric materials have evolved rapidly due to the development of modern technologies that require an unusual combination of properties that cannot be provided by polymers. Thermoplastic polymers are flexible and characterized by their mechanical properties but lack other properties that can make them more attractive such as intrinsic luminescence. By incorporating PCTA particles with luminescent properties due to aggregation induced emission (AIE), multifunctional composites with the typical properties of thermoplastic polymers and optical response to visible light are obtained.

In this work, a preparation of fluorescent nanoparticles of non-conjugated polymer with aggregation induced emission (AIE) by nanoprecipitation has been described. A series of characterization techniques have been carried out to certify the success of the nanoparticles without losing their initial properties as starting pellets. These nanoparticles have shown fluorescence in several regions of the spectrum, showing evident characteristics of CTE due to TSC. These nanoparticles can be excited with different wavelengths, collecting emissions in different ranges of the spectrum (blue, green, orange and red) being more intense in the red region. These nanoparticles show an excitation dependence in the emission. Considering the results, it is believed that it can be a good candidate to use these nanoparticles in the traceability and anti-copying of packaging made with the same material.

A system has been designed based on aggregated structures supported on the same material processed at high temperatures and used as packaging in the cosmetic and perfumery sector, where the luminescent contribution is exclusively found in the nanoparticles, regardless of the wavelength of the spectrum.

**References**

- [1] T. Song, Q. Wang, J. Li, X. Chen, S. Liu, and G. Wang, "Modifying the properties of poly(1,4-cyclohexylenedimethylene terephthalate) by hydroquinone bis(2-hydroxyethyl) ether," *Journal of Polymer Research*, vol. 29, no. 2, p. 48, Feb. **2022**, doi: 10.1007/s10965-021-02875-6.
- [2] J. Li, Y. Wang, X. Wang, and D. Wu, "Crystalline characteristics, mechanical properties, thermal degradation kinetics and hydration behavior of biodegradable fibers melt-spun from polyoxymethylene/poly(L-lactic acid) blends," *Polymers (Basel)*, vol. 11, no. 11, p. 1753, Oct. **2019**, doi: 10.3390/polym11111753.
- [3] V. V. Rajan, R. Wäber, and J. Wieser, "Online monitoring of the thermal degradation of POM during melt extrusion," *J Appl Polym Sci*, vol. 115, no. 4, pp. 2394–2401, Feb. **2010**, doi: 10.1002/app.31209.
- [4] X. Liu, Q. Yang, Z. Jiang, D. Feng, and G. Li, "Preparation and properties of fragrant acrylonitrile-butadiene-styrene composites," *Polym Plast Technol Eng*, vol. 48, no. 3, pp. 227–231, Feb. **2009**, doi: 10.1080/03602550802634709.
- [5] B. Briasco, P. Capra, A. Cozzi, B. Mannucci, and P. Perugini, "Packaging evaluation approach to improve cosmetic product safety," *Cosmetics*, vol. 3, no. 3, p. 32, Sep. **2016**, doi: 10.3390/cosmetics3030032.
- [6] R. Arppe and T. J. Sørensen, "Physical unclonable functions generated through chemical methods for anti-counterfeiting," *Nat Rev Chem*, vol. 1, no. 4, p. 0031, Apr. **2017**, doi: 10.1038/s41570-017-0031.
- [7] B. Yoon, J. Lee, I. S. Park, S. Jeon, J. Lee, and J. M. Kim, "Recent functional material based approaches to prevent and detect counterfeiting," *J Mater Chem C Mater*, vol. 1, no. 13, pp. 2388–2403, **2013**, doi: 10.1039/c3tc00818e.
- [8] "Fighting counterfeiting at the nanoscale," *Nat Nanotechnol*, vol. 14, no. 6, pp. 497–497, Jun. **2019**, doi: 10.1038/s41565-019-0484-0.
- [9] A. Abdollahi, H. Roghani-Mamaqani, B. Razavi, and M. Salami-Kalajahi, "Photoluminescent and chromic nanomaterials for anticounterfeiting technologies: recent advances and future challenges," *ACS Nano*, vol. 14, no. 11, pp. 14417–14492, Nov. **2020**, doi: 10.1021/acsnano.0c07289.
- [10] K. Abou-Melha, "Preparation of photoluminescent nanocomposite ink toward dual-mode secure anti-counterfeiting stamps," *Arabian Journal of Chemistry*, vol. 15, no. 2, Feb. **2022**, doi: 10.1016/j.arabjc.2021.103604.
- [11] S. Tang *et al.*, "Nonconventional luminophores: characteristics, advancements and perspectives," *Chem Soc Rev*, vol. 50, no. 22, pp. 12616–12655, **2021**, doi: 10.1039/D0CS01087A.

- [12] W. Zhang Yuan and Y. Zhang, "Nonconventional macromolecular luminogens with aggregation-induced emission characteristics," *J Polym Sci A Polym Chem*, vol. 55, no. 4, pp. 560–574, **2017**, doi: 10.1002/pola.28420.
- [13] K. Bauri, B. Saha, A. Banerjee, and P. De, "Recent advances in the development and applications of nonconventional luminescent polymers," *Polym Chem*, vol. 11, no. 46, pp. 7293–7315, **2020**, doi: 10.1039/d0py01285h.
- [14] R. Wang, W. Yuan, and X. Zhu, "Aggregation-induced emission of non-conjugated poly(amido amine)s: Discovering, luminescent mechanism understanding and bioapplication," *Chin J Polym Sci*, vol. 33, no. 5, pp. 680–687, May **2015**, doi: 10.1007/s10118-015-1635-x.
- [15] R. li Fu, J. hao Chu, H. Jiang, and X. Sun, "Field-induced luminescence quenching in electroluminescent conjugated polymers," *Chinese Physics Letters*, vol. 16, no. 10, pp. 764–766, **1999**, doi: 10.1088/0256-307X/16/10/023.
- [16] P. Wang, C. J. Collison, and L. J. Rothberg, "Origins of aggregation quenching in luminescent phenylenevinylene polymers," *J Photochem Photobiol A Chem*, vol. 144, no. 1, pp. 63–68, Oct. **2001**, doi: 10.1016/S1010-6030(01)00518-4.
- [17] W. Z. Yuan *et al.*, "Changing the behavior of chromophores from aggregation-caused quenching to aggregation-induced emission: development of highly efficient light emitters in the solid state," *Adv Mater*, vol. 22, no. 19, pp. 2159–2163, Mar. **2010**, doi: 10.1002/adma.200904056.
- [18] G. Chen *et al.*, "Conjugation-Induced rigidity in twisting molecules: filling the gap between aggregation-caused quenching and aggregation-induced emission," *Advanced Materials*, vol. 27, no. 30, pp. 4496–4501, Aug. **2015**, doi: 10.1002/adma.201501981.
- [19] J. Luo *et al.*, "Aggregation-induced emission of 1-methyl-1,2,3,4,5-pentaphenylsilole," *Chemical Communications*, vol. 18, pp. 1740–1741, **2001**, doi: 10.1039/b105159h.
- [20] R. li Fu, J. hao Chu, H. Jiang, and X. Sun, "Field-induced luminescence quenching in electroluminescent conjugated polymers," *Chinese Physics Letters*, vol. 16, no. 10, pp. 764–766, **1999**, doi: 10.1088/0256-307X/16/10/023.
- [21] J. Li, J. Wang, H. Li, N. Song, D. Wang, and B. Z. Tang, "Supramolecular materials based on AIE luminogens (AIEgens): construction and applications," *Chem Soc Rev*, vol. 49, no. 4, pp. 1144–1172, **2020**, doi: 10.1039/C9CS00495E.
- [22] Y. Xu *et al.*, "Aggregation-Induced Emission (AIE) in Super-resolution Imaging: Cationic AIE Luminogens (AIEgens) for Tunable Organelle-Specific Imaging and Dynamic Tracking in Nanometer Scale," *ACS Nano*, vol. 16, no. 4, pp. 5932–5942, Apr. **2022**, doi: 10.1021/acsnano.1c11125.

- [23] Q. Zhou *et al.*, “Clustering-Triggered Emission of Nonconjugated Polyacrylonitrile,” *Small*, vol. 12, no. 47, pp. 6586–6592, **2016**, doi: 10.1002/sml.201601545.
- [24] S. Zheng, T. Zhu, Y. Wang, T. Yang, and W. Z. Yuan, “Accessing tunable afterglows from highly twisted nonaromatic organic AIEgens via effective Through-Space Conjugation,” *Angewandte Chemie - International Edition*, vol. 59, no. 25, pp. 10018–10022, **2020**, doi: 10.1002/anie.202000655.
- [25] Y. Gong *et al.*, “Crystallization-induced dual emission from metal- and heavy atom-free aromatic acids and esters,” *Chem Sci*, vol. 6, no. 8, pp. 4438–4444, 2015, doi: 10.1039/c5sc00253b.
- [26] X. Chen, Z. He, F. Kausar, G. Chen, Y. Zhang, and W. Z. Yuan, “Aggregation-Induced dual emission and unusual luminescence beyond excimer emission of poly(ethylene terephthalate),” *Macromolecules*, vol. 51, no. 21, pp. 9035–9042, **2018**, doi: 10.1021/acs.macromol.8b01743.
- [27] A. Bell, C. J. Kibler, and J. G. Smith, “Preparation of elastomeric polymers by employing during the preparation of the polymer an aliphatic sulfur-containing compound,” U.S. Patent No 3,277,060, 4 Oct. **1966**.
- [28] S. R. Turner, “Development of amorphous copolyesters based on 1,4-cyclohexanedimethanol,” *J Polym Sci A Polym Chem*, vol. 42, no. 23, pp. 5847–5852, **2004**, doi: 10.1002/pola.20460.
- [29] S. Fujihara, “Luminescent thin films: fundamental aspects and practical applications,” in *Chemical Solution Deposition of Functional Oxide Thin Films*, Vienna: Springer Vienna, **2013**, pp. 725–745. doi: 10.1007/978-3-211-99311-8\_29.
- [30] H. Águas *et al.*, “Thin film silicon photovoltaic cells on paper for flexible indoor applications,” *Adv Funct Mater*, vol. 25, no. 23, pp. 3592–3598, Jun. **2015**, doi: 10.1002/adfm.201500636.
- [31] D. Pintossi, A. Colombo, M. Levi, C. Dragonetti, S. Turri, and G. Griffini, “UV-curable fluoropolymers crosslinked with functional fluorescent dyes: the way to multifunctional thin-film luminescent solar concentrators,” *J Mater Chem A Mater*, vol. 5, no. 19, pp. 9067–9075, **2017**, doi: 10.1039/C7TA01692A.
- [32] C. Zang, M. Xu, L. Zhang, S. Liu, and W. Xie, “Organic–inorganic hybrid thin film light-emitting devices: interfacial engineering and device physics,” *J Mater Chem C Mater*, vol. 9, no. 5, pp. 1484–1519, **2021**, doi: 10.1039/D0TC05059H.
- [33] A. S. Lemine, J. Bhadra, N. J. Al-Thani, and Z. Ahmad, “Promising transparent and flexible thermoelectric modules based on p-type CuI thin films—A review,” *Energy Reports*, vol. 8, pp. 11607–11637, Nov. **2022**, doi: 10.1016/j.egyr.2022.09.020.



- 
- 
- [34] H. P. Ho, W. W. Wong, and S. Y. Wu, "Multilayer optical storage disk based on the frequency up-conversion effect from rare-earth ions," *Optical Engineering*, vol. 42, no. 8, p. 2349, **2003**, doi: 10.1117/1.1588298.
- [35] A. G. Rodríguez-Hernández, J. A. Muñoz-Tabares, J. C. Aguilar-Guzmán, and R. Vazquez-Duhalt, "A novel and simple method for polyethylene terephthalate (PET) nanoparticle production," *Environ Sci Nano*, vol. 6, no. 7, pp. 2031–2036, **2019**, doi: 10.1039/C9EN00365G.
- [36] D. Bikiaris, "Can nanoparticles really enhance thermal stability of polymers? Part II: An overview on thermal decomposition of polycondensation polymers," *Thermochim Acta*, vol. 523, no. 1–2, pp. 25–45, Aug. **2011**, doi: 10.1016/j.tca.2011.06.012.
- [37] H. Zhang *et al.*, "Clusterization-triggered emission: Uncommon luminescence from common materials," *Materials Today*, vol. 32, no. February, pp. 275–292, **2020**, doi: 10.1016/j.mattod.2019.08.010.
- [38] Z. Zhao, H. Zhang, J. W. Y. Lam, and B. Z. Tang, "Aggregation-Induced Emission: new vistas at the aggregate level," *Angew Chem Int Ed*, vol. 59, no. 25, pp. 9888–9907, **2020**, doi: 10.1002/anie.201916729.
- [39] P. Liao, J. Huang, Y. Yan, and B. Z. Tang, "Clusterization-triggered emission (CTE): one for all, all for one," *Mater Chem Front*, vol. 5, no. 18, pp. 6693–6717, **2021**, doi: 10.1039/D1QM00808K.
- [40] Z. He, C. Ke, and B. Z. Tang, "Journey of aggregation-induced emission research," *ACS Omega*, vol. 3, no. 3, pp. 3267–3277, **2018**, doi: 10.1021/acsomega.8b00062.
- [41] D. P. Chatterjee, M. Pakhira, and A. K. Nandi, "Fluorescence in 'nonfluorescent' polymers," *ACS Omega*, vol. 5, no. 48, pp. 30747–30766, Dec. **2020**, doi: 10.1021/acsomega.0c04700.







## Chapter 5.

A physical unclonable function  
based on recyclable polymer  
nanoparticles for enabling the  
circular economy

Part of the work described in this Chapter has been published in ACS Appl.  
Nano Mater. **2022**, **5**, 10, 13752–13760



All-polymer physical unclonable functions (PUFs) can be made using polyester nanoparticles. PUFs on polyester packaging creating a recyclable, smartphone readable unique identifier on every product. We suggest that the unique ID is used to inform and incentivize recycling as part of the circular economy.



### **Abstract**

The circular economy requires that we know what a product is made of, that we can control that it is not a fake, and that we know how to recycle it. This requires a digital twin of each product, where the information is stored that we can access using a smartphone. Creating digital twins require connecting the physical and digital worlds, which in turn requires that all objects have a unique identifier that is valid in both domains. Realizing the intrinsic potential of creating digital twins of individual products, of linking physical and digital identities requires that the physical identifier is truly unique, and that it cannot be copied. Furthermore, the physical identifier should not interfere with the product lifecycle, in particular recyclability, as this would be a potential blocker in a circular economy. Here, we present a physical identifier based on a physical unclonable function (PUF) made from polymer nanoparticles and imbedded in a polymer laminate, where all components can be made from the same recyclable material. Such as materials commonly used for packaging in the fragrance and cosmetics industry. The development of the PUF system is presented, and each PUF was validated by using a proprietary smartphone application with a QR code as a common pattern defining PUF canvas. The functionality of the PUF was demonstrated across product types as diverse as lateral flow assays and construction materials. We conclude that polymer nanoparticle PUFs are a viable and directly recyclable solution for documenting authenticity and inform recyclability of polymers in the circular economy.



---

---

## Scientific background and state of the art

The approach to providing a digital ID for consumer goods that we present here is equivalent to creating ‘biometrics for things’. A direct link between a digital ID and a secure physical ID allows for an irrefutable link between the physical and digital world, enabling the creation of genuine digital twins for all consumer products. This pairing is presented as part of an integrated solution for object validation, authentication, and identification, where the immediate application lies as a solution to the problem of counterfeit goods [1–4]. Combatting counterfeiting is an old issue [5], but it is increasingly important due to the sheer scale of the problem [6], and the detrimental consequences to general human health and safety [7–11]. But an irrefutable optical authentication system directly available on portable devices allows for much more disruptive solution, from smart contracts bound to the physical object to direct transfer of ownership between consumer wallets [12–15]. Here we propose that secure physical IDs is also critical for realizing a circular economy.

Our proposed solution for a unique physical identifier is to use physical unclonable functions or PUFs [4,16,17]. PUFs are unique physical objects that contain vast amounts of information that can be recorded and compared [18–23]. Examples range from human fingerprints to the scattering of the random surface structure of paper [22,24–34]. While using PUFs is just emerging in optical authentication of goods, their application has been investigated in detail in electronics [19,21,24,35–38]. A solution that is to be implemented as an authentication and identification system for consumer goods requires that each PUF is cheap (far less than 0.10 USD per physical identifier), and if the solution is to be used as a driver of consumer behavior in a circular economy, the PUF must be an integral part of the product packaging to the extent that it is recycled with the product [39]. Plastics are the main material used for containers and packaging because they are economical, functional and lightweight. The most commonly used plastic materials are polyethylene (PE), polypropylene (PP), polystyrene (PS), polyesters (such as PET), polyamides (PA), and polyvinyl chloride (PVC).

The development of recyclable PUFs is a major challenge that can be overcome using advanced multifunctional polymer chemistry supported by nanotechnology [40–42]. A proposal towards a circular plastic economy is a more sustainable chemistry; our suggestion is to use nanotechnology to allow the consumer to perform the verification of originality, traceability, and to know the required manual sorting. With this purpose, nanotechnology might be able to offer a solution in preventing illicit copying of products by providing highly efficient and secure anti-counterfeiting and authentication methods to reach high and efficient security.

In this Chapter, we focus on polyesters used in many fields of industry such as beverage bottles, food packaging, pharmaceutical containers and cosmetic packaging. We present the use of polyester polymer nanoparticles to design novel PUFs based optical identification system aimed to enable the circular economy.

Figure 5.1 shows the functionality enabled by the direct link between the physical product and a digital twin a PUF creates when considering the circular economy. The full carbon cost is imprinted on the digital twin in the production and can be documented with the PUF along the product life cycle all the way to product recycling, where the carbon-ledger is sealed with proper disposal. For the consumer the PUF acts as a contract with the manufacturer, both documenting authenticity and environmental impact of the product. In the potential second life of the product, irrefutable provenance is added to the digital twin as part of the PUF. At end of life, the PUF can be coupled to correct recycling and thus mediate both corporate and individual carbon footprints. Many waste streams are readily sorted by the consumer, plastics in particular on esthetic products are not as readily recognized. As the current linear plastic economy is not sustainable, and even though we are improving [43], the complexity of polymer products hampers further progress [43,44]. One route to a circular plastic economy is new chemistry [45,46], our suggestion is to use nanotechnology to enable and maybe reward consumer to perform the required manual sorting. Here, we propose an ecosystem for the brand and the user in which a PUF enables incentivize the recycling of packaging and at the same

time to guarantee that the product is real. Incentivizing sorting/recycling is known i.e., beverage containers carry a fee that is returned when the container is recycled. We add to the general advantages of PUF marked products, by demonstrating a fully recycle PUFs and suggesting that the PUF is used to incentivize recycling.

The need for individual object authentication in the circular economy, the steps are: 1) the *design* includes PUF placement and required PUF functionality. 2) the *production* incorporates PUF patterns in (parts) of the product and define PUF canvas via printing or product structure, product carbon ledger and product information are burned into the digital twin of each product. 3) Product authenticity, care guides and carbon cost ensure *responsible use*. 4) *Re-use* and secondary use of products are ensured as ownership and carbon ledger can be transferred to other parties via the PUF ID. 5) *Sorting* by the end-user can be incentivized and quality controlled via the PUF on each product and i.e. a PUF on the recycling containers. 6) *Recycling* is readily done with only one material in each recycling stream.

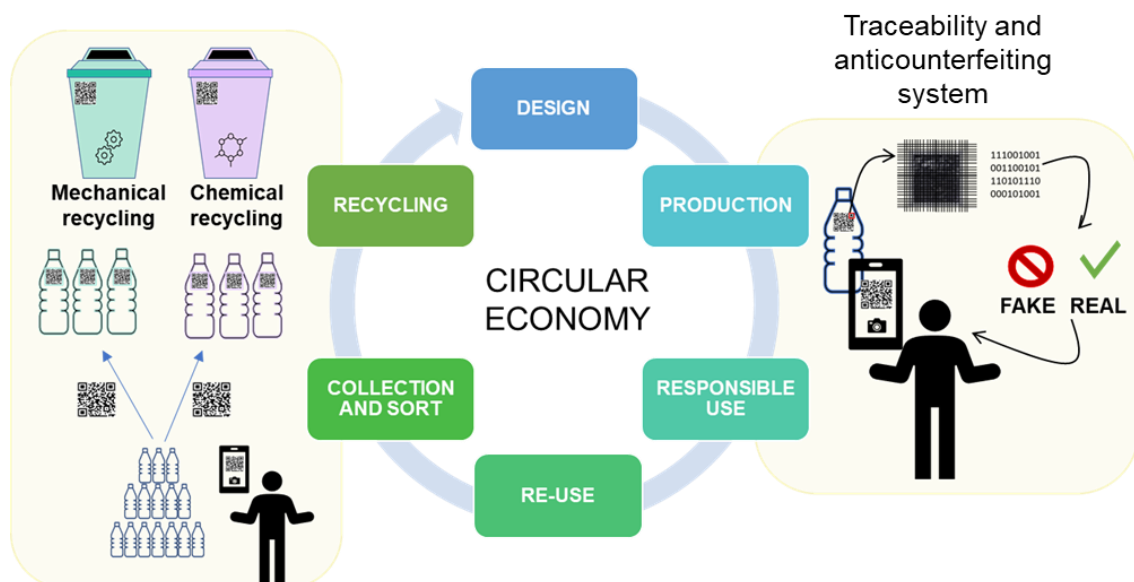


**Figure 5.1.** scheme of the proposed ecosystem for the brand and the user in which an PUF allows to encourage the recycling of packaging while ensuring that the product is real.

## Experimental procedures

The ink used for drop casting or knife coating was created by suspending polyester nanoparticles synthesized according to our previous work [47]. Briefly, the nanoparticles were synthesized by nanoprecipitation (Figure 5.2). First, polyester pellets were dissolved in DMSO (dimethylsulfoxide, Sigma-Aldrich) at high temperature. Then, the solution was added drop wise to a poor solvent under vigorous stirring. The nanoparticles were isolated as the precipitate were collected by filtration, washed with methanol, and dried. The full details are included in the reference 47. Table 5.1 includes the matrix of experimental parameters tested in order to prepare a PUF ink based on the patented nanoparticles. To produce the all-polymer PUFs, two PUF inks were created: the nanoparticles were either suspended at 1 % w/w in EtOH or in PVA/water (10 % w/w Sigma Aldrich).

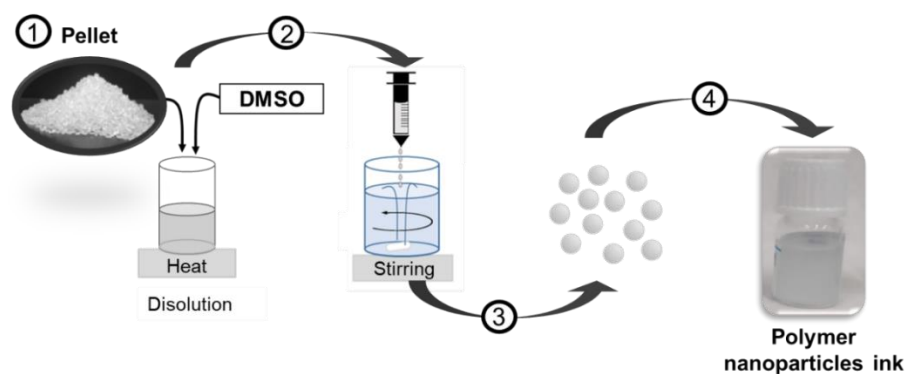


**Figure 5.2.** Synthesis of the polymer nanoparticles

**Table 5.1.** Experimental parameters tested for the creation of a PUF ink

Nanoparticles used	Solvents Tested	Polyester starting Concentration (g·l <sup>-1</sup> )
Nanoparticles formed by precipitates stored in metanol suspension	Methanol	0.1 0.5 1
	Ethanol	
	Petrol ether (60-80)	
	Diethyl eter	
	n-pentane	
	PVA	

QR codes were printed on different substrates such as recycled paper, polyethylene terephthalate (PET), low-density polyethylene (LDPE) using a conventional 1200 dpi laser printer.

Different multilayer laminates of PET (Optically Clear Adhesive Tape LUCIACS<sup>®</sup> CS986 Series), LDPE (ISTAD, resealable bag) and polypropylene (PP, transparent folders for A4) were created by depositing nanoparticles within the layers. The deposition method was either manual drop casting or knife coating. Table 5.2 shows the different combination of samples created by drop casting or knife coating of the two inks on the four substrates.

**Table 5.2.** Combinations of materials used to make all-polymer PUFs by applying a PUF ink on a substrate using different deposition methods

Substrate		PET	LDPE	PP	Paper
PUF ink	Particles	Polyester			
	Carrier liquid	PVA or Ethanol			
Deposition method		Knife coating or Drop Casting			
Contrast type		Scattering			

### Procedure used to fabricate 1<sup>st</sup> generation all-polymer PUFs

Drop casting was performed on different thin films of commercial polymers such as PET, PE and PP. For this purpose, solutions of the polymeric nanoparticles were prepared in ethanol at 0.5 g·l<sup>-1</sup>. The suspensions were homogenized by sonication at room temperature. Afterwards depositing the ethanol drop on the film, the substrate was dried at ambient condition, care was taken to ensure complete evaporation of the solvent. Then, the assembly was carried out by joining both layers of a laminate, with the help of a simple glue. Thus, multilayer films were obtained with the nanoparticles fixed inside.

### **Procedure used to fabricate 2<sup>nd</sup> generation all-polymer PUFs**

For the second generation of PUFs, we decided to increase the concentration of the polymer in the ink to  $1 \text{ g}\cdot\text{l}^{-1}$  in order to obtain better random patterns. Furthermore, the QR codes were printed directly on a PET film, and then the nanoparticles were deposited by drop casting directly on the PUF canvas of the QR code (Figure 5.3). After deposition, the solvent was evaporated, and the sandwich morphology was assembled using glue, thereby creating multilayer films with PUFs on the printed QR code in the form of polymer-embedded nanoparticles.

### **PUF Evaluation**

Each fabricated PUF was first evaluated by visual inspection (apparent randomness) and then by testing using the Pufin ID smartphone application. The app operates on a neural network trained on the QR based PUF we previously reported [17], and in developer mode the app allows for registration of new PUFs as well as validation of existing PUFs. Further, the developer mode reports a match score derived from an undisclosed distance measure in the embedding space scaled by the thresholds set for this particular PUF system. The neural network was trained on this match score is 99+ % for validation of PUF against the same PUF, and the match score is >5 % for validation of a PUF against a different PUF. The app only reports the match score for the five PUF in the embedding space most similar to the PUF being validated. When a PUF falls outside of the five most similar PUFs in a validation, we report a match score of zero.

The commercial version of the application can be downloaded for Android and iOS in the Google Play store and the Apple App store.

### **Results and Discussion**

The design concept for the recyclable optical physical unclonable function is shown in Figure 5.3. There are two significant differences between this design concept and previous reports of optical PUFs [4,17,39]: 1) the PUF is created as an integral part of the polymer laminate, and 2) high contrast reflective or

luminescent materials are not used to create the random pattern. In particular, the latter was initially of great concern.

The steps to follow to create all polymer-PUFs: Printing of the QR codes on the different substrates (1), drop-casting deposition of the nanoparticles (2), evaporation of the solvent (3), adhesion of both layers of laminates. The nanoparticle containing PUF ink is deposited in a polymer laminate on a QR code printed on a separate sheet of paper or the polymer bottom layer of the laminate. The corners of the QR code acts as PUF canvas, defining the regions where the PUFs the random patterns formed by the nanoparticles are read.

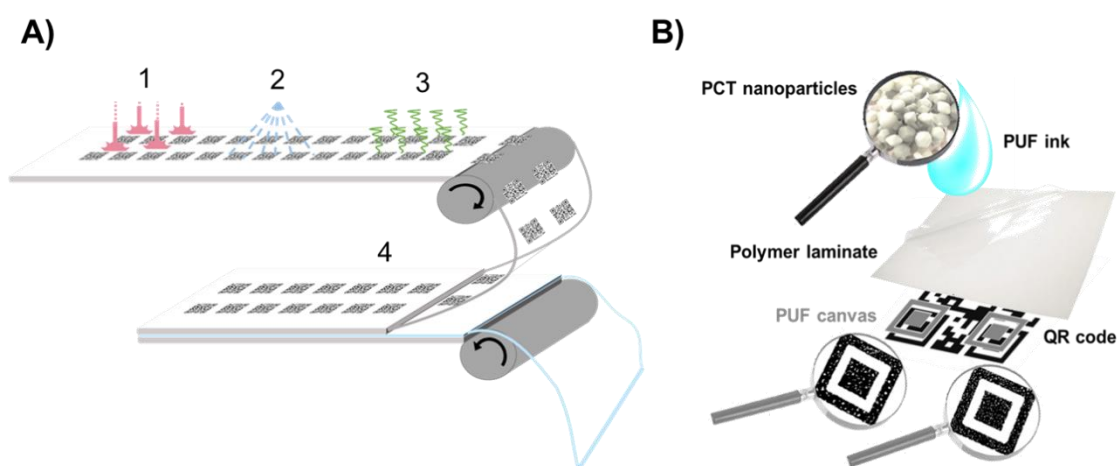


**Figure 5.3.** Design concept for all polymer PUFs. A) The steps to follow to create all polymer-PUFs B) multilayer films with PUFs on the printed QR code

Figure 5.3 shows how the PUF is made, and how the area containing the stochastic pattern is defined as a PUF canvas. Here, the PUF canvas is the corners of a QR code, where the black square is used to define the area of the random pattern that constitute the PUF. A PUF is in principle any random pattern, but to be operational it has to be read and associated to a unique ID. Used in an authentication system each PUF should only associate to one ID, and all others will give rise to a different ID. If a PUF is not registered, no ID will be returned. The algorithm used in this work validates all three corners of the QR code in parallel. In this manner, each QR code contains three independent PUFs.

### **An all-polymer PUF**

The nanoparticles used were synthesized according to a patented procedure [47]. These polyester nanoparticles show a spherical morphology with sizes between 160-200 nm as studied by SEM. However, it was demonstrated by DLS that when in solution, they agglomerate, reaching micrometer sizes, see also Figure 5.4. Thus, visible light scattering can be obtained, yet presumably with an efficiency inferior to common opacifiers like titanium dioxide and zirconia. Therefore, careful control of the agglomerate size must be achieved to the contrast needed to form an all-polymer PUF. By experimenting with various alcohols, pure solvents, mixtures and poly-ols as aqueous solution, and by changing the concentration of nanoparticles the optimal preparations of the PUF ink was discovered. The goal of maximum contrast and sufficient randomness in the patterns formed was achieved by drop casting from a suspension of nanoparticles in pure ethanol. To demonstrate the feasibility of the concept we first created physical unclonable functions by drop casting on PET, LDPE and PP films, which we placed on top of a QR code printed on paper. The first generation PUFs are shown in Figure 5.4. These 1<sup>st</sup> generation all-polymer PUFs did not provide the required contrast in most fabrications, twelve randomly selected PUFs are included in Figure 5.4 to demonstrate this point. By curating the prepared PUFs four were selected based on a selection criterion that was maximum black/white contrast in all three PUF canvas.

All the four PUFs in Figure 5.4 can be registered in the system and validated correctly using the Pufin ID smartphone application. While the true positive match scores lie in the 99 % range, the true negative significantly exceeds the 5 % that is indicative of a good PUF design for this particular neural network. Rather than training a new neural network, which is labor intensive, we decided to investigate and optimize the PUF fabrications.



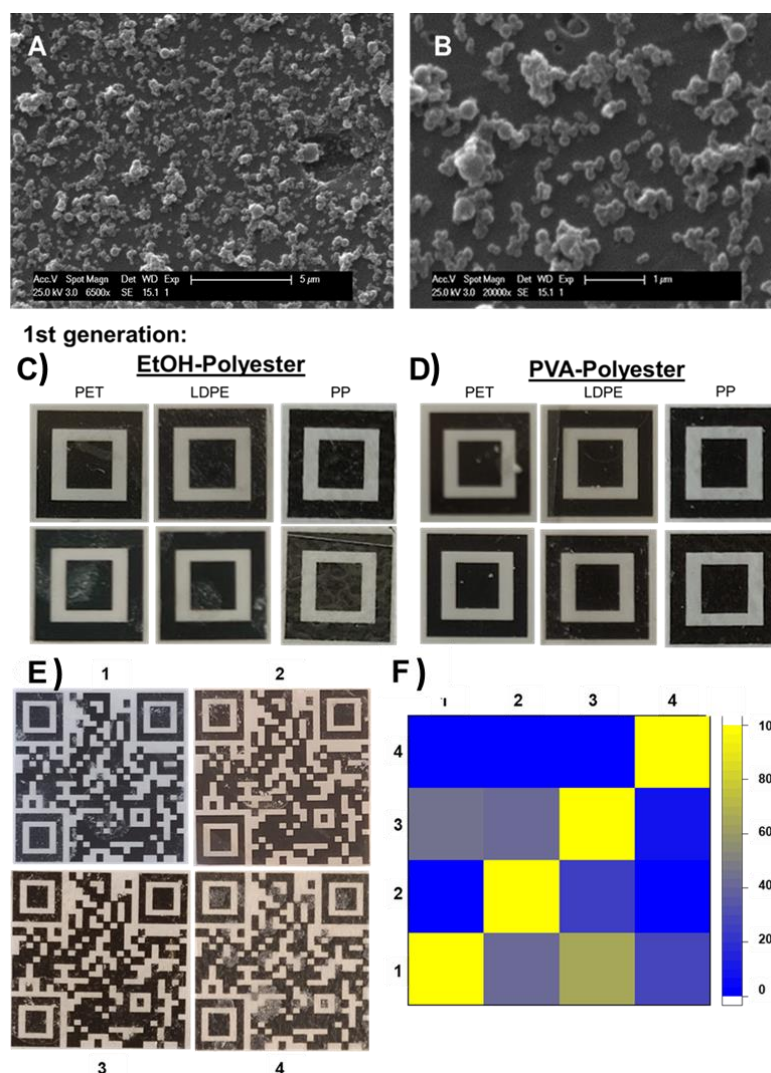


**Figure 5.4.** A) and B) SEM image of 0.5 g·l<sup>-1</sup> PCT/EtOH nanoparticles over PET-film. C) and D) First tests with Ethanol and PVA to create all polymer PUFs. E) The four first-generation PUFs created on QR codes printed on paper. The polymer laminates are made from PET(1), LDPE(2), PP(3,4). F) The match score (0-100 %) matrix using the Pufin ID app to first register and then validate these four PUFs

Figure 5.5 shows 120 2<sup>nd</sup> generation all-polymer PUFs that were created by increasing the nanoparticle concentration and tweaking the drop casting procedure in order to ensure that significant contrast are achieved on all PUF canvas. In this fabrication, the PUF canvas was created by printing the QR code directly on the polymer laminate.

Four of these PUFs were selected and registered in the authentication system. Subsequently, from the remaining 116, 40 QR codes were chosen at random

and validated to ensure that none were recognized as the same as those previously registered in the PUF database. The result of this experiment was evaluated using the match score reported by the Pufin ID app, where the match score of the true positive match and the match score for the closest five true negative matches are reported. All the match scores were recorded and compared. The result of this analysis is shown in Figure 5.6.

Cursory inspection of Figure 5.6 reveals that this second generation of fully recyclable all-polymer PUFs still show inferior performance using the smartphone application, when compared to the titanium dioxide based PUFs [16,17]. It should be noted that the smartphone application runs a neural network trained on PUFs made on paper using highly scattering titanium or zinc oxide. Thus, there are two possible reasons why the all-polymer PUF have inferior performances: 1) the PUFs created may be too similar that is the encoding capacity is too low [16], or 2) the neural network does not pick up the randomness in the all-polymer PUFs as it too different from the samples it was trained on.

### A) Registration

### B) Validation

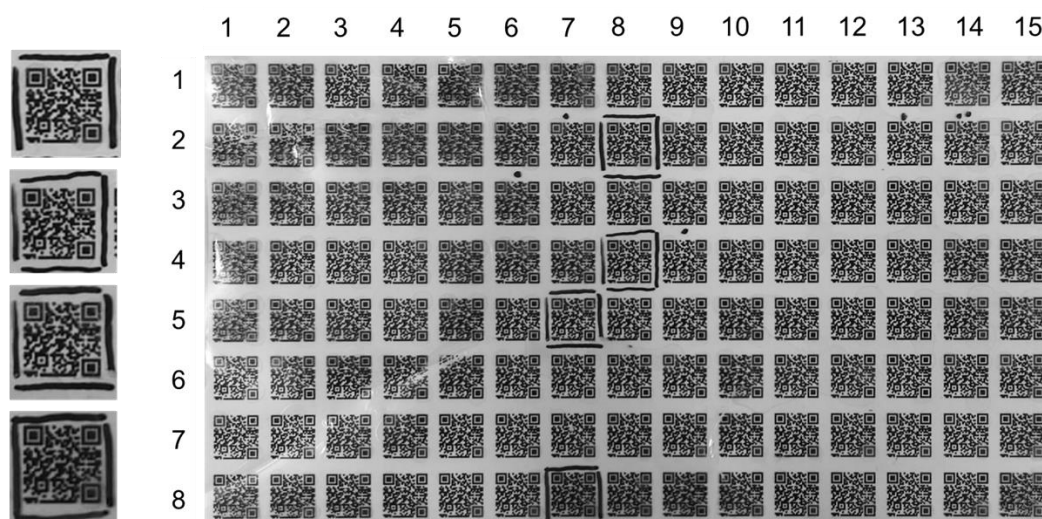


**Figure 5.5.** 120 QR codes printed on PET film (Optically Clear Adhesive Tape LUCIACS® CS986 Series) on which the nanoparticles have been deposited (NP 1 % w/w in EtOH), creating 120 new PUFs. A) 4 QR codes are selected and registered in the authentication system. B) The 4 QR codes are validated against 40 different QR codes

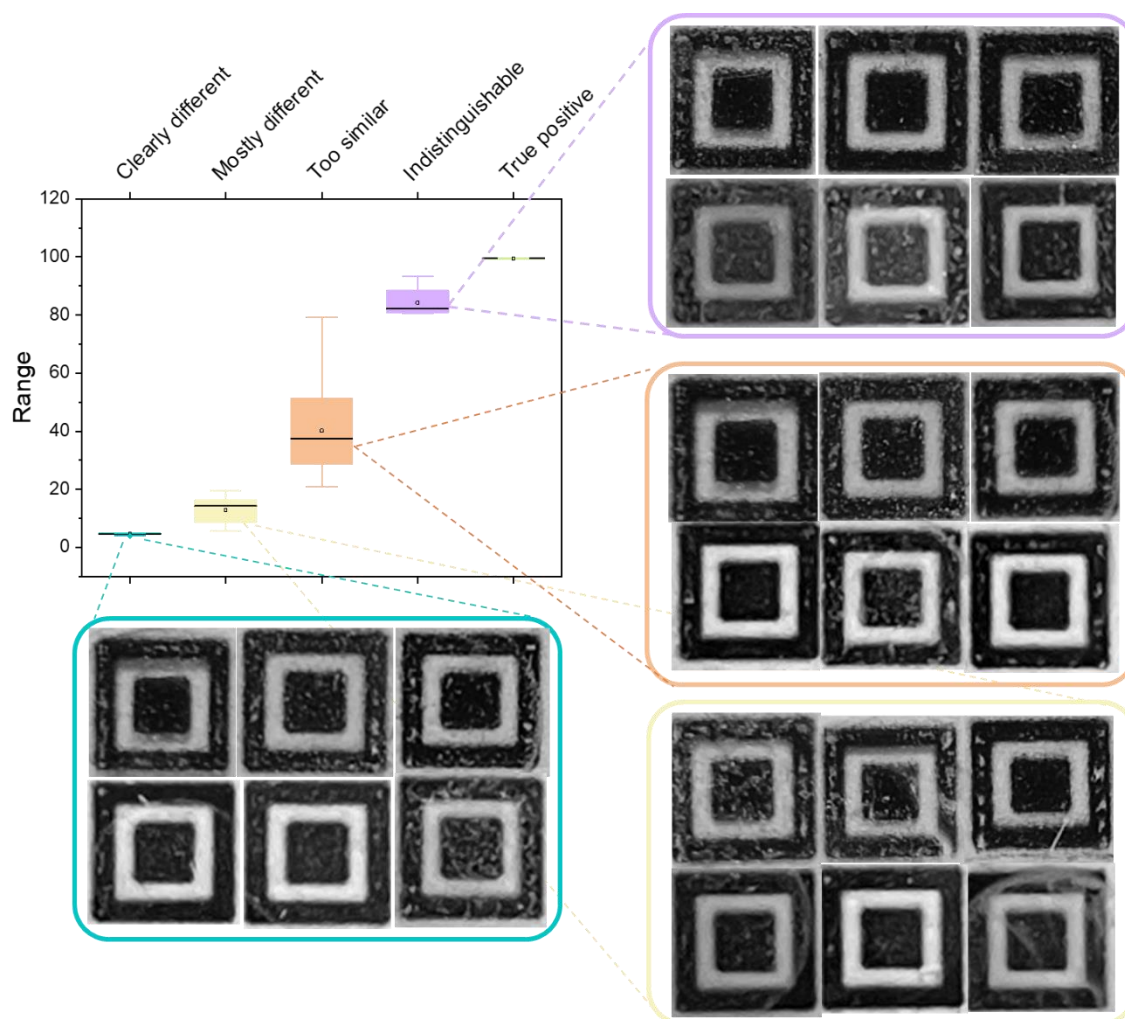


**Figure 5.6.** Box plot showing the result of validating 40 all-polymer PUFs and representative PUF canvas from each group of match scores. The box plot show match scores grouped by criteria taken from the distance measure in the embedding space of the neural network, each is represented by the actual pictures of PUFs giving rise to this match score. Note that the human eye would not assign any two PUFs shown as identical

To visualize the origin of the poor performance we included the images of groups of PUFs that give rise to poor match scores in Figure 5.6. It is worth noting that the neural network only performs a task of comparison similar to what we are capable of using our own eyes. The neural network has to be trained and is parameterized based on this training data. Therefore, it can only operate perfectly on similar samples. The question of poor performance of the all-polymer PUF using the Pufin ID optical authentication system can thus be decided by visual inspection of the PUFs. Considering the PUFs shown in Figure 5.6 they all are clearly random and contain significant amounts of

information [16,17]. Therefore, the failure is not in the PUF. This conclusion is further supported by the fact that the comparison 8/7 and 2/8 by human eye shows that each PUF is clearly unique and readily differentiated from the others. This is the case for all the 120 PUFs produced. There are two routes to a commercial grade optical authentication system from this point: 1) optimizing the means of fabrication to eliminate the 'too similar' and 'indistinguishable' groups in Figure 5.5, or 2) creating 10.000 PUFs and re-training the neural network.

### **Practical application of an all-polymer PUF**

The reason for moving from the oxide containing PUF system to an all-polymer PUF is that it can either be grafted on polymer products or be made an integral part of the product. An example: In the cosmetics and fragrance sectors, there are currently a wide variety of packaging available. The most commonly used containers are of the aromatic polyester family due to their high chemical and mechanical resistance. These materials allow for containers of different shapes and finishes. In order to protect these containers from counterfeiting, and to provide traceability of the product, polymeric nanoparticles of the same polymer as the containers can be used by incorporating them into the container. To do this, the multilayer technique is used. To implement a PUF technology, sheets and nanoparticles of the same polymer are used with an adhesive binder, thus creating a multilayer film. This film is then formed and welded to create the packaging, which is finished by printing and coating. The latter processes are as important as the former, as these will form the canvas of the PUF. The particle in the laminate carries the random pattern, the printed PUF canvas defines where it is read. The advantage of this implementation is that the PUF particles can be all over the packaging, can be used for product traceability, and can even inform about recyclability and thereby facilitate recycling. No additives, fluorescent dyes, fillers, oxides, or any materials that differ from the composition of the packaging have to be used. All is made from just a single polymer.

To illustrate the point, Figure 5.7 shows four examples of PUFs grafted onto polymer products with existing QR codes. Each PUF was registered in the optical authentication system and can be validated with a return of a unique ID

for each product. We consider this proof of concept, and it remains to the manufacturers to decide how to implement this unique ID in their Environmental, Societal, Governance (ESG) structure. We believe it is the only way to keep a true carbon-ledger. The PUF provides a unique ID for the physical product, but all advanced functionality relies on the digital platform that build on the digital ID, which in turn is linked to the physical ID. The investment in this digital platform may very well exceed the investment in production equipment needed to move from the demonstration in Figure 5.7 to mass produced PUFs.

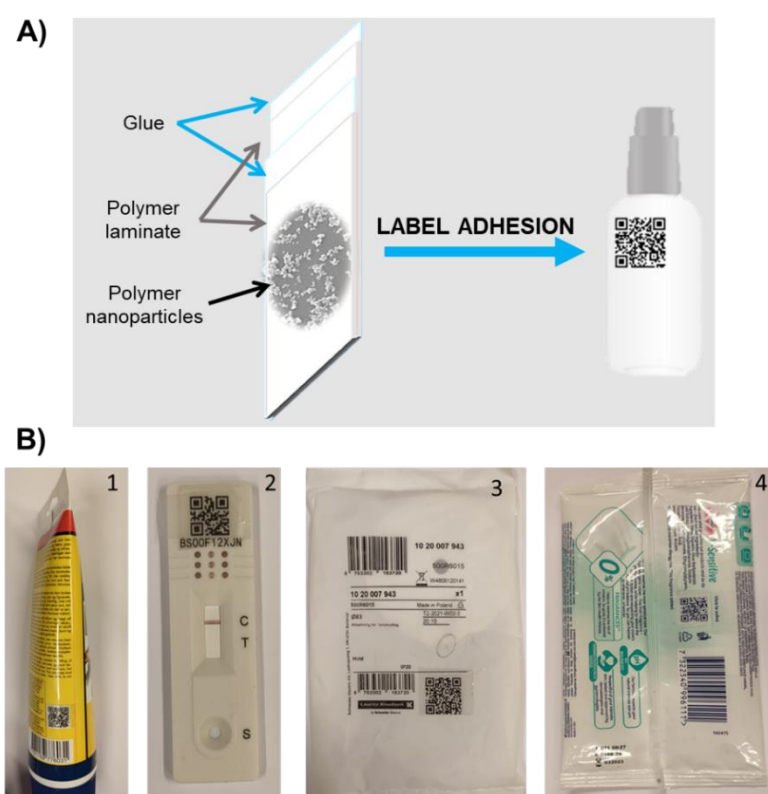


**Figure 5.7.** A) Adhesion of the all-polymer PUF label to commercial packaging already bearing a QR code. B) Commercial products examples made with different polymers (plastics) that have QR codes for proof of concept. DANA LIM filler extra 619 250 ml (1), Antigen test (2), Electronic product packaging from Lauritz Knudsen by Schneider Electrics (3) and Libresse product (4)

## Conclusions

We have shown that by using agglomerated nanoparticles it is possible to create an all-polymer physical unclonable function or PUF. Thus, we can use the same material (polymer) as the packaging to provide security and traceability to different products. In addition, the PUF facilitates the recycling since it provides information on how to recycle it, and the product can be recycled in its entirety, as it does not contain any additives.

We used the polymer nanoparticles to create random patterns on different polymer substrates. QR codes were used to define areas of the random patterns, creating distinct smartphone-readable PUFs. We demonstrated that the all-polymer PUF can be used in a smartphone based authentication system, creating a unique physical ID for products. The true potential of these physical IDs lies in linking them to a digital ID, creating digital twins, which in the right framework removes all barriers for tracking of individual products. While the transition to a circular economy still relies on human behavior, it can be enabled through personal and corporate carbon ledgers documented by PUFs.

As a transformative technology, the ability to link physical product to digital twins requires digital maturity of the producing corporation, and the actual ability to produce the PUF enabled physical product. We all have smartphones, so from the end user perspective we are ready. The natural next steps in commercializing PUF technology lies in integration in the industrial supply chain. Taking producers of products like perfume and cosmetics as an example. Step 1 is that PUF nanoparticles must be integrated into raw materials used to form the containers. Upon quality control using vision systems (Step 2), the material is formed into containers. These are coated, printing added to define the PUF canvas (Step 3), and the container is finished. The AI must be re-trained on the specific PUF design (Step 4). At the perfume and cosmetics supplier, the PUF on the container is registered using a dedicated vision system prior to filling (Step 5), and after filling the PUF is activated using a second vision system (Step 6) and a dedicated local server (Step 7) interfaced with cloud based software (Step 8). The activation of the PUF creates a digital twin of the product, and the physical product can now be authenticated. A

commercial PUF systems will require significant engineering and software development, but no further research. Using the PUF based digital twin as outlined here, requires further development of carbon ledgers, and enterprise software solutions for recycling carbon accounting.

## References

- [1] P. Aldhous, "Murder by medicine," *Nature*, vol. 434, no. 7030, pp. 132–134, Mar. **2005**, doi: 10.1038/434132a.
- [2] J. D. R. Buchanan *et al.*, "'Fingerprinting' documents and packaging," *Nature*, vol. 436, no. 7050, pp. 475–475, Jul. **2005**, doi: 10.1038/436475a.
- [3] C. Sheridan, "Bad medicine," *Nat Biotechnol*, vol. 25, no. 7, pp. 707–709, Jul. **2007**, doi: 10.1038/nbt0707-707.
- [4] R. Arppe and T. J. Sørensen, "Physical unclonable functions generated through chemical methods for anti-counterfeiting," *Nat Rev Chem*, vol. 1, no. 4, p. 0031, Apr. **2017**, doi: 10.1038/s41570-017-0031.
- [5] P. N. Newton, M. D. Green, F. M. Fernández, N. P. Day, and N. J. White, "Counterfeit anti-infective drugs," *Lancet Infect Dis*, vol. 6, no. 9, pp. 602–613, Sep. 2006, doi: 10.1016/S1473-3099(06)70581-3.
- [6] J. R. Yuva, "Fake Goods Represent 3.3 Percent of Global Trade," *Supply and Demand Chain Executive*, **2019**. <https://www.sdexec.com/riskcompliance/news/21060613/fake-goods-represent-33-percent-of-global-trade#platformComments> (accessed Oct. 19, 2022).
- [7] S. Boseley, "WHO warns of fake cancer drug made from paracetamol," *The Guardian*, **2019**. <https://www.theguardian.com/society/2019/feb/12/fake-cancer-drug-made-from-paracetamol-world-health-organization> (accessed Oct. 19, 2022).
- [8] I. Sample, "Fake drugs kill more than 250,000 children a year, doctors warn," *The Guardian*, **2019**. [https://www.theguardian.com/science/2019/mar/11/fake-drugs-kill-more-than-250000-children-a-year-doctors-warn?CMP=share\\_btn\\_link](https://www.theguardian.com/science/2019/mar/11/fake-drugs-kill-more-than-250000-children-a-year-doctors-warn?CMP=share_btn_link) (accessed Oct. 19, 2022).
- [9] M. Andrews, J. E. Jones, L. P. Harding, and S. J. A. Pope, "Luminescent probes based on water-soluble, dual-emissive lanthanide complexes: metal ion-induced modulation of near-IR emission," *Chem. Commun.*, vol. 47, no. 1, pp. 206–208, **2011**, doi: 10.1039/C0CC00210K.
- [10] FDA, "U.S. Department of Health and Human Services," **2016**.
- [11] G. M. L. Nayyar *et al.*, "Falsified and substandard drugs: stopping the pandemic," *Am J Trop Med Hyg*, vol. 100, no. 5, pp. 1058–1065, May **2019**, doi: 10.4269/ajtmh.18-0981.
- [12] D. Macrinici, C. Cartofeanu, and S. Gao, "Smart contract applications within blockchain technology: A systematic mapping study," *Telematics and*



---

---

*Informatics*, vol. 35, no. 8, pp. 2337–2354, Dec. **2018**, doi: 10.1016/j.tele.2018.10.004.

[13] W. Zou *et al.*, “Smart contract development: challenges and opportunities,” *Transactions on Software Engineering*, vol. 47, no. 10, pp. 2084–2106, Oct. **2021**, doi: 10.1109/TSE.2019.2942301.

[14] B. K. Mohanta, S. S. Panda, and D. Jena, “an overview of smart contract and use cases in blockchain technology,” in *2018 9th International Conference on Computing, Communication and Networking Technologies (ICCCNT)*, Jul. **2018**, pp. 1–4. doi: 10.1109/ICCCNT.2018.8494045.

[15] M. W. Karim, A. Haque, M. A. Ulfy, M. A. Hossain, and M. Z. Anis, “Factors influencing the use of E-wallet as a payment method among Malaysian young adults,” *Int J Bus Manag*, vol. 3, pp. 1–12, **2020**. Doi: 10.37227/jibm-2020-2-21

[16] M. R. Carro-Temboury, R. Arppe, T. Vosch, and T. J. Sørensen, “An optical authentication system based on imaging of excitation-selected lanthanide luminescence,” *Sci Adv*, vol. 4, no. 1, Jan. **2018**, doi: 10.1126/sciadv.1701384.

[17] R. Arppe-Tabbara, M. Tabbara, and T. J. Sørensen, “Versatile and validated optical authentication system based on physical unclonable functions,” *ACS Appl Mater Interfaces*, vol. 11, no. 6, pp. 6475–6482, Feb. **2019**, doi: 10.1021/acsami.8b17403.

[18] R. Pappu, B. Recht, J. Taylor, and N. Gershenfeld, “Physical one-way functions,” *Science (1979)*, vol. 297, no. 5589, pp. 2026–2030, Sep. **2002**, doi: 10.1126/science.1074376.

[19] T. McGrath, I. E. Bagci, Z. M. Wang, U. Roedig, and R. J. Young, “A PUF taxonomy,” *Appl Phys Rev*, vol. 6, no. 1, p. 011303, Mar. **2019**, doi: 10.1063/1.5079407.

[20] R. Maes, “Physically unclonable functions: properties,” in *Physically Unclonable Functions*, Berlin, Heidelberg: Springer Berlin Heidelberg, **2013**, pp. 49–80. doi: 10.1007/978-3-642-41395-7\_3.

[21] C. Herder, M.-D. Yu, F. Koushanfar, and S. Devadas, “Physical unclonable functions and applications: a tutorial,” *Proceedings of the IEEE*, vol. 102, no. 8, pp. 1126–1141, Aug. **2014**, doi: 10.1109/JPROC.2014.2320516.

[22] Y. Geng, J. Noh, I. Drevensek-Olenik, R. Rupp, G. Lenzini, and J. P. F. Lagerwall, “High-fidelity spherical cholesteric liquid crystal Bragg reflectors generating unclonable patterns for secure authentication,” *Sci Rep*, vol. 6, no. 1, p. 26840, Jul. **2016**, doi: 10.1038/srep26840.

- [23] R. Horstmeyer, B. Judkewitz, I. M. Vellekoop, S. Assaworrorarit, and C. Yang, "Physical key-protected one-time pad," *Sci Rep*, vol. 3, no. 1, p. 3543, Dec. **2013**, doi: 10.1038/srep03543.
- [24] M. Lehtonen, N. Oertel, and H. Vogt, "Features, identity, tracing, and cryptography in product authentication," *IEEE International Technology Management Conference (ICE)* (pp. 1-8), **2007**.
- [25] D. Mehta, L. Zhou, K. Aono, and S. Chakrabartty, "Self-powered sensing and time-stamping of tampering events," in *2018 IEEE 61st International Midwest Symposium on Circuits and Systems (MWSCAS)*, Aug. **2018**, pp. 968–971. doi: 10.1109/MWSCAS.2018.8623916.
- [26] R. Cowburn, "Laser surface authentication – reading Nature's own security code," *Contemp Phys*, vol. 49, no. 5, pp. 331–342, Sep. **2008**, doi: 10.1080/00107510802583948.
- [27] T. Takahashi, Y. Kudo, and R. Ishiyama, "Mass-produced parts traceability system based on automated scanning of 'Fingerprint of Things,'" in *2017 Fifteenth IAPR International Conference on Machine Vision Applications (MVA)*, May **2017**, pp. 202–206. doi: 10.23919/MVA.2017.7986836.
- [28] T. Haist and H. J. Tiziani, "Optical detection of random features for high security applications," *Opt Commun*, vol. 147, no. 1–3, pp. 173–179, Feb. **1998**, doi: 10.1016/S0030-4018(97)00546-4.
- [29] B. Wigger, T. Meissner, A. Förste, V. Jetter, and A. Zimmermann, "Using unique surface patterns of injection moulded plastic components as an image based Physical Unclonable Function for secure component identification," *Sci Rep*, vol. 8, no. 1, p. 4738, Dec. **2018**, doi: 10.1038/s41598-018-22876-8.
- [30] E. Burzurí, D. Granados, and E. M. Pérez, "Physically unclonable functions based on single-walled carbon nanotubes: a scalable and inexpensive method toward unique identifiers," *ACS Appl Nano Mater*, vol. 2, no. 4, pp. 1796–1801, Apr. **2019**, doi: 10.1021/acsanm.9b00322.
- [31] B.-H. Wu, C. Zhang, N. Zheng, L.-W. Wu, Z.-K. Xu, and L.-S. Wan, "Grain boundaries of self-assembled porous polymer films for unclonable anti-counterfeiting," *ACS Appl Polym Mater*, vol. 1, no. 1, pp. 47–53, Jan. **2019**, doi: 10.1021/acsapm.8b00031.
- [32] Z. Hu *et al.*, "Physically unclonable cryptographic primitives using self-assembled carbon nanotubes," *Nat Nanotechnol*, vol. 11, no. 6, pp. 559–565, Jun. **2016**, doi: 10.1038/nnano.2016.1.
- [33] Y. Liu *et al.*, "fabrication of anticounterfeiting nanocomposites with multiple security features via integration of a photoresponsive polymer and upconverting nanoparticles," *Adv Funct Mater*, vol. 31, no. 37, p. 2103908, Sep. **2021**, doi: 10.1002/adfm.202103908.

- 
- 
- [34] W. Ren, G. Lin, C. Clarke, J. Zhou, and D. Jin, "Optical nanomaterials and enabling technologies for high-security-level anticounterfeiting," *Adv Mater*, vol. 32, no. 18, p. 1901430, May **2020**, doi: 10.1002/adma.201901430.
- [35] G. E. Suh and S. Devadas, *Physical unclonable functions for device authentication and secret key generation. 44th ACM/IEEE Design Automation Conference* (pp. 9-14). **2007**.
- [36] Y. Liu *et al.*, "Inkjet-printed unclonable quantum dot fluorescent anti-counterfeiting labels with artificial intelligence authentication," *Nat Commun*, vol. 10, no. 1, p. 2409, Dec. **2019**, doi: 10.1038/s41467-019-10406-7.
- [37] Z. Gao, Y. Han, and F. Wang, "Cooperative supramolecular polymers with anthracene–endoperoxide photo-switching for fluorescent anti-counterfeiting," *Nat Commun*, vol. 9, no. 1, p. 3977, Dec. **2018**, doi: 10.1038/s41467-018-06392-x.
- [38] J. Yuan, P. R. Christensen, and M. O. Wolf, "Dynamic anti-counterfeiting security features using multicolor dianthryl sulfoxides," *Chem Sci*, vol. 10, no. 43, pp. 10113–10121, **2019**, doi: 10.1039/C9SC03948A.
- [39] L. Tarjan, I. Šenk, S. Tegeltija, S. Stankovski, and G. Ostojic, "A readability analysis for QR code application in a traceability system," *Comput Electron Agric*, vol. 109, pp. 1–11, Nov. **2014**, doi: 10.1016/j.compag.2014.08.015.
- [40] H. Liu, D. Xie, H. Shen, F. Li, and J. Chen, "Functional micro–nano structure with variable colour: applications for anti-counterfeiting," *Advances in Polymer Technology*, vol. 2019, pp. 1–26, Dec. **2019**, doi: 10.1155/2019/6519018.
- [41] N. Torun, I. Torun, M. Sakir, M. Kalay, and M. S. Onses, "Physically unclonable surfaces via dewetting of polymer thin films," *ACS Appl Mater Interfaces*, vol. 13, no. 9, pp. 11247–11259, Mar. **2021**, doi: 10.1021/acsami.0c16846.
- [42] C. Adhikari, "Polymer nanoparticles-preparations, applications and future insights: a concise review," *Polym-Plast Tech Mat*, pp. 1–29, Jul. **2021**, doi: 10.1080/25740881.2021.1939715.
- [43] K. Ragaert, L. Delva, and K. van Geem, "Mechanical and chemical recycling of solid plastic waste," *Waste Management*, vol. 69, pp. 24–58, Nov. **2017**, doi: 10.1016/j.wasman.2017.07.044.
- [44] Z. O. G. Schyns and M. P. Shaver, "Mechanical recycling of packaging plastics: a review," *Macromol Rapid Commun*, vol. 42, no. 3, p. 2000415, Feb. **2021**, doi: 10.1002/marc.202000415.
- 
-

[45] G. W. Coates and Y. D. Y. L. Getzler, “Chemical recycling to monomer for an ideal, circular polymer economy,” *Nat Rev Mater*, vol. 5, no. 7, pp. 501–516, Jul. **2020**, doi: 10.1038/s41578-020-0190-4.

[46] T. Thiounn and R. C. Smith, “Advances and approaches for chemical recycling of plastic waste,” *Journal of Polymer Science*, vol. 58, no. 10, pp. 1347–1364, May **2020**, doi: 10.1002/pol.20190261.

[47] A. Fernández-Benito, M. Hoyos, M. Lopez-Manchado, R. Verdejo, D. Andrinal-Lopez, and R. Cisneros de los Arcos, “Agregados fluorescentes de poli(tereftalato de ciclohexilendimetileno), procedimiento de obtención y uso como etiqueta físicamente no clonable para identificar y/o trazar envases para productos cosméticos y/o perfumes,” ES1641.1644, **2021**





## **Conclusions of Section II**





After the studies shown in this Section, it can be concluded that most of the company's main objectives have been achieved by complying with requirements such as:

1. The optimum material has been studied for the packaging required for the company. Tests have been carried out under standard to certify the research.
2. Through polymer nanotechnology a novel anti-counterfeiting system has been designed without using semiconducting polymers or organic dyes. A process for the preparation of photoluminescent nanoparticle aggregates has been protected.
3. The first proof of concept has been performed by creating physical unclonable functions with the use of the synthesized polymer nanoparticles, demonstrating its potential use as real security system.



## **Chapter 6.**

### **Summary and final remarks**



---

---

## **General conclusions and future work**

### **General conclusions**

In this Ph.D. Thesis, polymeric nanoparticles of diverse nature combining different properties depending on the final application for which they have been designed are developed. The main results have provided an excellent understanding of the impact of the particle size and chemical composition on the functional properties. The use of nanoscience and nanotechnology was applied throughout the research activities of this Ph.D. Thesis in order to achieve the desired objectives. It was possible to control their morphology, particle size from the synthetic strategy used to make them. The possibility of designing functional polymeric nanoparticles will contribute to different sectors such as the sustainable energy storage field and the circular economy of plastics manufacture, and in the protection and traceability of packaging.

### **Outlook and future work**

This Ph.D. Thesis offers a fundamental vision of the potential impact of nanotechnology in our society. The new results presented here may be the beginning of new lines of research opening the way for nanoparticles in the development of new polymer electrolytes and in the wide industry of anti-counterfeiting. However, this is only a small part because many questions remain to be answered and many challenges to be solved.

In Chapter 2, the effect of different polypyrrole chemistries in the design of redox-active polymeric nanoparticles and their impact on the new properties of energy storage and CO<sub>2</sub> capture might be tackled.

In Chapter 3, the new block copolymer can also serve as a material's platform for different applications. Although the results have not been presented here, we have been studying the design of an electrolyte with the incorporation of the viologen compound within the macromolecular structure of the synthesized

block copolymer. It would be important to continue with this line of research and thus create a redox flow system with electroactive nanoparticles in aqueous media and with the use of a porous membrane by using different redox chemistries anchored to the copolymer backbone.

As for Chapter 4, it would be necessary to focus on better design and control of the nanoparticles by tuning their luminescence as a function of aggregates and nanoparticle sizes in order to try to delimit in which region of the spectrum it emits. So far, we have a multicolor response, ideally just by modifying the aggregate size we can modify the range of emission. Another line that is open is to synthesize from scratch this type of block copolymers by condensation trying to incorporate a chromophore within the chain and subsequently form the polymeric nanoparticles and use it as has been done with those presented in this Ph.D. Thesis. This study has been carried out in parallel during the development of the Thesis, but the results are not shown here. In addition, it would be interesting to study other commercial polymers used in packaging to synthesize new polymeric nanoparticles with the same methodology and study their photophysical properties and their possible use as anti-counterfeiting systems.

Search for new detection methodologies and collaborate with companies on recyclability area. Give them options such as the one proposed here for better recycling and safety, creating new ecosystems between brands and users.

To contact companies interested in the patent of the luminescent aggregates to sell them and implement them in final products. In fact, this finding is of great interest in the industrial sector.







# Appendix



---

---

## Publications related to this Ph.D. Thesis

1. **Fernández-Benito, A.**, Rivera-Gálvez, F.J., Cisneros-Ruiz, P., Sanz-Horta, R., Jasso-Gastinel, C.F., López-Manchado, M.A., Carretero-González, J. Novel ferrocene-containing amphiphilic block copolymer nanoparticles as high-capacity charge carriers in aqueous redox flow systems. **Materials Today Chemistry**, 2023, 27, 101271 (**Impact factor: 7.613, Q1**)
2. **Fernández-Benito, A.**, Hoyos, M., López-Manchado, M.A., Sørensen, T.J. A physical unclonable function based on recyclable polymer nanoparticles to enable the circular economy. **ACS Applied Nano Materials**, 2022, 5(10), 13752-13760 (**Impact factor: 6.140, Q2**)
3. **Fernández-Benito, A.**, Rodríguez, G., Arenas-Esteban, D., Sjödin, M., Navalpotro, P., Rodríguez-Caballero, D., Ávila-Brandé, D., López-Manchado, M.A., Carretero-González, J. Multifunctional metal-free rechargeable polymer composite nanoparticles boosted by CO<sub>2</sub>. **Materials Today Sustainability**, 2020, 10, 100048. (**Impact factor: 7.244, Q1**)

## Patents related to this Ph.D. Thesis

1. Carretero-González, J., **Fernández-Benito, A.**, Rodríguez-Caballero, D., Rodríguez, G., & López-Manchado, M.Á. *Electrochemically active nanoparticulate polymer material*. WO2021037441 A1 (**2021**)
2. **Fernández-Benito, A.**, López-Manchado, M.Á., Verdejo, R., Hoyos, M., Andrinal, D., & Cisneros, R. *Agregados fluorescentes de poli(tereftalato de ciclohexilendimetileno), procedimiento de obtención y uso como etiqueta físicamente no clonable para identificar y/o trazar envases para productos cosméticos y/o perfumes*. PCT/ES2022/070023 (**2022**)

---

---

## Dissemination article

1. Fernández-Benito, A. El Desafío Energético: Baterías Poliméricas de Flujo Redox. Revista de Plásticos Modernos. **2019**, **117** (745), 21-25

## Oral contributions

1. Electroactive nanoparticulate polymer composite. 4<sup>th</sup> Young Polymer Scientists Seminar (SEJIPOL2019). Madrid, Spain. October **2019**
2. Synthesis of novel electroactive copolymers for sustainable energy storage. Polímeros para el siglo XXI, X congreso de jóvenes investigadores en polímeros (JIP19). Burgos, Spain. May **2019**

## Dissemination activities

1. Interview, “Día internacional de la mujer y la niña en la ciencia” Amparo Fernández Benito. 11F. February **2020**.  
(<https://www.youtube.com/watch?v=QdDiG2j1mJc&t=2s>)
2. Araujo-Morera, J.; Utrera-Barrios, S.; Peñas-Caballero, M.; **Fernández-Benito, A.** La metamorfosis del neumático. PHOTOPOL **2019**. Categoría: Sostenibilidad, valorización y reciclado de polímeros. **(Second prize)**
3. I Edición del concurso tu tesis doctoral en un hilo de Twitter: #HiloTesis. April **2021**.  
(<https://twitter.com/Lamparet/status/1385626260852903939>)
4. 4º ESO + Empresa. May **2019**

---

---

## Direction of internships and Master's Thesis

1. Co-direction of the Master's Thesis, in the Master of High Specialization in Plastics and Rubber. Leandro Conti Persino. Menendez Pelayo University. **2020**.
2. Co-direction of external curricular internships. Marta Vizuete Vidal, Degree in Chemistry. Complutense University of Madrid (UCM). **2021**.

## Visits and research stays

During the course of the Ph.D. Thesis, some measurements have been carried out at other research centers.

1. Centro Nacional de Biotecnología (CNB): The cryoEM measurements were carried out with the help of Rocio Arranz. I learned how samples are prepared for cryoEM measurements and became familiar with the equipment and data processing.  
(<https://www.cnb.csic.es/index.php/es/investigacion/servicios-cientificos/microscopia-crioelectronica>).
2. Instituto de Investigaciones Biomédicas "Alberto Sols" (CSIC-UAM): I became familiar with the confocal fluorescence microscopy equipment and learned how to prepare the samples for later measurement. All this with the assistance of Mónica Martín and Lucía Guerrero.  
<https://www.iib.uam.es/portal/web/microscopia/funciones>
3. I have also done a research stay at the University of Copenhagen (23/08/21 to 01/12/21) in Thomas Just Sorensen Group.  
(<https://sites.google.com/view/tjsgroup/thomas-just-s%C3%B8rensen>).

Where a system for optical authentication of polymeric nanoparticles based on their own materials has been developed. The aim of the visit was to develop a fully recyclable optical authentication system combining

---

---

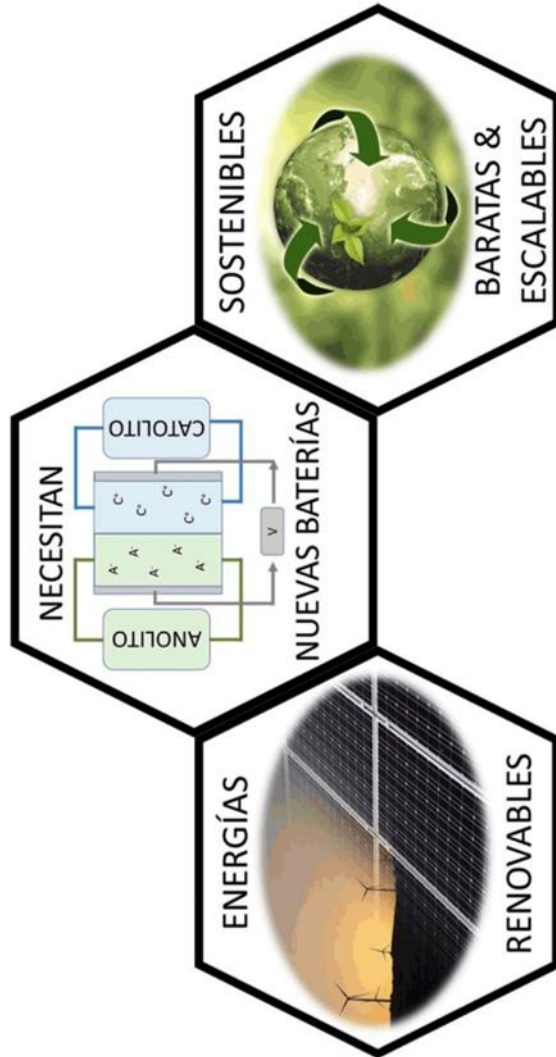
the knowledge of non-clonable physical function of Prof. Thomas Just Sørensen and my experience in polymeric materials.

During the stay, work was done with various forms of luminescence microscopy and spectroscopy. In addition, I attended some advanced photophysics classes.

# El Desafío Energético: Baterías Poliméricas de Flujo de Redox

**Autora:** Amparo Fernández Benito

Instituto de Ciencia y Tecnología de Polímeros, ICTP-CSIC  
C/ Juan de la Cierva, nº 3, 28006, Madrid  
amparo\_fb@ictp.csic.es



## Resumen

El almacenamiento de energía eléctrica, proveniente de energías renovables intermitentes ha experimentado un notable crecimiento en los últimos años. Las energías renovables presentan grandes fluctuaciones en la producción de energía, siendo este su principal problema. Por eso surge la necesidad de crear nuevos sistemas de almacenamiento de energía capaces de acumular los excedentes de energía que no puedan ser adsorbidos por la red, y posteriormente utilizarlos a demanda. Se requiere, por tanto, de sistemas de almacenamiento de bajo coste, sostenible y escalable. En este artículo se describen los tipos

de baterías de flujo redox (BFR) que existen actualmente y la sustitución de los metales convencionales como material activo-redox, por materiales orgánicos/poliméricos. Las características que poseen los materiales orgánicos como su gran versatilidad estructural, propiedades modificables, ligereza, bajo coste y respeto con el medio ambiente, los hacen idóneos para aplicaciones de almacenamiento de energía estacionaria; proporcionando una alternativa prometedora para las futuras baterías de flujo redox.

**Palabras clave:** energías renovables, baterías de flujo redox, polímeros, almacenamiento electroquímico de energía.

## Abstract

The storage of electrical energy from intermittent renewable sources has experienced a remarkable growth in recent years. The main problem is that renewable sources such as wind and sun present great fluctuations in the production of energy. For this reason, the need arises to create new energy storage systems capable of accumulating the excess of energy that cannot be absorbed by the grid, and then use them on demand. Low-cost, sustainable and scalable storage systems are therefore required. This article describes the types of redox flow batteries that currently exist and the substitution of conventional

metals as active-redox material by organic/polymer materials. The characteristics of organic materials such as their great structural versatility, tunable properties, lightweight, low cost and environmentally friendly, make them suitable for stationary energy storage, providing a promising alternative for future batteries redox flow systems.

**Key words:** renewable energies, redox flow batteries, polymers, electrochemical energy storage.



Índice

Noticias



Contents lists available at ScienceDirect

## Materials Today Sustainability

journal homepage: <https://www.journals.elsevier.com/materials-today-sustainability>

## Multifunctional metal-free rechargeable polymer composite nanoparticles boosted by CO<sub>2</sub>



A. Fernández-Benito<sup>a</sup>, G. Rodríguez<sup>a</sup>, D. Arenas-Esteban<sup>b</sup>, M. Sjödin<sup>c</sup>, P. Navalpotro<sup>a</sup>,  
D. Rodríguez-Caballero<sup>a</sup>, D. Ávila-Brande<sup>b</sup>, M.Á. López-Manchado<sup>a</sup>,  
J. Carretero-González<sup>a,\*</sup>

<sup>a</sup> Polymer Nanomaterials and Biomaterials Department, Institute of Polymer Science and Technology (ICTP-CSIC), Madrid, Spain

<sup>b</sup> Department of Inorganic Chemistry, Faculty of Chemistry, Universidad Complutense de Madrid, Madrid, Spain

<sup>c</sup> Department of Engineering Sciences, Uppsala University, Uppsala, Sweden

## ARTICLE INFO

## Article history:

Received 19 March 2020

Received in revised form

28 May 2020

Accepted 30 June 2020

Available online 8 July 2020

## Keywords:

Multifunctional electrolyte

Energy storage

CO<sub>2</sub> utilization

Polymer nanomaterials

Flow batteries

## ABSTRACT

Herein, we present a multigram scale-up route for the preparation of novel polymer composite nanoparticles as potential multifunctional rechargeable material for future, sustainable batteries. The nanoparticles (20 nm) comprise three innocuous yet functional interpenetrated macromolecular networks: polypyrrole, methylcellulose, and lignin. They are uniquely assembled in strands or chains (~200 nm) such as *necklace beads* and show long-term stability as water dispersion. We find that an aqueous suspension of this hierarchical nanomaterial shows two sets of reversible redox peaks, separated by ~600 mV, originating from the catechol moieties present in the lignin biopolymer. Remarkably, the addition of carbon dioxide increased the capacity of one of the redox processes by 500%. Importantly, the three redox stages occur in the presence of the same nanostructured polymer so being a potentially bifunctional material to be used in advanced electrochemical systems. The new properties are attributed to an intrinsic chemical and electronic coupling at the nanoscale among the different building blocks of the metal-free polymer composite and the structural rearrangement of the interpenetrated polymer network by the incorporation of CO<sub>2</sub>. We have provided both a new electrochemically multifunctional hierarchically structured material and a facile route that could lead to novel sustainable energy applications.

© 2020 Elsevier Ltd. All rights reserved.

## Introduction

The increase of pollution levels in the atmosphere and their global impact on human health and on climate change are pushing rapid integration of energy from wind and sun into the electric grid as well as the electrification of the transport sector [1]. In addition, to reach a low-carbon and climate-resilient future, highly efficient, low-cost, and large-scale methods to decrease the CO<sub>2</sub> concentration in urban and industrial areas are also needed [2]. Batteries have not yet achieved the degree of versatility and functionality to, simultaneously, store electricity and CO<sub>2</sub>. In addition, the use of more sustainable energy storage materials to minimize the original

carbon dioxide footprint of fabricating and recycling the battery is highly needed [3].

In search for superior battery performance, one of the strategies adopted by researchers has been the development of electroactive materials structured on the nanometer scale [4]. By diminishing particle sizes [5] or the layer thickness [6] to nanometer size, the solid-state ion diffusion distances decrease while the surface area increases, thus enabling capacity values close to the theoretical ones even at high cycling rates. Nanostructured electrodes can also accommodate large strain without pulverization, providing mechanical flexibility and sustained electronic contact under stress [7].

However, the fabrication of nanostructured electrodes and electroactive nanoparticles normally involves complex synthetic routes with several reaction steps and often with the use of harmful chemicals. Moreover, these methods usually provide a very low amount of functional material, making the overall process highly

\* Corresponding author.

E-mail address: [jcarretero@ictp.csic.es](mailto:jcarretero@ictp.csic.es) (J. Carretero-González).<https://doi.org/10.1016/j.mtsust.2020.100048>

2589-2347/© 2020 Elsevier Ltd. All rights reserved.



# A Physical Unclonable Function Based on Recyclable Polymer Nanoparticles to Enable the Circular Economy

Amparo Fernández-Benito,\* Mario Hoyos, Miguel A. López-Manchado, and Thomas Just Sorensen\*

Cite This: *ACS Appl. Nano Mater.* 2022, 5, 13752–13760

Read Online

ACCESS |

Metrics &amp; More

Article Recommendations

**ABSTRACT:** The circular economy requires that we know what a product is made of, that we can control that it is not a fake, and that we know how to recycle it. This requires a digital twin of each product where the information is stored and that we can access using a smartphone. The creation of digital twins requires a connection between the physical and digital worlds, which in turn requires that all objects have a unique identifier valid in both domains. The realization of the intrinsic potential of creating digital twins of individual products that link physical and digital identities in turn requires that the physical identifier is truly unique and that it cannot be copied. Furthermore, the physical identifier should not interfere with the product lifecycle, in particular recyclability, as this would be a potential blocker in a circular economy. Here, we present a physical unclonable function (PUF) made from polymer nanoparticles and imbedded in a polymer laminate, where all components can be made from the same recyclable material. Such materials are commonly used for packaging in the fragrance and cosmetics industry. The development of the PUF system is presented, and each PUF was validated using a proprietary smartphone application with a QR code as a common pattern defining the PUF canvas. The functionality of the PUF was demonstrated across product types as diverse as lateral flow assays and construction materials. We conclude that polymer nanoparticle PUFs are a viable and directly recyclable solution to document authenticity and inform on recyclability of polymers in the circular economy.

**KEYWORDS:** physical unclonable function, polymer nanoparticles, recycling, nanomaterials, authentication systems, digital twins



## INTRODUCTION

The approach to providing a digital ID for consumer goods that we present here is equivalent to creating "biometrics for things". A direct link between a digital ID and a secure physical ID allows for an irrefutable link between the physical and digital worlds, enabling the creation of genuine digital twins for all consumer products. This pairing is presented as part of an integrated solution for object validation, authentication, and identification, where the immediate application lies as a solution to the problem of counterfeit goods.<sup>1–4</sup> The fight against counterfeiting is an old issue,<sup>5</sup> but it is increasingly important due to the sheer scale of the problem<sup>6</sup> and the detrimental consequences to general human health and safety.<sup>7–11</sup> However, an irrefutable optical authentication system directly available on portable devices allows for much more disruptive solutions ranging from smart contracts bound to the physical object to the direct transfer of ownership between consumer wallets.<sup>12–15</sup> Here, we propose that secure physical IDs are also critical for the realization of a circular economy.

Our proposed solution for a unique physical identifier is to use physical unclonable functions (PUFs).<sup>4,16,17</sup> PUFs are

unique physical objects that contain vast amounts of information that can be recorded and compared.<sup>18–23</sup> Examples range from human fingerprints to the scattering of the random surface structure of paper.<sup>22,24–34</sup> While using PUFs is just emerging in the optical authentication of goods, their application has been investigated in detail in electronics.<sup>19,21,24,35–39</sup> A solution that is to be implemented as an authentication and identification system for consumer goods requires that each PUF is cheap (less than 0.10 USD per physical identifier), and if the solution is to be used as a driver of consumer behavior in a circular economy, the PUF must be an integral part of the product and packaging to the extent that it is recycled with the product.<sup>40</sup> Plastics are the main material used for containers and packaging because they are economical, functional, and lightweight. The most commonly

**Special Issue:** Professor Sir Fraser Stoddart's 80th Birthday Forum

**Received:** February 22, 2022

**Accepted:** April 24, 2022

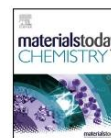
**Published:** May 9, 2022





Contents lists available at ScienceDirect

Materials Today Chemistry

journal homepage: [www.journals.elsevier.com/materials-today-chemistry/](http://www.journals.elsevier.com/materials-today-chemistry/)

## Novel ferrocene-containing amphiphilic block copolymer nanoparticles as high-capacity charge carriers in aqueous redox flow systems



A. Fernández-Benito <sup>a, b</sup>, F.J. Rivera-Gálvez <sup>c</sup>, P. Cisneros-Ruiz <sup>a</sup>, R. Sanz-Horta <sup>a</sup>,  
C.F. Jasso-Gastinel <sup>c</sup>, M.A. López-Manchado <sup>a</sup>, J. Carretero-González <sup>a, \*</sup>

<sup>a</sup> Institute of Polymer Science and Technology (ICTP), CSIC, 28006, Madrid, Spain

<sup>b</sup> Organic and Inorganic Chemistry Department, Universidad de Alcalá de Henares, Madrid, Spain

<sup>c</sup> Chemical Engineering Department, Universidad de Guadalajara, Guadalajara, Mexico

### ARTICLE INFO

#### Article history:

Received 7 June 2022

Received in revised form

20 September 2022

Accepted 23 October 2022

Available online xxx

#### Keywords:

Redox amphiphilic block copolymers

Polymer nanoparticles

Redox flow batteries

And energy storage

### ABSTRACT

Size-exclusion polymer electrolytes are promising charge carriers to diminish the crossover and allowing commercially available low-cost porous membranes in redox flow batteries. Boosting the solubility in water and maximizing the number of redox sites to enhance the capacity of these polymeric systems is challenging. New highly water dispersed amphiphilic diblock copolymers are reported here, with an average concentration value of  $1.7 \cdot 10^{-3}$  mmol of Ferrocene (Fc)-linked moieties per mg of polymer, determined by total X-ray reflection fluorescence. These redox amphiphilic block copolymers are stabilized in water as spherical nanoparticles (20 nm) by using a simple phase solvent inversion procedure. We evidence a maximum polymer dispersibility value of 6 g/L in water, for long-term stable polymer nanoparticle suspensions, yielding a theoretical capacity value of 4.78 mAh at 10.5 mM Fc. Further adjustment of the ionic conductivity and pH of these stable redox block copolymer suspensions has rendered a conductivity value of 44.5 mS/cm at pH values close to a neutral one, by adding a variety of salt supports. Studies using a 3-electrode configuration cell reveal an efficient charge transport between each of the Fc motifs in the polymer nanoparticle. A capacity value of 3.1 mAh with no transient of the polymer nanoparticles crosswise the cheap porous membrane is evidenced when cycled as polycatholyte material in a Zn hybrid aqueous redox flow battery. The particle size and electronic changes of these novel amphiphilic redox block copolymer electrolytes during consecutive redox cycles have also been monitored by dynamic light scattering and ultraviolet-visible spectroscopy, respectively. The analysis of the results enables the understanding of the main mechanisms behind their non-fully reversible capacity. Among them, aggregation and sedimentation, along with retention inside the graphite felt electrode acting the latter as a filter. These insights will aid the design of future polymer electrolyte materials and redox flow battery components with better performance and cost.

© 2022 Elsevier Ltd. All rights reserved.

### 1. Introduction

Replacing non-renewable energy sources with sustainable alternatives such as solar and wind energies is crucial for the ecological transition toward a safe, zero-carbon future [1–4]. Redox flow batteries (RFBs) show promise for large-scale energy storage from these intermittent renewable sources [5]. Generally, RFBs are comprised of two electrolytes containing redox active compounds

that are continuously pumped from two external tanks into an electrochemical cell where the electroactive species are oxidized or reduced swapping electrons through the external circuit. Ions migrate through an ion-selective polymer membrane to balance the charges. So far, the most studied and commercially extended RFB system has been based on vanadium chemistry [6] but it requires expensive membranes [7], and electrolytes that are also scarce and/or costly, and not particularly eco-friendly [8].

These drawbacks might be reduced by using redox polymer electrolytes to diminish the material crossover between the poly(catholyte) and poly(anolyte) and allow commercially available low-cost porous membranes [9,10]. In addition, the use of aqueous

\* Corresponding author.

E-mail address: [jcarretero@ictp.csic.es](mailto:jcarretero@ictp.csic.es) (J. Carretero-González).

<https://doi.org/10.1016/j.mtchem.2022.101271>

2468-5194/© 2022 Elsevier Ltd. All rights reserved.

(12) INTERNATIONAL APPLICATION PUBLISHED UNDER THE PATENT COOPERATION TREATY (PCT)

(19) World Intellectual Property  
Organization  
International Bureau



(43) International Publication Date  
04 March 2021 (04.03.2021)

WIPO | PCT

(10) International Publication Number  
WO 2021/037441 A1

- (51) International Patent Classification:  
C08B 11/02 (2006.01) H01B 1/12 (2006.01)
- (21) International Application Number:  
PCT/EP2020/070521
- (22) International Filing Date:  
21 July 2020 (21.07.2020)
- (25) Filing Language: English
- (26) Publication Language: English
- (30) Priority Data:  
19382731.8 28 August 2019 (28.08.2019) EP
- (71) Applicant: **CONSEJO SUPERIOR DE INVESTIGACIONES** [ES/ES]; C/ Serrano, 117, 28006 Madrid (ES).
- (72) Inventors: **CARRETERO GONZÁLEZ, Javier**; INSTITUTO DE CIENCIA Y TECNOLOGIA DE POLIMEROS, C/ Juan De La Cierva, 3, 28006 Madrid (ES). **FERNÁNDEZ BENITO, Amparo**; INSTITUTO DE CIENCIA Y TECNOLOGIA DE POLIMEROS, C/ Juan De La Cierva, 3, 28006 Madrid (ES). **RODRIGUEZ CABALLERO, Daniel**; INSTITUTO DE CIENCIA Y TECNOLOGIA DE POLIMEROS, C/ Juan De La Cierva, 3, 28006 Madrid (ES). **RODRIGUEZ RODRIGUEZ, Giovanna**; INSTITUTO DE CIENCIA Y TECNOLOGIA
- DE, POLIMEROS, C/ Juan De La Cierva, 3, 28006 Madrid (ES). **LÓPEZ MANCHADO, Miguel Ángel**; INSTITUTO DE CIENCIA Y TECNOLOGIA DE POLIMEROS, C/ Juan De La Cierva, 3, 28006 Madrid (ES).
- (74) Agent: **PONS ARIÑO, Angel**; Glorieta Rubén Darío, 4, 28010 Madrid (ES).
- (81) Designated States (unless otherwise indicated, for every kind of national protection available): AE, AG, AL, AM, AO, AT, AU, AZ, BA, BB, BG, BH, BN, BR, BW, BY, BZ, CA, CH, CL, CN, CO, CR, CU, CZ, DE, DJ, DK, DM, DO, DZ, EC, EE, EG, ES, FI, GB, GD, GE, GH, GM, GT, HN, HR, HU, ID, IL, IN, IR, IS, IT, JO, JP, KE, KG, KH, KN, KP, KR, KW, KZ, LA, LC, LK, LR, LS, LU, LY, MA, MD, ME, MG, MK, MN, MW, MX, MY, MZ, NA, NG, NI, NO, NZ, OM, PA, PE, PG, PH, PL, PT, QA, RO, RS, RU, RW, SA, SC, SD, SE, SG, SK, SL, ST, SV, SY, TH, TJ, TM, TN, TR, TT, TZ, UA, UG, US, UZ, VC, VN, WS, ZA, ZM, ZW.
- (84) Designated States (unless otherwise indicated, for every kind of regional protection available): ARIPO (BW, GH, GM, KE, LR, LS, MW, MZ, NA, RW, SD, SL, ST, SZ, TZ, UG, ZM, ZW), Eurasian (AM, AZ, BY, KG, KZ, RU, TJ, TM), European (AL, AT, BE, BG, CH, CY, CZ, DE, DK, EE, ES, FI, FR, GB, GR, HR, HU, IE, IS, IT, LT, LU, LV, MC, MK, MT, NL, NO, PL, PT, RO, RS, SE, SI, SK, SM,

(54) Title: ELECTROCHEMICALLY ACTIVE NANOPARTICULATE POLYMER MATERIAL

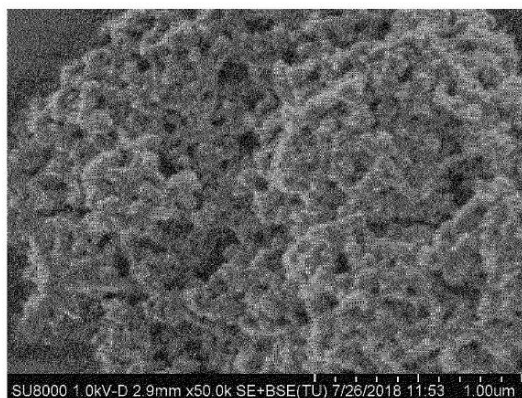


Fig. 1

(57) Abstract: The present invention relates to an electrochemically active nanoparticulate polymer material comprising methylcellulose, sulfonated lignin and polypyrrole with a hierarchical structure and method of obtaining thereof, for use as an electrochemical material dispersed in an aqueous medium. The present invention belongs to the field of sustainable electrochemical systems mainly for converting and storing energy from renewable sources and capturing and transporting CO<sub>2</sub> gas from the combustion of fossil fuels in the industry sector.

[Continued on next page]

WO 2021/037441 A1

**TRATADO DE COOPERACIÓN EN MATERIA DE PATENTES  
NOTIFICACIÓN DE LA RECEPCIÓN DE LOS DOCUMENTOS QUE  
CONSTITUYEN SUPUESTAMENTE UNA SOLICITUD INTERNACIONAL  
PRESENTADA DE FORMA ELECTRÓNICA.**

**(Instrucciones Administrativas del PCT, Parte Séptima)**

- 1.-Se notifica al solicitante que la Oficina Receptora ha recibido en la fecha de recepción indicada más abajo, los documentos que supuestamente constituyen una solicitud internacional.
- 2.-Se llama la atención del solicitante sobre el hecho de que la Oficina Receptora no ha comprobado aún si estos documentos satisfacen las condiciones del art. 11.1, es decir, si cumple los requisitos para que le sea atribuida una fecha de presentación internacional. En cuanto la Oficina Receptora haya comprobado los documentos, avisará al solicitante.
- 3.-El número de la supuesta solicitud internacional indicado más abajo ha sido otorgado automáticamente a estos documentos. Se invita al solicitante a mencionar este número en toda la correspondencia con la Oficina Receptora.

Número de presentación	300437696	
Solicitud Número PCT	PCT/ES2022/070023	
Fecha de recepción	19 enero 2022	
Oficina Receptora	Oficina Española de Patentes y Marcas, Madrid	
Referencia del expediente del solicitante o mandatario	PCT1641.1644	
Solicitante	CONSEJO SUPERIOR DE INVESTIGACIONES CIENTÍFICAS (CSIC)	
Número de solicitantes	2	
País	ES	
Título de la invención	AGREGADOS FLUORESCENTES DE POLI(TEREFTALATO DE CICLOHEXILENDIMETILENO), PROCEDIMIENTO DE OBTENCIÓN Y USO COMO ETIQUETA FÍSICAMENTE NO CLONABLE PARA IDENTIFICAR Y/O TRAZAR ENVASES PARA PRODUCTOS COSMÉTICOS Y/O PERFUMES	
Documentos presentados	eolf-pkda.xml eolf-appb.xml eolf-vlog.xml eolf-appb-P000002.pdf (2 p.)	eolf-requ.xml eolf-fees.xml eolf-appb-P000001.pdf (13 p.) eolf-appb-P000003.pdf (1 p.)



